Formulation of nano-structured emulsions for use in food and healthcare applications

Elahi, Shabnam

Award date:
2015

Awarding institution:
University of Bath

Formulation of nano-structured emulsions for use in food and healthcare applications

Shabnam Elahi

A thesis submitted in candidature

for the degree of Doctor of Philosophy

University of Bath

Department of Chemical Engineering

June 2015

Copyright:

Shabnam Elahi

ABSTRACT

Nano-emulsions are a centre of attention for many industrial applications in different fields such as pharmaceutical, cosmetic, food and agriculture due to their interesting physical properties such as transparency, larger surface area to volume ratio and long-term physical stability. This PhD project focuses on the preparation of stable nano-emulsions using different emulsification methods with an attempt to find the optimum formulation to produce stable nano-emulsions for food and healthcare applications.

The emulsification methods studied in this project were rotor-stator homogeniser (Ultra-Turrax), Phase Inversion Temperature (PIT), dead-end and cross-flow membrane emulsification methods. The model system soybean oil/water/Brij 97 was used to investigate the emulsification methods. However, in the case of two membrane emulsification methods, it was decided to use Tween series surfactants as Brij 97 didn't work for our experiments.

Our study showed that stable nano-emulsions containing 10 % (w/w) oil phase ratio can be produced by Homogeniser, PIT and dead-end membrane emulsification methods with droplet sizes in the range of 9 - 90 nm depending on the employed method, surfactant concentration and various experimental conditions. Cross-flow emulsification method failed to produce stable nano-emulsions in this study. PIT method yielded the smallest drop sizes in the range of 9 – 19 nm and lowest energy consumption (200 - 280 J g^{-1}). However, for producing stable nano-emulsions by this method, the minimum amount of surfactant required were found to be 10.5 % (w/w). Dead-end membrane emulsification was also found to be a promising method for producing stable nano-emulsions with using surfactant concentration as low as 4 % (w/w) in oil, bearing also in mind that Tween series surfactants are more biocompatible than Brij 97. The only drawback for this method is its higher energy consumption than PIT method as Ultra-Turrax was used to prepare the premix. If a more energy efficient method for mixing the emulsion components is employed, this method could be a more suitable option than PIT method for food and healthcare applications. Nevertheless, PIT method could still be considered as the favourable choice when shear sensitive materials are used.

ACKNOWLEDGEMENTS

I wish to express my utmost gratitude to my supervisors, Dr Tom Arnot and Dr Pawel Plucinski for their supervision, guidance and advice throughout this PhD project.

I would like to acknowledge all the administrative and technical staff in the Department of Chemical Engineering, University of Bath for their practical help.

I also want to thank the EPSRC and University of Bath for their financial support of my work.

My final thanks go to my husband, my parents and Mehdi for their endless support and encouragement.

TABLE OF CONTENTS

LIST OF FIGURES

LIST OF TABLES

ABBREVIATIONS

AAO	Anodic aluminium oxide
ADI	Acceptable daily intake
AFM	Atomic force microscopy
CCD	Charge-coupled device
CIP	Cleaning in place
CMC	Critical micelle concentration
CMT	Critical micelle temperature
Cryo-TEM	Cryogenic transmission electron microscopy
DDS	Drug delivery systems
DLS	Dynamic light scattering
EPDM	Ethylene propylene diene monomer
FDA	Food and Drug Administration
FTU	Formazine turbidity unit
HCC	Hepatocellular carcinoma
HLB	Hydrophile-Lipophile Balance
HPH	High-pressure homogeniser
IUPAC	International Union of Pure and Applied Chemistry
MC	Microchannel emulsification technique
ME	Membrane emulsification
MPG	Micro-porous glass membranes
NTA	Nanoparticle tracking analysis
O/W	Oil-in-water
O/W/O	Oil-in-water-in-oil
P & ID	Piping and instrumentation diagram/drawing
PCS	Photon correlation spectroscopy
PCTE	Polycarbonate track-etched membrane
PdI	Polydispersitry index
PIT	Phase inversion temperature
PTFE	Polytetrafluoroethylene
RO	Reverse osmosis
rpm	revolutions per minute

SBO	Soybean oil
SDS	Sodium dodecyl sulfate
SEM	Scanning electron microscopy
SIP	Sterilisation in place
SPG	Shirasu porous glass
TMP	Transmembrane pressure
UHT	Ultra-high temperature processing
UT	Ultra-Turrax
US	Ultrasonic
W/O	Water-in-oil
W/O/W	Water-in-oil-in-water

NOMENCLATURE (SI unit)

English letters:

A	Surface area of the membrane (m^2)
A_p	Surface area of the pore (m^2)
A_t	Total area of the pores in the image (m^2)
A_T	Total area of the image (m^2)
a_o	Optimal surface area per head group (m^2)
C_e	Arbitrary experimental constant
C_p	Specific heat capacity of the material (J kg^{-1} °C^{-1})
D	Diffusion coefficient (m^2 s^{-1})
D_R	Diameter of the rotor (m)
d_{av}	Average droplet diameter (m)
d_d	Droplet diameter (m)
d_i	Final particle size in the *i*th pass (m)
d_{max}	Maximum droplet diameter (m)
d_m	Mean pore size (m)
d_p	Membrane pore diameter (m)
d_x	Droplet diameter corresponding to x vol. % on a relative cumulative droplet diameter distribution curve (m)
E_v	Energy density (J m^{-3})
F_B	Buoyancy force (N)
F_D	Viscous drag force (N)
F_{sp}	Static pressure difference force (N)
F_γ	Interfacial tension force (N)
g	Gravitational force (m s^{-2})
J	Permeate flux (kg m^{-2} s^{-1})
J_d	Dispersed phase flux (m^3 m^{-2} s^{-1})
J_i	Trans-membrane flux in the *i*th pass (m^3 m^{-2} s^{-1})
J_{4-25}	Equivalent of membrane water flux at 4 bar TMP and 25 °C
$J_{Exp,T}$	Measured flow at T °C (m^3 s^{-1})
K	Membrane permeability (m^2)
k_B	Boltzmann's constant (J K^{-1})

k_t	Coefficient of temperature
L	Membrane thickness (m)
l_c	Critical chain length (m)
l_w	Kolmogorov length scale (m)
m	Mass of the material (kg)
m_e	Total mass of the emulsion (kg)
N	Rotation speed (rpm)
P	Power input into the machine (W)
P_d	Pressure of the dispersed phase (Pa)
$P_{c,in}$	Pressure of the flowing continuous phase at the inlet of membrane module (Pa)
$P_{c,out}$	Pressure of the flowing continuous phase at the outlet of membrane module (Pa)
P_c	Critical pressure (Pa)
Q	Energy required to increase the temperature of a material (J)
r	Radius of the spherical particle (m)
r_D	Radius of the droplet (m)
r_{Di}	Initial radius of the droplet (m)
R_{fi}	Fouling resistance in the *i*th pass (m^{-1})
R_m	Membrane resistance (m^{-1})
r_P	Radius of the pore (m)
T	Absolute temperature of the system (K)
V	Velocity of dispersed phase ($m\ s^{-1}$)
V_c	Volume of the hydrocarbon chain (m^3)
V_e	Volume of emulsion (m^3)
V_o	Volume of oil (m^3)
$\dot{V}$	Volume flow rate ($m^3\ s^{-1}$)
$\dot{V}_d$	Volume flow rate of the dispersed phase ($m^3\ s^{-1}$)
υ_c	kinematic viscosity of continuous phase ($m^2\ s^{-1}$)
W	Work done by applied pressure (J)

Greek symbols:

a	Distance between the two slots of the motor (m)
γ	Interfacial tension between the phases (N m^{-1})
γ_{ow}	Interfacial tension between oil and water (N m^{-1})
γ_{LS}	Interfacial tension between the liquid and the solid (N m^{-1})
γ_{GS}	Interfacial tension between the gas and the solid (N m^{-1})
γ_{LG}	Interfacial tension between the liquid and the gas (N m^{-1})
ΔA	Increase in interfacial area (m^2)
ΔF_{form}	Free energy of formation of the emulsion (J mol^{-1})
ΔP	Laplace pressure (Pa)
ΔP_{tm}	Transmembrane pressure (Pa)
ΔS	Configurational entropy of the system (J mol^{-1} K^{-1})
ΔT	Variation in temperature during heating (°C)
$\Delta\gamma$	Interfacial tension between the phases (N m^{-1})
ε	Power density (W m^{-3})
ε_m	Power density per unit mass (W kg^{-1})
δ	Standard deviation of the droplet diameters (m)
μ	Dynamic viscosity (Pa s)
μ_c	Viscosity of the continuous phase (Pa s)
μ_d	Viscosity of the dispersed phase (Pa s)
μ_e	Mean viscosity of emulsions inside the pores (Pa s)
θ	Interfacial contact angle (°)
ρ_d	Density of the dispersed phase (kg m^{-3})
ρ_c	Density of the continuous phase (kg m^{-3})
σ_W	Wall shear stress (Pa)
$\sigma_{W,P}$	Wall shear stress inside the pore (Pa)
τ	Membrane tortuosity
φ	Membrane porosity
φ_d	Volume fraction of the dispersed phase (vol %)

1. Introduction

An emulsion is formed when two immiscible liquid phases in the presence of an emulsifying agent are mixed together with a sufficient amount of energy to break up one of the phases into smaller droplets, which remain dispersed throughout the other phase. Emulsions are non-equilibrium systems. Thus, they are not formed spontaneously and not only the thermodynamic conditions (*i.e.*, composition, temperature, or pressure) but also the preparation methods and the order of component addition can affect their properties [1].

Regarding the droplet size there are three types of emulsions; Macro-emulsions, Micro-emulsions and Nano-emulsions which are different not only in size but also in stability and application [2]. This PhD project focuses on the preparation of nano-emulsions. Nano-emulsions are a type of emulsions with small droplet diameters in the range of 20–200 nm with high kinetic stability and low viscosity. They have either bluish semi-opaque appearance, or optical transparency resembling micro-emulsions. To prepare nano-emulsions usually high amount of energy input from mechanical devices or from the chemical potential of components is required as they cannot be formed spontaneously due to being non-equilibrium system [3]. However, unlike micro-emulsions which need a high surfactant concentration, usually in range of 20 % and higher, nano-emulsions can be prepared using lower surfactant concentration in order to be more favourable for food and healthcare applications [4].

Nano-emulsions are a centre of attention for many industrial applications in different fields such as pharmaceutical, cosmetic, food and agriculture. The main distinguishing factor which makes the nano-emulsions more attractive than ordinary emulsions is their interesting physical properties, which are their transparency, larger surface area to volume ratio and long-term physical stability [5]. The optical transparency of nano-emulsions makes them suitable for potential applications in beverage fortification where certain products are required to be optically clear *e.g.* fortified soft drinks and waters [6]. By using food-grade ingredients, nano-emulsions are being growingly employed in the food industry to encapsulate, protect, and deliver hydrophobic functional components *e.g.* bioactive lipids and lipophilic flavours, vitamins, preservatives, and nutraceuticals, and in the pharmaceutical

industry as drug delivery system [7]. Due to their large surface area to volume ratio and small particle sizes, it has been shown that nano-emulsions can enhance the bioavailability of the encapsulated ingredients when used as a delivery system through the 'rough' skin surface or oral ingestion [4] [8]. The transparent nature and the fluidity of nano-emulsion systems (at reasonable concentrations) and also the absence of any thickeners give them a pleasant aesthetic character and skin feel which makes them suitable for cosmetic applications. They can be also applied for delivery of fragrances, which may be incorporated in many personal care products as well as in perfumes, which are desirable to be formulated alcohol free [4].

For many commercial applications within food, healthcare and cosmetic industries, oil-in-water (O/W) emulsions are favoured over water-in-oil (W/O) emulsions [9]. Many biologically-active components are lipophilic molecules. Therefore, oil-in-water emulsions are more suitable vehicles for oral delivery of these bioactive nutraceutical and pharmaceutical products [10]. O/W emulsions have also some interesting advantages such as lower viscosity and consistency indices when compared to water-in-oil emulsions due to their lower oil phase ratio. Because of less feeling of oiliness, they offer a better skin application property and skin feel [9]. The other reason for their preference over water-in-oil emulsions is their lower manufacturing cost. For producing water-in-oil emulsions, higher concentrations of oil are required. Furthermore, the W/O emulsifiers are generally more expensive than those used for stabilising O/W emulsions [11].

With regards to the amount of energy required for emulsification, the methods applied for preparation of nano-emulsions can be categorized into two groups of high-energy methods such as high pressure homogeniser, high shear stirring (Rotor-Stator method) and ultrasound generators and low-energy methods like phase inversion temperature (PIT) method and membrane emulsification.

The high-energy emulsification methods are broadly used in industry for producing stable fine emulsions. However, the limitations of these methods due to their high energy requirements, such as high equipment and operating costs and not being suitable for shear-sensitive components made the low-energy methods a promising alternative especially in the food and healthcare industries where the delicate ingredients can lose their functionality or nutritional value with high shear stresses.

1.1 Aims and scope

The overall aim of this project is to find the optimum formulation using low-toxicity components to produce stable nano-emulsions for food and healthcare applications by employing different emulsification methods. In order to fulfill the main aim, the following objectives set at the beginning of this study can be summarised as:

- Investigating oil-in-water emulsions prepared by rotor-stator homogeniser (Ultra-Turrax), as an example energy intensive method, and comparing them with those produced by Phase Inversion Temperature (PIT) as a low energy emulsification technique
- Investigating oil-in-water emulsions produced by two membrane emulsification methods of 'dead-end' and 'cross-flow' as two novel low-energy methods
- Studying the main factors affecting the quality of the prepared emulsions with an attempt to find the optimum formulation. Depending on the emulsification method, these main factors include temperature, surfactant concentration, volume fraction of the dispersed phase, membrane characteristics and finally amount of energy or pressure applied to the system.

1.2 Thesis structure

This thesis is composed of 7 chapters:

Following the Introduction, Chapter 2 provides the necessary background needed to understand the principles of emulsions, emulsification methods and all the affecting parameters, overviewing the previous studies in the relevant areas. In the first part of this section, some basic concepts have been explained such as what emulsions are and how they are formed. Then, the different types of emulsification methods are explained. Furthermore membrane emulsification as a novel method is discussed in detail together with all its affecting parameters.

Chapter 3 (Material and Methods) gives full details of the materials used to produce emulsions, and all the methods and devices utilised in this study to investigate the emulsification process and characterise the prepared nano-emulsions.

Chapter 4 presents the results for emulsions prepared by rotor-stator homogeniser (Ultra-Turrax) and their comparison with those produced by Phase Inversion Temperature (PIT)) in terms of droplet size, polydispersitry index (PdI) stability over time and finally their energy consumption.

Chapter 5 concentrates on the dead-end emulsification method. It provides results for the emulsions using ceramic or polycarbonate flat sheet membranes focusing on the effects of various parameters on the droplet size and droplet size distribution of these emulsions as well as on their stability over time. The estimated energy consumption of this method is given in the last section of this chapter.

Chapter 6 explains the attempt to design an experimental rig for cross-flow membrane emulsification and provides the results for the emulsions produced by this method as well as the estimated energy consumption.

Chapter 7 summarises conclusions from the experimental findings in this project and suggests potential future work for further investigation in this area of research.

2. Literature Review

2.1 Basic concepts

2.1.1 Definition of Emulsions

An emulsion is a heterogeneous system of two immiscible liquid phases where one of the phases is dispersed in another in the form of droplets and stabilized by emulsifying agent [12]. Milk and rubber latex are examples of natural emulsions [13].

The International Union of Pure and Applied Chemistry (IUPAC) has defined the emulsion as "*A dispersion of droplets of one liquid in another one with which it is incompletely miscible. Emulsions of droplets of an organic liquid (an oil) in an aqueous solution are indicated by the symbol O/W and emulsions of aqueous droplets in an organic liquid as W/O. In emulsions the droplets often exceed the usual limits for colloids' sizes''* [14].

Emulsions are generally categorized into two types; simple and multiple emulsions. Simple emulsions, *e.g.*, oil-in-water (O/W) and water-in-oil (W/O) only consist of two phases while the complex or multiple emulsions have three or more phases, such as water-in-oil-in-water (W/O/W) (Figure 2.1). The simplest multiple emulsions are double emulsions. A double emulsion is defined as an emulsion in an emulsion. Two main types of double emulsions are water-in-oil-in-water (W/O/W) emulsions, in which a W/O emulsion is dispersed in an aqueous phase, and oil-in-water-in-oil (O/W/O) emulsions, in which an O/W emulsion is dispersed as droplets in an oil phase. Among the two types of double emulsions the W/O/W emulsions are more common. Double emulsions have more interface than single emulsions and are also more thermodynamically unstable [1].

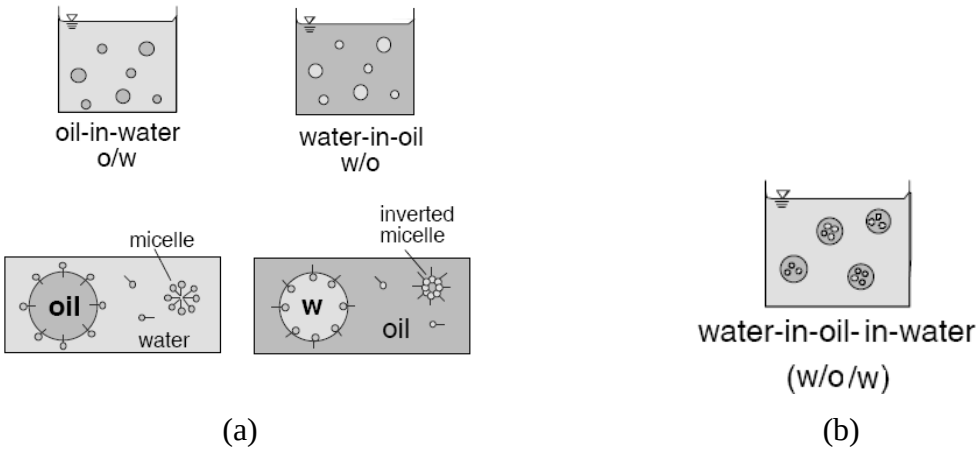

Figure 2.1: (a) Simple types of emulsions; (b) An example of multiple emulsions [15].

Emulsions are non-equilibrium systems. Thus, they are not formed spontaneously and not only the thermodynamic conditions (*i.e.*, composition, temperature, or pressure) but also the preparation methods and the order of component addition can affect their properties [1]. Regarding the droplet size there are three types of emulsions; Macro-emulsions, Micro-emulsions and Nano-emulsions which are different not only in size but also in stability and application [2] (Table 2.1).

Table 2.1: Types of emulsions in term of size

Type of emulsion	**Droplet size**	**Stability**	**Appearance**
Macro-emulsion	>1µm	kinetically stable	Creamy / Opaque
Nano-emulsion	10-200 nm	kinetically stable	Transparent
Micro-emulsion	5-100 nm	Thermodynamically stable	Transparent

2.1.2 Applications of Emulsions

Emulsions have been used in different fields such as pharmaceutical, cosmetic, food and agriculture [16]. Double emulsions have many interesting applications in food and drug industries. Producing low calorie products and drug delivery systems are two examples of their applications. Besides that, they can be used in skin care products due to their spreadability and ability to encapsulate ingredients in both phases (water and oil) [17].

2.1.3 Emulsion formation

An emulsion is formed when the oil phase, aqueous phase and surfactant are mixed together with a sufficient amount of energy to break up either the oil or the water phase into smaller droplets, which remain dispersed throughout the other liquid, by using mixer or a homogeniser. Enough agitation is required to disperse one liquid into small droplets, and sufficient surfactant is required to stabilize the dispersed droplets [18]. In emulsion formation (*i.e.*, emulsification) two major considerations are essential: first the formation of the correct type of emulsion (O/W, W/O, multiple emulsions) with the required droplet size distributions and second the stabilization of dispersed droplets which are formed in the continuous phase.

The formation mechanism can be explained by the expression of free energy of formation of the emulsion which is given by the following equation:

$$\Delta F_{form} = \gamma \Delta A - T \Delta S \qquad \text{Equation 2.1}$$

Where ΔF_{form} is the free energy of formation of the emulsion (J mol^{-1}), γ: the interfacial tension between the phases (N m^{-1}), ΔA: the increase in interfacial area (m^2), T: the temperature of the system (K) and ΔS is the configurational entropy of the system (J mol^{-1} K^{-1}) [19].

In most cases the free energy of formation is positive which means forming emulsion requires energy input to the system, thus indicating it is not a spontaneous process. A spontaneous system arises when $\gamma \Delta A$ is significantly small. For this condition to happen, γ must be very small ($<< 10^{-5}$ *N m*$^{-1}$). The free energy can then be shown to be negative [20].

Emulsions are traditionally made by colloid mills, rotor-stator systems or high pressure homogeniser [21]. Within the dispersing zone of these machines, droplets of a premix are deformed and disrupted which requires high energy input [22]. Because of great stresses applied to deform and disrupt the larger droplets in these machines, shear-sensitive emulsifiers and stabilizer such as proteins or starch may lose their functional properties [23].

2.1.4 Stability

Emulsion stability is a kinetic concept. An emulsion is a thermodynamically unstable system and tends to separate over a period of time, thus it is important to produce an emulsion resistant to physical and chemical changes over time. Creaming (sedimentation), coalescence, flocculation and Ostwald ripening are four important examples of physical instability, whereas oxidation and hydrolysis are the consequences of chemical instability [24]. Ostwald ripening is the consequence of droplet size increase due to large droplets growing at the expense of smaller ones [25].

Figure 2.2 shows some types of emulsion instability. Coalescence is the collision of two particles and the formation of a larger particle which is irreversible. Flocculation is the attachment of emulsion particles to form flocs which in many cases can be a reversible process. Colloidal interaction between the droplets has an effect on flocculation [26]. Creaming is the result of gravitational force and occurs when the dispersed droplets separate from the continuous medium and is reversible. (It can be returned to the original state by gentle agitation) [27]. The rate of creaming mainly depends on the difference between the density of continuous and dispersed phase and is given by Stokes' law:

$$V = \frac{2{r_D}^2(\rho_d - \rho_c)g}{9\mu} \qquad \text{Equation 2.2}$$

Where:

V is the velocity of dispersed phase (m s^{-1})
r_D is the radius of dispersed phase droplet (m)
ρ_d is the density of the dispersed phase (kg m^{-3})
ρ_c is the density of the continuous phase (kg m^{-3})
g is the gravitational force (m s^{-2})
μ is the viscosity of continuous phase (Pa s) [28].

Breaking or inversion is the separation of an emulsion in to two or more phases and it is an irreversible process leading to complete phase separation. Phase inversion occurs when an O/W emulsion inverts to W/O emulsion or vice versa.

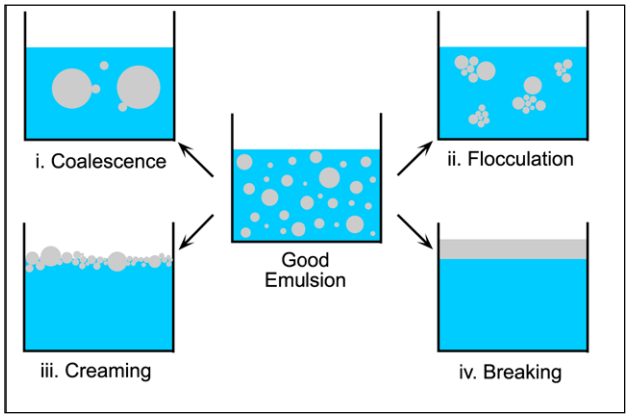

Figure 2.2: Different types of emulsion instability [29]

Droplet interfacial free energy is a primary driving force that causes phase separation. By applying surface active ingredients *e.g.* surfactant which adsorbs at the oil-water interface and lowers interfacial tension the system becomes more stable [26]. Therefore the stability of an emulsion considerably depends upon the surfactant.

Other factors which have an impact on stability of emulsions are droplet size, density difference between dispersed and continuous phases, viscosity of the continuous phase, electrostatic and/or steric repulsion between droplets, net charge and the physical and mechanical property of adsorbed film [30].

Another parameter showing the stability of an emulsion is whether the emulsion is monodisperse or polydisperse. The emulsion is called monodisperse when the droplets are all of the same size while an emulsion that contains droplets with a range of different sizes is called polydisperse. A polydispersed emulsion tends to break-up faster than a monodispersed one [31].

The dispersity of the droplets can be expressed in terms of the coefficient of variation (relative standard deviation) or the relative span factor. The coefficient of variation is defined as Equation 2.3.

$$CV = \left(\frac{\delta}{d_{av}}\right) \times 100 \qquad \text{Equation 2.3}$$

Where δ is the standard deviation of the droplet diameters (m) and d_{av} is the average droplet diameter (m). It has been defined that the emulsions are monodispersed for a coefficient of variation equal or smaller than 0.35. The relative span factor (or span) is determined using Equation 2.4.

$$Span = \frac{d_{90} - d_{10}}{d_{50}} \qquad \text{Equation 2.4}$$

Where d_x is the diameter (m) corresponding to x vol. % on a relative cumulative droplet diameter distribution curve [32]. Span (*i.e.* polydispersity index) is a dimensionless estimate of the width of the particle size distribution and is scaled from 0 to 1. Under 0.08, the sample is nearly monodispersed. On the contrary, over 0.7, it is very polydispersed [33].

Distribution of emulsion droplets is the most important parameter in characterising of any emulsion. Droplet size distribution affects the stability of emulsion and resistance to creaming. The larger the particle size, the greater the tendency to coalesce. Hence smaller droplet size improves the emulsion stability. Generally, emulsion stability is characterised by measuring the droplet size distribution as a function of time. Measuring can be done by optical microscopy, light scattering techniques or other methods. An emulsion is considered physically stable when there is no change in its droplet size distribution independently of time and place [34].

2.1.5 Definition of Micro-Emulsion and Nano-Emulsion

2.1.5.1 Micro-Emulsions

According to Danielsson and Lindman, *"A micro-emulsion is a system of water, oil and an amphiphile which is a single optically isotropic and thermodynamically stable liquid solution."* [35]

Micro-emulsions are translucent or optically transparent solutions with dispersed droplet sizes in range of 5-100 nm. They are isotropic, have low viscosity and are thermodynamically stable [2]. Their optical transparency is due to their very small droplet size, which does not scatter visible light as compared to larger aggregates like droplets in a coarse emulsion.

There are some substantial differences between a micro-emulsion and a normal emulsion, although they are both dispersions of oil in water stabilized by an interfacial film of amphiphilic molecules. The main difference between the two systems is that a micro-emulsion forms spontaneously while forming an emulsion requires mechanical force and a large input of energy. The other major difference between a normal emulsion and a micro-emulsion is their size and stability [36]. The size and shape of the droplets dispersed in the continuous phase shows the two systems are different in terms of thermodynamic stability. Emulsions are kinetically stable and thermodynamically unstable which leads them to coalesce and cause separation of the two phases during storage, while micro-emulsions are thermodynamically stable and will not separate during storage. Micro-emulsions and normal emulsions can also be easily distinguished by their transparency. As mentioned before, micro-emulsions are transparent whereas normal emulsions have an opaque appearance (see Table 2.2).

Micro-emulsions have a variety of applications in different industries. Beverage concentrates, pesticide formulations and pharmaceutical products are a few examples. In recent years they have received considerable interest as potential drug delivery systems. Advantages associated with micro-emulsions include their ease of formation, solubilization capacity, low viscosity, transparency and thermodynamic stability [37].

The composition of micro-emulsions can be explained in the context of ternary phase diagrams (Figure 2.3). Ternary phase systems or three component systems are represented by the use of triangular phase diagrams to illustrate the phase behavior of surfactant, oil and water, at well defined temperature and pressure. The vertices of the triangle represent pure components and each of the triangle sides corresponds to possible compositions of binary mixtures including micelles and reverse micelles. Any point inside the triangle characterises a ternary mixture in specific proportions for each component. To produce single-phase micro-emulsions first a suitable surfactant dissolves in the oil phase and then the water will be added slowly with gentle shaking. Micro-emulsions form spontaneously and the system rapidly becomes translucent and then optically transparent. As shown in Figure 2.3 micro-emulsions can be prepared over a wide range of surfactant concentrations and oil-to-water ratios, however in most systems, a micro-emulsion exists only within a confined range of concentrations. In fact a micro-emulsion is only one of a number of possible oil, water and surfactant association structures that can form, depending on the chemical nature and concentration of each of the components, and additionally on the temperature and pressure (other structures include gels and various mesomorphic phases). No matter if a micro-emulsion is formed or not, at very low surfactant concentrations, a large multiphase region is normally seen, while at very high surfactant concentrations, liquid crystalline phases are usually formed. It is obvious from Figure 2.3 that the microstructure of the micro-emulsion must be different over the range of possible micro-emulsion compositions. At low oil or water volume fractions, micro-emulsions are generally believed to be a dispersion of either oil or water micelles stabilized by an interfacial film of surfactant and if appropriate, cosurfactant. These micellar structures are the most commonly encountered type of micro-emulsion microstructure [36].

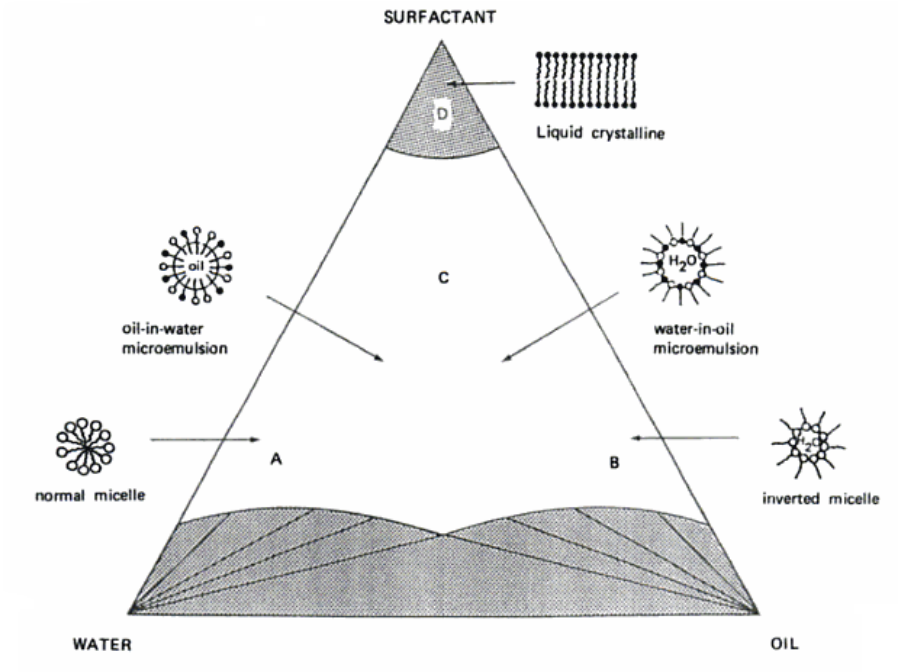

Figure 2.3: Schematic ternary phase diagram of an oil-water-surfactant micro-emulsion system consisting of various associated microstructures. A. Normal micelles or O/W micro-emulsions. B. Reverse or W/O micro-emulsions, C. Concentrated micro-emulsion domain. D. Liquid-crystal or gel phase. Shaded areas represent multiphase regions. Adapted from [38]

2.1.5.2 Nano-emulsions

Nano-emulsions belong to a wide category of multiphase colloidal dispersions [5]. Solans *et al.* defined Nano-emulsions as a type of emulsion with small droplet diameters, typically in the range of 20–200 nm showing narrow size distributions. They appear transparent to the naked eye (Figure 2.4 and 2-5) and possess stability against sedimentation or creaming [39].

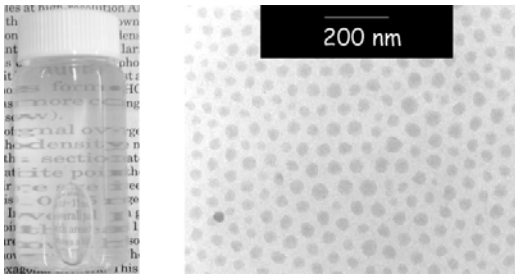

a b

Figure 2.4: (a) Visual appearance and (b) a Cryo-TEM picture of nano-emulsion [41]

Figure 2.5: Transparency of a nano-emulsion (left) as opposed to the milky appearance of a macro-emulsion (right) [39]

The fundamental difference between micro-emulsions and nano-emulsions is that micro-emulsions are equilibrium systems (*i.e.* thermodynamically stable) whereas nano-emulsions are non-equilibrium systems with a spontaneous and instinctive tendency to separate into their constituent phases. Nevertheless, nano-emulsions may keep a relatively high kinetic stability even for several years [40].

The main distinguishing factor which makes the nano-emulsions more attractive than ordinary emulsions is their interesting physical properties, which are their transparency and larger surface area to volume ratio. Ordinary micro-scale emulsions typically show strong multiple scattering of visible light which leads to a white appearance, by contrast most nano-emulsions appear optically transparent [5].

Table 2.2: The main difference between Micro-emulsions, Nano-emulsions (Mini-emulsions) and Emulsions [37]

Properties	Emulsions		Microemulsions
	Nano-emulsion	Macro-emulsion	
Visual aspect			
Typical characteristic size	20 – 200 nm	> 1 µm	5 – 100 nm
Stability	Kinetic		Thermodynamic
Formation	Energy input		Spontaneous
Surfactant concentration	Low		High

2.1.6 Properties of Nano-Emulsions

As stated before, nano-emulsions have high kinetic stability, low viscosity and optical transparency. They are a centre of attention for many industrial applications; for instance, in the pharmaceutical field as drug delivery systems (DDS), food industry and cosmetics. Some advantages of nano-emulsions can be summarised as follows [4]:

(i) No creaming or sedimentations during storage: This is due to the very small droplet size which causes a large reduction in the gravity force. On the other hand, Brownian motion may be sufficient for overcoming gravity.

(ii) The system remains dispersed with no separation: This is again because of the very small droplet size which prevents any flocculation of the droplet.

(iii) No coalescence: The small size droplets and also the significant surfactant film thickness prevent disruption and coalescence between the droplets.

(iv) Nano-emulsions are suitable for efficient delivery of active ingredients through the skin: The large surface area of the emulsion system and their small sizes allows rapid penetration of actives through the 'rough' skin surface.

(v) Pleasant aesthetic character and skin feel: It is due to the transparent nature and the fluidity of nano-emulsion systems (at reasonable concentrations) and also the absence of any thickeners.

(vi) Unlike micro-emulsions which need a high surfactant concentration, usually in range of 20 % and higher, nano-emulsions can be prepared using reasonable surfactant concentration. For instance, for a 20 % O/W nano-emulsion, a surfactant concentration of 5-10 % can be sufficient.

(vii) The droplets deposit uniformly on substrates because of their small size. Besides that, the low surface tension of the whole system and the low interfacial tension of the O/W droplets lead to the enhancement of wetting, spreading and penetration.

(viii) Nano-emulsions can be applied for delivery of fragrances, which may be incorporated in many personal care products as well as in perfumes, which are desirable to be formulated alcohol free [4].

2.1.7 Preparation of Nano-emulsions

To prepare nano-emulsions high amount of energy input from mechanical devices or from the chemical potential of components is required as nano-emulsions are non-equilibrium systems and cannot be formed spontaneously [3].

Besides that, this high amount of energy can also be explained by considering the Laplace pressure (*P)* (Equation 2.5). The smaller droplet size, the higher energy is required to overcome the Laplace pressure.

$$\Delta P = \frac{2\gamma}{r_D} \qquad \text{Equation 2.5}$$

Where ΔP: The pressure difference between inside and outside the spherical droplet (Pa), r_D: Radius of droplet (m) and γ is the interfacial tension (N m^{-1}) [4].

2.2 Emulsification methods to produce nano-emulsions

Figure 2.6 and Table 2.3 show an overview of the most frequently used emulsification methods.

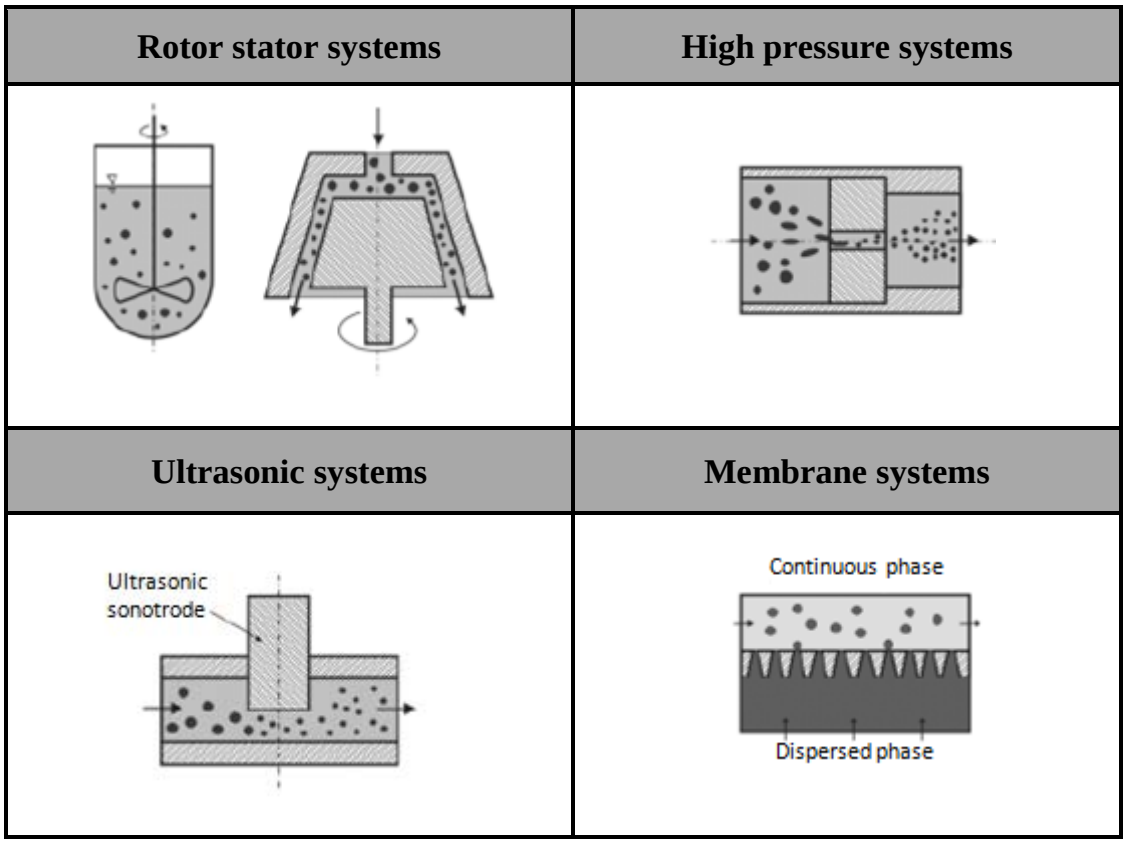

Figure 2.6: Schematic view of different emulsifying systems [42]

Table 2.3: Methods for emulsification [42]

	Rotor Stator systems		High pressure systems	Membrane systems	Ultrasonic System
Mode of operation	Discontinuous Quasi-continuous	Continuous	Continuous	Continuous	Discontinuous Quasi-continuous
Examples	Mixer Gear rim disperser	Colloid Mills Gear rim disperser Intensive mixer	Radial diffuser Counter jet disperser Axial nozzle systems	Glass/ceramic membrane	Ultrasonic sonotrode
Breakup mechanism	Shear/inertia stress in turbulent flow	Shear stress in laminar flow and/or Shear/inertia stress in turbulent flow	Shear/inertia stress in turbulent flow; Cavitation; Laminar extension flow	Pore diameter; Dispersed phase flux	Cavitation; Micro-turbulences
Throughput	Middle	High	High	Low	Low
Product stress	Middle to high	Very high	Very high	Low	Very high
Application	Industrial production			Laboratories / product from development	

With regards to the amount of energy required for emulsification, the methods applied for preparation of nano-emulsions can be categorized into two groups:

- High-energy methods
- Low-energy methods

The actual amount of energy required to form an emulsion depends on the type of method used and the operating condition. During the emulsification process droplets are disrupted and the higher the energy density the smaller the droplets after disruption [21]. Thus the formation of small droplets (Nano-emulsions) requires a larger amount of energy.

In Figure 2.7 the mean droplet size is given as a function of energy density. Energy density can be calculated from Equation 2.6 as follows:

$$E_v = \frac{P}{\dot{V}} = \Delta p \qquad \text{Equation 2.6}$$

Where,

E_v is the energy density (J m^{-3}), P is the power input into the machine (W), $\dot{V}$ is the volume flow rate (m^3 s^{-1}) and Δp is the pressure difference (Pa) [43].

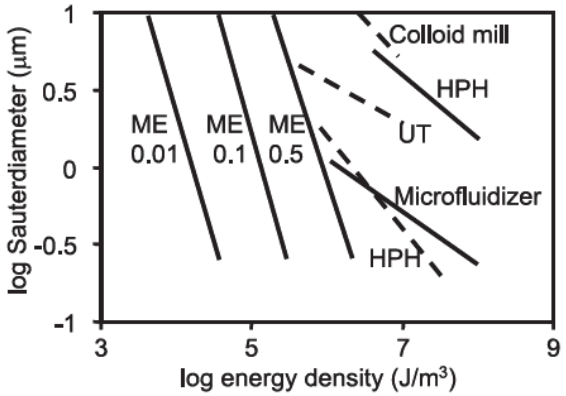

Figure 2.7: Droplet diameter as a function of the energy consumption supplied by different types of equipment. (ME: cross-flow membrane emulsification. Numbers represent the dispersed phase fraction; HPH: high-pressure homogeniser; UT: Ultra Turrax [44].

2.2.1 High-energy emulsification methods

Nano-emulsions can be produced by the so-called dispersion or high-energy emulsification techniques *i.e.* high pressure homogeniser, high shear stirring (Rotor-Stator method) and ultrasound generators. It has been shown that the smallest size can be achieved by devices which supply the available energy in the shortest time and have the most homogeneous flow [39].

2.2.1.1 High-pressure homogenisers (HPH)

High-pressure homogenisers are the most important continuously operated emulsifying devices. As they are operated in a continuous mode high production rates can be obtained, which is one of the reasons behind their wide uses in industries for making finely dispersed emulsions [45]. Homogenisers are the most common methods of producing fine emulsions in the food industry. They are widely utilized to prepare nano-emulsions (see Figure 2.8).

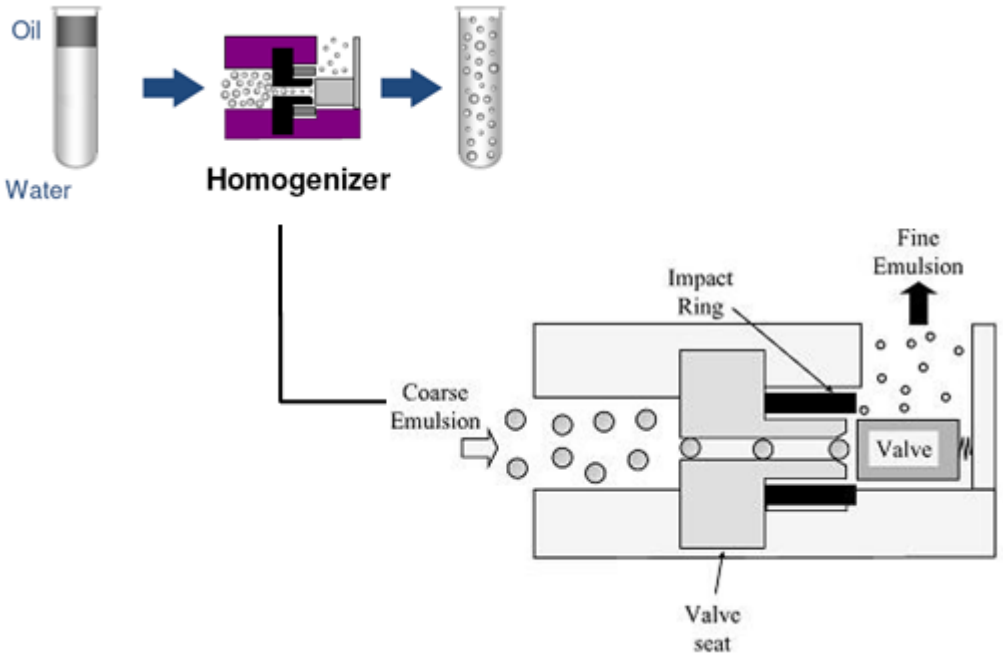

Figure 2.8: High pressure homogeniser [46]

High-pressure homogenisers consist of a high-pressure pump and a homogenizing nozzle [39]. Essential parameters affecting the properties of the final product are the order of ingredient addition and homogenization. In this system, emulsification is carried out by turbulence and cavitation effect using a high amount of energy (up to 10^8 J m^{-3}). A coarse emulsion pre-mixture of dispersed phase, continuous phase and emulsifier is passed through a narrow orifice causing the droplets to be deformed and disrupted to the smaller sizes. It leads to the formation of very fine but polydispersed

droplets. Furthermore, the small droplets have to be stabilized against coalescence by adsorbing emulsifier molecules.

Rapid emulsifier adsorption makes the droplets more stable while slow adsorption causes coalescence (Figure 2.9). This process may be coupled with the use of ultrasound or electric fields. The driving pressures in this method of emulsification are commonly in the range 5.0×10^{6} to 3.5×10^{7} Pa. Besides the high energy required in this method, it is also difficult to control the droplet size and droplet size distribution, and because of high shear-stress it is not suitable for production of shear sensitive emulsions [1].

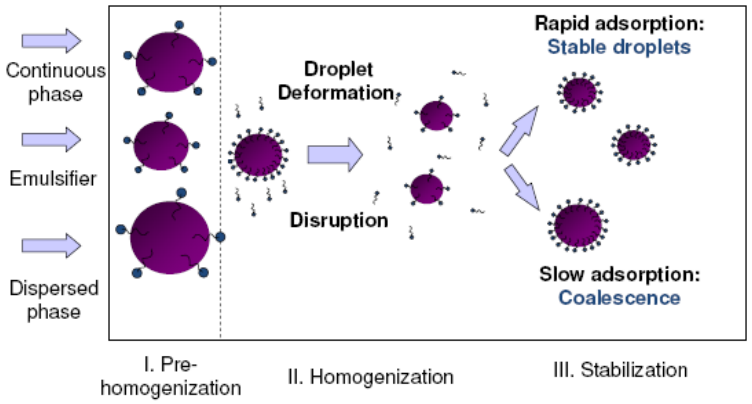

Figure 2.9: Schematic of homogenization process [46]

2.2.1.2 Rotor-Stator method

Rotor-stator systems are high pressure dispersing systems used to produce emulsions. Rotor-stator is the simplest type of emulsification equipment available which can be operated both continuously and discontinuously (batch-wise). Normally, gear-rim dispersing machines are used for discontinuous or quasi-continuous production while colloid-mills with smooth or toothed rotors and stators, gear-rim dispersing machines and intensive mixers are utilized for continuous operation [47]. In the rotor-stator system, emulsification is carried out under very high shear rate (up to 10^{7} s^{-1}) in a very narrow gap (*e.g.* 0.1 mm) between a high speed rotor and stator surface (Figure 2.10). The liquids enter at the bottom through suitable tubes and then flow through

the narrow slit between the stator and the rotor and finally leave the system. In the dispersing zone of these machines droplets of a premix are deformed and disrupted. Shear sensitive emulsifiers and stabilizers, *e.g.* proteins or starch, may lose functional properties if too great stresses are applied in these machines.

According to Tadros *et al*. (2004) and McClements (2004) [4] [24], the droplet size in an emulsion that has been prepared by the homogenization method is controlled by the interaction between droplet break-up and coalescence. Droplet break-up is governed by the type and amount of shear applied by the homogeniser and also by the resistance of the surfactant-induced droplets to deformation (Laplace pressure). The rate of droplet coalescence, which is related to droplet stability, depends on how quickly the surfactant can adsorb to the surface of newly formed droplets; this is controlled by surfactant surface activity and concentration [49]. Therefore, the droplet size decreases as the energy input increases (with time) until it reaches a steady state value where the rate of droplet rupture to droplet coalescence becomes constant so that the mean droplet size does not change anymore.

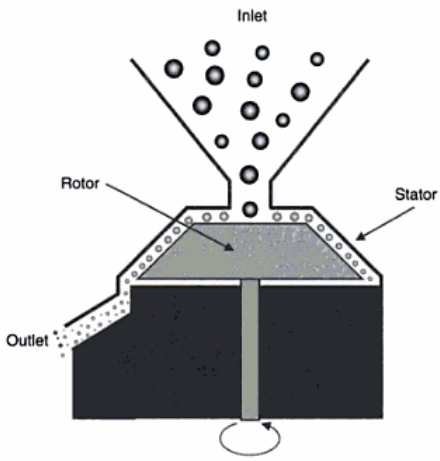

Figure 2.10: Schematic view of a rotor stator system (colloid mill) [24]

Rotor-stator systems are used for the production of emulsions with medium to high viscosities (20–5000 mPa s) [47]. Colloid mill is one of different forms of this device and can produce emulsions with smaller particle sizes (1 – 100 μm) comparing to the ones prepared using fixed gap rotor-stator mixers. Colloid mills are extensively used in the food industry processes for homogenizing intermediate and highly viscous materials.

2.2.1.3 Ultrasonic method

The ultrasonic method can be operated continuously or discontinuously. Although this method is efficient in reducing droplet size, it is only suitable for small batches (<50 ml). Hence, it is more frequently used at the lab scale [25][39].

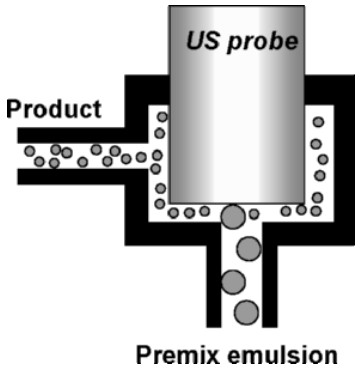

Figure 2.11: Schematic view of ultrasonic method [48]

According to Kentish *et al.*, Ultrasonic emulsification is believed to happen through two mechanisms.

a) Interfacial waves produced by an acoustic field become unstable, ultimately resulting in the eruption of the oil phase into the water medium in the form of droplets.

b) The application of low frequency ultrasound leads to the formation of micro bubbles defined as acoustic cavitation, and their subsequent collapse (*i.e.*, an implosion on a microscopic scale) due to the pressure fluctuations of a simple sound wave. These micro-implosions cause extreme levels of highly localized turbulence which act as a very effective way to break up the dispersed oil droplets into droplets of sub-micron size [49].

A comparison of different high energy methods is summarized in Table 2.4 (see also Table 2.3).

Table 2.4: A comparison of different high energy methods

	High pressure systems	Rotor Stator systems	Ultrasonic System
Energy consumption (Jm^{-3})	10^8	10^7	10^7
Minimum droplet size	0.1 µm	1 µm	0.1 µm
Range of viscosity	Low to medium (1-200 mPa s)	Medium to high (20-5000 mPa s)	Low to medium (1-200 mPa s)
Application	Lab and/or Industrial: Pharmaceutical Cosmetics	Lab and/or Industrial: Food Pharmaceutical Cosmetics	Lab.

2.2.2 Low-energy emulsification methods

The second group of emulsification methods are referred to as low-energy emulsification, where the energy requirement is much lower than conventional emulsifying systems. The two more frequently-used low-energy methods for producing nano-emulsions *i.e.* phase inversion temperature (PIT) method and membrane emulsification, are described in this section.

2.2.2.1 Phase inversion temperature (PIT) Method

The phase inversion temperature (PIT) may be defined as the temperature at which an oil-in-water emulsion changes to water-in-oil emulsion or vice versa. This method is one of the low energy emulsification methods that may be applied for the preparation of nano-emulsions. The Phase Inversion Temperature (PIT) method requires a much lower level of energy than conventional emulsifying systems.

In the PIT method, emulsions are formed by rapid temperature changes passing through the phase inversion temperature (*i.e.* the hydrophile-lipophile balance (HLB)

temperature) and stabilized by appropriate nonionic surfactants [50]. The HLB temperature is a characteristic property of an emulsion at which the hydrophilic-lipophilic property of non-ionic surfactant just balances [51]. Below this temperature, the surfactant is more hydrophilic; preferentially encapsulate oil as droplets in water. One the other hand, at higher temperature (above the PIT), surfactants become more hydrophobic and give W/O emulsions (Figure 2.12).

The PIT emulsification method consists of preparing the emulsions at the HLB temperature in order to take advantage of the low interfacial tension achieved, followed by a rapid cooling or heating of the samples to produce O/W or W/O emulsions, respectively [52]. The emulsions produced by this method are long-term stable because of the nano-scale particle size. This stability lasts as long as coalescence of the oil droplets does not occur [53]. It has been reported that stable oil-in-water emulsions can be obtained by the PIT method if the temperature of the sample is quickly lowered to a temperature approximately 30 °C below its PIT. In those conditions, droplet coalescence becomes almost negligible as the surfactant molecules form an efficient physical barrier preventing the droplets from merging when colliding [28][31].

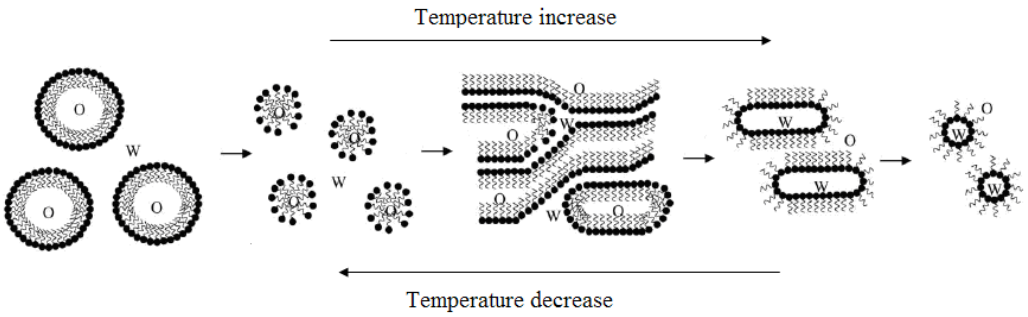

Figure 2.12: Schematic diagram of the PIT process [54]

2.2.2.2 Membrane emulsification methods

Tado Nakashima proposed membrane emulsification method at the annual meeting of the Society of Chemical Engineers, Japan, in 1988 [55]. This method involves either passing pure disperse phase through a membrane into cross-flowing

continuous phase or the permeation of a coarse premix through a membrane. Membrane emulsification has received increasing attention over the last 15 years for its effectiveness in producing narrow droplet size distribution over a broad range of mean droplet sizes (mainly controlled by the membrane pore size) at low energy consumption; with potential application in many fields such as food, cosmetics and the drug industry. The membrane emulsification principles and its potential applications have been studied and reviewed by several researchers such as Nakashima *et al.* , (2000); Joscelyne and Trägårdh, 2000; Charcosset *et al*., 2004; Charcosset and Fessi, 2005, Gijsbertsen-Abrahamse *et al*., 2004; Vladisavljevic´ and Williams, 2005.

There are currently two methods of membrane emulsification: pre-mix membrane emulsification, and cross-flow membrane emulsification.

2.2.2.2.1 Pre-mix membrane emulsification

Premix membrane emulsification is an emulsification method which has received increasing attention over the past years. This method was first introduced by Suzuki and co-workers in 1998 [56] [60]. In this method, which is also known as dead-end membrane emulsification, coarse pre-mix emulsions are forced through a porous membrane where they breakup into finer droplets [1]. Figure 2.13 illustrates a schematic view of the pre-mix membrane emulsification process.

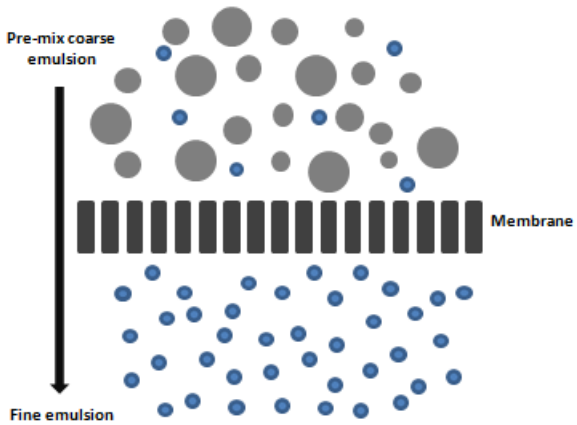

Figure 2.13: Schematic view of the pre-mix membrane emulsification as introduced by Suzuki and co-workers.

The narrow droplet size distribution obtained at low energy costs, along with high flows and high volume fractions of dispersed phase, makes this method more attractive and a good alternative to conventional emulsification methods for bulk production of emulsions [58]. The droplet size distribution achieved with this method is insignificantly wider than that achieved with cross-flow membrane emulsification [56]. A considerable advantage of pre-mix membrane emulsification is that high fluxes (up to 10 $m^3 m^{-2} h^{-1}$) can be achieved [59]. Besides that, a fine emulsion can be easily obtained from a low-concentrated coarse emulsion at high emulsifying rates [32].

As stated before, in this method a preliminary coarse emulsion is used as the dispersed phase. The coarse emulsion can be prepared by mixing the two immiscible liquids using a conventional stirrer mixer. Premix membrane emulsification can be performed in two ways; premix membrane emulsification without phase inversion and premix membrane emulsification with phase inversion. When an oil-in-water emulsion passes through a hydrophilic membrane the resulting fine emulsion will be oil-in-water, on the other hand, if a hydrophobic membrane is used phase inversion occurs and the resulting emulsion will be water-in-oil. Phase inversion can happen when the dispersed phase wets the membrane wall and appropriate surfactants are dissolved in both liquid phases, *i.e.* during the phase inversion a coarse O/W emulsion may be turned into a fine W/O emulsion and vice versa [32].

In the pre-mix membrane emulsification method, the resulting fine emulsion may be repeatedly passed through a membrane a number of times to gain greater droplet size reduction and improved size uniformity [32]. Some premix membrane emulsification investigations reported so far are summarized in Table 2.5.

Table 2.5: Some previous investigations carried out regarding the premix membrane emulsification [32]. (SPG: Shirasu porous glass, PTFE: Polytetrafluoroethylene)

Membrane Material	**System**	**Mean pore size, d_p (µm)**	**Product emulsion**	**Mean droplet size and span**	**Flux ($m^3 m^{-2} h^{-1}$)**	**Ref.**
Tubular SPG	Cross flow	2.7 and 4.2	O/W	1.4 - 2.1 d_p, span = 0.4 - 0.62	0.03-3.5	[32]
Flat PTFE	Dead-end	1.0	O/W and W/O	2 - 4.1 d_p	Up to 9	[32]
Flat PTFE	Dead-end with phase inversion	1.0	O/W and W/O	2.8 - 4.0 d_p	1-5.5	[60]
Flat PTFE	Dead-end, multi-pass (n=1-3)	1.0	O/W	1.2 - 2.6 d_p, span = 0.55 - 0.9	2-18	[32]
Flat cellulose acetate	Dead-end	0.2, 0.45, 0.8 and 3.0	W/O/W	1.0 - 3.5 d_p	Not given	[61]
Flat polycarbonate	Dead-end, multi-pass (n=1-18)	0.33, 0.38, 0.44, 0.6 and 1.0	O/W	≤1.6 d_p for n>12	0.2-0.6	[62]
Tubular SPG	Dead-end, multi-pass (n=3)	1.1	S/O/W	0.9 d_p	1.6	[63]
Tubular SPG	Dead-end, multi-pass (n=1-5)	10.7	W/O/W	0.4 - 1.2 d_p, span = 0.28 - 0.6	0.8-37	[64]

The premix ME has some advantages over direct ME which are as follows [65]:

a) The optimal transmembrane fluxes regarding droplet size uniformity are generally above 1 $m^3 m^{-2} h^{-1}$, which is one to two orders of magnitude higher than in direct ME method (0.01-0.1 $m^3 m^{-2} h^{-1}$).

b) The mean droplet sizes which can be achieved while using the same membrane and phase compositions are smaller than that in direct ME.

c) Simpler experimental set-up in comparison with direct ME. For instance, no moving parts such as cross flow pump or stirrer are required (except for preparing the pre-emulsion)

d) Unlike direct ME the operation and control are easier in premix ME as the driving pressure and emulsifier properties are not so critical for the successful outcome.

The higher droplet polydispersity obtained in premix ME is one of the disadvantages of this method as compared to direct ME. Attempts have been made to mix the advantages of these two techniques in the form of multi-pass ME [61] [64], in which the fine emulsion is repeatedly forced through the same membrane a number of times to obtain extra droplet size reduction and enhanced size uniformity.

2.2.2.2.2 Cross-flow membrane emulsification

Cross-flow membrane emulsification is a technique in which a liquid phase or to be dispersed phase is forced through the pores of a microporous membrane with uniform pore size by a low pressure (typically 200 kPa), to form droplets at the permeate side of the membrane. The droplets are carried away by a continuous phase flowing alongside the membrane surface. By using this method, and under specific conditions, monodisperse emulsions can be prepared for pharmaceutical, cosmetic and food applications. The energy requirement in this technique is much lower than conventional emulsifying systems and because of the low shear stresses, shear-sensitive ingredients for new products can be developed [21][22][23][66].

A schematic view of a typical membrane emulsification setup is shown in Figure 2.14. The system consists of a tubular microfiltration membrane, a pump and a feed vessel. The dispersed phase is pumped under gas pressure through the membrane module [22].

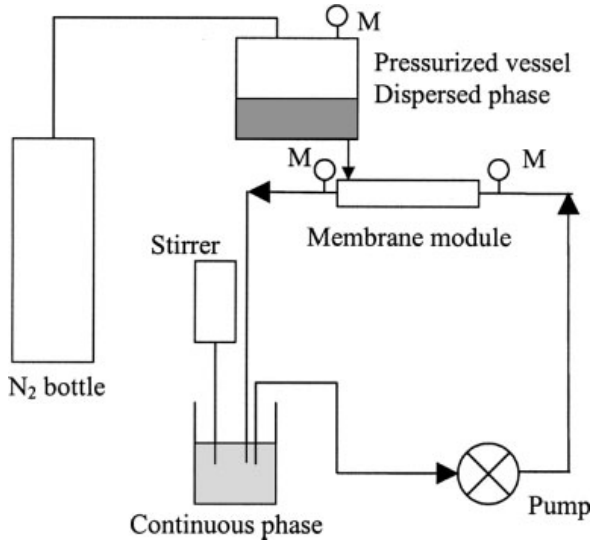

Figure 2.14: Experimental set-up for the membrane emulsification process (M: Monometer) [22]

Due to its simplicity, potentially lower energy consumption, need for less surfactant and the resulting narrow droplet size distribution, the membrane emulsification method has received increasing attention over the last few years. Membrane technique can be employed to the production of oil-in-water (O/W) food emulsions (*e.g.* salad dressing), to UHT (ultra-high temperature) products, artificial milk and also cream liqueurs in which the droplet size needs to be less than 1 µm in order to have a stable emulsion [21]. The distinguishing feature of this method is that the droplet size is primarily controlled by the choice of the membrane and not by the generation of turbulent droplet break-up in zones of high energy density (Figure 2.15) [22]. The main drawback of this method when compared to the pre-mix ME is its relatively low dispersed phase flux leading to lower productivity. Also, at high dispersed phase fraction, it is difficult to obtain uniform droplets [57].

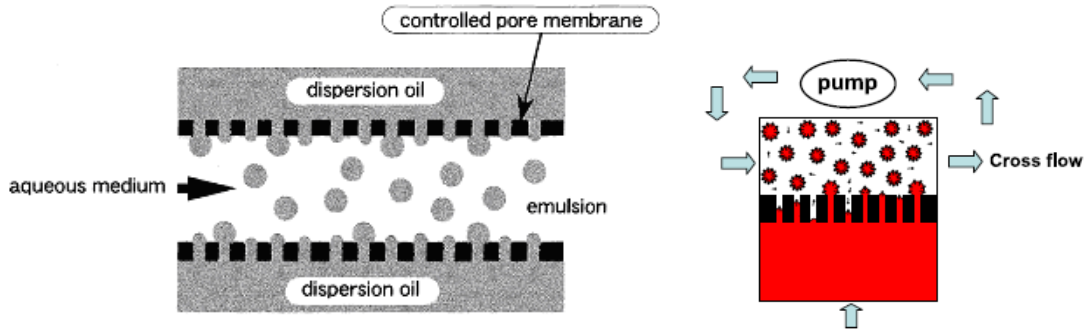

(a) (b)

Figure 2.15: (a) Preparation of oil-in-water (O/W) emulsion by using Membrane emulsification method, (b) Cross-flow membrane emulsification [67] [32]

One of the essentials in this method is that the membrane must not wetted by the dispersed phase, which means that hydrophilic membranes are suitable to produce oil-in-water (O/W) emulsions and hydrophobic membranes for water-in-oil emulsions (W/O) [17].

Some of the advantages of membrane emulsification methods for preparation of nano-emulsions compared to other methods are as follows:

a. *Low energy consumption:* Membrane emulsification method allows the production of emulsions at lower energy input (10^4 - 10^6 J m^{-3}) compared with conventional mechanical methods (10^6 - 10^8 J m^{-3}) [22].

b. *Control of droplet size and droplet size distribution:* As stated before, the droplet size in this method is primarily controlled by the choice of the membrane.

c. *Uniformity of droplets:* The particle size of the emulsion produced by membrane emulsification technique compared to other conventional method is remarkably uniform.

d. *Low shear stress:* Only mild shear stresses are applied in membrane emulsification which makes this process a very suitable method for producing shear sensitive double emulsions. Double emulsions have an interesting potential for the production of low calorie food products, encapsulation of medicines and other high value products [1].

2.3 Parameters affecting the droplet formation in membrane emulsification

Droplet formation and detachment from the membrane pores depends on various parameters (Figure 2.16), and these are described in this section.

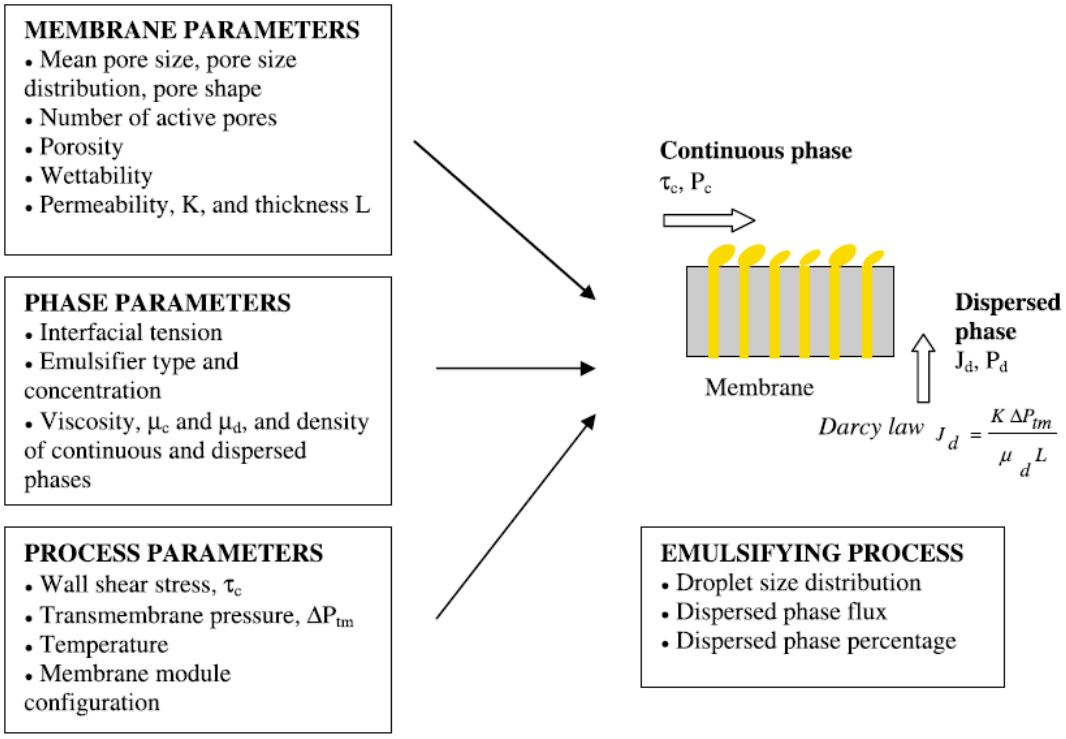

Figure 2.16: Parameters affecting droplet formation [68]

2.3.1 Membrane material

Shirasu porous glass (SPG) membrane developed by Nakashima *et al.* is the most common membrane used for the preparation of emulsion. It is prepared by phase separation of a glass composition. SPG is synthesized from $CaO–Al_2O_3–B_2O_3–SiO_2$-type glass made from 'Shirasu', a Japanese volcanic ash and has a very uniform pore size distribution [22]. Apart from SPG other membranes used in membrane emulsification studies are sintered ceramic membranes, microchannels and microsieve membranes. Microporous ceramic aluminium oxide (α-Al_2O_3) is one of

the examples of ceramic membranes [17] [69]. The broad range of other types of membranes used in membrane emulsification investigations is reported in Table 2.6.

Table 2.6: Microporous membranes (Excl. Shirasu Porous Glass (SPG)) used by different investigators for membrane emulsification [32]

Membrane material	**Membrane form**	**Inherent surface affinity**	**Mean pore size (μm)**	**Effective membrane area (cm^2)**	**Ref.**
Coated α-alumina or zirconia	Tubular	Hydrophilic	0.02-3	50-460	[21][32] [70][71]
Anodic porous alumina	Flat	Hydrophilic	0.125	-	[72]
Sol-gel porous glass	Tubular	Hydrophilic	0.6	-	[73]
Stainless steel with laser drilled pores	Tubular	Hydrophilic	100-150	4	[32][74]
Microporous nickel	Tubular	Hydrophilic	2.9-5.2	-	[75]
Polypropylene	Hollow fiber	Hydrophilic	0.4	10^3	[32]
Polyamide	Hollow fiber	Hydrophilic	10 nm	36	[76]
Polytetrafluoroethylene (PTFE)	Flat	Hydrophilic or hydrophobic	0.5-5	3-17	[32][60] [77]
Polycarbonate, track-etched	Flat	Hydrophilic	0.6-10	1.5-14	[61][62]
Cellulose acetate	Flat	Hydrophilic	0.2-3	4	[61]
Microengineered silicone nitride microsieve	Flat	Hydrophilic	7	3×10^{-4}	[66][78]
Straight-through silicon microchannels	Flat	Hydrophilic	10-17	1	[79][80]

2.3.2 Membrane pore size

There is close relation between membrane pore size and the size of droplets formed in membrane emulsification. Particle-size distribution of emulsions corresponds to pore-size distribution of the membrane. The larger pore size of membrane used, the larger particle size of emulsion is prepared [55].

According to Charcosset *et al.* the average droplet diameter, increases with the average membrane pore diameter by a linear relationship, for given operating condition [22]:

$$\bar{d}_d = c\bar{d}_p \qquad \text{Equation 2.7}$$

Where, $\bar{d}_d$: Droplet diameter (m), $\bar{d}_p$: Membrane pore diameter (m) and c is a constant ranged from 2 to 10 [17][22].

Figure 2.17 is a graph plotting the average particle size of emulsion as a function of the average pore size of the membrane which shows this linear relation [21][55].

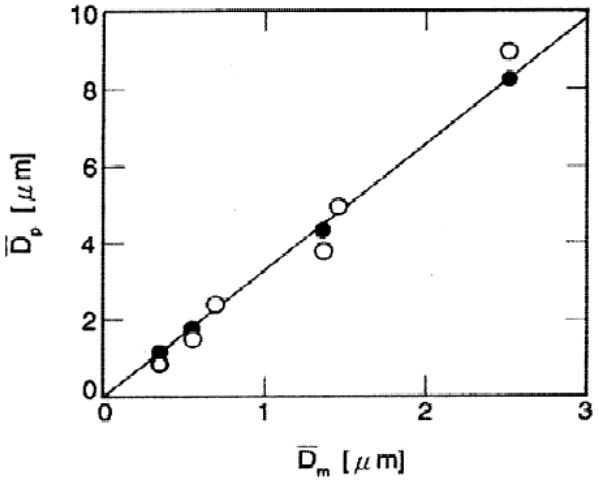

Figure 2.17: Relation between particle size of the emulsion and the membrane pore size in a cross-flow membrane emulsification system. The white and black markers represent average particle sizes in preparing an oil-in-water emulsion and a water-in-oil emulsion, respectively [55].

According to Peng and Williams, droplet formation from an individual pore of membrane consists of two stages: droplet growth (*i.e.* inflating the droplet at the pore mouth) and droplet detachment (*i.e.* breaking off the droplet and moving away from

the pore mouth). A droplet at a pore has a tendency to form a spherical shape under the action of interfacial tension, but some distortion may happen depending upon the flow rate of the continuous phase and the contact angle between the droplet and membrane surface. It is also important that the membrane not be wetted by the phase to be dispersed which means hydrophilic membranes are suitable to produce O/W emulsions and hydrophobic membranes for W/O emulsions (Figure 2.18) [17].

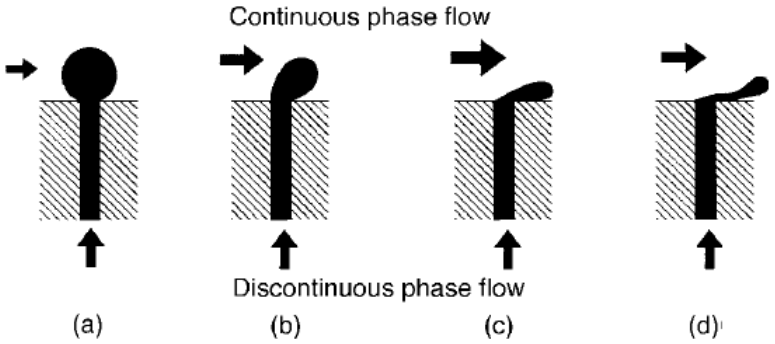

Figure 2.18: Droplet formation and detachment from a pore mouth under different conditions (a) negligible or low shear force; (b) high shear force in comparison to the interfacial tension; (c) very small contact angle or extremely high shear force; (d) membrane surface wetted by dispersed phase [81].

Contact angle measurement is a conventional method used to define the hydrophobic or hydrophilic behaviour of a material. Contact angle (θ) is the angle between the outline tangent of a drop deposited on a solid and the surface of the solid (Figure 2.19) [152]. For a membrane to be defined as hydrophilic, this angle should be less than 90 ° (Figure 2.20). The more the water drop spreads on the membrane surface, the smaller this angle is [153].

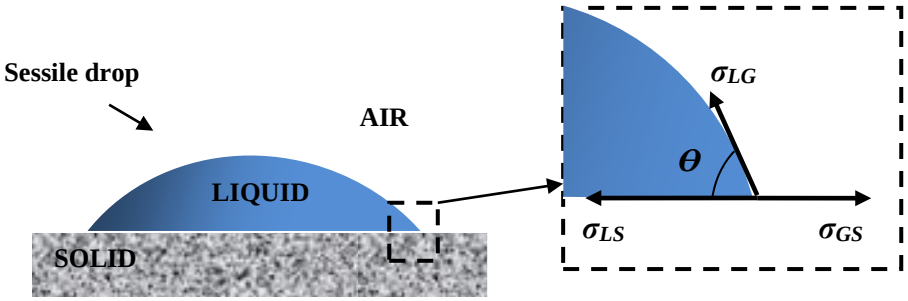

Figure 2.19: Contact angle formed by a liquid at the three phase boundary where a liquid, gas and solid intersect.

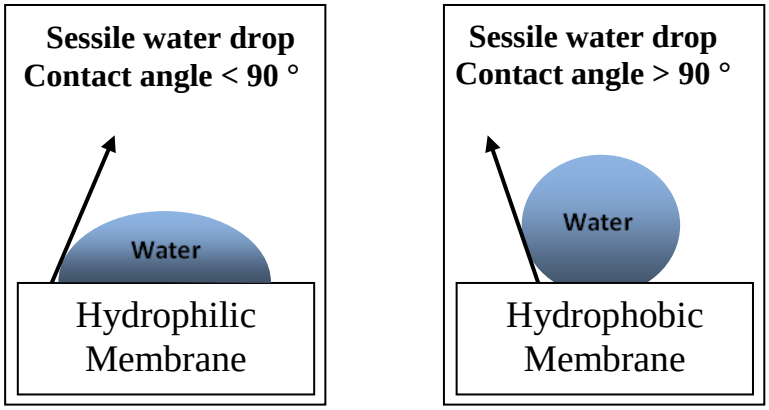

Figure 2.20: The relation between contact angle and membrane wettability

The shape of the drop and consequent magnitude of the contact angle are determined by the interaction between the interfacial tensions of the three phases involved (solid, liquid and gas), which is expressed by Young's Equation [153]:

$$\Delta\gamma = \gamma_{LS} - \gamma_{GS} = \gamma_{LG}\cos\theta \qquad \text{Equation 2.8}$$

Where,

γ_{LS} is the interfacial tension between the liquid and the solid (N m^{-1}), γ_{GS} is the interfacial tension between the gas and the solid (N m^{-1}) and γ_{LG} is the interfacial tension between the liquid and the gas (N m^{-1}).

Many studies have been carried out using tubular micro-porous glass membranes (MPG) or Shirasu porous glass membranes (SPG) which are assumed to have cylindrical, interconnected , uniform micropores and a narrow pore size distribution regularly ±15 %. Other membranes in published investigations are ceramic membranes (α-Al_2O_3) coated with titainia oxide or zirconia oxide. Multicoating can result in smaller pore size and narrower size distribution. All membranes mentioned above come in different nominal pore sizes in the range of 0.05-14 μm [17].

If the membrane pore size distribution is sufficiently narrow monodispersed emulsions may be produced [17]. Schubert and Schröder used a ceramic α-Al_2O_3 membrane to form oil-in-water emulsion (O/W) and they found that smaller nominal membrane pore size results in smaller minimum droplet size, and to reach this diameter smaller shear stress was needed. A wall shear stress >2 Pa was needed for the 0.1 and 0.5 μm membranes and >20 Pa for the 0.8 μm membrane [23]. Finally, the final droplet size and size distribution are not only affected by the pore size and size distribution of the membrane, but also by the degree of coalescence [17][81].

2.3.3 Membrane porosity

The distance between two adjacent pores is determined by the porosity of the membrane surface, which is the surface area fraction of the pores. This distance is critical to ensure two adjacent droplets do not come adequately close to each other to cause coalescence. Nevertheless, low porosity results in a low dispersed flux [81]. According to Schröder *et al.* a ratio of the droplet size to pore diameter of >1.6, for a membrane porosity of 0.3, leads to a significant degree of coalescence [82].

The top limit of the droplet size of the final product is also determined by the membrane porosity. A minimum distance greater than the droplet diameter is needed to avoid coalescence during the formation process, therefore, for a given desired final droplet size, the membrane needs to be confined to such a value that ensures an average distance between any two adjacent pores is more than the droplet diameter desired (Figure 2.21) [81].

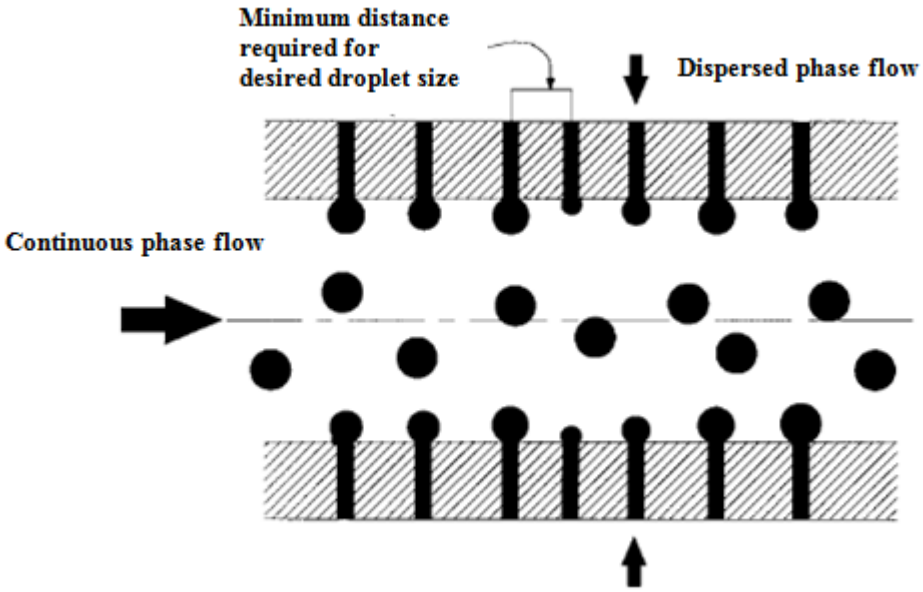

Figure 2.21: Schematic of membrane emulsification showing minimum distance required for desired droplet size [81].

Abrahamse *et al.* calculated the maximum limit for membrane porosity to prevent coalescence of droplets growing on adjacent pores with 5 µm diameters to be 1.5 %. However, a low porosity leads to a low dispersed flux [22][83].

The maximum porosity to be used while preventing coalescence providing that all pores are active can be predicted by assuming a square array of pores. The distance between the pores should at least be equal to the droplet diameter. The membrane porosity (φ) follows from the following equation.

$$\varphi = \frac{0.25\pi {d_p}^2}{{d_d}^2} = 0.25\pi \left(\frac{1}{x}\right)^2 \qquad \text{Equation 2.9}$$

Where, d_p: pore diameter (m), d_d: droplet diameter (m) and x is ratio of droplet diameter over pore diameter [84].

2.3.4 Surfactant

During emulsification droplets not only break up, but at the same time they may recoalesce to larger droplets. Both phenomena are influenced conclusively by surfactant molecules in the continuous phase [85].

Surfactants (emulsifiers) are molecules which occupy the interface between the oil and the water phase during the formation of droplets in order to protect the droplets against fusion while colliding [86]. Surfactants play two main roles in the formation of emulsions. Firstly they reduce the interfacial tension which consequently facilitates droplet distribution, reduces the mixing energy and decreases the minimum emulsification pressure. Secondly they stabilize the droplets against coalescence and/or aggregation [22].

The adsorption kinetics of the emulsifier determines the time required to stabilize the droplets against coalescence, both during the formation process and inside the flowing continuous phase after detachment [82].

According to Bancroft's rule *"The emulsifier stabilizes the emulsion type where the continuous phase is the medium in which it is most soluble"* it is more efficient to have the surfactant in the continuous phase [87].

The concentration of surfactants is an important factor on droplet formation, the higher surfactant concentration the smaller droplets achieved at smaller times. According to Graaf *et al.*, low concentration of surfactants leads to a relatively large droplets which is a direct result of a high interfacial tension during droplet formation [86].

One of the performance characteristics of the surfactant is Critical Micelle Concentration (CMC). When the concentration of a surfactant in an aqueous solution exceeds a critical level, micelles are formed spontaneously [24]. The lower the CMC value, the higher the surface activity (Figure 2.22) [88].

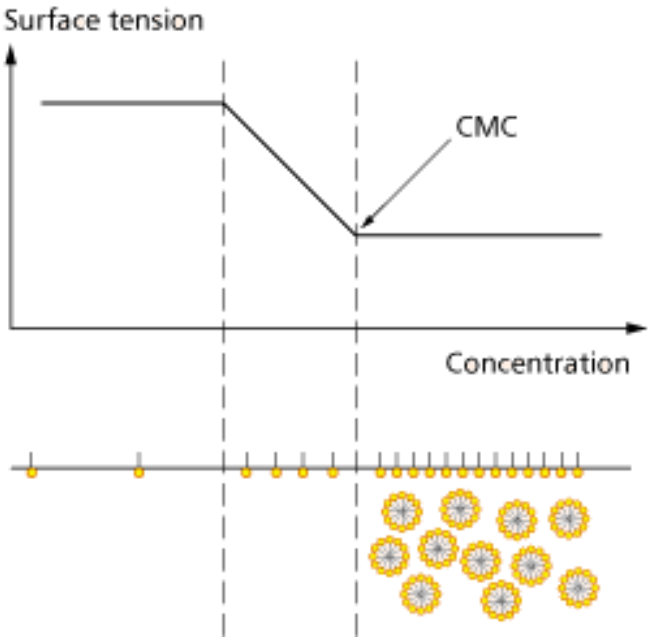

Figure 2.22: Critical micelle concentration (CMC): As the concentration of the surfactants increases to a certain level known as CMC (arrow), the surfactant molecules begin to form aggregates in which the hydrophilic groups are oriented outside (to water) and the hydrophobic groups are oriented inside to avoid water. These aggregates are called micelle [88] [89].

The type of surfactants used in membrane emulsification also has a significant effect on the droplet formation behaviour [80]. Surfactants can be categorized by their hydrophilic groups into four families: Anionic, Cationic, Nonionic and Amphoteric. Different types of surfactant are used for membrane emulsification; anionic surfactants such as SDS and nonionic surfactant such as Tween 20. According to Nakashima *et al.* both lead to successful emulsification and producing excellent monodispersions [55]. Nonionic surfactants play an important role in preparing food and pharmaceutical emulsions [90]. The surfactants commonly used in food emulsions are summarized in Table 2.7.

Table 2.7: Surfactants which are commonly used in food emulsions. ADI is the acceptable daily intake, NL; not limited (Adapted from Krog (1997) and Faergemand and Krog (2003)) [24].

Chemical Name	**Abbreviation**	**EU Number**	**U.S. FDA**	**ADI (mg kg^{-1})**	**Solubility**
Ionic					
Lecithin		E 322	184.1400	NL	Oil/Water
Fatty acids salts	FA	E 470	172.863	NL	Oil/Water
Sodium stearoyl lactylate	SSL	E 481	172846	0-20	Water
Calcium stearoyl lactylate	CSL	E 482	172.844	0-20	Oil
Citric acid esters of MG	CITREM	E 472c	172.832	NL	Water
Diacetyl tartaric acid esters of MG	DATEM	E472e	184.1101	0-50	Water
Nonionic					
Monoglycerides	MG	E 471	184.1505	NL	Oil
Acetic Acid esters of MG	ACETEM	E 472a	172.828	NL	Oil
Lactic acid esters of MG	LACETEM	E 472b	172.852	NL	Oil
Succinic acid esters of FA	SMG	----	172.830	----	
Polyglycerol esters of FA	PGE	E 475	172.854	0-25	Water
Propylene glycol esters of FA	PGMS	E 477	172.856	0.25	Oil
Sucrose esters of FA		E 473	172.859	0-10	Oil/Water
Sorbitan monostearate	SMS	E 491	172.842	0-25	Water
Sorbitan tristearate	STS	E 492	----	0-15	Oil
Polyoxyethylene (20) sorbitan monostearate	Polysorbate 60	E 435	172.836	0-25	Water
Polyoxyethylene (20) sorbitan tristearate	Polysorbate 65	E 436	172.838	0-25	Water
Polyoxyethylene (20) sorbitan monooleate	Polysorbate 80	E 433	172.840	0-25	Water

A surfactant molecule consists of a hydrophilic head and a hydrophobic tail. The tendency of surfactants to disperse in polar or non-polar liquids is defined as the Hydrophilic-Lipophilic Balance value (HLB). There is a numerical HLB scheme for classifying surfactants with regard to their relative solubility in aqueous and oily liquid phases [5]. The HLB value helps to determine the phase in which the

surfactant is most soluble and also gives an indication whether the surfactant is suitable for formation of oil-in-water (HLB number 8-18) or water-in-oil emulsion (HLB number 4-6) [91] (Table 2.8). Surfactants with high HLB values (more hydrophilic) preferentially encapsulate oil as droplets in water, and vice versa, surfactants with low HLB values (more hydrophobic) give W/O emulsions (Figure 2.23).

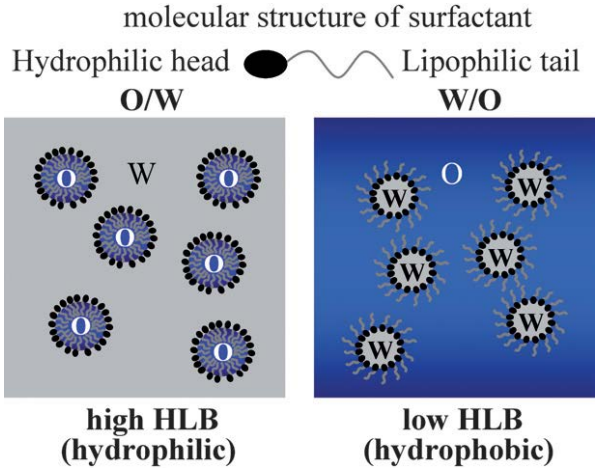

Figure 2.23: Surfactant structure and emulsion types corresponding to HLB values. O: oil, W: water [92]

Table 2.8: Classification of Surfactants (surface-active agents) by HLB value [93]

HLB Value	Use	Example
1	Antifoaming Agent	Oleic Acid
2	Antifoaming Agent	Sorbitan Tristearate
3	Antifoaming Agent	Glyceryl Monostearate
4	Emulsifying Agent W/O	Sorbitan mono-oleate (Span 80)
5	Emulsifying Agent W/O	Glyceryl Monostearate
6	Emulsifying Agent W/O	Diethylene glycol monolaurate
7	Wetting and Spreading Agent	{none}
8	Emulsifying Agent W/O, Wetting and Spreading Agent	Sorbitan monolaurate (Span 20)
9	Emulsifying Agent O/W, Wetting and Spreading Agent	Polyethylene lauryl ether (Brij 30)
10	Emulsifying Agent O/W	Methyl Cellulose (Methocel 15 cps)
11	Emulsifying Agent O/W	Polyoxyethylene monostearate (Myrij 45)
12	Emulsifying Agent O/W	Triethanolamine oleate
13	Emulsifying Agent O/W, Detergents	Polyethylene glycol 400 monolaurate
14	Emulsifying Agent O/W, Detergents	{none}
15	Emulsifying Agent O/W, Detergents, Solubilizing Agents	Polyoxyethylene sorbitan mono-oleate (Tween 80)
16	Emulsifying Agent O/W, Solubilizing Agents	Polyoxyethylene sorbitan monolaurate (Tween 20)
17	Emulsifying Agent O/W, Solubilizing Agents	Polyoxylene lauryl ether (Brij 35)
18	Emulsifying Agent O/W, Solubilizing Agents	Sodium oleate
19	Solubilizing Agents	{none}
20	Solubilizing Agents	Potassium oleate

The ability of surfactant molecules to provide the required curvature of the interfacial film to produce emulsions has been related to their packing parameter, which is an essential geometric quantity associated with the surfactant aggregation shape [94]. This relationship was first explained by Israelachvili *et al.* (1976) through the following equation [95]:

$$Critical\ packing\ parameter = \frac{V_c}{a_o l_c}$$ Equation 2.10

Where,

V_c is the volume of the hydrocarbon chain (m^3),

a_o is the optimal surface area per head group (m^2),

l_c is the critical chain length (m).

Theoretically, a surfactant with a critical packing parameter between 0 and 1 is suitable for producing oil in water emulsions as this gives the interfacial film a spontaneous positive curvature (i.e. toward water) [96].

2.3.5 Interfacial tension

Applying higher surfactant concentrations results in smaller droplets and shorter droplet formation times due to a reduction in the interfacial tension [86]. With an increase in the interfacial tension the droplet diameter increases significantly.

A lower interfacial tension means a lower Laplace pressure and the latter results in a lower transmembrane pressure for droplet formation. For droplets to be formed the transmembrane pressure has to at least exceed the critical Laplace pressure. The critical Laplace pressure can be measured by:

$$\Delta p = \frac{2\gamma_{ow}}{r_{Di}} = \frac{2\gamma_{ow}}{r_p}$$ Equation 2.11

Where Δp is the Laplace pressure (Pa), γ_{ow} : the interfacial tension (N m^{-1}), r_{Di} :the initial radius of the droplet (m) and r_p is the radius of the pore (m).

As mentioned before the critical pressure is the pressure at which droplets start to be formed. It can be seen from Equation 2.11 that the initial radius of the droplet is corresponding to the radius of the pore, r_p. When exceeding the critical pressure, the droplet will grow more [86].

2.3.6 Crossflow velocity (velocity of continuous phase)

The droplets formed at the membrane surface are detached and carried away under the influence of the flowing continuous phase. The characteristic parameter of the flowing continuous phase is the crossflow velocity which is often expressed in terms of wall shear stress (Pa). Wall shear stress and the drag force on the detaching droplet are related to the crossflow velocity of the continuous phase. By increasing the crossflow velocity of the continuous phase the wall shear stress can be increased [97]. According to Charcosset *et al.*, as the wall shear stress increases the droplet size becomes smaller [22]. In other words, the risk of droplets grows and coalesces at the surface of membrane before being detached is more at low shear stresses [21]. This influence on droplet size is greater for small wall shear stresses (see Figure 2.24). At high wall shear stresses, the further decrease in mean droplet size is prevented by the forming droplets hindering each other in detaching from the pores. Hence, droplets forming at the pore openings are being surrounded by other droplets, and as a result, the continuous phase fluid cannot flow freely around them, but rather it flows above them. [17][98][99]. Schröder *et al.*, using ceramic α-Al_2O_3 membranes to make o/w emulsions, found that droplet size decreases with increasing continuous water phase flow rate as a result of the increased drag force; particularly at relatively low wall shear stresses. However the effect of wall shear stress on reducing droplet size is dependent on the membrane pore size and is more effective for smaller pore size [22][23]. The crossflow velocity ranges typically between 0.8 and 8 m s^{-1} [17]. The action of the shear force may change depending on the concentration of the dispersed phase, and if there is a significant change in this value then it may affect the droplet size. Williams *et al.* [70] found that up to 30 % oil in O/W emulsion had no observable influence.

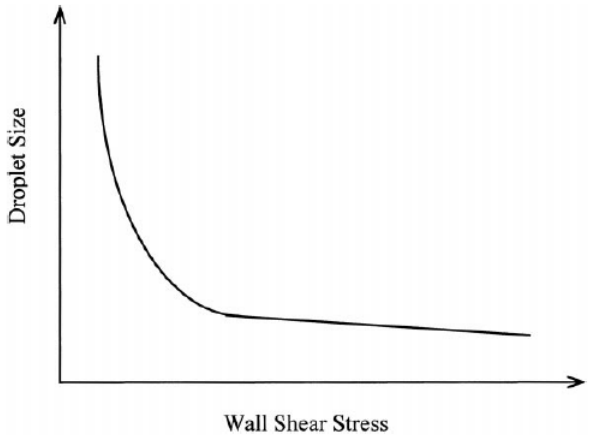

Figure 2.24: Effect of wall shear stress on droplet size for oil-in-water emulsions produced by membrane emulsification, (schematically shown) [17].

2.3.7 Dispersed phase flux (through membrane)

Dispersed phase flux is an essential parameter with regard to the economy of the whole process of membrane emulsification [82]. The more disperse phase flux, the less production time and the more cost effective the process for large scale industrial purposes.

The flux of the dispersed phase through a membrane is likely to be quite low for producing emulsions with narrow droplet-size distributions. For producing O/W emulsions, the fluxes are typically in a range of 2 to 40 l m^{-2} h^{-1} for membranes having a nominal pore size from 0.2 to 0.8 µm, respectively [21]. The flow rate of dispersed phase or dispersed phase flux is defined as:

$$J_d = \frac{\dot{V}_d}{A} \qquad \text{Equation 2.12}$$

Where J_d is the dispersed phase flux (m^3 m^{-2} s^{-1}), $\dot{V}_d$ is the volume flow rate of the dispersed phase (m^3 s^{-1}) and A is the membrane surface area (m^2) [23].

According to Joscelyne and Tragardh, at higher fluxes the average droplet size and also the size distribution tend to increase due to increased droplet coalescence at the

membrane surface. Hence, an increase in flux and hence production rate may be at the expense of size distribution [21][22].

2.3.8 Dispersed and continuous phase viscosities

The viscosity of the dispersed and the continuous phase is also an important parameter which affects the performance of the membrane emulsification process. The flux of the dispersed phase is inversely proportional to the dispersed phase viscosity. According to Darcy's law, when the dispersed phase viscosity is increased the dispersed phase flux decreases, which consequently leads to larger droplet diameters [22]. However, According to Yuan *et al.*, by increasing the dispersed phase viscosity the uniformity of the droplet size can be predominantly improved [100].

The viscosity of the continuous phase affects the pumping cost. To pump a viscous fluid through the membrane module more power is required. By increasing the temperature of the continuous phase (with certain limitations) the viscosity of the continuous phase can be reduced [17].

2.3.9 Transmembrane pressure

Transmembrane pressure is required to force the dispersed phase to permeate through the membrane into the continuous phase. According to Darcy's law, when the transmembrane pressure is increased the flux of the dispersed phase through the membrane increases [22]. The effect of transmembrane pressure depends upon operating conditions such as crossflow velocity and type of surfactant [22].

To form droplets a minimum transmembrane pressure is required [23]. It is defined as the difference between the pressure of the dispersed phase, and the mean pressure of the continuous phase using Equation 2.13:

$$\Delta P_{tm} = P_d - \frac{(P_{c,in} + P_{c,out})}{2}$$ Equation 2.13

Where P_d: the pressure of the dispersed phase (Pa), $P_{c,in}$: the pressure of the flowing continuous phase at the inlet of membrane module (Pa) and $P_{c,out}$ is the pressure at the outlet of membrane module (Pa) [22].

A minimum transmembrane pressure, also called the critical pressure is essential to overcome the capillary pressure of the membrane pores, so the dispersed phase can permeate through the pores to form the emulsion. This is described as the Laplace pressure. The applied transmembrane pressure needed to make the dispersed phase flow can be estimated from the capillary pressure, assuming that the pores are ideal cylinders, using Equation 2.14 [75]:

$$P_c = \frac{4\gamma \cos\theta}{\bar{d}_p}$$ Equation 2.14

Where,
P_c is the critical pressure (Pa), γ is the equilibrium interfacial tension between the continuous and dispersed phase (N m^{-1}), θ is the contact angle of the droplet against the membrane surface well wetted with the continuous phase and $\bar{d}_p$ is the average pore diameter (m).

However the actual transmembrane pressure required to make the dispersed phase permeate through the pores, may be greater than that predicted by this equation due to the tortuosities in the pores, irregular pore openings at the membrane surface and the significant effects of surface wettability [22]. Williams *et al.* have suggested that the usable range of transmembrane pressure is between 2 and 10 times the minimum pressure [70].

According to Darcy's law the dispersed phase flux is related to the transmembrane pressure (Equation 2.15):

$$J_d = \frac{K\Delta P_{tm}}{\mu L}$$ Equation 2.15

Where J_d is the dispersed phase flux ($m^3\ m^{-2}\ s^{-1}$), $\Delta P_{tm:}$ transmembrane pressure (Pa), μ: the dispersed phase viscosity (Pa s), L: membrane thickness (m), and K *is* membrane permeability (m^2) which can be calculated from Hagen–Poiseuille Equation:

$$K = \frac{n{r_p}^2}{8\pi} \qquad \text{Equation 2.16}$$

Where n is the number of uniform cylindrical pores of radius r_p (m) [22] [23].

Figure 2.25 shows the relationship between transmembrane pressure and dispersed phase flux for the SPG and α-Al_2O_3 membranes. It can be seen from this figure that the dispersed phase flux increases with increasing the transmembrane pressure and mean pore size [101].

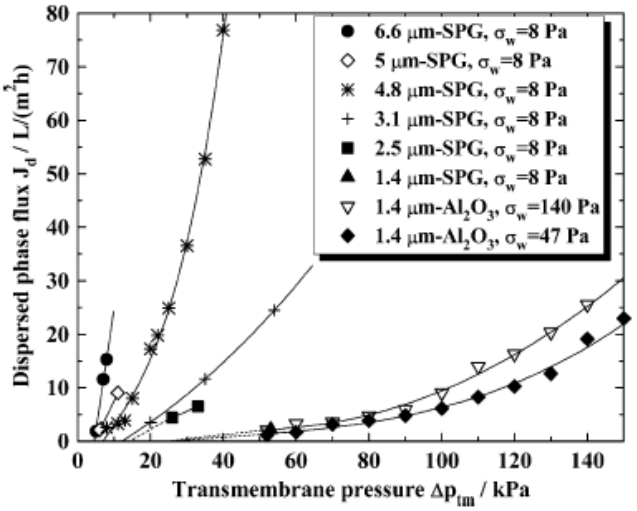

Figure 2.25: Relationship between transmembrane pressure and dispersed phase flux for the SPG and α-Al_2O_3 membranes. σ_w is shear stress in continuous phase at membrane surface (wall shear stress, Pa) [101].

Abrahamse *et al.* has investigated the relationship between the transmembrane pressure and the droplet formation. Their study shows that the dispersed phase flux increases when the tansmembrane pressure increases and by increasing the transmembrane pressure smaller droplets were obtained. That is because the number

of active pores increases linearly with the transmembrane pressure (Figure 2.26) [66].

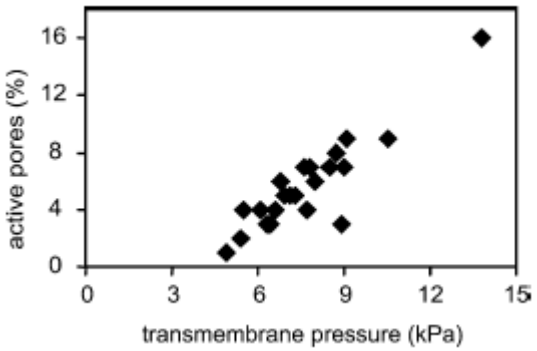

Figure 2.26: Percentage of active pores as a function of the transmembrane pressure (using a microsieve) [66]

On the other hand, droplet formation time is significantly decreased by increasing the transmembrane pressure. But according to Schröder and Schubert (1999) the dispersed phase flux may be increased by increasing the transmembrane pressure, but in many cases larger droplets will result [23].

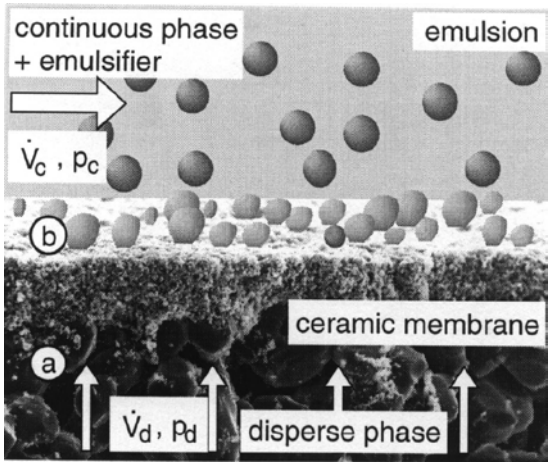

Figure 2.27: A schematic view of membrane emulsification process showing velocity and pressure of dispersed and continuous phases as the affecting parameters [23]

Joscelyne and Trägårdh (2000) have shown that for making O/W emulsions, the typical values of transmembrane pressure for emulsification using 0.2, 0.5, and 0.8 µm pore size membranes lie between about 20 and 500 kPa [17].

2.3.10 Membrane thickness

Membrane thickness has an indirect effect on the droplet size. At a given transmembrane pressure the membrane thickness is one of the factors determining the dispersed phase flux J_d [44]. By choosing a thinner membrane the flux through the pores increases which results in a higher droplet expansion rate [44]. Dependence of flux on membrane geometry is shown by the following equation:

$$J_d = \left(\frac{\varphi {r_P}^2}{8L\tau}\right)\left(\frac{\Delta P_{tm}}{\mu}\right) \qquad \text{Equation 2.17}$$

Where J_d is the dispersed phase flux ($m^3\ m^{-2}\ s^{-1}$), φ the porosity, r_P the average pore radius (m), ΔP_{tm} the differential pressure across the membrane (Pa), μ viscosity (Pa s), τ the tortuosity and L is the membrane thickness (m) [102].

2.3.11 pH

Membrane surface properties often depend on the pH of the continuous phase. They might show an iso-electric point at a given pH, where the surface has no net charge. Huisman *et al.* have measured the iso-electric points of different ceramic membranes which were in the range of 5.2 to 8 [103]. At pH values above and below these points, the membranes were negatively and positively charged, respectively. The charge on the membrane may have a serious influence on which surface active agents adsorb [17]. As a result, a hydrophilic membrane might turn hydrophobic with changes of pH, which consequently affects the resulting emulsion droplet size [104].

2.4 The main forces affecting droplet formation

Several different forces act on a droplet during the membrane emulsification process (see Figure 2.28).

a. *Interfacial tension force*, F_γ, represents the effect of dispersed phase adhesion around the edge of the pore opening, and is the dynamic effect of the pressure difference between the phases [82].

b. *Static pressure difference force*, F_{SP}, the pressure difference between the dispersed phase and the continuous phase at the membrane surface.

c. *The drag force*, F_D, created by the continuous phase flowing past the droplet, parallel to the membrane surface.

d. *The dynamic lift force*, F_L, which results from the asymmetric velocity profile of the continuous phase near the droplet.

e. *The buoyancy force*, F_B, due to the density difference between the continuous phase and the dispersed phase.

f. *The inertial force*, F_I, caused by the dispersed phase flow moving through the capillary as it inflates the droplet [22]. The inertial force is associated with the mass of fluid flowing out from the opening of the pore [105].

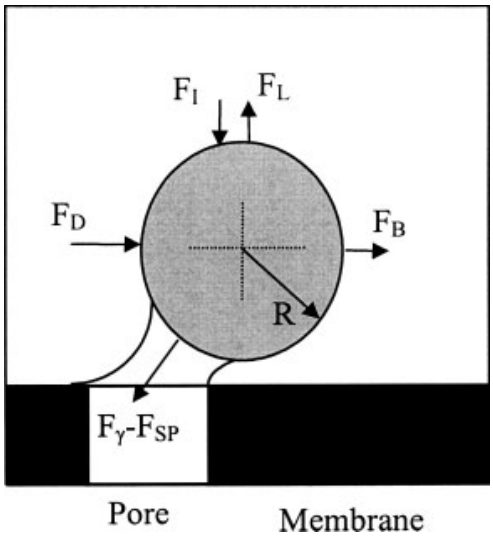

Figure 2.28: Forces acting on a droplet during the membrane emulsification process. F_γ : interfacial tension force, F_{SP}: static pressure difference force, F_D: drag force, F_L : dynamic lift force, F_B: buoyancy force, F_I: inertial force [22].

The balance between the drag force on the droplet, the buoyancy of the droplet, the interfacial tension force and the driving force determine the growth of droplet at pores to a certain size and subsequent detaching [17].

The three most important forces which have a key role in formation of small droplets during membrane emulsification are interfacial tension force that holds the droplets connected at a pore of the membrane, the drag force which detaches the droplets and finally the static pressure difference force. These forces can be determined using the following equations [70][106]:

$$F_\gamma = 2\pi\gamma r_p = F_D + F_B \qquad \text{Equation 2.18}$$

$$F_{sp} = \Delta P_{tm} A_p = \frac{2\gamma}{r_D}\pi {r_P}^2 = F_\gamma \frac{r_P}{r_D} \qquad \text{Equation 2.19}$$

$$F_D = 6\pi {r_D}^2 \sigma_W \qquad \text{Equation 2.20}$$

Where F_γ is interfacial tension force (N), γ the interfacial tension (N m^{-1}), r_P radius of the pores (m), F_D viscous drag force (N), F_B buoyancy force (N), F_{sp} static pressure difference force (N), ΔP_{tm} the transmembrane pressure (Pa), A_p surface area of the pore (m^2), r_D radius of the droplet (m), and σ_W wall shear stress (Pa).

By using Equations 2.18 to 2.20 the radius of the droplets can be estimated as a function of the different forces:

$$r_D = \sqrt{\frac{r_P \gamma}{3\sigma_w}} = \sqrt{\frac{F_\gamma}{6\pi\sigma_w}} = \frac{F_\gamma r_P}{\Delta P_{tm} A_p} \qquad \text{Equation 2.21}$$

Equation 2.21 shows that the radius of the droplet is proportional to the ratio of the interfacial tension force to the static pressure difference force, inversely proportional to the wall shear stress due to the flux of the continuous phase, and finally proportional to the radius of the pore [105][106].

Figure 2.29 shows a framework of all the forces and torques acting on a droplet, which can be categorised into two groups; detachment torques and adhesion torques. It is based on their respective roles to drive droplets off the pore, and hold droplets on the pore [106].

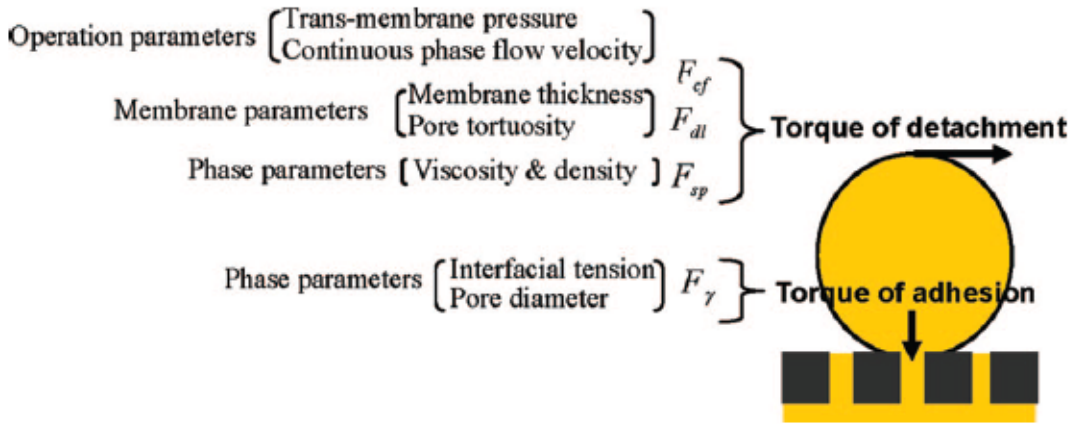

Figure 2.29: Torques on the global droplet. F_{cf} is the crossflow drag force, F_{dl} dynamic lift force and F_{sp} is the static pressure difference force [106].

2.5 Applications of membrane emulsification

2.5.1 Large-scale applications

The membrane emulsification process is suitable for large-scale production. By adding more membranes modules the process can be easily scaled-up. However there are not many documented products produced by this method [22].

Williams *et al.* have shown that pilot-scale membrane emulsification can be operated successfully in both batch and semi continuous mode. However, until now, one documented product has been produced using membrane emulsification (Yes light, a very low fat spread, Moringa Milk industry, Japan) [22] [55] [70].

The low level of dispersed phase flux through the membrane is one of the main limiting factors with regards to industrial scale-up. This especially happens when small submicron droplets are required [21].

2.5.2 Small-scale applications

The membrane emulsification method is suitable for the production of both single and multiple emulsions, which can be used for the preparation of drug delivery system (DDS) and also in food industry [22].

2.5.2.1 Drug delivery systems (DDS)

A drug delivery system is one of the most attractive applications of membrane emulsification. Nanoemulsions have been used as a vehicle to deliver active pharmaceutical ingredients and other bioactive compounds. This is mainly attributed to their optical transparency, long kinetic stability and high surface area [108]. Various studies have shown their efficiency for intravenous, oral and ocular drug administrations, reducing drug side effects and improving the pharmacological

effects of the drugs [109] [111] [112]. Most anticancer drugs are used in the form of emulsions in order to control release rates of medicine and to prevent strong side effects of the drug [107].

2.5.2.2 Food emulsions

Emulsions play an important role in the formulation of food products, in the form of oil-in-water (O/W) emulsions *e.g.*, salad dressing, artificial milk, cream liqueurs, and water-in-oil emulsions such as margarine and low fat spreads. A high flux is important for production of food emulsions in large scale using membrane emulsification method as it decreases the production time [21].

Production of low calorie spread is one of the interesting large-scale applications of ME in food industry [110]. For instance, a low fat spread has been developed and commercialized in the milk industry in Japan using ME [55].

2.6 Conclusions

In this chapter, by reviewing the previous studies, the necessary background needed to understand the principles of emulsions, emulsification methods and all the main affecting parameters were provided. It has been shown that in recent years there has been an increasing interest in using low-energy emulsification methods for producing fine stable emulsions for food and healthcare applications. Membrane emulsification was found to be an attractive method due to low energy consumption, easy control of droplet size and size distribution and low shear stress applied to the ingredients. However, in most previous studies, the SPG membranes with the pore sizes in the micrometer range were used. Therefore, one of the research gaps in this area is the investigation of other types of membranes such as ceramic and polycarbonate membranes and also more importantly using nano-scale porous membranes. Moreover, there have been several studies focusing on the production of nano-emulsions by direct or indirect membrane emulsification methods. However, for the potential applications in food and healthcare industries, the possibility of using

biocompatible components needs to be considered in any new research in this area. Although there are a few reports in the literature regarding the successful production of stable nano-emulsions using the aforementioned methods, the reproducibility of the reported formulations after scaling-up for commercialisation is still challenging.

3. Materials and Methods

3.1 Materials

This section contains details of the generic materials used throughout this project. All the chemical components were purchased from Sigma-Aldrich Ltd, Dorset, UK.

3.1.1 Emulsions

To make oil-in-water (O/W) emulsions, different compositions of RO water, surfactant and soybean oil were used. A reverse osmosis-based water purification system, supplied by Elga Ltd., was utilised to obtain pure water.

Soybean oil (density= 0.917 g ml^{-1} at 25 °C) supplied by Sigma Aldrich, was chosen as the dispersed phase due to its potential application in food and healthcare products and its status as a food-grade component. It is considered as a good model oil for both pharmaceutical and food applications [114]. It is a long chain triglyceride (C16-C22) with the major unsaturated fatty acids of linolenic acid (C18:3), linoleic acid (C18:2) and oleic acid (C18:1) [115].

3.1.2 Surfactants

All surfactants used in this study were supplied by Sigma Aldrich. The choice of surfactants in this project was on the basis of their compatibility with the food and healthcare applications, their suitability for making oil-in-water emulsions and finally on the basis of previous studies in which the selected surfactants were shown to provide a model system that can be characterised. As explained in Section 2.3.4, surfactants with HLB number values of 8 to 18 are suitable for formation of oil-in-water emulsion.

3.1.2.1 Brij 97 (polyoxyethylene-10-oleoyl ether)

Brij 97 (Sigma) was chosen as the main surfactant on account of its potential applicability, widespread availability, and low toxicity [117]. Brij 97 (polyoxyethylene-10-oleoyl ether, $C_{38}H_{76}O_{11}$) is a nonionic surfactant with a molecular mass of 709 g mol^{-1} and a density of 1000 kg m^{-3} at 25 °C. It is a white to pale yellow liquid or semi-solid with critical micelle concentration (CMC) of 0.029 % (w/v) in water. Having a HLB value of 12.4 and the critical packing parameter of 0.45 [118] make it suitable for producing an oil-in-water emulsion. Due to its availability, applicability and low toxicity, Brij 97 is favoured in the pharmaceutical and food industries , having been used in the study of drug delivery systems by many researchers in the past [114][119][120][121][122]. It has a drug solubility of 74.32 mg ml^{-1}, which is the second highest after Tween 80 (with a drug solubility of 87.25 mg ml^{-1}) [123]. It was also already mentioned in the literature for its ability to emulsify soybean oil [114][124]. Therefore, Brij 97 was selected as a model surfactant to investigate different emulsification methods in this study.

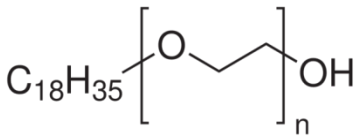

Figure 3.1: Structure of the Brij 97 molecule

3.1.2.2 Tween 20 (Polyoxyethylene (20) sorbitan monolaurate)

As the main objective of this project was to find the optimum formulation to produce stable nano-emulsions for food and healthcare applications using different emulsification methods, the food-grade Tween 20 (Sigma) with the hydrophilic–lipophilic balance (HLB) value of 16.7 was considered as an alternative surfactant in case the model surfactant Brij 97 failed to produce nano-emulsions in any emulsification methods under study. Tween 20 (Polyoxyethylene (20) sorbitan monolaurate, $C_{58}H_{114}O_{26}$) also known as (Polysorbate 20) (E432) is a nonionic surfactant with a molecular mass of 1228 g mol^{-1} and the critical micelle

concentration (CMC) of 0.007 % (w/v) in water [125]. It is a clear yellow viscous liquid with a density of 1100 kg m^{-3}, having a high level of stability and a low level of toxicity and therefore is extensively used for the production of emulsions in a variety of food, pharmaceutical and cosmetic applications [126].

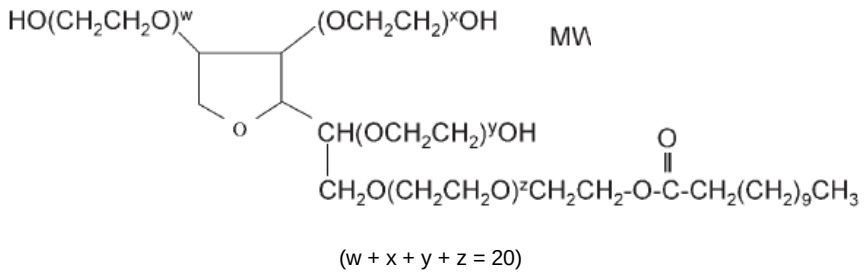

Figure 3.2: Structure of the Tween 20 molecule

3.1.2.3 Tween 80 (Polyoxyethylene (20) sorbitan monooleate)

Finally, Tween 80 (Sigma) was used as alternative to Tween 20 for experimental comparison. Tween 80 (Polyoxyethylene (20) sorbitan monooleate, $C_{64}H_{124}O_{26}$) also known as (Polysorbate 80) (E433) is a nonionic surfactant with a molecular mass of 1310 g mol^{-1}. Having a density of 1060 – 1090 kg m^{-3}, it resembles Tween 20 in terms of appearance and level of stability and toxicity, making it a suitable alternative to Tween 20 in the preparation of emulsions specifically for medical and food applications. The HLB and CMC of Tween 80 is 15 and 0.0016 % (w/v) in water, respectively [125].

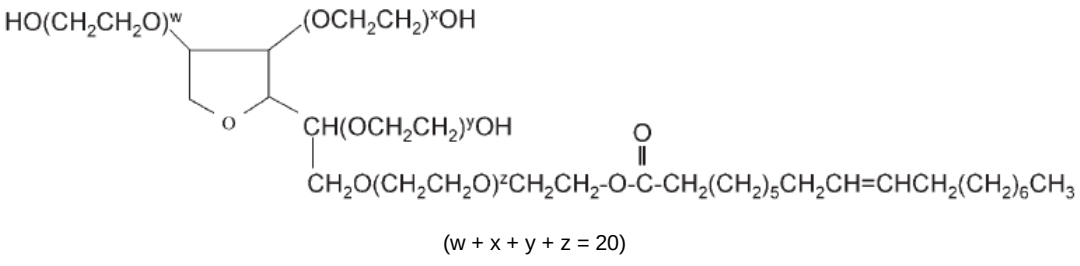

Figure 3.3: Structure of the Tween 80 molecule

3.1.3 Membranes

As explained in Section 2.2.2.2, in order to obtain O/W emulsions using premix membrane emulsification, a hydrophilic membrane is required. The membranes used in this work were selected from the available types of commercial filtration membrane.

3.1.3.1 Flat-sheet ceramic membranes

Ceramic membranes are one of the well-known commercially available membranes for water filtration. The flat-sheet type of these membranes (Figure 3.4), which is made up of Anodic Aluminium Oxide (AAO) was purchased from Synkera Technologies Inc., USA to a specification suitable for the LiposoFast LF-50. They were 25 ± 0.2 mm in diameter with two different pore sizes (see Table 3.1).

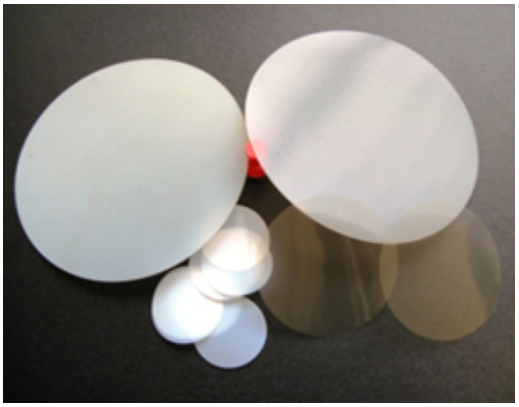

Figure 3.4: Flat-sheet ceramic membranes [149]

Table 3.1: The specification of the ceramic membranes used in this work, supplied by Synkera Technologies Inc., USA

Pore size	Pore density	Porosity	Thickness
55 ± 6 nm	5×10^9 cm^{-2}	12 %	98 ± 1 µm
100 ± 10 nm	2×10^9 cm^{-2}	15 %	48 ± 1 µm

Anodic alumina is a self-organized nanostructured material which contains densely-populated uniform cylindrical pores aligned perpendicular to the surface of the material. The pores, which pass through the whole thickness of the material, are formed when aluminium is electrochemically oxidized in certain solutions. They are separated from the aluminium by a thin dense layer of Aluminium Oxide. The pore diameter is in the range of 5 nm to several hundred nm, while the corresponding pore density of 10^{12} to 10^{9} cm^{-2} is achievable by optimising the synthetic conditions. Anodic Aluminium Oxide (AAO) is optically transparent, electrically insulating, chemically inactive and resistant to thermal and mechanical stresses [149]. The SEM images taken of newly purchased ceramic membranes with pore sizes of 55 ± 6 and 100 ± 10 nm were shown in Appendix B.

3.1.3.2 Flat-sheet polycarbonate membranes

The Nuclepore™ track-etched polycarbonate membranes (Figure 3.5) purchased for this study from Whatman, UK were produced from high-quality polycarbonate film and had a diameter of 25 mm and two different pore diameters of 50 and 100 nm with respective porosity of 30 % and 32 % (see Table 3.2). As stated by the supplier, the membranes have clearly defined pore sizes, high flow rates with a high chemical resistance and a good thermal stability for use with a wide range of samples. The Nuclepore™ membranes have a smooth flat surface enabling good visibility of the particles and also feature a very low level of protein binding and extractables, ensuring no sample contamination [150].

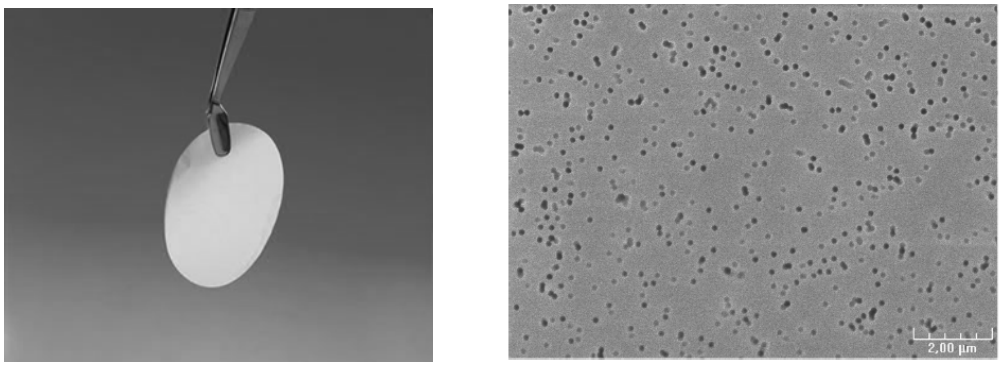

A B

Figure 3.5: A) The Nuclepore™ track-etched polycarbonate membrane. It is used with the shiny surface face up. B) SEM image of a polycarbonate membrane [151]

Table 3.2: The specification of the Nuclepore™ polycarbonate membranes used in this work, supplied by Whatman, UK.

Pore size	Porosity	Thickness
50	30.1 %	10 ± 0.1 µm
100	32 %	10 ± 0.1 µm

3.1.3.3 Tubular ceramic membranes

The membranes used for the cross-flow membrane emulsification method in this study were tubular monochannel inorganic membranes named Kerasep™. These membranes which were developed by Novasep (Novasep process, France) are insensitive to solvents; highly resistant to radiation, heat, chemical and mechanical constraints; and finally ageing. Based on the manufacturer's catalogue, the key features of Kerasep™ membranes and their characteristics are summarized in Appendix E.

3.1.4 Experimental rig for cross-flow emulsification

3.1.4.1 Membrane module

The module and the operating kit were supplied by Novasep (France) (Figure 3.6). As stated by the manufacturer: *'The Micro Carbosep®/Kerasep™ module is specially designed for low volume treatment by tangential ultrafiltration and microfiltration allowing feasibility trials to be performed under ideal conditions.'* (Novasep Process (France) 2001)

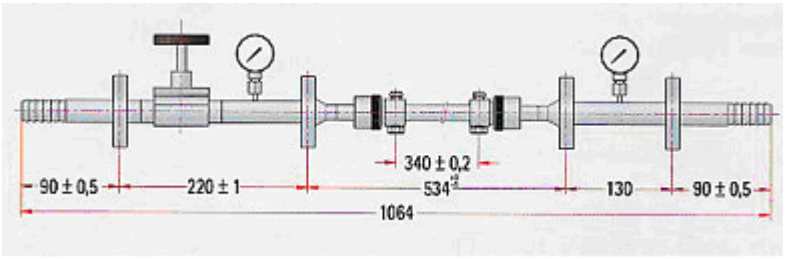

Figure 3.6: Membrane module, Novasep (France) [164]

The stainless steel Carbosep® / Kerasep™ module is equipped with pressure gauges, retentate valve, gaskets, polyamide tube, and PVC tube. There is also a back pressure control valve which is essential to regulate trans-membrane pressure, and two permeate outlets with PVC tube connections. The back pressure valve becomes less important when forming emulsions because, in order for the dispersed phase to be pushed through the membrane from outside the tube to the inside, the inner pressure (the permeate side) requires to be less than the feed/retentate side. Figure 3.7 shows a skeleton diagram of Axial Outlet Stainless Steel Micro Carbosep® / Kerasep™ Modules.

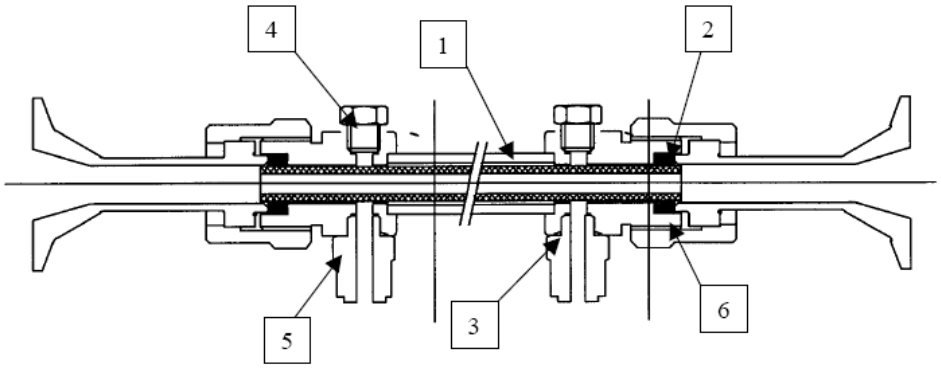

Figure 3.7: Diagram of Axial Outlet Stainless Steel Micro Carbosep® / Kerasep™ Modules [164].

1. Casing
2. End connectors (x2)
3. O-ring seals
4. Plastic plugs (x2)
5. Quick-action unions (x2)
6. Membrane seals (x2)

3.1.4.2 Pump

The circulation pump used in this experimental set-up was a NMO21BY02S12B Netzsch NEMO® progressing cavity pump, supplied by NETZSCH PUMPS LTD. and is equipped with a NEMO® STP 2A stator dry running protection device (Figure 3.8).

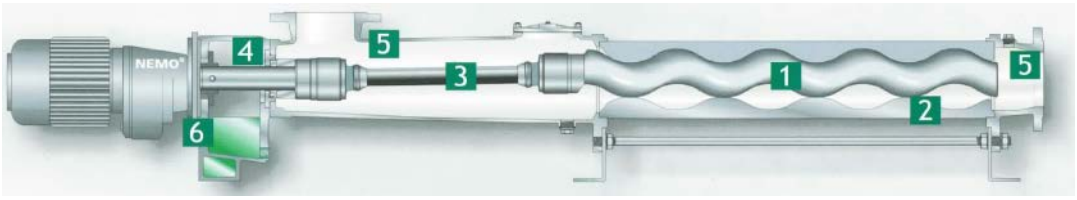

Figure 3.8: Netzsch NEMO® pump and its different parts [165]

1. Rotor
2. Stator
3. Drive Chain
4. Shaft Seal
5. Suction and Pressure Housing
6. Block Construction Design

This pump was primarily selected for this application for its notably low flow pulsation at all discharge pressures which is an important consideration when analysing the flow behaviour through the membrane module. Two important key features of this pump which make it ideal for this work are the ability to produce a

wide variation of flow rates and capability of operating a high pressure system. These features are particularly important in preliminary tests to check the suitability of the membrane for producing emulsions, but also to test whether it is fouled due to previous applications. Also higher pressures are required when working with high viscosity fluids.

3.1.4.3 Rotameters, Pressure gauges and transducers

Two 24-E rotameters measuring flows of 2-20 l min^{-1}, manufactured by GEC Elliot Process Instruments Ltd were used to measure the flow rate of the continuous phase in the inlet and outlet of the membrane module (Figure 6.2). The module is also equipped with Norgren and Ashcroft pressure gauges (Figure 6.3, G1 - 2) and PDCR 510 pressure transducers supplied by Druck, England.

3.1.4.4 Pressure vessel

A stainless steel pressure vessel supplied by Alloy Products Corporation is used in this system for pushing the dispersed phase into the continuous phase through the membrane (Figure 6.2). The vessel is pressurised by Nitrogen (N_2) supplied by an attached cylinder connected to the permeate line (Figure 3.9). The maximum capacity of the pressure dispensing vessel is 5 litres. There is a pressure gauge on the vessel that shows the pressure applied to the vessel (Figure 6.3, G3). The concept is that oil placed in the pressurised vessel can be forced into the annular space of the module and then permeate through the membrane at a specific pressure.

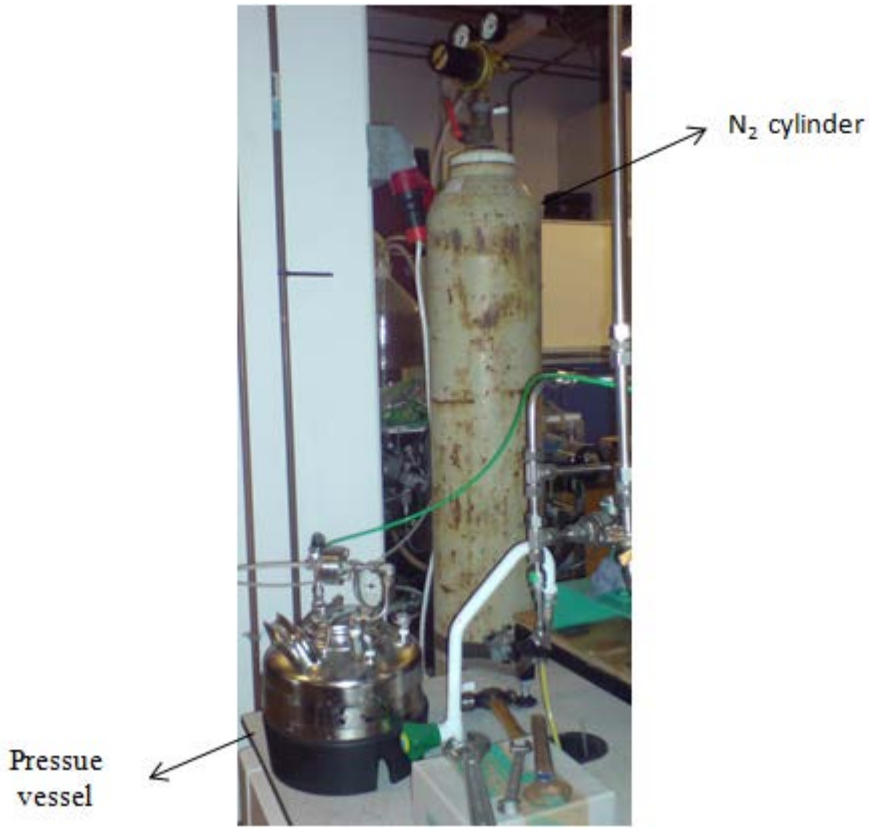

Figure 3.9: Pressure vessel and attached N_2 cylinder

3.2 Methods

3.2.1 Emulsification methods

The emulsification methods which have been used in this project to produce nano-emulsions are listed below.

- Rotor-stator homogeniser (Chapter 4)
- Phase inversion temperature (PIT) method (Chapter 4)
- Dead-end membrane emulsification (Chapter 5)
- Cross-flow membrane emulsification (Chapter 6)

For any investigated method in this study, each experiment was carried out at least three times to check for reproducibility. The maximum error in the measurements was found to be less than 5 %.

3.2.1.1 Rotor-stator homogeniser

A rotor-stator homogeniser (Ultra-Turrax, Janke & Kunkel, Staufen, Germany) was used to prepare oil-in-water emulsions. This device is a high-shear mixer with a motor rating input of 700 W and maximum speed of 25,000 rpm. It consists of an outer stationary saw-toothed edged tube and an inner motor-driven tube, each with radially distributed holes at their lower edges corresponding to each other. When the inner tube is rotated by the motor, it causes the samples to be moved outwards through the holes. Because the two sets of holes constantly and rapidly come into and out of alignment the samples break up into smaller sizes and are subsequently emulsified by the shear between the rotating and stationary tubes.

In order to prepare the emulsions, different concentrations of surfactant were added to the aqueous phase and pre-heated to a desired temperature. The soybean oil (which was also pre-heated separately) was then added to the mixture under continuous stirring to form a coarse oil-in-water emulsion. Finally, the prepared coarse emulsions were further homogenised using the Ultra-Turrax rotor-stator homogeniser for a particular period of time, at a specified rotation speed of 13,500 rpm, while resting in a water bath in order to keep the temperature constant. The rotation speed of 13500 rpm was selected for emulsification process in our study because the preliminary experiments showed that emulsification at any speed lower than this resulted in producing highly polydispersed emulsions with poor stability. Higher speeds were also ruled out in favour of energy efficiency. Each test was repeated at least in triplicate in order to confirm its reproducibility. Samples were then taken in order to measure the mean droplet size and polydispersity index and also to investigate the characterization of the rheological properties of the formed emulsions.

3.2.1.2 Phase inversion temperature method

In this study, different concentrations of Brij 97 (in the range of 10 % to 25 % w/w), 10 % (w/w) soybean oil and RO water in 50 g batches were mixed by stirring at room temperature and then gradually brought to the PIT temperature and then rapidly cooled in an ice bath while stirring on a magnetic stirrer. Samples were prepared at least three times to check the reproducibility of the method.

3.2.1.3 Dead-end membrane emulsification

To investigate the premix membrane emulsification process a LiposoFast LF-50 extruder (Avestin Inc, Ottawa, Canada), designed for the preparation of lipid vesicles, was used. The extruder is supplied with polycarbonate track-etched membranes with a diameter of 25 mm. In this work, ceramic membranes were used in addition to polycarbonate in order to investigate the effect of membrane type on the quality of the emulsions produced.

The LiposoFast LF-50 is a medium pressure extruder constructed from corrosion resistant material in which the sample, in a cylinder with a maximum capacity of 50 ml, is forced through a membrane or a number of membranes by applying a pressure of up to 600 psi / 41 bar. The required pressure is provided by a cylinder of compressed gas connected to the sample chamber; the gas head pressure forces the starting material through the membrane in dead end mode. The processed sample, which now contains reduced particle sizes, is then collected in a 50 ml flask. Samples as small as 5ml can be processed with the LiposoFast LF-50. Figure 3.10 shows a schematic view of the extruder system [148].

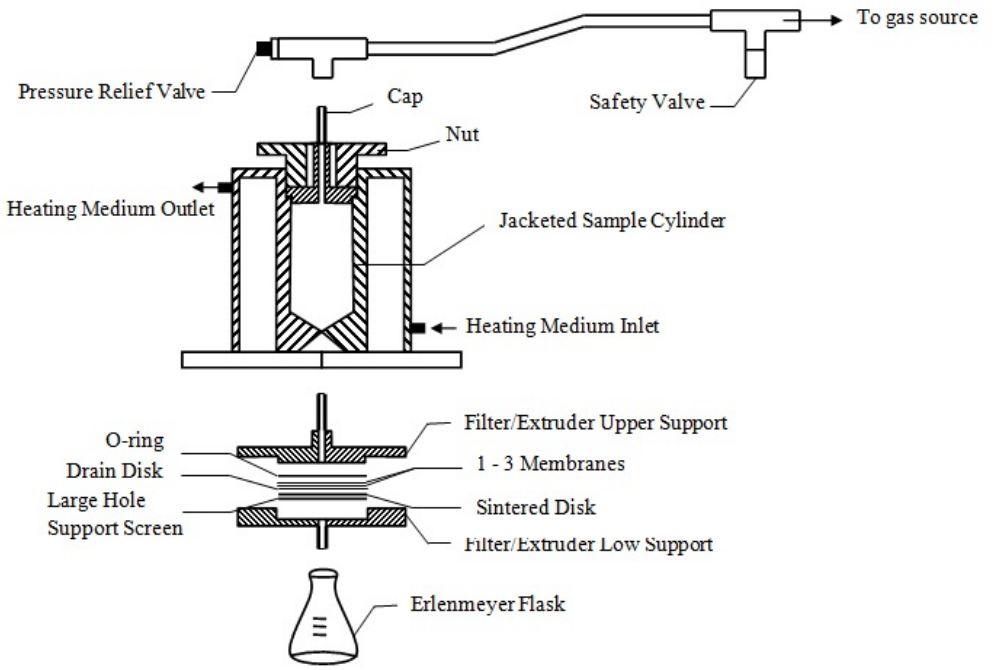

Figure 3.10: Schematic representation of LF-50 extruder [148]

The central sample cylinder of the LiposoFast LF-50 is sealed within a stainless steel jacket and, depending on the experimental conditions, the temperature of the starting material can be increased or decreased by circulating a temperature-controlled heat transfer liquid (such as water) between the sample cylinder and the external jacket. The low volume of the jacket and the high flow-through enables optimum heat transfer. Sample temperatures may be as high as 200 °C [148].

The extruder parts (Figure 3.11) were cleaned by sonicating for 15 minutes and then rinsing first with pure ethanol and then several times in RO water before and after each experiment, to remove any trace of surfactant molecules or chemicals. There was no need to dry the parts, and they were then stored in a clean beaker between experiments. For each set of experiments, the extruder was assembled according to the manufacturer's instructions [148] in the order shown in Figure 3.10, i.e. by positioning the large-holed support screen first followed by the sintered disk, polyester drain disk, membrane(s), and finally the o-ring. The assembled device was tested for leaks with RO water prior to each experiment.

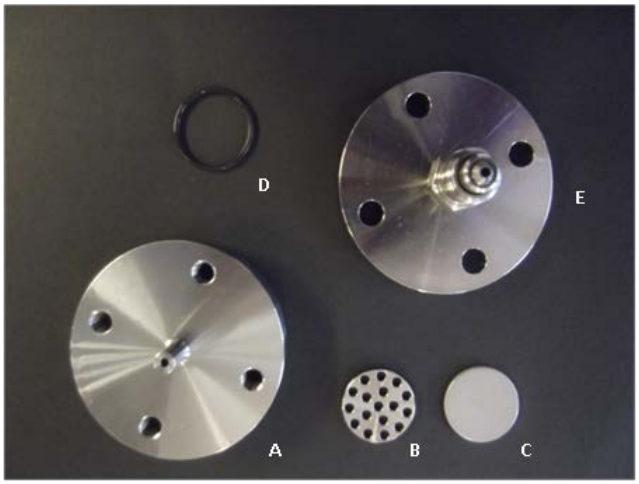

Figure 3.11: LipsoFast LF-50 extruder parts: A) Filter/Extruder low support, B) Support screen, C) Sintered disk, D) O ring and E) Filter/Extruder upper support

In this work, oil in water (O/W) emulsions were produced in a two stage process. In the first stage, oil and surfactant were pre-heated together to reach the desired temperature. RO water was also heated to the same temperature and was then added gradually to the mixture of oil and surfactant. Finally, this mixture was emulsified using an Ultra-Turrax homogeniser set at 13,500 rpm for 4 min to form a pre-mix emulsion. In the next stage, the pre-mix coarse emulsion was loaded into the sample cylinder of the LiposoFast extruder. Nitrogen gas pressure forced the sample through the membrane, while maintaining the desired temperature via a circulating water bath connected to the jacket. The fine emulsion resulting from this process was collected in an Erlenmeyer flask.

3.2.1.4 Cross-flow membrane emulsification

Membrane emulsification experiments were carried out using three different ceramic membranes with the pore sizes of 0.1, 0.2 and 0.45 µm. Throughout the experiments, the inlet and outlet pressure of the continuous phase were kept constant at zero bar and the dispersed phase (*i.e* soybean oil) were forced through the membrane into the continuous phase under 3-4 bar at the ambient temperature of 20 ± 1 °C. The continuous phase consisted of water and different concentrations of Tween 20 as surfactant, and was circulated in the system by the pump set at 50 %, corresponding

to a flow rate of 2.50 l min^{-1}. The experiment was stopped when air bubbles started to appear in the tube connecting the pressurised vessel to the membrane module and samples were taken from the feed tank for further investigations.

3.2.2 Droplet size determination

3.2.2.1 Dynamic Light Scattering (DLS)

The Malvern Zetasizer Nano Series 4S 0.31 (Malvern Instruments Ltd., Malvern, Worcestershire, UK) was used for measuring the drop size and drop size distribution of the samples prepared by the emulsification devices. Figure 3.12 shows a DLS device and its different parts.

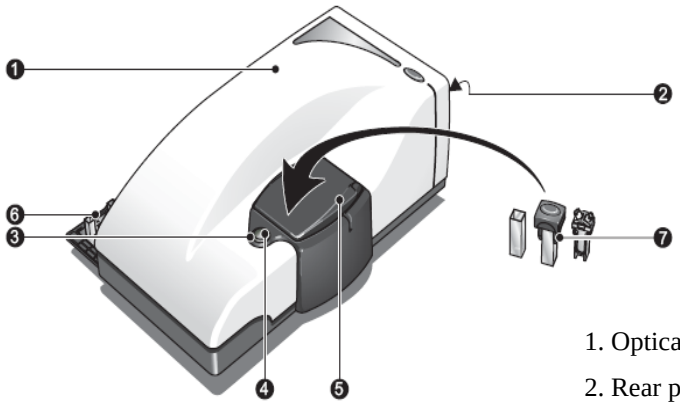

1. Optical unit
2. Rear panel
3. Status indicator
4. Cell access button
5. Cell area
6. Cuvette holder
7. Cells and cuvettes

Figure 3.12: Schematic view of a DLS device [127]

Dynamic Light Scattering (DLS), also known as Photon Correlation Spectroscopy (PCS), is a non-invasive, well-known technique for calculating the size of molecules and particles that are in the sub-micron region, such as small emulsion droplets,

protein aggregates and surfactant micelles which are below the lower limit of static light-scattering techniques [24]. Typical applications of DLS are the determination of the size and size distribution of particles emulsions and molecules which are dispersed or dissolved in a liquid [127].

The DLS technique is based on the fact that droplets in an emulsion continuously move around due to Brownian motion. This is the motion induced by the bombardment of solvent molecules having their own movement due to their thermal energy [127]. If the particles or molecules are illuminated with a laser beam, the intensity of the scattered light fluctuates at a rate directly related to the motion of the molecule (Figure 3.13). The faster the particles move through the solvent, the faster the intensity will change. The diffusion of the molecules is typically controlled by three factors: temperature, viscosity of the solvent and finally the size of the molecules. In the case of constant temperature and viscosity of the solvent, therefore, variation in the intensity of the scattered light is directly related to the size of the molecule [128].

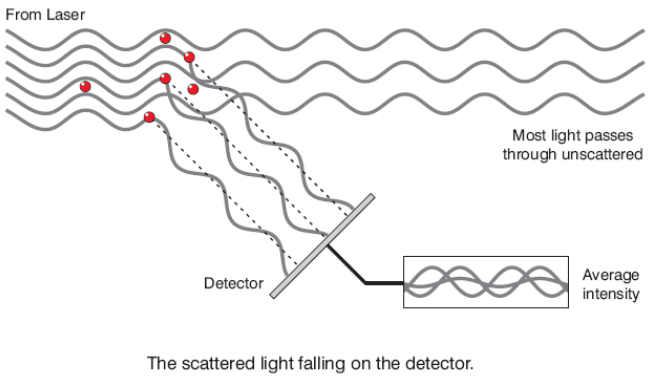

Figure 3.13: Schematic illustration of light scattering fluctuations being detected by DLS [127]

By measuring the timescale of light intensity fluctuations, DLS can give the average size, size distribution and polydispersity of molecules and particles in solution. Analysis of these intensity fluctuations provides the diffusion coefficient of the particles, which is inversely proportional to the decay time of the light scattering fluctuations. Consequently the particle size is determined using the Stokes-Einstein equation assuming the emulsion droplets to be spherical [24].

$$r = \frac{k_B T}{6\pi\mu D}$$ Equation 3.1

Where

r is the radius of the spherical particle (m).

D is the diffusion coefficient ($m^2\ s^{-1}$).

k_B is Boltzmann's constant = 1.38064×10^{-23} ($J\ K^{-1}$).

T is the absolute temperature (K).

μ is viscosity (Pa s).

The diameter measured in Dynamic Light Scattering (hydrodynamic diameter) refers to how a particle diffuses within a fluid. This is the diameter of the sphere defined by the molecule moving in all directions plus the hydration layer, and has the same translational diffusion coefficient as the particle being measured (Figure 3.14). This is actually also an indication of how easy it is for the molecule to move through the solvent [128]. Figure 3.15 illustrates an example of the data display from DLS analysing software, from which the Z-average (i.e the mean hydrodynamic diameter) and PdI are the data used for the evaluation of droplet size and size distribution, respectively. For each sample, a series of six measurements was carried out.

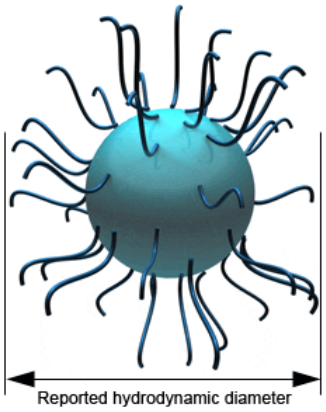

Figure 3.14: Hydrodynamic diameter being measured by DLS [129]

		Size (d.nm):	% Intensity	Width (d.nm):
Z-Average (d.nm): 69.42	Peak 1:	84.12	100.0	39.74
PdI: 0.163	Peak 2:	0.000	0.0	0.000
Intercept: 0.968	Peak 3:	0.000	0.0	0.000
Result quality : Good				

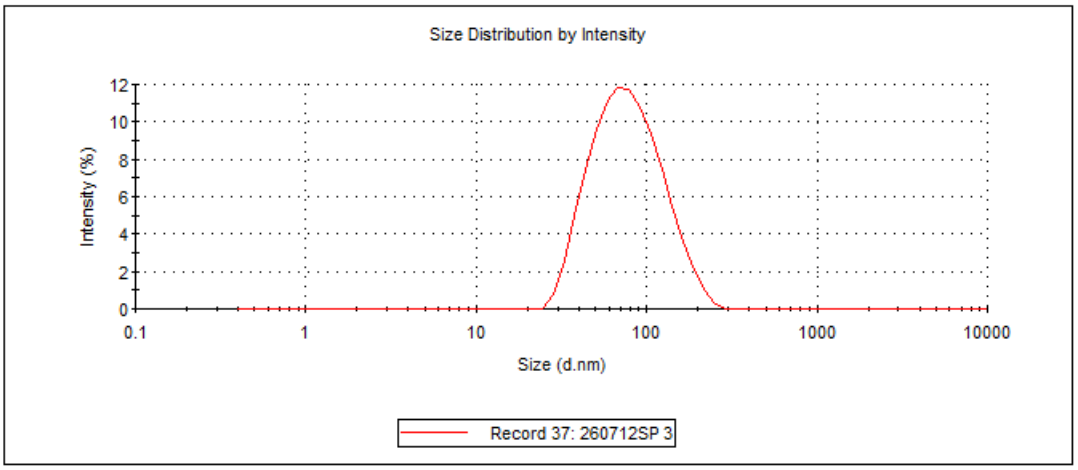

Figure 3.15: Data display from the DTS Data Software

3.2.2.2 Nanoparticle Tracking Analysis (NTA)

NanoSight (NTA 2.1, NanoSight NS500; NanoSight Ltd., Wiltshire, United Kingdom) was another device used in this work for measuring the drop size and drop size distribution of the samples prepared by the emulsification devices (Figure 3.16).

Figure 3.16: NTA 2.1, NanoSight NS500; (NanoSight Ltd., Wiltshire, United Kingdom)

Nanoparticle Tracking Analysis (NTA) is a recently introduced method for analysing nano-emulsions through a direct visualisation of the nano-scale particles in real-time. Based on a conventional optical microscope and by using a laser light source, the nanoparticles, which are moving under Brownian motion in a 0.3 ml sample, are separately tracked as point scatters in real-time by a CCD camera and analysed using particle tracking image analysis software. As each particle is tracked and analysed separately, the determination of particle size and particle size distribution does not have the limitation of being an intensity weighted z-average distribution, as is the case in conventional techniques. The Nanosight instrument records the Brownian motion of the particles, and by subsequently applying the Stokes-Einstein equation determines the particle size (in term of hydrodynamic diameter) and concentration [130][131].

The measurement process in NTA consists of three steps. First, the sample is diluted by pure water and placed in the 0.3 ml sample chamber. Then, the light scattered from the laser-illuminated particles in the sample is captured by a high sensitivity camera via the microscope, with the moving particles being illustrated on a computer screen as dots of light. This image is stored as a movie at a rate of 30 frames per second. Finally the captured movie is play backed via NTA software showing individually tracked particles. The NTA process is shown schematically in Figure 3.17.

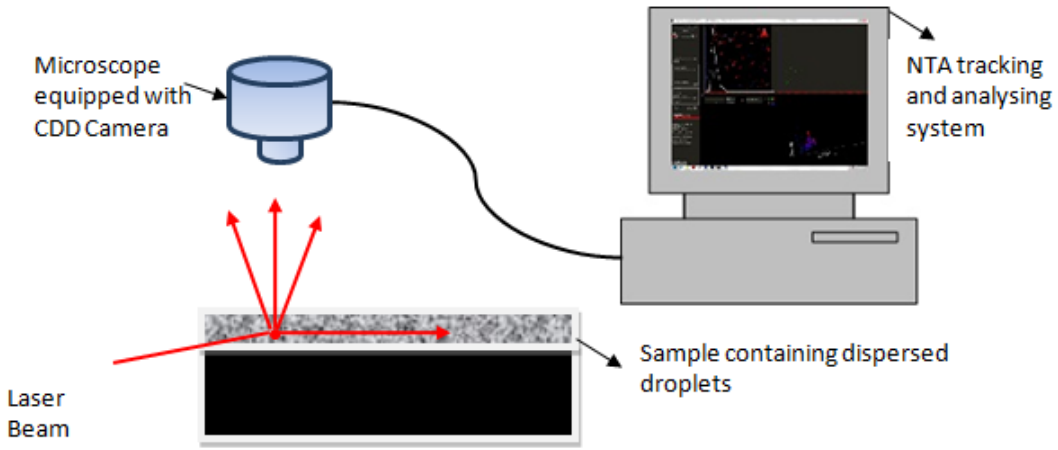

Figure 3.17: Schematic illustration of Nanoparticle Tracking Analysis (NTA)

The NTA device also has the ability to measure the zeta potential of the particles in the sample. This is done using the ZetaSight system which is an upgrade module added to the NanoSight NS500. The zeta potential of a system, which is defined as "the *electric potential at the slip plane between the bound layer of diluent molecules surrounding the particle, and the bulk solution*" [132], is an indication of charge stability and is in control of all particle-particle interactions in a suspension. When determining the stability of a nanoparticle suspension it is extremely important to investigate the zeta potential: the higher the level of the zeta potential, the greater the electro-static repulsion between the particles, resulting in less aggregation or flocculation over time (i.e better stability). Generally, samples with zeta potentials of between -30 mV and +30 mV incline to aggregate. The exact stability threshold, however, depends on the particle type [132].

The ZetaSight system, which measures the zeta potential of individual nano-scale particles in aqueous suspension, illustrates a detailed view of the particle distribution in terms of electrical potential and related stability. A variable electric field, applied by platinum electrodes fitted in the sample chamber, induces the movement of both the sample particles and the aqueous diluent, known as electro-phoresis and electro-osmosis, respectively. The apparent drift velocity, which is a superposition of these two motions, is then recorded by the NanoSight technique for every tracked particle. By examining the total velocity at various depths within the sample chamber, these two components can be separated to determine the electro-phoretic velocity, and subsequently the zeta potential of the particles [132] [133].

3.2.3 Transparency measurements

3.2.3.1 Refractive indices

Refractive indices were measured using a digital handheld refractometer (Reichert Instruments, Depew, NY) at room temperature. Three drops of prepared emulsion samples were placed on the measuring prism of the refractometer and the respective refractive index was read from the screen.

3.2.3.2 Turbidity measurements

Turbidity readings, expressed as Formazine Turbidity Units or FTU, were taken with the use of a portable microprocessor turbidity meter (HANNA HI 93703, Hanna Instruments, Kehl, Germany). According to supplier manual, the HI 93703 Turbidity meter, which complies with ISO 7027 [134], is based on light-angle scattered light detection. The light source is an infrared LED with a wavelength of 890 nm.

3.2.3.3 UV-Visible characterization

Ultraviolet (UV) spectrophotometric analyses were carried out using a UV1601 spectrophotometer (Shimatzu, Japan). The absorbance values of the diluted emulsions were determined by measuring the percentage absorbance through a U.V. Spectrophotometer. Each set of measurements was performed at 590 nm by using purified water as a blank sample followed by three replicates for each sample.

3.2.4 Viscosity measurements

The apparent viscosity measurements were made using a calibrated glass capillary viscometer (Cannon-Fenske Routine Viscometer) filled with the sample at room temperature (25 °C) and then thermostatted in a water bath at 40 °C for 10 minutes prior to reading. The size of viscometer was chosen based on the viscosity range of the samples and the measurements were carried out in triplicates. The Kinematic viscosity of each sample was calculated by multiplying the efflux time by the viscometer constant at 40 °C. The efflux time is the time in seconds for the liquid to pass from mark A to mark B inside the tube, as shown in Figure 3.18. Based on the calibration data certified by Cannon Instrument Co., the viscometer constant at 40 °C is 0.00799 $mm^2\ s^{-2}$; assuming the viscometer is filled at room temperature. If the filling temperature (T_F) is substantially different than the room temperature, the viscometer constant at test temperature (T_T) can be calculated by using the following equation:

$$C = C_0\ (1 - B[T_T - T_F])$$ Equation 3.2

Where,

C is the viscosity constant at test temperature ($mm^2\ s^{-2}$)

C_0 is the viscosity constant when filled and tested at the same temperature ($mm^2\ s^{-2}$)

B is the temperature dependence factor ($°C^{-1}$)

T_T and T_F are the test temperature and filling temperature, respectively (°C).

The values for C_0 and B given by Cannon Instrument Co. on their certificate of calibration are 0.008 $mm^2\ s^{-2}$ and 88 ($\times\ 10^{-6}$ /°C) respectively; and have been based on a coefficient of thermal expansion typical to that of a mineral oil.

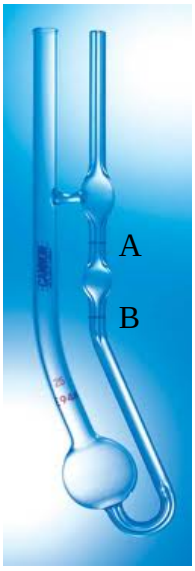

Figure 3.18: Cannon-Fenske Routine Viscometer. Marks A and B are the starting and finishing points of the efflux time measurement.

3.2.5 Membrane characterization

Membrane characterization is the determination of structural and morphological properties of a membrane, such as porosity, pore size, pore size distribution, pore shape, etc. By using this information one can aim to predict the membrane performance for a given application (see Equation 2.9). There are different characterization techniques available for porous membranes such as Scanning

Electron Microscopy (SEM), Atomic Force Microscopy (AFM), Bubble point and Permeation measurement.

Scanning Electron Microscopy (SEM), which was used in this work for membrane characterisation, has the ability to scan the sample surface and provide high quality images at magnifications up to 100,000×. In this device, a focused beam of high-energy electrons are used to generate a variety of signals derived from electron-sample interactions at the surface of a solid sample. These signals give some information about the sample such as external morphology (texture), chemical composition, and the crystalline structure and orientation of materials making up the sample [135]. As it has a large depth of field, SEM can be focused on the entire surface of a sample which makes it a good technique for membrane characterisation with respect to surface porosity and thickness of the active layer.

Cross-sections of membranes used in this project were observed by SEM (JEOL-JSM-6480 LV, University of Bath). In order to analyse the membrane surface using SEM, and to get clear and well magnified images, the samples must first be prepared. Since the SEM uses electrons to produce an image, it is important that the samples be electrically conductive. For this purpose, a conductive coating is applied to the surface of the samples. In this experiment a gold coating was used for the membrane samples. Preparation of the samples for SEM observation was as follows:

a) The membrane samples were cut to appropriate sizes.

b) By using a double-sided carbon adhesive tape each sample was fixed to an aluminium dish.

c) The samples were placed in a small vacuum chamber of an automated sputter coater for coating a thin, conductive layer of gold over the samples (about a few nanometers). This process takes about 4 to 5 minutes.

d) The samples were then allowed to cool to room temperature.

The prepared samples were then observed using SEM. Images captured by a camera linked to the microscope were later analysed using a public domain image-processing software called ImageJ (developed by National Institutes of Health, USA) in order to investigate the membrane morphology such as thickness, pore size and shape, the

grains' structure and finally the porosity. The software can be calibrated to the scale bar on the SEM image. The ImageJ software was downloaded from http://rsbweb.nih.gov/ij/ (2010).

3.2.6 Contact angle measurement

The FTA200, supplied by FTA Europe, UK, is an instrument used to measure contact angle and surface tension by means of the pendant drop method. The instrument contains a pumping system driven by a stepper motor by which the oil sample in a highly accurate syringe is injected into a rectangular acrylic container (filled with the continuous phase) in the form of droplets. The syringe can be used in accordance with a variety of commercially available needles. The pumping system of the FTA200 is designed to be used with 10 ml syringes; however, it can be adapted to use smaller syringes of 5 ml capacity. The process of drop formation in the tip of the I-shaped needle is captured by a built-in high-speed video camera system. By analysing a still image extracted from the captured video in the time just before drop detachment, the interfacial tension, drop volume and contact angle can be measured. Figure 3.19 illustrates the FTA200 device used in this study.

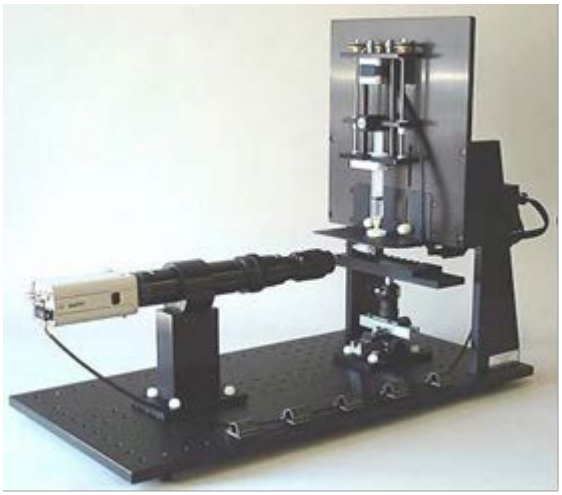

Figure 3.19: A photograph of the FTA200 instrument (FTA Europe, UK)

4. Batch Emulsion formulation: Comparison of Homogeniser and PIT methods

4.1 Introduction

Emulsification methods can be categorised according to their energy consumption as high and low energy emulsification techniques, as discussed earlier in Chapter 2. Energy-intensive emulsification techniques use applied shear forces, via mixing methods, to produce smaller droplets, whereas low energy techniques take advantage of physiochemical properties of the system. The purpose in this chapter is to investigate oil-in-water emulsions prepared by rotor-stator homogeniser (Ultra-Turrax), as an example energy intensive method, and compare them with those produced by Phase Inversion Temperature (PIT) (i.e. low energy emulsification technique) in terms of droplet size, polydispersitry index (PdI) and stability. Previous studies reported formation of emulsions using water/soybean oil/polyoxyethylene 10 oleoyl ether (Brij 97) system [114][124] and hence this system was chosen as a model to study these two emulsification mechanisms and characterise nano-emulsions produced via these techniques.

4.2 Rotor-stator homogeniser (Ultra-Turrax)

4.2.1 Effect of temperature

To study the effect of temperature on emulsions, a series of samples with various surfactant concentrations were prepared at three different temperatures of 45, 75 and 85 °C, and investigated for droplet size, polydispersity and transparency. The results of these tests are shown in Figure 4.1.

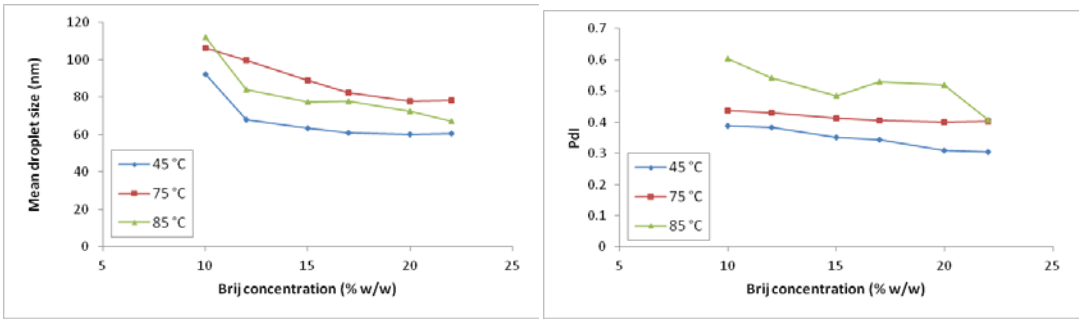

A B

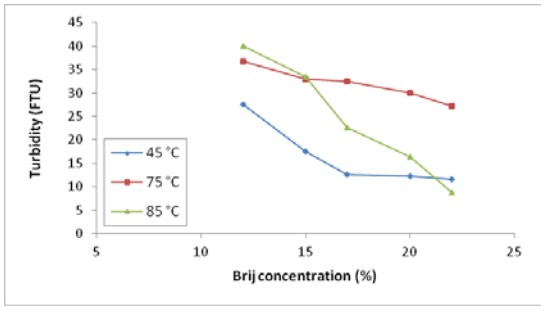

C

Figure 4.1: Effect of temperature on the droplet size (A), polydispersity index (B) and turbidity (C) of the emulsions containing 10 % (w/w) oil and different Brij 97 concentrations produced by Ultra-Turrax; emulsified for 15 min at a rate of 13,500 rpm.

As it can be seen in Figures 4.1 A and Figure 4.1 B, the emulsions prepared at 45 °C had the smallest droplet sizes and the narrowest size distributions (i.e. PdI) compared to the ones produced at higher temperatures. The emulsions prepared at 45 °C also showed the lowest turbidity (Figure 4.1 C), and hence they were more visually transparent. The resulting emulsions had a slight yellowish appearance with droplet sizes of less than 100 nm, i.e. smaller than the wavelength of light, which explains their transparency. The appearance of prepared samples is tabulated in Table 4.1.

Table 4.1: Appearance of the fresh emulsions containing 10 % (w/w) oil and different Brij 97 concentrations produced by Ultra-Turrax; emulsified at room temperature for 15 min at a rate of 13,500 rpm after pre-heating the components to three different temperatures of 45, 75 and 85 °C.

	Emulsions prepared by UT (15 min)		45 °C			75 °C			85 °C		
			Appearance			Appearance			Appearance		
1	SBO	10 % (w/w)			Opaque			Opaque			Opaque
	Brij 97	10 % (w/w)									
	Water	80 % (w/w)									
2	SBO	10 % (w/w)			Slightly transparent			Opaque			Slightly transparent
	Brij 97	12 % (w/w)									
	Water	78 %									
3	SBO	10 % (w/w)			Transparent			Opaque			Slightly transparent
	Brij 97	15 % (w/w)									
	Water	75 % (w/w)									
4	SBO	10 % (w/w)			Transparent			Slightly transparent			Transparent
	Brij 97	17 % (w/w)									
	Water	73 % (w/w)									
5	SBO	10 % (w/w)			Transparent			Transparent			Transparent
	Brij 97	20 % (w/w)									
	Water	70 % (w/w)									
6	SBO	10 % (w/w)			Transparent			Transparent			Transparent
	Brij 97	22 % (w/w)									
	Water	68 % (w/w)									

Temperature has a complex effect on droplet formation mechanism. An increase in temperature reduces both interfacial tension and viscosity. Low interfacial tension decreases the Laplace pressure and hence the energy required to break droplets to smaller ones (see Equation 2.11). However, reduction in the viscosity has a complex effect on the final droplet size in an energy-intensive method: a reduction in the viscosity of continuous phase can increase the collision frequency and coalescence rate consequently, whereas lowering the viscosity of the dispersed phase can result in formation of smaller droplets [137]. These can explain the increase in droplet size as temperature rises. Although the increase in temperature results in decrease in interfacial tension, variations in viscosity and coalescence rate can result in formation of larger droplets at high temperatures (Figure 4.1 A). As mentioned, our

results show that the smallest droplets were obtained at 45 °C. Also, Figure 4.1 B clearly shows that the polydispersity index of emulsions increases as the temperature increases, which can be attributed to the change in viscosity and increasing the coalescence rate. In addition, as explained in Section 2.2.2.1, the affinity of non-ionic surfactants towards oil or water (i.e. HLB value) varies with temperature which can affect the final results. Based on the obtained results in this section, 45 °C was selected as the mixing temperature for further experiments in our study where investigating other factors affecting the emulsion properties.

4.2.2 Effect of mixing time

In this section, the effect of mixing time on the droplet size and size distribution were investigated while keeping the rotation speed constant at 13500 rpm. In order to find the optimum emulsification time, a set of experiments was carried out, using 10 % (w/w) oil and different Brij 97 concentrations. Emulsion components were first pre-heated to 45 °C and then mixed together for up to 30 minutes while samples were taken after 5, 10, 15 and 30 minutes. The variation in mean droplet size and PdI are depicted in Figure 4.2.

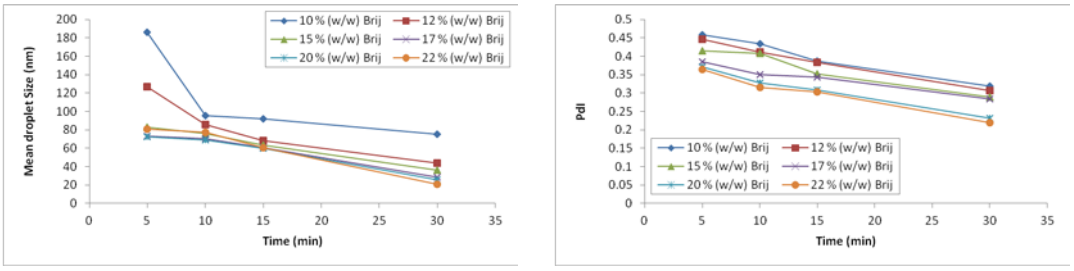

A B

Figure 4.2: Effect of mixing time and different Brij 97 concentrations on the droplet size (A) and polydispersity index (B) of the emulsions containing 10 % (w/w) oil produced by Ultra-Turrax; emulsified at room temperature at 13,500 rpm (after pre-heating the components to 45 °C).

As it can be seen in Figure 4.2 A and Figure 4.2 B, the droplet sizes and polydispersity indices decrease as surfactant concentrations increase. At lower surfactant concentrations, the graphs show two relatively linear regimes: transient and steady state regimes. The initial sharp decrease in mean droplet size with time is the transient period, during which the rate of droplet rupture is higher than that of droplet coalescence. The mean droplet size becomes relatively constant during the steady-state period, in which the rate of droplet rupture and coalescence is relatively constant. However, there was no initial sharp drop in mean droplet size at higher surfactant concentrations. This can be attributed to the fact that the interfacial tension between two phases decreases significantly at very high surfactant concentrations and therefore very small droplets were formed even at relatively lower energy input. The effect of surfactant concentration will be discussed in detail in Section 4.2.3.

Results show that the steady-state droplet size is achieved after 15 minutes, and therefore, taking into consideration that higher mixing times are less energy efficient, 15 minutes was selected as appropriate emulsification time for future experiments in our study.

4.2.3 Effect of different surfactant concentration

To study the effect of surfactant concentration on the size and polydispersity of the formed droplets within the oil-in-water emulsions, a series of emulsions were prepared at room temperature (21 °C ± 2), using 10 % (w/w) oil and different Brij 97 concentrations**.** Emulsion components were first pre-heated to 45 °C and then mixed together by Ultra-Turrax for 15 minutes at the rate of 13,500 rpm. In order to avoid the temperature rise during homogenisation the container was immersed in a water bath in which the temperature was the same as room temperature.

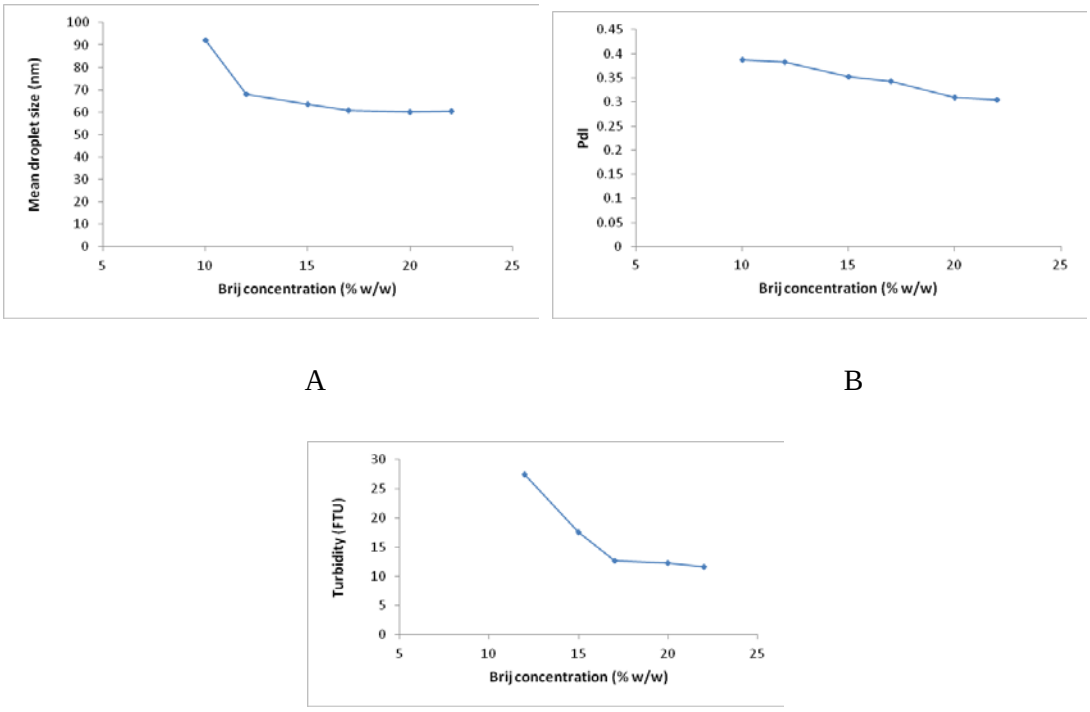

Figure 4.3: Effect of different Brij 97 concentrations on the droplet size (A), polydispersity index (B) and turbidity (C) of the emulsions containing 10 % (w/w) oil produced by Ultra-Turrax; emulsified for 15 min at room temperature at 13,500 rpm (after pre-heating the components to 45 °C).

Figure 4.3 A shows that the droplet size decreased as surfactant concentration increased until the surfactant concentration of 17 % and then remained almost constant for higher concentrations due to presence of adequate amount of surfactant in the system to cover all the droplets and prevent coalescence. However, the polydispersity index decreased for all surfactant concentrations as shown in Figure 4.3 B. This resulted in more transparent emulsions as indicated in both the turbidity measurements and the absorbance values (Figures 4.3 C and 4.4).

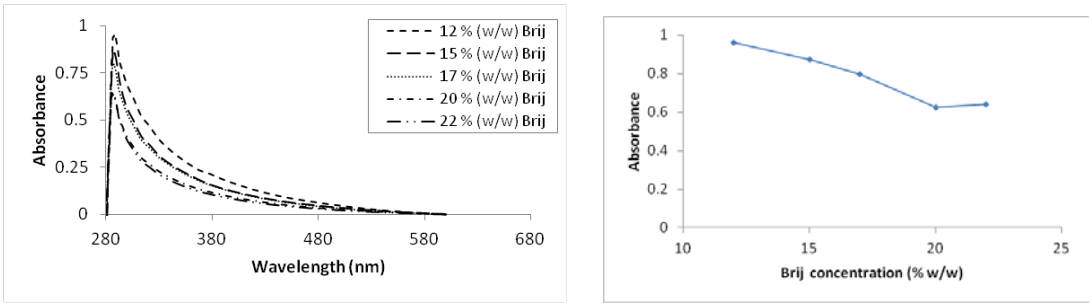

Figure 4.4: Absorbance of samples containing different surfactant concentrations. Pre-heated samples were mixed at room temperature for 15 minutes at 13,500 rpm. Samples were diluted 30 times with deionised water.

As mentioned in Section 2.2.1.2, the surfactant concentration plays an important role in determining the droplet size, polydispersity and stability of the produced emulsions by controlling the interaction between the droplet break-up and coalescence. During the emulsification process, and due to the shear applied by the Ultra-Turrax homogenisation, the oil droplets are deformed, resulting in a new interfacial area and subsequent breakup. The size of the newly formed droplets depends on the interfacial tension during the deformation. The surfactant lowers the interfacial tension and consequently eases droplet rupture. The effect of surfactant on droplet size, however, depends on to the extent it can reduce the interfacial tension and also the speed of adsorption of surfactant at the newly formed interface. A slow adsorption leads to poor coverage of newly formed interfaces/droplets making them susceptible to coalescence [138]. This explains why an increase in surfactant concentration results in smaller droplet size and PdI, as high surfactant concentration leads to presence of excess surfactant which is adsorbed quickly at the recently formed interface/droplets and stabilises them. The surfactant layer at the interface stabilises droplets by hindering coalescence through two mechanisms. The surfactant-covered interface not only acts as a physical barrier to prevent the coalescence of droplets when colliding, but also lowers the thermodynamic drive towards coalescence by decreasing the interfacial tension (see Equation 2.1). In other words, the relationship between emulsion droplet size and Brij 97 content can be explained in terms of surfactant surface coverage. At low Brij 97 concentrations there are insufficient surfactant molecules to cover the droplet surfaces, and they are therefore unable to prevent the newly formed droplets from coalescing, leading to larger droplet sizes. As it can be seen in Figure 4.5, the emulsions with higher

surfactant concentrations have higher viscosity. It can be explained mainly by the presence of more surfactant molecules in the system and also by the increase in droplet interactions. The decrease in droplet size when increasing the surfactant concentration results in an increase in the number of droplets and also the interfacial area between two phases. It escalates the interaction between droplets leading to more viscous emulsions [113].

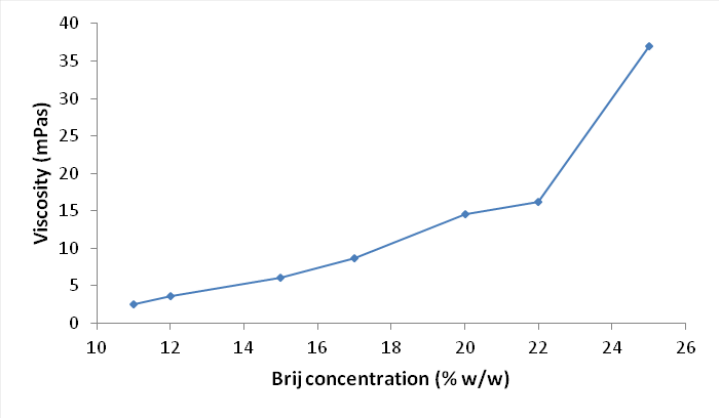

Figure 4.5: Effect of different Brij 97 concentrations on viscosity of the emulsions containing 10 % (w/w) oil produced by Ultra-Turrax; emulsified for 15 min at room temperature at 13,500 rpm (after pre-heating the components to 45 °C).

4.2.4 A model to predict the average droplet size

When a high mechanical shear and turbulent flow is applied to the emulsion components, the droplet size distribution are controlled by the size distribution of the micro-eddies in the flow pattern (which are responsible for droplet breakage). According to the Hinze-Kolmogorov theory, two different regimes can be distinguished in a turbulent flow: 1) the turbulent-viscous regime, in which the eddies are larger than the droplets and thus act like a mill; 2) the turbulent-inertial regime, in which the size of the turbulent eddies are similar to or smaller than the dispersed droplets and thus break them by collision [139]. Generally, the droplets produced in the viscous regime are smaller in size than the ones produced in the

inertial regime. The maximum droplet diameter (d_{max}) which can be produced in these two regimes (i.e. the Kolmogorov Diameter) is expressed as follows:

$$d_{max} \approx \varepsilon^{(-1/2)} \gamma_{ow} \mu_c^{(-1/2)} \quad \text{(Viscous regime)} \quad \text{Equation 4.1}$$

$$d_{max} \approx \varepsilon^{(-2/5)} \gamma_{ow}^{(3/5)} \rho_c^{(-1/5)} \quad \text{(Inertial regime)} \quad \text{Equation 4.2}$$

Where,

γ_{ow} is the oil/water interfacial tension (N m^{-1}),

ρ_c and μ_c are the density (kg m^{-3}) and viscosity (Pa s) of the continuous phase, respectively,

ε is the input mechanical energy per unit time and unit volume (*i.e.* power density) (W m^{-3}), which can be estimated for a rotor-stator homogeniser using the following Equation as introduced by Brocart *et al.* (2002) [140][141]:

$$\varepsilon = \rho_c \frac{(2\pi D_R N)^3}{4a} \quad \text{Equation 4.3}$$

Where,

N is the rotation speed (rpm),

D_R is the diameter of the rotor (m),

a is the distance between the two slots of the motor (m),

ρ_c is the density of the continuous phase (kg m^{-3}).

Here it should be noted that this equation estimates mechanical energy input which is generated through the rotation of rotor and turbulent mixing within the rotor/stator slut. According to Equation 4.3, the rate and amount of shear applied to the droplets

can be increased by increasing the mixing time as well as the rotation speed of the homogeniser. Given the diameter of the rotor (*D*) and the distance between the two slots of the motor as 14 mm and 2 mm respectively, the power density (ε) applied to the system per time unit was estimated at approximately 9.7 x 10^8 W m^{-3}, when the device motor was set to 13,500 rpm. Another method, used in the literature, for calculation of energy density is the electrical energy consumption of the emulsifying device which can be calculated as the energy consumption of the device per total mass of emulsion (see Section 4.3.4) [142].

Boundary between the viscous and inertial regimes can be estimated according to the Kolmogorov length scale. Droplets larger and smaller than the Kolmogorov length scale lie within the inertial and viscous regimes, respectively The Kolmogorov length scale can be estimated by:

$$l_w = (\frac{\upsilon_c^3}{\varepsilon_m})^{1/4} \qquad \text{Equation 4.4}$$

where l_w is the Kolmogorov length scale (m), υ_c is the kinematic viscosity of continuous phase (m^2 s^{-1}) and ε_m (W kg^{-1}) is the power density per unit mass.

The Kolmogorov length scale for the system under study (considering υ_c=1.0×10^{-6} m^2 s^{-1} and ε_m=9.7×10^5 W kg^{-1}) is estimated to be 1.007 μm which is above the mean drop size of emulsions produced. In order to simplify calculations, the density of emulsion was considered to be equal to water (*i.e.* 1000 kg m^{-3}). An estimation of power density and Kolmogorov length scale at various rotor speeds are shown in Figure 4.6. These results clearly show that Kolmogorov length scale decreases as the energy input to the system increases.

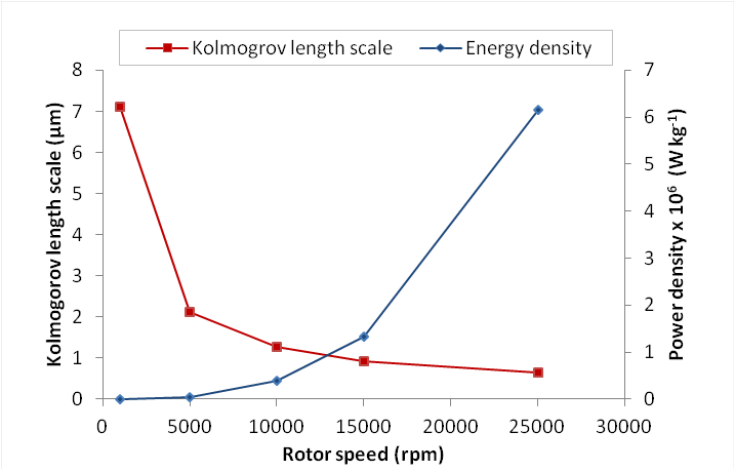

Figure 4.6: Variation in power density (ε_m) and Kolmogrov length scale (l_w) with rotor speed (N).

Comparison between estimated Kolmogorov length scale and obtained droplet sizes confirms that the viscous regime is predominant in the system under study and therefore Equation 4.1 can be used to estimate the mean droplet size. Equation 4.1 can be rewritten as:

$$d_{max} = C_e\, \varepsilon^{(-1/2)}\, \gamma_{ow}\, \mu_c{}^{(-1/2)} \qquad \text{Equation 4.5}$$

Where C_e is the arbitrary experimental (dimensionless) constant which can be fitted according to the experimental setup [142][143].

The interfacial tension between soybean oil and water at various Brij 97 concentrations (at 45 °C) were measured using the "FTA200" system (see Section 3.2.6) and shown in Figure 4.7. Results show that the interfacial tension between two phases decreases until surfactant concentration of 10 % (w/w) and remains mostly constant for higher concentrations.

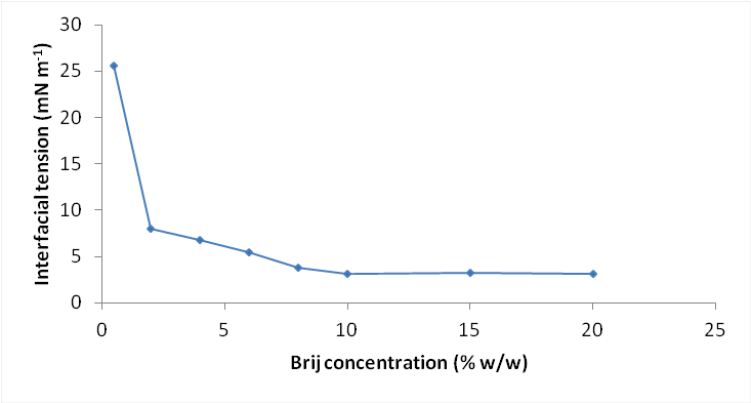

Figure 4.7: Variation in interfacial tension between water and soybean oil with Brij 97 concentration.

It should be noted that μ_c in Equation 4.5 is the viscosity of the continuous phase. However in an emulsion, with a high oil phase ratio, water cannot be assumed to be the continuous phase anymore and presence of droplets changes the viscosity of continuous phase and the energy transferred to droplets. Therefore, overall viscosity of emulsions (shown in Figure 4.5) can be considered as the viscosity of continuous phase, known as effective viscosity [142].

The experimental constant can be estimated by rewriting Equation 4.5 as:

$$C_e = \frac{d_{max}}{[\varepsilon^{(-1/2)}\, \gamma_{ow}\, \mu_c{}^{(-1/2)}]} \qquad \text{Equation 4.6}$$

Experimental droplet sizes at various surfactant concentrations were considered and C_e for the system under study for two different mixing times of 15 and 30 min were found to be C_e= 0.06 and C_e= 0.03, respectively. These values are in line with those reported previously. Nazarzadeh *et al*. (2010) have used the arbitrary constant values of 0.012 and 0.025 for their study depending on the surfactant concentration and found these values to provide satisfactory fits to the data [142]. The constant values reported by Pacek *et al*. (1998) were 0.022 and 0.052 [144]. Arbitrary experimental constant was then used to estimate the mean droplet size of emulsions produced using Ultra-Turrax. The estimated average droplet sizes for two different mixing times (from Equation 4.5) and their comparison with experimental results are shown

in Figure 4.8 and 4.9. The model provides a relatively good estimation for the emulsion produced in this study.

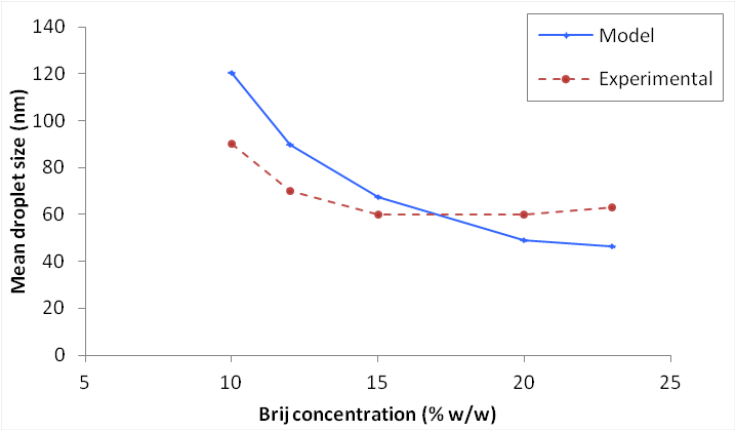

Figure 4.8: Comparison between experimental and model fit results (Equation 4.5) for the variation in mean droplet size of emulsions with surfactant concentration, using 10 % (w/w) soybean oil as dispersed phase. Samples were emulsified for 15 min at room temperature at 13,500 rpm (after pre-heating the components to 45 °C).

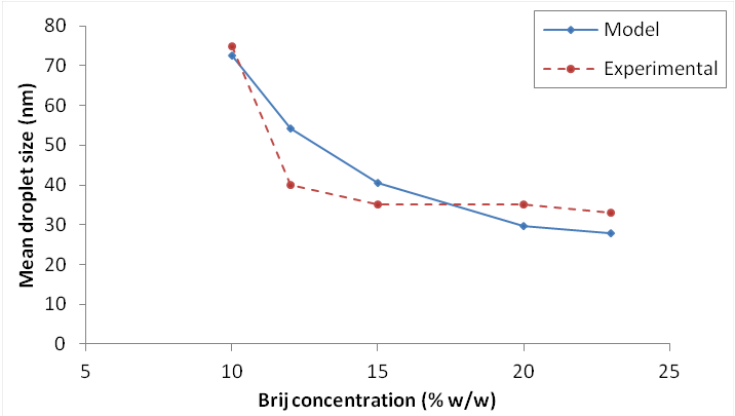

Figure 4.94: Comparison between experimental and model fit results (Equation 4.5) for the variation in mean droplet size of emulsions with surfactant concentration, using 10 % (w/w) soybean oil as dispersed phase. Samples were emulsified for 30 min at room temperature at 13,500 rpm (after pre-heating the components to 45 °C).

4.2.5 Effect of different oil concentrations

In order to investigate to what extent an increase in oil concentration affected the quality of the produced emulsions, two set of samples were prepared containing 5 %

and 20 % (w/w) soybean oil, respectively. The quality of the prepared emulsions was then compared with the ones containing 10 % soybean oil. Figure 4.10 shows the variation in droplet size and PdI for three soybean oil phase ratios of 5, 10 and 20 % (w/w) at different surfactant (i.e. Brij 97) concentrations.

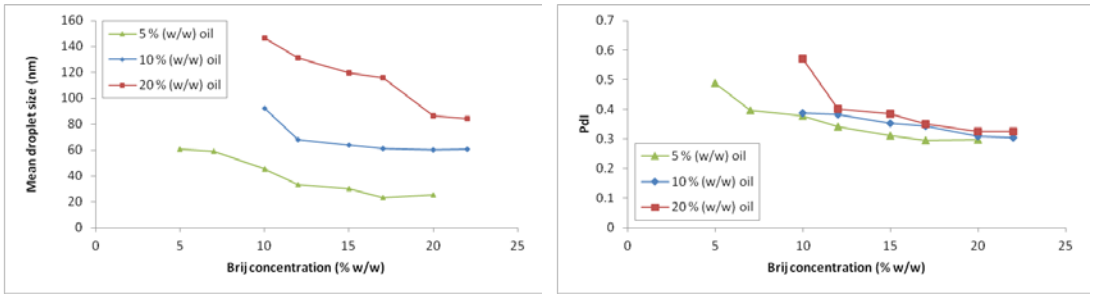

A B

Figure 4.10: Effect of different soybean oil concentrations on the droplet size (A) and polydispersity index (B) of the emulsions containing different Brij 97 concentrations produced by Ultra-Turrax; emulsified for 15 min at room temperature at 13,500 rpm (after pre-heating the components to 45 °C).

The mean droplet size of emulsions decreases as the oil phase ratio decreases. Emulsions comprised of 20 % (w/w) oil show large mean droplet sizes in range of 80 to 150 nm whereas the mean droplet size of emulsions with 5 and 10 % (w/w) oil phase ratio are in range of 60 to 95 nm and 20 to 60 nm, respectively. There are a number of potential reasons for this. Firstly, increasing disperse volume fraction may prevent the formation of eddies due to the increase in the effective viscosity of emulsion (as discussed in Section 4.2.4), and reduce the energy transfer from the continuous phase to the dispersed phase. Secondly, given the same concentration of surfactant, there may be inadequate surfactant molecules to fully cover the droplets when the oil concentration increases, and finally the rate of droplet collision and subsequent coalescence rises when there are more oil droplets in the system [145]. The PdI of emulsions shows nearly the same trend with the exception that PdI of all emulsions at high surfactant concentrations are in the range of 0.3 to 0.4, regardless of their oil phase ratio. Also, results for all oil phase ratios show a decrease in mean droplet size by increasing the surfactant concentration. The decrease in the mean droplet size is relatively sharper for 20 % (w/w) oil phase ratio, compared to 5 and 10

% (w/w). Furthermore, the appearance and stability of these emulsions are summarised in Tables 4.2 and 4.3.

Table 4.2: Appearance and stability of the emulsions containing 5 % oil and different Brij 97 concentrations produced by Ultra-Turrax; emulsified at room temperature for 15 min at a rate of 13,500 rpm after pre-heating the components to 45 °C.

	Emulsions prepared by UT (15 min)		Appearance (fresh samples)		Stability (over 1 month)
1	SBO	5 % (w/w)		Opaque	No creaming
	Brij 97	10 % (w/w)			
	Water	85 % (w/w)			
2	SBO	5 % (w/w)		Transparent	No creaming
	Brij 97	12 % (w/w)			
	Water	83 % (w/w)			
3	SBO	5 % (w/w)		Transparent	No creaming
	Brij 97	15 % (w/w)			
	Water	80 % (w/w)			
4	SBO	5 % (w/w)	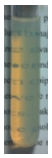	Transparent	No creaming
	Brij 97	17 % (w/w)			
	Water	78 % (w/w)			
5	SBO	5 % (w/w)		Transparent	No creaming
	Brij 97	20 % (w/w)			
	Water	75 % (w/w)			
6	SBO	5 % (w/w)		Transparent	No creaming
	Brij 97	22 % (w/w)			
	Water	73 % (w/w)			

Table 4.3: Appearance and stability of the emulsions containing 20 % oil and different Brij 97 concentrations produced by Ultra-Turrax; emulsified at room temperature for 15 min at a rate of 13,500 rpm after pre-heating the components to 45 °C.

	Emulsions prepared by UT (15 min)		Appearance (fresh samples)		Stability (over 1 month)
1	SBO	20 % (w/w)		Opaque	Creaming
	Brij 97	10 % (w/w)			
	Water	70 % (w/w)			
2	SBO	20 % (w/w)		Opaque	Creaming
	Brij 97	12 % (w/w)			
	Water	68 % (w/w)			
3	SBO	20 % (w/w)		Opaque	Creaming
	Brij 97	15 % (w/w)			
	Water	65 % (w/w)			
4	SBO	20 % (w/w)		Opaque	Creaming
	Brij 97	17 % (w/w)			
	Water	63 % (w/w)			
5	SBO	20 % (w/w)		Opaque/ Gel	No creaming
	Brij 97	20 % (w/w)			
	Water	60 % (w/w)			
6	SBO	20 % (w/w)		Opaque/ Gel	No creaming
	Brij 97	22 % (w/w)			
	Water	58 % (w/w)			

It can be seen that the emulsions containing 5 % soybean oil were similar to the ones with 10 % (w/w) oil in terms of appearance and stability, in that all samples were transparent and stable (*i.e.* no creaming observed) apart from the one with the lowest amount of surfactant, which had an opaque appearance. When the oil concentration was increased from 10 % to 20 % (w/w), however, the stability decreased drastically and creaming occurred within 24 hours of preparation, except for the samples with

extremely high concentration of Brij 97 (*i.e.* the 20 and 22 % samples). All samples had an opaque/ milky appearance due to the higher oil volume ratio. According to Gravis (2008), by increasing the dispersed phase volume fraction the number of droplets which scatter the light in the system increases, leading to more opaque appearance. Additionally, larger droplets scatter more light than smaller droplets and for droplets larger than 100 nm, it results in opaque nano-emulsions [167].

4.3 Phase inversion temperature method (PIT) and its comparison with Homogeniser method

In this section, a series of samples were prepared using phase inversion temperature method (PIT) and compared with those produced by Homogeniser in terms of appearance, droplet size, polydispersity and stability. Finally, energy consumption in two methods were estimated and compared. The various experiments which were carried out on the prepared samples are summarised in Table 4.4.

Table 4.4: Characteristics of the emulsions prepared by the PIT method using different concentrations of Brij 97 and 10 % (w/w) soybean oil. (The PIT values were evaluated by visual observation)

Brij Concentration (% w/w)	Phase inversion temperature (°C)	Stability	Appearance	Viscosity (mPas)	Size (nm)	PDI	Turbidity (FTU)	Absorbance	Refractive Index
10	....	Not stable	Milky	....	104.1	0.38	>40	>1	....
11	85	Stable	Transparent	2.00	18.06	0.141	>40	0.883	1.3632
12	80	Stable	Transparent	2.25	17.11	0.111	26.18	0.618	1.3648
15	78	Stable	Transparent	2.79	12.18	0.102	19.79	0.539	1.3669
17	78	Stable	Transparent	4.50	11.26	0.085	15.57	0.519	1.3723
20	78	Stable	Transparent	7.61	10.28	0.063	12.89	0.428	1.3739
22	75	Stable	Transparent	8.94	10.12	0.042	10	0.417	1.3764
25	73	Stable	Transparent	30.12	9.043	0.054	9.58	0.172	1.3786

In general, the average droplet size of emulsions decreases by increasing the surfactant concentration. The lowest required surfactant concentration, to stabilize 10 % (w/w) soybean oil, was found to be around 10.5 % (w/w) and attempts to produce stable nano-emulsion with surfactant concentrations lower than 10 % (w/w) failed. However, stable nano-emulsions were produced at all surfactant concentrations higher than 11 % (w/w). These nano-emulsions were transparent in appearance, with mean droplet sizes in range of 9 to 19 nm (see Table 4.4).

Failure of producing stable nano-emulsions at low concentrations can be correlated to the droplet formation mechanism during the PIT method. Two mechanisms were proposed in literature for formation of nano-emulsions through the PIT method. The first is based on transition of the system through a stage at which the interfacial tension between phases is at its lowest value [52][54], where a high coalescence rate is also expected [28][31]. Therefore, one might conclude that the surfactant concentration at values below 11 % was not enough to prevent the coalescence rate so that no stable emulsion could be obtained at these low concentrations.

Another mechanism, as reported by Roger *et al*. (2010) [146], is transition through a clear/transparent structure to obtain a fine nano-emulsion. The structure of this clear/transparent structure is expected to be a lamellar or cubic micellar structure, where a single phase solution is formed. Any variation in the structure of this system may lead to inversion of the curvature of the surfactant layer (through a homogeneous nucleation), which results in formation of nano-emulsion. The cubic micellar structure is a very viscous (or gel-like) structure. It was noticed during the experiments that the mixture became very viscous during the heating process and then became transparent at higher surfactant concentration, whereas no transparent solution was obtained at low surfactant concentrations. It can be concluded that the viscous structure which was obtained during the heating process might be cubic structure which broke due to a sudden change in temperature, resulting in the formation of nano-size droplets. As formation of single phase cubic structure requires a relatively high surfactant structure, it couldn’t be formed at low surfactant concentrations and therefore failed to produce nano-emulsions.

Also, the polydispersity index (PdI) of emulsions decreases by increasing the surfactant concentrations (Table 4.4). This can be correlated to the fact that at high

concentration, formed droplets are better protected against coalescence and therefore a fine nano-emulsion with narrow size distribution was obtained.

4.3.1 Appearance

As it can be seen in Table 4.5, all the samples produced by PIT method showed some level of transparency and stability except for the one prepared using the lowest amount of surfactant (10 % w/w) which had a milky appearance and became biphasic in less than 24 hours after preparation. Similar to the results in Homogeniser method, as the concentration of surfactant increased the samples became visually more transparent. It was later confirmed by absorbance measurements as shown in Figure 4.11, in which, the absorbance values of the samples produced by these two methods were plotted as a function of different surfactant concentrations. The absorbance of the samples was measured at a wavelength of 590 nm using a UV-Vis Spectrophotometer. The samples were first diluted 30 times with deionised water. The lower the absorbance number, the more transparent the sample is.

Table 4.5: Appearance and stability of emulsions produced by PIT method

	Prepared emulsions		Appearance (fresh samples)			Stability (over 1 month)
1	SBO	10 % (w/w)			Milky	Not stable
	Brij 97	10 % (w/w)				
	Water	80 % (w/w)				
2	SBO	10 % (w/w)			transparent	Stable
	Brij 97	10.5 % (w/w)				
	Water	79.5 % (w/w)				
3	SBO	10 % (w/w)			Transparent	Stable
	Brij 97	11 % (w/w)				
	Water	79 % (w/w)				
4	SBO	10 % (w/w)			Transparent	Stable
	Brij 97	12 % (w/w)				
	Water	78 % (w/w)				
5	SBO	10 % (w/w)			Transparent	Stable
	Brij 97	15 % (w/w)				
	Water	75 % (w/w)				
6	SBO	10 % (w/w)			Transparent	Stable
	Brij 97	17 % (w/w)				
	Water	73 % (w/w)				
7	SBO	10 % (w/w)			Transparent	Stable
	Brij 97	20 % (w/w)				
	Water	70 % (w/w)				
8	SBO	10 % (w/w)			Transparent	Stable
	Brij 97	22 % (w/w)				
	Water	68 % (w/w)				

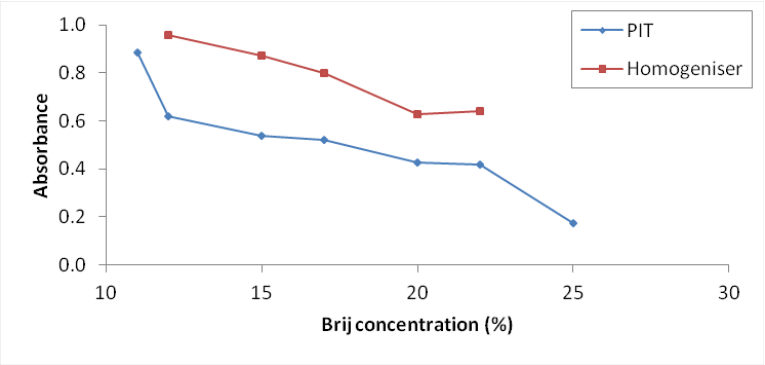

Figure 4.11: Effect of different surfactant concentrations on absorbance: Comparison of absorbance values between homogeniser (45 °C, 15 min) and PIT methods using the same formulation containing 10 % (w/w) soybean oil and different surfactant concentrations. Samples were diluted 30 times with deionised water.

Turbidity measurements were also carried out and appeared to be in line with the absorbance values, as illustrated in Figure 4.12. The decrease in the turbidity and absorbance as the surfactant concentration is increased can be correlated to the decrease in the droplet size at higher surfactant concentration. As the droplet size drops below the wavelength of visible light, the system becomes more transparent and less turbid.

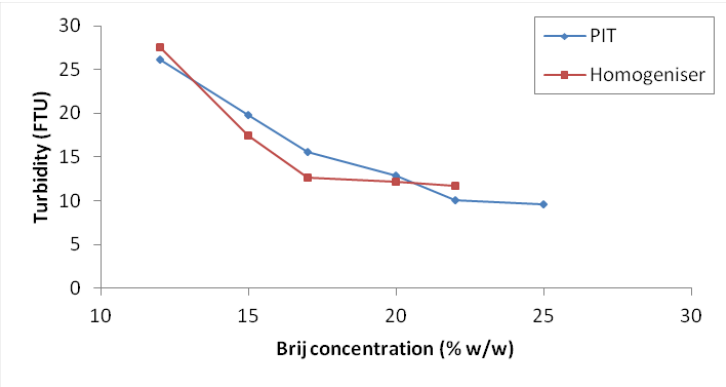

Figure 4.12: Effect of different surfactant concentrations on turbidity: Comparison of turbidity values between homogeniser (45 °C, 15 min) and PIT methods using the same formulation containing 10 % (w/w) soybean oil and different surfactant concentrations.

In comparison, the emulsions prepared using the PIT method were generally more transparent than those produced using Ultra-Turrax, because they contained smaller droplet sizes with lower PdI.

4.3.2 Droplet size and polydispersity index

As mentioned in Section 4.3, the results showed a decrease in both droplet size and polydispersity index (PdI) as surfactant concentration increased (Table 4.4); which clearly results in more transparent emulsions. Figure 4.13 illustrates a comparison of the emulsions prepared using the homogeniser and PIT methods in terms of their droplet size and polydispersity index.

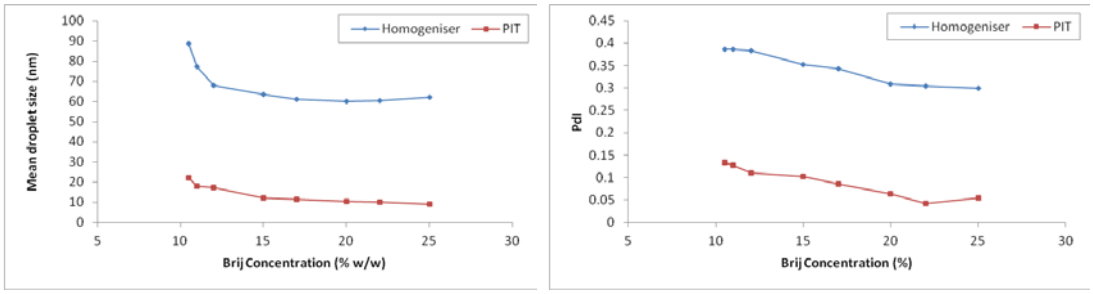

A B

Figure 4.13: Effect of different surfactant concentrations on droplet size and polydispersity index: Comparison of droplet sizes (A) and polydispersity indices (B) between homogeniser (45 °C, 15 min) and PIT methods using the same formulation containing 10 % (w/w) soybean oil and different surfactant concentrations.

As can be seen in these graphs, while in both methods the droplet size and polydispersity index reduced as the surfactant concentration increased, the emulsion prepared using the PIT method had much smaller droplets (as low as 9 nm) and narrower polydispersity compared to those emulsified using the homogeniser. The smaller droplet size of nano-emulsions prepared via PIT, when compared to the homogeniser method, is due to the droplet formation mechanisms in these methods. The PIT method takes advantage of passing through the minimum interfacial tension during the heating process, easing the droplet rupture; whereas the interfacial tension is constant during homogenization. Lower interfacial tension during the PIT method results in formation of smaller droplets. Also, the rapid cooling of the system during PIT method increases the interfacial tension rapidly so that the probability of coalescence for surfactant-coated droplets decreases, improving the polydispersity index of emulsions produced via the PIT method.

Here it should be noted that, as discussed in Section 4.2.1, emulsions produced using Ultra-Turrax at 75 and 85 °C consisted of larger droplets whereas very fine emulsion was obtained at 45 °C. This might be concluded that such a large increase in temperature during Ultra-Turrax resulted in a change of the HLB of the system and when the emulsions were left to slowly cool down to room temperature, the coalescence rate increased as the system is more susceptible to coalescence when the interfacial tension is the lowest at HLB optimum (i.e. PIT temperature). On the contrary, the rapid cool down of the emulsions produced via the PIT results in a quick transition through the optimum HLB value and therefore fine emulsions were formed.

In both methods, when surfactant concentrations exceeded 15 % (w/w), the rate of reduction in the droplet size slowed down considerably (Figure 4.19). This also elaborates the fact that the rate of droplet rupture to droplet coalescence became comparable at surfactant concentrations higher than 15 % (w/w), showing that droplets are fully covered and protected against droplet coalescence. Figure 4.14 illustrates the changes in the viscosity of the emulsions in both methods when the surfactant concentration increases, showing a direct relationship, as explained in Section 4.2.3. In other words, the viscosity of nano-emulsions increases as the surfactant concentration increases [113].

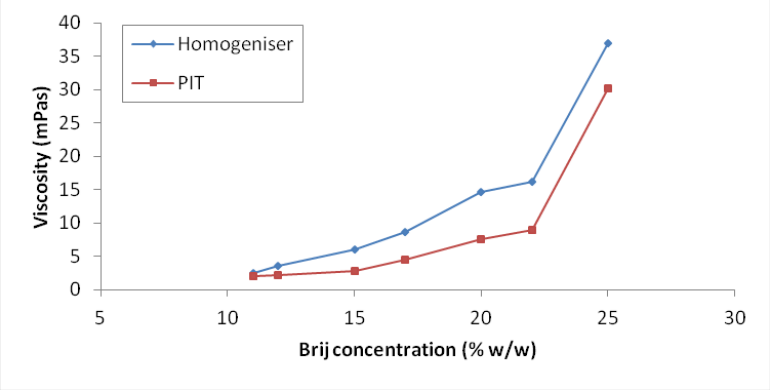

Figure 4.14: Effect of different surfactant concentrations on viscosity: Comparison of emulsion viscosities between homogeniser (45 °C, 15 min) and PIT methods using the same formulation containing 10 % (w/w) soybean oil and different surfactant concentrations.

This increase in viscosity can be correlated to either higher concentration of surfactant or droplet size of nano-emulsions. According to supplier's data sheet, the viscosity of Brij 97 is around 100 mPa s, which is 100 times of that of water and therefore, can affect the viscosity of the mixture significantly. Also, as the droplet size decreases, droplets form a finer and more packed structure so that a higher stress is required to break the structure, which results in a higher viscosity.

As seen in Figure 4.14, the emulsions prepared by the PIT method were less viscous than those emulsified by homogeniser. Although it is expected that emulsions with smaller droplets are more viscous, the higher viscosity of emulsions produced by homogeniser with larger droplets than the ones prepared via PIT might be correlated to their higher polydispersity indices.

4.3.3 Stability

Emulsion stability refers to the ability of prepared emulsions to maintain their properties unaltered over a period of time. Emulsion stability, however, is not absolute but relative, since emulsions are thermodynamically unstable in nature. The stability of an emulsion, therefore, is measured in terms of how slowly these changes occur. There are various instability phenomena that can change the emulsion properties, as has been explained in detail in Section 2.1.4. In this work, the stability of emulsions prepared using the homogeniser and PIT methods were studied by investigating two particular instability phenomena: creaming and coalescence. This was achieved by recording any changes in appearance and in droplet sizes at different time intervals over a period of one month. The latter may results in coalescence.

4.3.3.1 Creaming

As soybean oil has a lower density than water, the dispersed droplets tend to move up to form a layer at the top (i.e. creaming). Intrinsic stability was studied for each formulation. The test tubes were filled with 8 ml of the emulsion and then

hermetically closed. They were then stored vertically at room temperature (21 °C ± 2) and observed periodically to detect the occurrence of any creaming. All the experiments were performed in triplicate. The observation results for both methods of preparation are summarised in Table 4.6.

Table 4.6: Creaming observations in emulsions prepared using homogeniser and PIT methods using the same formulation containing 10 % (w/w) soybean oil and different surfactant concentrations. (X: when creaming is observed)

Homogeniser	**Creaming**							
	Homogeniser				**PIT**			
Brij 97 Concentration (%)	Fresh	14 Days	21 Days	30 Days	Fresh	14 Days	21 Days	30 Days
10.5	-	X	X	X	-	-	X	X
11	-	-	X	X	-	-	X	X
12	-	-	X	X	-	-	-	-
15	-	-	-	-	-	-	-	-
20	-	-	-	-	-	-	-	-
22	-	-	-	-	-	-	-	-
25	-	-	-	-	-	-	-	-

It can be seen that in both methods creaming occurred only in the emulsions containing lower amounts of surfactant (less than 12 % w/w). In these cases creaming occurred after three weeks, apart from the emulsions prepared using the Ultra-Turrax with 10.5 % (w/w) Brij 97, in which a slight creaming was seen in week 2. In all samples, however, the height of the cream layer was less than 2 mm, which indicates the role of the surfactant in lowering the creaming rate, bearing in mind that a creaming rate of < 1 mm per day can be neglected [24][26]. Also, the emulsions produced via Ultra-Turrax with 12 % (w/w) surfactant creamed after 21 days while those produced via PIT were stable. This indicated a better adsorption of surfactant at the interface for this method, resulting in producing finer emulsion.

According to Stokes' law (see Section 2.1.4), the creaming velocity can be reduced by minimising the density difference between the droplets and the continuous phase, whether by reducing the droplet size and/or by increasing the continuous phase viscosity. The added surfactant, in this case Brij 97, plays an important role in these three mechanisms. It not only reduces the density difference, since its density (*i.e.* 1 g ml^{-1}) is closer to the water density, but it also decreases the droplet size, as explained earlier. Finally, it can act as a thickening agent, increasing the continuous phase viscosity.

4.3.3.2 Alteration in droplet size and distribution

Furthermore, to investigate the changes in droplet size and polydispersity indices over time, which can eventually lead to coalescence, droplet size measurements were repeated at intervals up to 1 month. Measurements were taken in triplicate. Figures 4.15 and 4.16 illustrate the changes in droplet size and PdI for the emulsions prepared by the two methods.

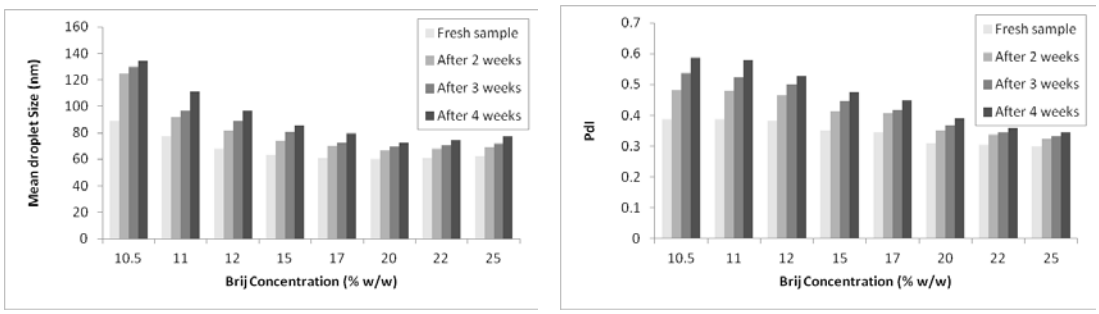

A B

Figure 4.15: Changes over time in the droplet size (A) and polydispersity index (B) of emulsions produced using the homogeniser method.

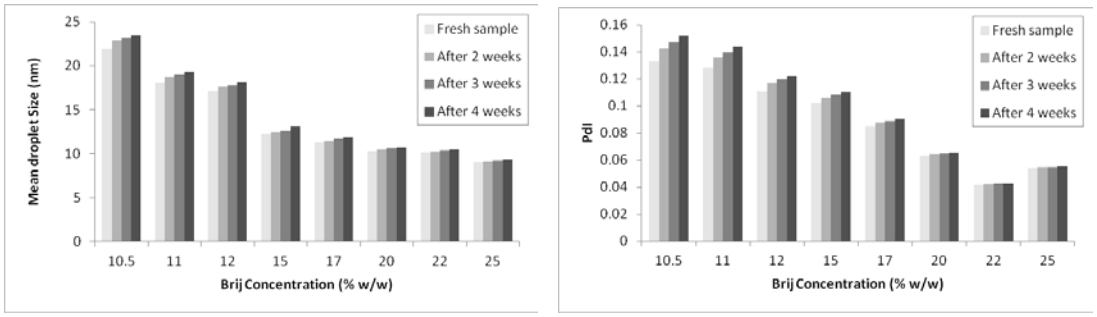

A B

Figure 4.16: Changes over time in the droplet size (A) and polydispersity index (B) of emulsions produced using the PIT method.

It can be seen that for both methods of emulsification, the droplet sizes and their polydispersity increase over time. As surfactant concentrations increase, however, the rate of change reduces. This effect is more prominent in the PIT method, where the droplet sizes in the emulsions with the highest concentrations of surfactant (more than 20 % w/w) remain almost unchanged (an increase of less than 4 % in diameter in one month was recorded). It can also be concluded from Figures 4.15 and 4.16 that the emulsions containing initially smaller droplet sizes were more stable over time than those with larger droplets. In other words, the larger the droplets in the emulsion, the more sensitive its stability is to surfactant concentration. Indeed, droplet size has a substantial effect on the dependence of stability to the level of surfactant concentration [147]. It can be seen that increasing the Brij 97 concentration has a more noticeable effect on the stability of the emulsions produced by the Ultra-Turrax, in which the initial droplet sizes are higher than those prepared using the PIT method. Figure 4.17 shows a comparison between the two methods in terms of the percentage increase in size and PdI over time. It is clear in this figure that the droplet sizes and polydispersity indices of the emulsions prepared using the PIT method did not change considerably, even when they contained the lowest amount of surfactant. In other words, they exhibited better stability compared to those produced by the homogeniser.

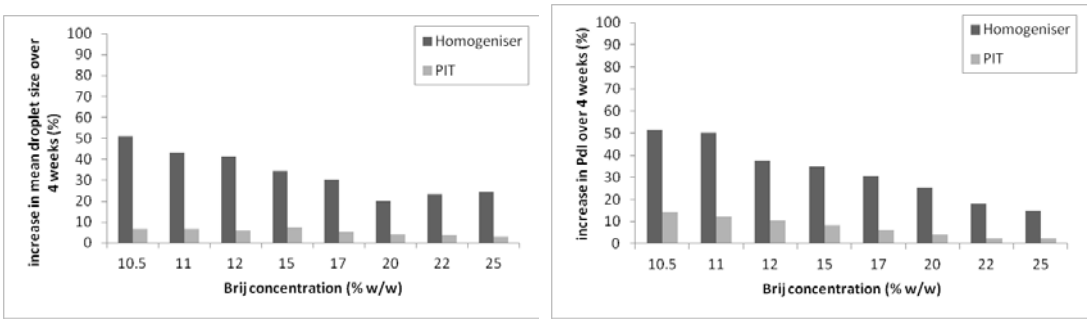

A B

Figure 4.17: Comparison of homogeniser and PIT methods in terms of percentage changes in droplet size (A) and polydispersity index (B) of the prepared emulsions over 4 weeks.

4.3.4 Energy consumption

In order to have a better understanding of the difference between these two methods in term of energy consumption, the required energy for the homogenisation and phase inversion temperature to produce emulsions were estimated.

According to the Ultra-Turrax manual, it consumes 700 W energy to run at 25,000 rpm. Therefore, it can be estimated that 378 W is required to run the device at 13,500 rpm. The specific energy consumption for Ultra-Turrax between 5 and 30 minutes was calculated to be in range of 2,000 to 14,000 J g^{-1} (Figure 4.18).

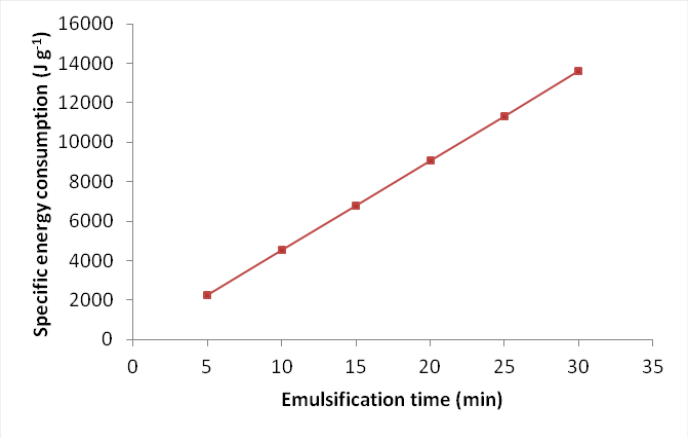

Figure 4.18: Specific energy consumption of Ultra-Turrax for different mixing times running at 13,500 rpm.

The energy consumption during PIT method can be estimated by using the thermal energy equation (see Appendix A). Experimental results (see Table 4.4) showed that the phase inversion temperature varies according to the surfactant concentration which should be considered when estimating the energy consumption. The specific energy consumption (joule per gram of emulsion) was then calculated by dividing the total energy consumption by 50 g (*i.e.* weight of emulsion). Figure 4.19 shows the variation in the specific energy consumption of PIT method at various surfactant concentrations.

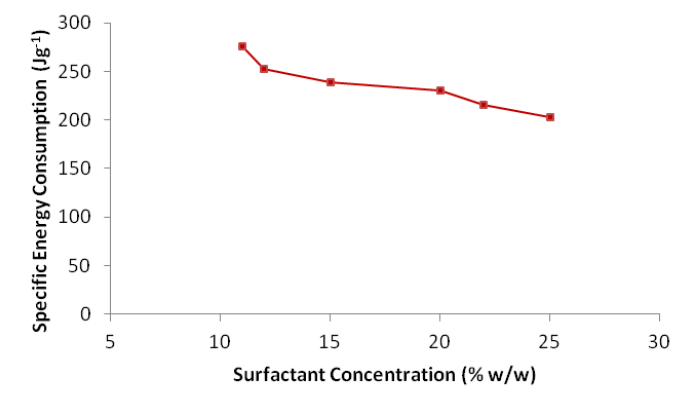

Figure 4.19: Specific energy consumption during PIT method for different surfactant concentrations

As can be seen in Figure 4.19, the required energy decreases as surfactant concentration increases. This is due to the decrease in the interfacial tension and therefore the free energy of the system (See Equation 2.1) as the surfactant concentration increases.

From a cross comparison between Figure 4.18 and 4.19, it can be seen that lower amount of energy is required during the PIT method. In addition, comparing the final average droplet size of emulsions produced via these methods with their energy input can highlight their efficiency. Figure 4.20 shows that PIT method is capable of producing relatively smaller droplets at much lower energy consumption whereas Ultra-Turrax consumes nearly 50-60 times more energy.

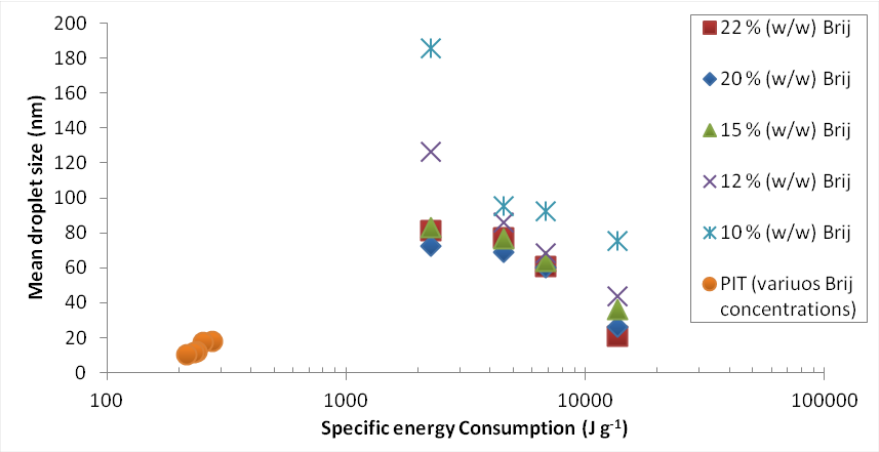

Figure 4.20: Comparison of energy consumption between homogeniser (at different mixing times) and PIT methods according to their final mean droplet sizes.

4.4 Summary

In this chapter, the oil-in-water emulsions, prepared using the rotor-stator homogeniser (Ultra-Turrax), were compared with the ones produced using the Phase Inversion Temperature (PIT) method, when using the same model system (*i.e.* water/soybean oil/Brij 97).

In the first part of this chapter, formation of nano-emulsions via Ultra-Turrax was studied. Results showed that nano-emulsions, containing 10 % oil (w/w), with mean droplet sizes as small as 60 nm were formed after mixing for 15 minutes at 13,500 rpm. This means droplet size is significantly smaller than the droplet sizes previously reported for Ultra-Turrax which were in range of 1 µm [54]. This was achievable by pre-heating the emulsion components to 45 °C. However, further increase in temperature failed to produce fine nano-emulsions due to the change in viscosity and increasing the coalescence resulting in larger droplets and higher polydispersity indices.

Investigating the effect of mixing time on the prepared emulsion showed that the steady-state droplet size in which the rate of droplet rupture and coalescence is relatively constant can be achieved after 15 minutes. Results also show that increasing the surfactant concentration leads to a better surface coverage of droplets and formation of emulsions with smaller mean droplet size. Also, increasing the oil

phase ratio results in formation of emulsions with larger mean droplet sizes, 80 to 150 nm for 20 % (w/w) oil phase ratio compared to 20 nm in the case of 5 % (w/w) oil phase ratio.

Considering the Kolmogorov length scale and experimental results, it was found that droplets lie within the viscous regime and therefore viscous equation was employed, as model, to estimate the final mean droplet size of emulsions produced via Ultra-Turrax. It was determined that arbitrary experimental constants for Ultra-Turrax at 13,500 rpm and two different mixing times of 15 and 30 min are C_e= 0.06 and C_e= 0.04, respectively, which provide a close estimation of mean droplet size to those obtained from experimental results. Also, viscosity of emulsions increases as their surfactant concentration increases and their droplet size decreases.

In the second part of this chapter, emulsions prepared by PIT method containing different concentrations of Brij 97, 10 % (w/w) soybean oil and RO water were investigated and compared with those prepared by Ultra-Turrax. The result showed that by PIT method stable nano-emulsions were produced at all surfactant concentrations higher than 11 % (w/w). These nano-emulsions were transparent in appearance, with mean droplet sizes in range of 9 to 19 nm. Therefore, the results tended to favour the use of the PIT method as for the same formulation (containing 10 % (w/w) soybean oil), PIT method yielded emulsions with approximately 80 % smaller droplet sizes than those produced by homogeniser method at much lower consumed energy. The emulsions produced by PIT were also about 65-80 % less polydispersed depending on the surfactant concentration and showed a better stability over time as opposed to those prepared by homogeniser.

All in all, it can be concluded that the PIT method is better than the homogeniser method for producing stable nano-emulsions, especially when shear sensitive materials are used. For materials with higher heat sensitivity, however, the homogeniser seems to be the more suitable method.

5. Premix (dead-end) membrane emulsification

5.1 Introduction

The purpose of the work in this chapter is to investigate the parameters affecting droplet size and size distribution in emulsions produced using the premix membrane emulsification method. Effects of various parameters on the emulsion including temperature and trans-membrane pressure; surfactant type/concentration; and finally membrane type and pore size were investigated. Through studying these parameters the aim was to find the optimum formulation for membrane emulsification to produce stable nano-emulsions. Each experiment was carried out at least three times to check for reproducibility. The maximum error in the measurements was found to be 5 %.

5.2 Contact angle measurements

In order to investigate the suitability of the ceramic and polycarbonate membranes for producing O/W emulsions, contact angle measurements were carried out using the sessile drop method. The results, as shown in Figures 5.1 and 5.2, demonstrated that both types of membranes were hydrophilic and could therefore be used in this study for O/W emulsion formation. The contact angles were measured as 55.05 ° and 59.30 ° for ceramic and polycarbonate membranes respectively.

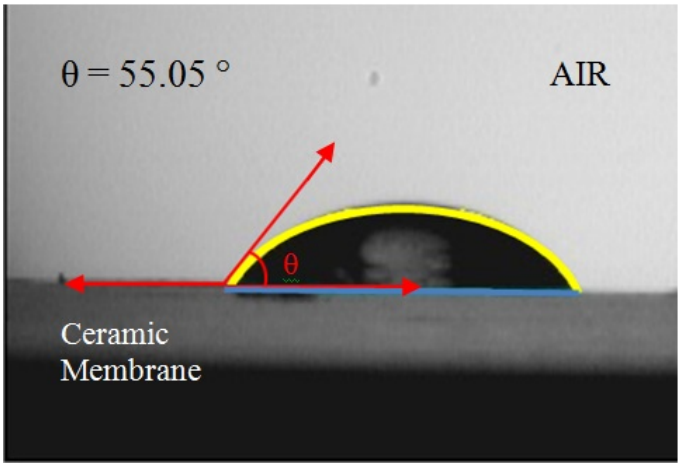

Figure 5.1: Contact angle measurement of a ceramic membrane.

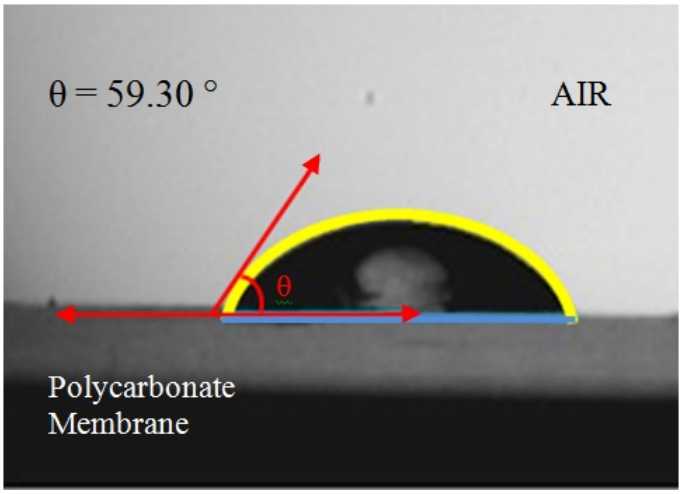

Figure 5.2: Contact angle measurement of a polycarbonate membrane.

5.3 Water flux for new membranes

As mentioned in Section 2.3.7, the dispersed phase flux (permeate flux) is one of the essential parameters in determining the final droplet size of the emulsion. It has been stated that the premix membrane emulsification outcome depends not only on the droplet size and dispersity of the resulting emulsion, but also on the flux of the emulsion through the membrane [82]. The latter is important with regard to the

economy of the whole process of membrane emulsification: the more the dispersed phase flux, the less the production time and thus the more cost effective the process for large scale industrial purposes. The permeate flux of the emulsion through the membrane during premix membrane emulsification can be calculated by the following equation:

$$J = \frac{m_e}{tA} \qquad \text{Equation 5.1}$$

Where;

J is the permeate flux (kg m^{-2} s^{-1}),

m_e is the total mass of the emulsion (kg),

t is the time required for the total mass to pass through the membrane (s),

A is the membrane area (m^2).

Fouling of the membrane is one of the main factors that can irreversibly reduce the effective pore diameter, and hence the permeate flux, and lead to inaccurate results. In order to make sure that the membrane has not been fouled during the experiments, the experimental membrane needs to be compared with newly purchased membranes in terms of their respective pure water fluxes. A successfully cleaned membrane should have a flux for clear water which can be recovered after use by the cleaning process.

The flux of pure water through the new membranes at room temperature were measured and used as a reference for the fouling investigation. RO water was forced through the membranes at different pressures applied by the nitrogen bottle connected to the sample cylinder. The water flows were measured at a time interval of 1 minute. All the measured flows in term of the dispersed phase velocity (ml s^{-1}) were then converted to water flux (kg m^{-2} h^{-1}) for the given membrane area of 4.91×10^{-4} m^2. Each measurement was performed at least three times. The measured values

were then compared with theoretical values obtained from the Hagen–Poiseuille equation (Equation 5.2).

$$J_d = \left(\frac{\varphi {r_P}^2}{8L\tau}\right)\left(\frac{\Delta P_{tm}}{\mu}\right) \quad \text{Equation 5.2}$$

where J_d is the phase flux ($m^3\ m^{-2}\ s^{-1}$), φ the porosity, r_P the average pore radius (m), ΔP_{tm} the differential pressure across the membrane (Pa), μ viscosity (Pa s), τ the tortuosity and L is the membrane thickness (m) [102]

According to Hagen–Poiseuille equation, flux rate is indirectly correlated to membrane thickness and tortuosity. In order to find the tortuosity of the membranes, the Hagen–Poiseuille equation was first rearranged as:

$$\tau = \left(\frac{\varphi {r_P}^2}{8LJ_d}\right)\left(\frac{\Delta P_{tm}}{\mu}\right) \quad \text{Equation 5.3}$$

Experimental flux values were then used to estimate the tortuosity of membranes under study. Tortuosity of ceramic and polycarbonate membranes were found to be 4.04 and 2.20, respectively. Also, the tortuosity of three polycarbonate membranes was calculated to be 7.08. Water density and viscosity were considered as 1 kg l^{-1} and 0.001 Pa s, respectively, and the porosity of three polycarbonate membrane was assumed to be as that of one membrane (i.e. 30 %). The estimated tortuosity values were then used to calculate the theoretical water fluxes using Hagen–Poiseuille equation. Graphs of experimental and theoretical water fluxes against different pressures were plotted for each membrane (Figure 5.3).

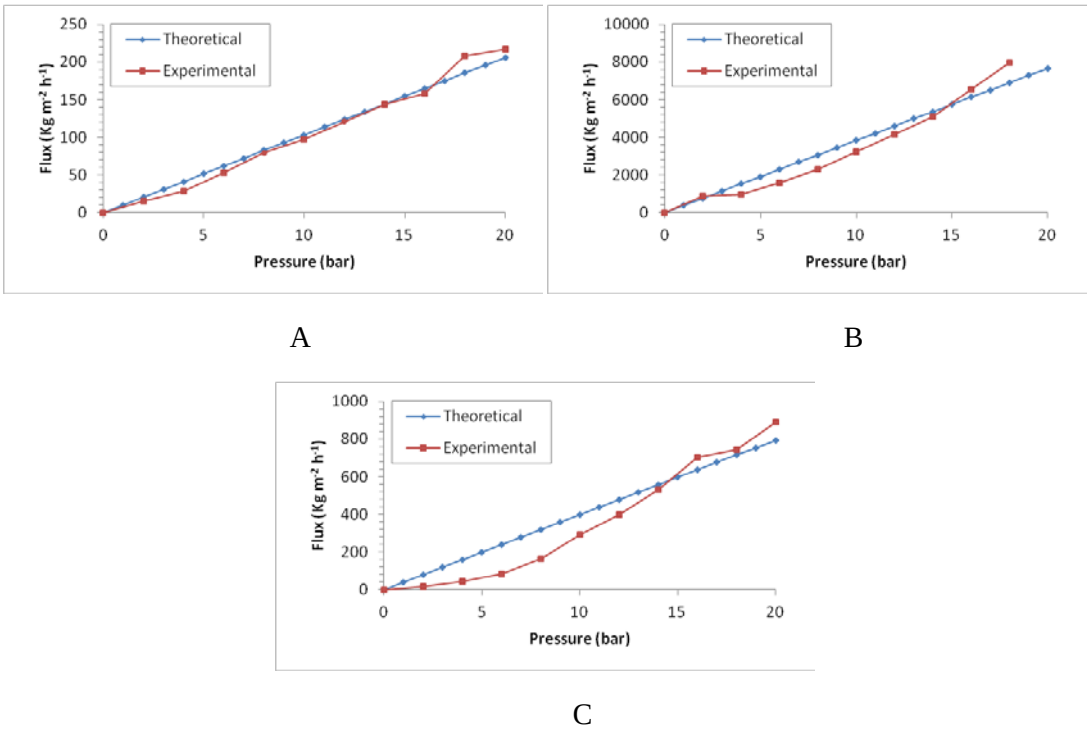

Figure 5.3: Experimental and theoretical values for water flux against pressures: A) 55 ± 6 nm ceramic membrane, B: 50 nm polycarbonate membrane, C: three polycarbonate 50 nm membranes. Experimental fluxes were measured at room temperature (20 ± 1 °C).

As it is evident in the above figures, and according to Darcy's Law (see Section 2.3.9), increasing the pressure of the dispersed phase increases the flux of water through the membrane. It has been stated by Vladisavljević (2004) that there is a direct relationship between the transmembrane pressure and water flux through the membrane [101]. However, the slight deviation of experimental values from those calculated by Hagen-Poiseuille equation could be attributed to possible errors in estimating tortuosity values.

As mentioned before, membrane fouling is another important parameter that can severely affect the membrane flux. This is a major issue in the pre-mix emulsification method. Although fouling generally happens when a large molecule such as protein is being used as a stabiliser, the oil droplets can also accumulate on the membrane surface and inside the pores and significantly reduce the effective pore size [154]. In order to prevent this phenomenon, the ceramic membranes used in this study, which were not disposable like the polycarbonate membranes, had to be

cleaned after each use. This was carried out by extruding RO water through the membrane, followed by ethanol and finally RO water again to clear any oil residues from the membrane.

5.4 Characterisation of the prepared emulsions

In this study, emulsions prepared using the pre-mix membrane emulsification method using two different types of membranes (ceramic and polycarbonate), were investigated and compared in terms of droplet size, size distribution and stability over time. Initially, Brij 97 was used to prepare the emulsions. However, preliminary experiments showed that the pre-mix emulsions contained Brij 97 failed to pass through the pores, resulting in membrane clogging. Therefore, it was decided to employ Tween 20 as main surfactant instead of Brij 97 for membrane emulsification methods. Tween 80 was then used as alternative to Tween 20 for experimental comparison.

5.4.1 Emulsification with a 55 ± 6 nm ceramic membrane

Four series of emulsions were prepared containing 10 % soybean oil and 4 % surfactant (in oil) using a 55 ± 6 nm ceramic membrane. First, the mixture of oil and surfactant was pre-heated to reach the desired temperature. This solution was then mixed with RO water (which was also preheated separately) for 4 min with an Ultra-Turrax homogeniser at a speed of 13,500 rpm. Finally, the produced coarse emulsion was loaded into the premix reservoir of the LiposoFast extruder and forced through the membrane by the pressure supplied by the nitrogen gas, set at 5 bar, while maintaining a constant temperature by means of a water bath.

For two series of emulsions, Tween 20 was used as the surfactant while the other two contained Tween 80. The emulsions were prepared at 70° and 20 °C when containing Tween 20 and at 60° and 20 °C in the case of Tween 80. The main reason for choosing 60 °C as one of the emulsification temperatures for Tween 80, as opposed

to 70 °C for Tween 20, is related to the cloud point of these surfactants. The cloud point is one of the temperature related properties of non-ionic surfactants. This is the point where the temperature passes the critical micelle temperature (CMT) resulting in phase separation of the emulsion; *i.e.* a process in which the mixture separates into two surfactant-rich and aqueous layers giving a cloudy appearance due to the dehydration of the surfactants upon temperature elevation [155]. According to the supplier's manual, the cloud points of Tween 20 and Tween 80 are 76 °C and 65 °C, respectively; so a lower temperature of 60 °C was selected as the experimental preparation temperature for the mixtures containing Tween 80 in order to avoid the phenomenon of phase separation. The droplet size and size distribution of the prepared emulsions were determined and monitored at intervals up to 1 month from the date of the experiment to evaluate their stability over time. Measurements were in triplicate. The results are summarised in Table 5.1.

Table 5.1: Characteristics of the four series of prepared emulsions over time (emulsified at 5 bar with a 55 ± 6 nm ceramic membrane). All emulsions contained 10 % soybean oil, 4 % surfactant in oil pre-mixed with RO water using Ultra-Turrax (13,500 rpm, 4 min)

Emulsion composition (w/w) (Soybean oil-Surfactant : Water) (10 % : 90 %)		**Mean droplet size (nm)**			**Polydispersity index**		
		Fresh	After 4 weeks	% change	Fresh	After 4 weeks	% change
Tween 20 (4 % in oil)	70 °C	85.3	95.1	11.49	0.448	0.547	22.10
	20 °C	96.37	112.9	17.15	0.56	0.589	5.18
Tween 80 (4 % in oil)	60 °C	51.24	57.12	11.48	0.493	0.584	18.46
	20 °C	85.1	90.2	5.99	0.582	0.624	7.22

As can be seen in Table 5.1, elevated preparation temperature resulted in formation of emulsions with smaller droplets. Also, emulsions produced with Tween 80 have smaller droplets compared to those produced with Tween 20. Droplet size is based on the forces acting on the droplet formation at the mouth of the pore. These forces, in the absence of a cross flow, are the interfacial force which acts as an adhesive

force; and detachment (i.e. shear) forces applied due to the pore wall shear and pressure gradient across the membrane [106]. Therefore, the final droplet size during membrane emulsification, in absence of cross flow, is dependant on interfacial tension, pore size, trans-membrane pressure and area of the pore as expressed by the following equation [105]:

$$r_D = \frac{F_\gamma r_p}{\Delta P_{tm} A_p} \qquad \text{Equation 5.4}$$

Where, r_D is the final droplet size (m),

F_γ is the interfacial tension force (N),

r_p is the pore radius (m),

ΔP_{tm} is the trans-membrane pressure (Pa),

A_p is the area of the pore (m^2).

Considering all membrane properties are constant, the final drop size is solely reliant on interfacial tension at constant transmembrane pressure. Figure 5.4 shows the interfacial tension between RO water and soybean oil in presence of Tween 20 and Tween 80. These values are in the range of values reported in previous studies [156][157]. It should be noted that these values are measured at room temperature (~20 °C) and surfactant is dissolved in the oil phase. Values obtained for interfacial tension between RO water and soybean oil are lower in presence of Tween 80, compared to Tween 20. This can explain formation of smaller droplets in emulsions with Tween 80. Also, as discussed in previous chapters, elevated temperatures result in a decrease in interfacial tension, which can be correlated to formation of smaller droplets at elevated temperatures for systems under study. The polydispersity indices of all samples were in the range of 0.4-0.6 showing an acceptably moderate level of monodispersity. With regard to the stability of the produced emulsions, the lowest changes in droplet sizes over time were detected in the emulsions containing Tween

80 and prepared at 20 °C with approximately 6 % alteration in droplet diameter over 4 weeks.

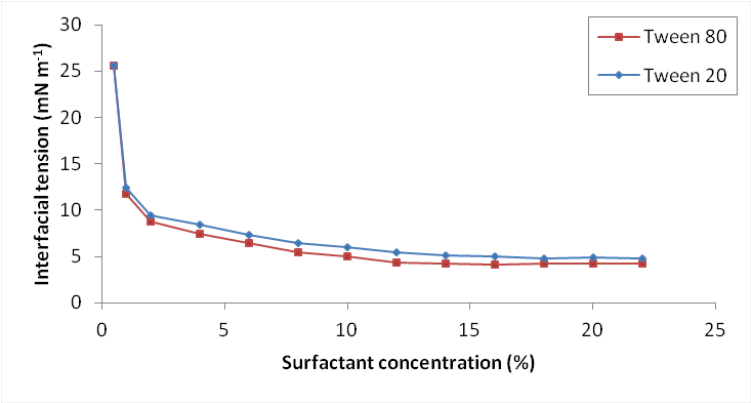

Figure 5.4: Variations in interfacial tension between RO water and soybean oil with Tween 20 and Tween 80 concentrations at 20 °C.

5.4.1.1 Effect of different oil concentrations

In order to study the effect of dispersed phase content on the droplet size and size distribution of the prepared emulsions, a new set of experiments was carried out for each of the formulations by conducting experiments at higher oil phase ratios of 20 % and 30 % with 4 % surfactant in oil. The emulsions were prepared at 70° and 20 °C when containing Tween 20 and at 60° and 20 °C in the case of Tween 80. The droplet sizes and polydispersity indices were determined for the fresh samples and at intervals within one month while storing at room temperature. The results were plotted against time, as seen in Figures 5.5 to 5.8, in order to allow comparison with the values obtained for the emulsions containing 10 % oil.

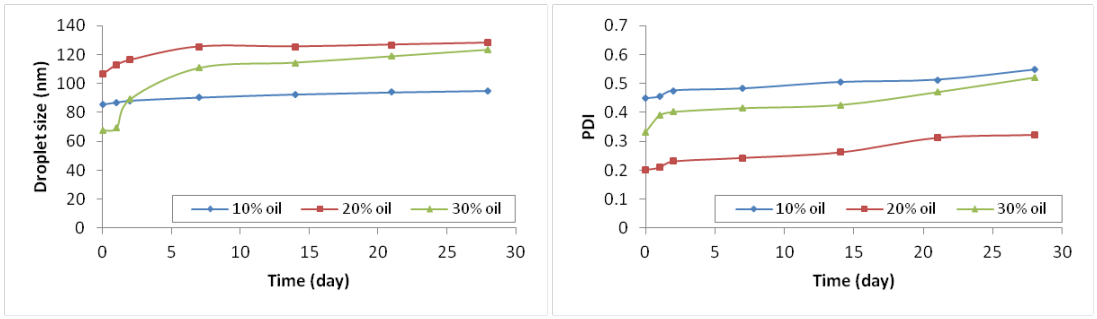

A B

Figure 5.5: Average droplet size (A) and polydispersity indices (B) over time for emulsions containing 4 % Tween 20 in oil and different oil concentrations, prepared using the pre-mix membrane emulsification method, emulsified at 70 °C and 5 bar with a 55 ± 6 nm ceramic membrane and stored at room temperature.

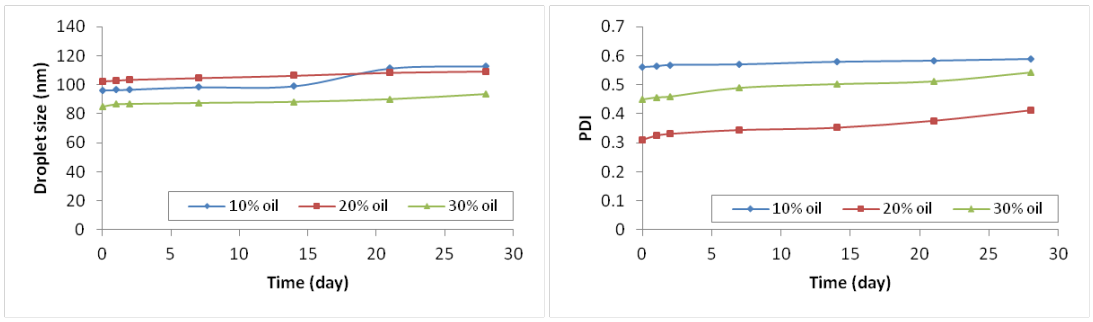

A B

Figure 5.6: Average droplet size (A) and polydispersity indices (B) over time for emulsions containing 4 % Tween 20 in oil and different oil concentrations, prepared using the pre-mix membrane emulsification method, emulsified at 20 °C and 5 bar with a 55 ± 6 nm ceramic membrane and stored at room temperature.

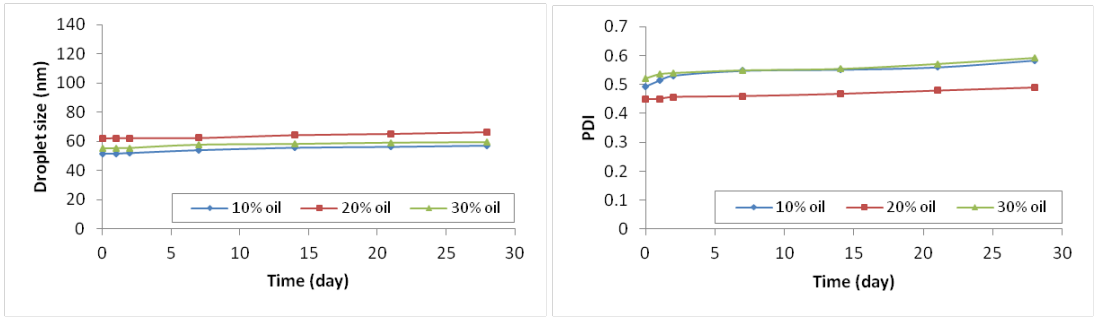

A B

Figure 5.7: Average droplet size (A) and polydispersity indices (B) over time for emulsions containing 4 % Tween 80 in oil and different oil concentrations, prepared using the pre-mix membrane emulsification method, emulsified at 60 °C and 5 bar with a 55 ± 6 nm ceramic membrane and stored at room temperature.

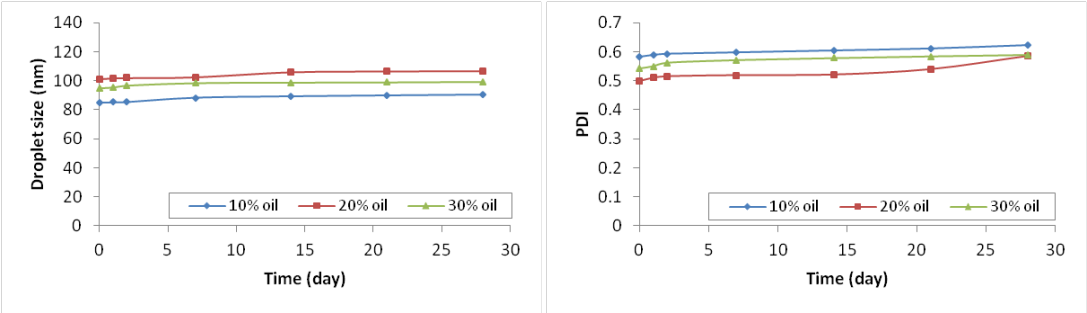

A B

Figure 5.8: Average droplet size (A) and polydispersity indices (B) over time for emulsions containing 4 % Tween 80 in oil and different oil concentrations, prepared using the pre-mix membrane emulsification method, emulsified at 20 °C and 5 bar with a 55 ± 6 nm ceramic membrane and stored at room temperature.

As can be seen in Figures 5.5 to 5.8, in all four formulations, the emulsions containing 20 % soybean oil had larger droplet size than those with 10 % oil content. Regardless of the emulsification temperature, in emulsions stabilized by both Tween 20 and Tween 80, a 20 % oil phase ratio resulted in formation of largest droplet size followed by 30 % and 10 % oil phase ratios. In the case of emulsions produced with Tween 20 at 20 °C, the droplets were even smaller in the emulsions with 30 % oil phase ratio than those with 10 % oil. With regard to the polydispersity indices, the emulsions prepared with 20 % soybean oil showed the narrowest polydispersity in all four formulations.

Here it should be noted that the surfactant was dissolved in oil phase. Therefore, as seen in Table 5.2, increasing the oil phase ratio results in presence of more surfactant in the formulation (i.e. lower interfacial tension) which can be correlated to formation of emulsions with smallest drop size at highest oil phase ratio (i.e. 30 %).

Table 5.2: Overall concentration of surfactant in the prepared emulsions at different oil phase ratios when containing 4 % surfactant in oil

Emulsion composition in % (w/w) (Soybean oil-surfactant in oil : water)	**Surfactant concentration in emulsion % (w/w)**
(10 % : 90 %)	0.4
(20 % : 80 %)	0.8
(30 % : 70 %)	1.2

However, it seems that the mean droplet sizes in an emulsion produced using pre-mix membrane emulsification is independent of the oil concentration of the dispersed phase. Indeed, according to Vladisavljević *et al*. (2004), one of the interesting features of pre-mix membrane emulsification method is that, under certain experimental conditions, the average droplet size is not dependent on the oil concentration over a wide range of 1-60 vol %. This behaviour is different from that for high-pressure homogenisers, in which, when applying a constant pressure, the average droplet size may be significantly dictated by the dispersed phase content, even in a range as small as 0.05–0.2 vol % [64][154].

According to Darcy's Law, when the oil concentration in the dispersed phase is increased, the transmembrane flux considerably decreases. At significantly low fluxes, the oil droplets may be quickly stabilised by the surfactant while passing through the membrane. Therefore, the opportunity for the droplets to coalesce as they come out of the pores becomes almost negligible [158]. In the absence of coalescence, the final mean diameter of the droplets is mainly governed by the membrane pore size and the wall shear stress inside the pores. The latter, which is the main mechanism for droplet disruption and break-up in the pre-mix membrane emulsification, is expressed by the following equation:

$$\sigma_{w,p} = \frac{8\mu_e J_d \tau}{\varphi d_m}$$ Equation 5.5

where,

$\sigma_{w,p}$ is the wall shear stress (Pa),

μ_e is the mean viscosity of emulsions inside the pores (Pa s),

τ is the mean tortuosity of the pores,

φ is the mean membrane porosity,

d_m is the mean pore size (m),

J_d is trans-membrane flux ($m^3\ m^{-2}\ s^{-1}$).

The Equation 5.5 indicates that the wall shear stress is directly related to the transmembrane flux. At higher oil concentrations, the flux is smaller; however, the dispersed phase viscosity is higher, so that at given operating conditions, the wall shear stress, and consequently the final droplet size, may become independent of the oil content [64]. This will be discussed in more detail in Section 5.4.1.6

5.4.1.2 Effect of different trans-membrane pressures

The pressure applied to the system is the most significant determining factor in the premix membrane emulsification process as, due to Darcy's Law (see Section 2.3.9), it substantially affects the dispersed phase flow through the membrane (i.e. the transmembrane flux). This subsequently influences the wall shear stress inside the membrane pores, being responsible for oil droplet disruption as explained in previous section (see Equation 5.4). Effect of wall shear stress is discussed in more detail in Section 5.4.1.6. In other words, in pre-mix membrane emulsification, transmembrane pressure provides not only the driving force for the emulsion flow through the membrane but also the required energy for droplet break-up [158].

The effect of pressure on the emulsification yield was investigated in this study by extruding coarse emulsions prepared with the same formulations as previously through the membrane, but at different trans-membrane pressures. A pre-mixture of 10 % soybean oil, 4 % Tween 20 in oil and RO water, preheated to 70 °C, was forced through the membrane when applying two different pressures of 5 and 10 bar. The droplet size and size distribution of the produced emulsions were determined and monitored at intervals over 1 month from the date of the experiment while stored at room temperature. The results are shown in Figure 5.9.

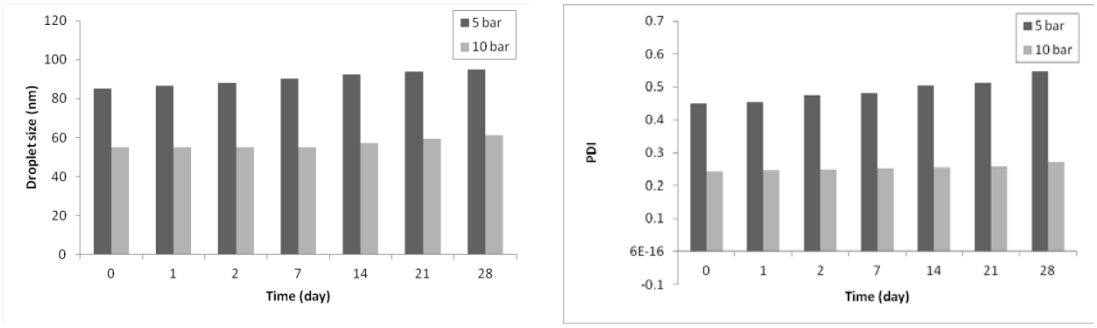

A B

Figure 5.9: Changes of droplet sizes (A) and polydispersity indices (B) over time in emulsions prepared at 70 °C and containing 10 % oil with 4 % Tween 20 in oil (10 % Soybean oil-Tween 20 : 90 % water), using the pre-mix membrane emulsification method under two different pressures of 5 and 10 bar.

From Figure 5.9, it can be concluded that smaller droplet sizes and narrower polydispersity are obtained by applying higher pressure. The same behavior was reported by Suzuki (1998) and Vladisavljević (2004) [56] [64]. The emulsions prepared at 10 bar appeared to go through less change over time, implying that they were more stable, when compared to the ones emulsified at 5 bar.

As discussed earlier, and shown in Equation 5.5, smaller droplet size at higher pressure (which is the disruption force) is due to the increase in the transmembrane flux, and consequently shear stress inside the pores, resulting in a more intensive droplet disruption. At transmembrane pressures lower than the critical pressure p_c, the droplets in the coarse emulsion, which are generally larger than the pore size, cannot pass through the membrane as the applied pressure is not sufficient to overcome the interfacial tension and deform the droplets (Figure 5.10 A). Critical pressure can be estimated according to:

$$P_c = \frac{4\gamma \cos\theta}{d_p}$$ Equation 5.6

where γ, θ and d_p are interfacial tension (N m^{-1}), contact angle (°) and pore diameter (m), respectively. The critical pressures of ceramic and polycarbonate membranes for the mixtures containing different surfactant concentrations were estimated and tabulated in Table 5.3. All estimated values are below the minimum applied pressure in this study (*i.e.* 5 bar), and hence flux through membrane is achieved.

Table 5.3: The critical pressures of ceramic and polycarbonate membranes for the mixtures containing 10 % soybean oil, different surfactant concentrations in oil and RO water, pre-mixed using Ultra-Turrax (13,500 rpm, 4 min)

Membrane	Surfactant (% w/w in oil)		Interfacial tension (mN m^{-1})	Contact angle (°)	Critical pressure (bar)
Ceramic (55 nm)	Tween 20	2	9.4	55.05	3.92
		4	8.4	55.05	3.52
		6	7.3	55.05	3.03
		8	6.4	55.05	2.67
	Tween 80	2	8.8	55.05	3.67
		4	7.4	55.05	3.08
		6	6.5	55.05	2.71
		8	5.4	55.05	2.25
Polycarbonate (50 nm)	Tween 20	2	9.4	59.3	3.85
		4	8.4	59.3	3.45
		6	7.3	59.3	2.97
		8	6.4	59.3	2.62
	Tween 80	2	8.8	59.3	3.59
		4	7.4	59.3	3.02
		6	6.5	59.3	2.65
		8	5.4	59.3	2.21

At transmembrane pressures above this critical pressure, all droplets, regardless of their size, can eventually pass through the membrane. The final droplet size, however, is dependent on the level of shear stress inside the pores. At moderate shear stresses, the large droplets of the premix are deformed at the pore inlets enabling them to enter the pores. This is followed by a moderate disruption inside the pores due to friction between the droplets and the pore walls, leading to finer droplets. The final droplet size, however, is larger than the pore size so that the droplets need to be

deformed one more time at the pore outlets to recover their spherical shape (Figure 5.10 B). Finally, at higher shear stresses, the final droplets are smaller than the pore size due to intensive disruption inside the pores caused by droplet/droplet and droplet/pore wall collisions (Figure 5.10 C). There is also no droplet deformation at the pore outlets as the final droplet size is smaller than the pore size [64].

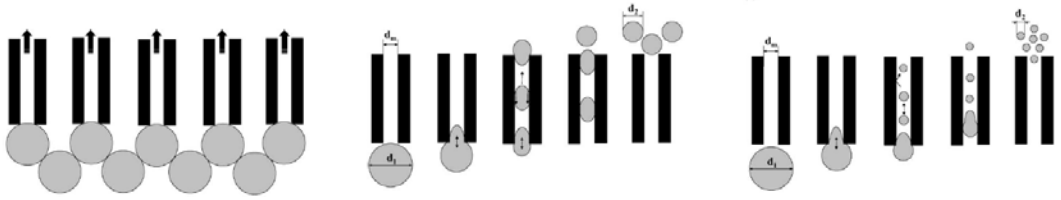

A B C

Figure 5.10: Effect of wall shear stress on droplet beak-up in premix membrane emulsification: A) no emulsification below a critical pressure, B) moderate break-up at smaller shear stresses ($d_m < d_2 < d_1$), C) intensive break-up at higher shear stresses ($d_2 < d_m < d_1$) *[64].

*d_m: membrane pore size, d_1: initial droplet size, d_2: final droplet size

5.4.1.3 Effect of different temperatures

The temperature at which the emulsion components are emulsified is one of the parameters that can affect the final outcome of the pre-mix emulsification. Temperature can affect the system in different ways, causing variation in viscosity, interfacial tension and the nature and solubility of surfactant. [17].

In order to study the effect of temperature on the droplet size and size distribution, the results obtained from the samples containing 10 % soybean oil, 4 % Tween 20 in oil prepared at 20 and 70 °C under 5 bar (see Section 5.4.1) were compared in Figure 5.11.

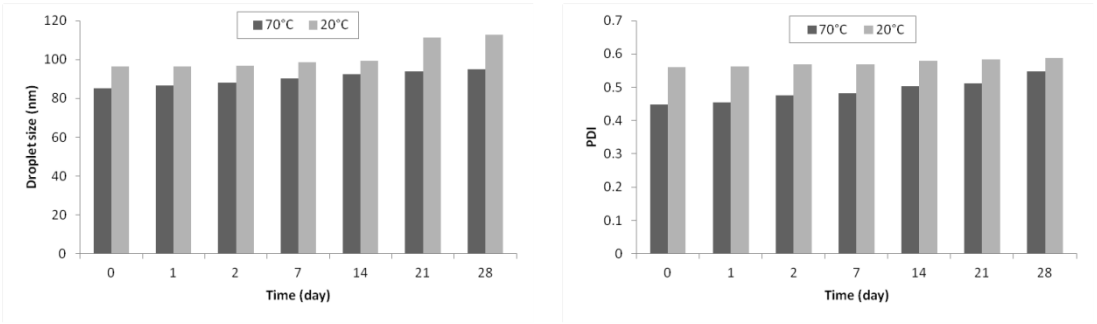

A B

Figure 5.11: Changes of droplet sizes (A) and polydispersity indices (B) over time in emulsions prepared using the pre-mix membrane emulsification method containing 10 % oil, with 4 % Tween 20 in oil (10 % Soybean oil-Tween 20 : 90 % water) and an applied pressure of 5 bar and emulsified at two different temperatures of 20 and 70 °C.

The results show that increasing the temperature from 20 °C to 70 °C resulted in smaller droplet sizes and narrower polydispersity. The emulsions prepared at 70 °C were more transparent to the naked eye and also more stable over time in that the droplet size alteration over 1 month was less than those prepared at room temperature.

The effect of increasing temperature on droplet size reduction can be explained by the influence of temperature on the viscosity of the dispersed phase and interfacial tension between two phases. Generally, surface tensions and consequently the interfacial tensions between phases decrease with increase in temperature. This is due to the higher molecular thermal activity at elevated temperature which leads to a decrease in cohesive forces [159]. According to Joscelyne and Tragardh (2000), one can increase the fluidity of the oil phase by employing elevated temperatures when producing O/W emulsions [17]. When the temperature is increased, the viscosity of the dispersed phase decreases, leading to higher transmembrane flux according to Darcy's Law. Figure 5.12 shows the effect of viscosity on flux rate in a ceramic membrane with pore size of 55 nm and estimated tortuosity of 4.04. The higher the flux and hence the higher the shear stress inside the pore, the smaller the droplets produced. This will be discussed in details in trans-membrane flux Section 5.4.1.6.

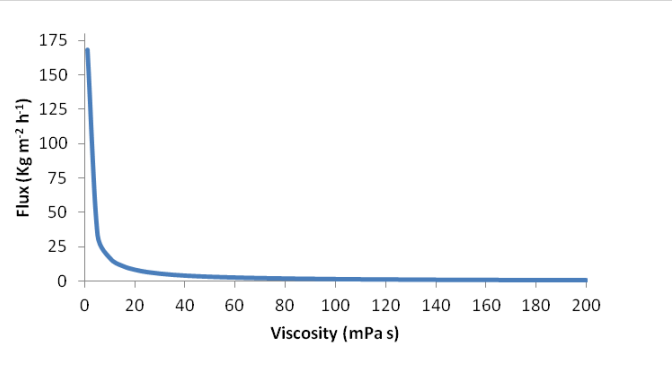

Figure 5.12: Variation in flux with viscosity of emulsion (for 55 ± 6 nm ceramic membrane, with tortuosity of 4.04 and porosity of 12 %).

5.4.1.4 Effect of different surfactants

As discussed in Section 4.2.3, the surfactant plays an important role in determining the droplet size, polydispersity and stability of the produced emulsions. In order to compare the effect of the two types of surfactants used in this study (i.e. Tween 20 and Tween 80) on the droplet size and size distribution, the results obtained from the samples containing 10 % soybean oil, 4 % Tween 20 in oil prepared at 70 °C were compared with those containing 10 % soybean oil, 4 % Tween 80 in oil prepared at 60 °C (see Section 5.3.1.1) in Figure 5.13.

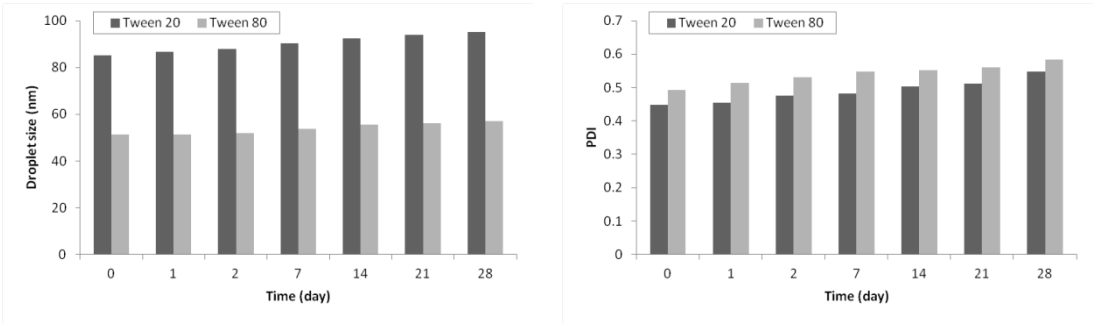

A B

Figure 5.13: Changes of droplet sizes (A) and polydispersity indices (B) over time in emulsions prepared using the pre-mix membrane emulsification method containing 10 % oil and 4 % surfactant in oil at an applied pressure of 5 bar and stabilised with two different surfactants (Tween 20 and Tween 80) at 70 °C and 60 °C respectively. (Composition: 10 % Soybean oil-Tween 20/80 : 90 % water)

As can be seen in Figure 5.13, the results showed that in the emulsions stabilised using Tween 80, the final droplet sizes were smaller than those containing Tween 20. However, their polydispersity is higher than those produced using Tween 20. With regard to the stability of the produced emulsions, however, in terms of droplet size alteration over time, no significant difference was found between two formulations.

The reason for the smaller droplets in the case of Tween 80 may be explained with regard to either their interfacial tension or their critical micelle concentration (CMC). The CMC of Tween 80 (0.0016 w/v %) is lower than that of Tween 20 (0.0074 w/v %). It has been stated that a surfactant with a lower CMC has a higher surface activity than one with a higher CMC [160]. This is also projected in lower interfacial tension between water and soybean oil in presence of Tween 80. In other words, at a given concentration, a low-CMC surfactant lowers the interfacial tension more than a high-CMC one, resulting in formation of smaller droplets. This is because the higher surface activity results in newly formed droplets being covered more quickly by the surfactant molecules required for the prevention of coalescence. In addition, as mentioned earlier, the cloud point of Tween 80 is around 65 °C. The emulsification temperature for Tween 80 is set at 60 °C which is very close to the cloud point of the surfactant and might result in ultra-low interfacial tension between oil and water, producing smaller droplets. However, the ultra low interfacial tension results in a higher coalescence rate [161] which can explain the higher polydispersity index of emulsions produced with Tween 80.

5.4.1.5 Effect of surfactant concentration

It was found in this study that by using 4 % Tween 20 in oil, stable nano-emulsions can be produced. In order to study the effect of higher surfactant concentrations on emulsions produced using the pre-mix membrane emulsification method, however, new sets of emulsions were prepared in which the concentration of Tween 20 was increased to 6 % and then to 10 %. The emulsions contained 10 % oil and were emulsified at 70 °C under a pressure of 5 bar. Each experiment was carried out at least three times to check for reproducibility. The droplet size and size distribution of

the prepared emulsions were determined and compared with those contained 4 % Tween 20 as presented in Figure 5.14.

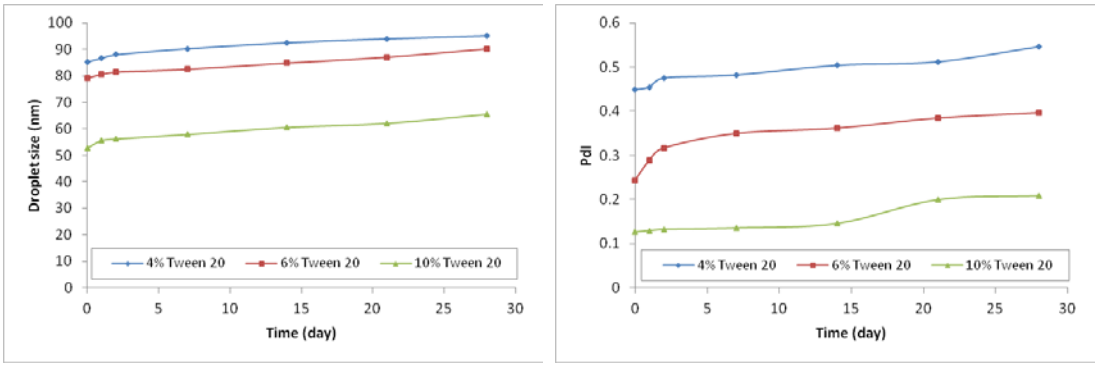

A B

Figure 5.14: Changes of droplet sizes (A) and polydispersity indices (B) over time in emulsions containing 10 % oil prepared using the pre-mix membrane emulsification method at 70 °C under 5 bar and stabilised with different concentrations of Tween 20.

The results showed that the droplet size and size distribution in the emulsions decreased with an increase in the surfactant concentration. The droplet size of emulsion produced with 10 % surfactant is very close to the membrane pore size. This can be explained by the surfactant's role in droplet formation and subsequent stabilization, as explained in detail in Section 4.2.3. The higher the surfactant concentration, the lower the interfacial tension is; leading to the formation of smaller droplets. Also, at a higher surfactant concentration, the surface of newly formed droplets is more quickly covered by the surfactant molecules, which reduces the coalescence probability during collision.

5.4.1.6 Effect of pressure and temperature on membrane flux

As mentioned in Section 2.3.7, the dispersed phase flux is an essential parameter with regard to the droplet size and size distribution of the produced emulsions, as well as the economy of the whole process of membrane emulsification. In previous sections it has been explained that the transmembrane pressure and experimental temperature had a determining influence on the droplet sizes by affecting the

transmembrane flux according to Darcy's Law. In this section, the effects of pressure and temperature on the dispersed phase flux were investigated by determining the fluxes for the pre-mixed emulsions containing different concentrations of soybean oil and 4 % Tween 20 in oil when emulsified at two different temperatures of 20 and 70 °C under two pressures of 5 and 10 bar. The calculated fluxes are compared in Figure 5.15 for different pressures and temperatures.

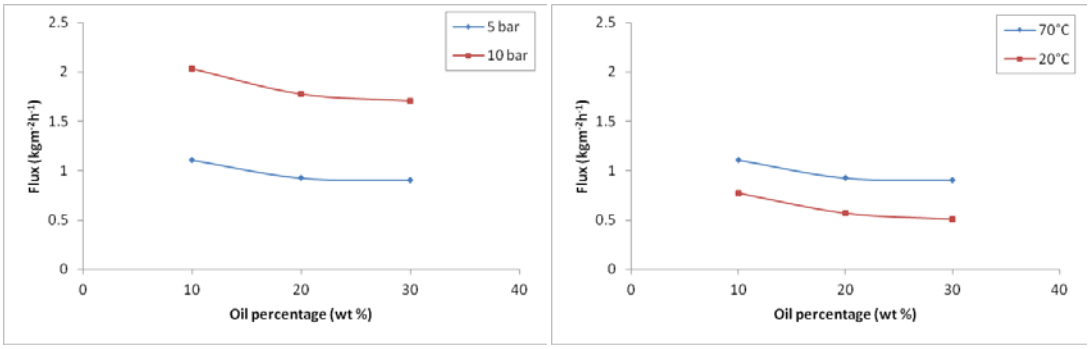

A B

Figure 5.15: Comparison of fluxes through the 55 ± 6 nm ceramic membrane with different oil concentrations: A) emulsified under two different pressures of 5 and 10 bar. (Pre-mixed emulsions contained 4 % Tween 20 in oil and were emulsified at 70 °C), B) emulsified at different temperatures of 20 and 70 °C. (Pre-mixed emulsions contained 4 % Tween 20 in oil and were emulsified under 5 bar).

As can be seen in Figure 5.15, the trans-membrane flux is inversely proportional to the oil content due to the increase in the viscosity of the dispersed phase. The results also showed that increasing the temperature or pressure led to an increase in transmembrane flux which is consistent with Darcy's Law.

Figure 5.15 shows fluxes of emulsions with different oil concentrations at different transmembrane pressures and at room and elevated temperatures. The transmembrane flux increases with increasing the transmembrane pressure and temperature; whereas it decreases with increasing oil phase ratio. As discussed earlier, Equation 5.2 (Hagen–Poiseuille equation) correlates the trans-membrane flux to membrane properties (i.e. porosity, tortuosity and thickness of membrane), transmembrane pressure and viscosity of the phase. In order to estimate the viscosity

of emulsions at various conditions outlined in Figure 5.15, the Hagen–Poiseuille equation was rearranged as:

$$\mu = \left(\frac{\varphi {r_P}^2}{8L\tau}\right)\left(\frac{\Delta P_{tm}}{J_d}\right) \qquad \text{Equation 5.7}$$

For these calculations, membrane thickness, porosity, and tortuosity were considered to be 98 μm, 12 % and 4.04. The estimated viscosities are given in Table 5.4. Apparent viscosity of emulsions increases with their oil phase ratio and transmembrane pressure, whereas it decreases with increasing temperature.

Furthermore, replacing these values into Equation 5.5 (see Section 5.4.1.1), the wall shear stress in membrane pores is calculated. The pore wall shear stress is constant for both room and elevated temperatures amounted to 70.15 Pa whereas it nearly doubled by increasing the transmembrane pressure reaching 140.31 Pa. According to these theoretical calculations, it can be concluded that smaller droplet sizes at higher transmembrane pressure is due to the higher wall shear stress inside pores. However, it appears that wall shear stress has very low effect on emulsions at higher temperature and therefore it can be concluded that lower interfacial tension at elevated temperature is the main reason for formation of emulsions with smaller droplet sizes.

Table 5.4 Estimated viscosity and wall shear stress for emulsions with different oil phase ratios at room and elevated temperatures.

Temperature °C	**Oil phase ratio (%)**	**Pressure (Bar)**	**viscosity (mPa s)**	**Flux (kg m^2 h^{-1})**	**wall shear stress (Pa)**
70°C	10	5	46.66	1.105	70.15
	20	5	55.70	0.926	70.15
	30	5	56.89	0.907	70.15
	10	10	50.63	2.037	140.31
	20	10	57.95	1.780	140.31
	30	10	60.32	1.710	140.31
20°C	10	5	66.66	0.774	70.15
	20	5	90.47	0.570	70.15
	30	5	101.49	0.508	70.15

Results in this section show that in premixed membrane emulsification, using a membrane with 55 nm pore size can produce emulsions with average droplet size of 51 to 96 nm that is in the range of 1.08 to 1.74 of the membrane pore size. This elaborates the effect of pore wall shear on droplet formation in premixed membrane emulsification. In order to have a better understanding of the effect of pore size on the final droplet size, a series of experiments were carried out using membrane with 100 nm pore size in next section.

5.4.2 Emulsification with a 100 ± 10 nm ceramic membrane

To study the effect of membrane pore size on the droplet size and size distribution of emulsions produced using the pre-mix membrane emulsification method, another set of experiments was carried out using 100 ± 10 nm ceramic membranes. Each experiment was carried out at least three times to check for reproducibility. A pre-mixture of different oil concentrations (10, 20 and 30 %), 4 % Tween 20 in oil and RO water which were preheated to 70 °C and mixed for 4 min with an Ultra-Turrax homogeniser at a speed of 13,500 rpm, was forced through the LiposoFast extruder under 5 bar.

The resulting emulsions, however, were found to be opaque and unstable. This can probably be explained with regard to the membrane thickness. The 100 ± 10 nm ceramic membranes are 48 ± 1 µm thick, almost half the thickness of the 55 ± 6 nm membranes (*i.e.* 98 ± 1 µm). It is reported in the literature that thicker membranes produce more uniform emulsions, due to the higher rate of droplet break-up inside the pores [162]. Therefore, emulsions were passed three times through the membrane to obtain emulsions with smaller droplet sizes and narrow size distribution, which are known to have better stability. Figures 5.16 to 5.18 show the resulting droplet sizes and polydispersity indices for the prepared emulsions containing different oil concentrations after each pass and their changes over time.

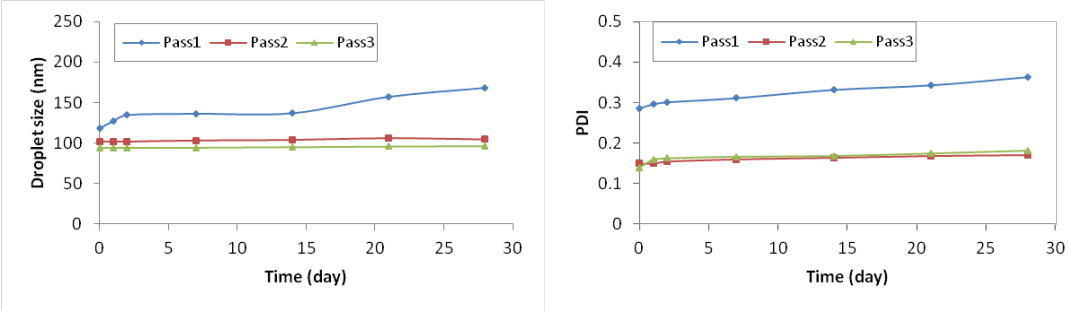

A B

Figure 5.16: Changes of droplet sizes (A) and polydispersity indices (B) over time in emulsions containing 10 % soybean oil and 4 % Tween 20 in oil prepared using the pre-mix membrane emulsification method at 70 °C and 5 bar and passed through a 100 ± 10 nm ceramic membrane three times. (Composition: 10 % Soybean oil-Tween 20 : 90 % water)

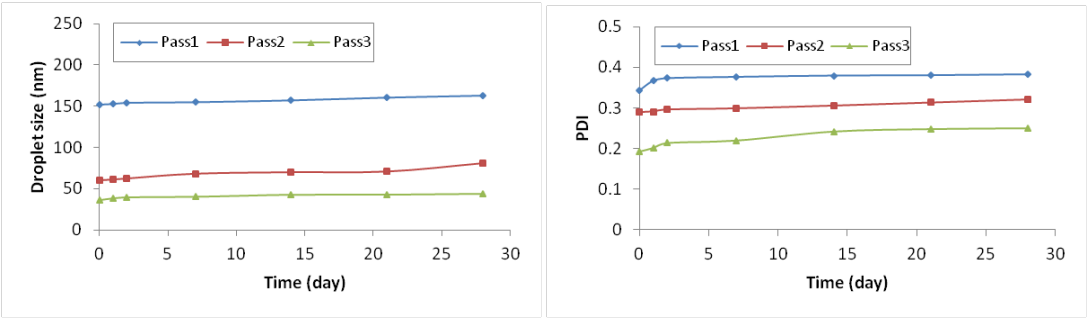

A B

Figure 5.17: Changes of droplet sizes (A) and polydispersity indices (B) over time in emulsions containing 20 % soybean oil and 4 % Tween 20 in oil prepared using the pre-mix membrane emulsification method at 70 °C and 5 bar and passed through a 100 ± 10 nm ceramic membrane three times. (Composition: 20 % Soybean oil-Tween 20 : 80 % water)

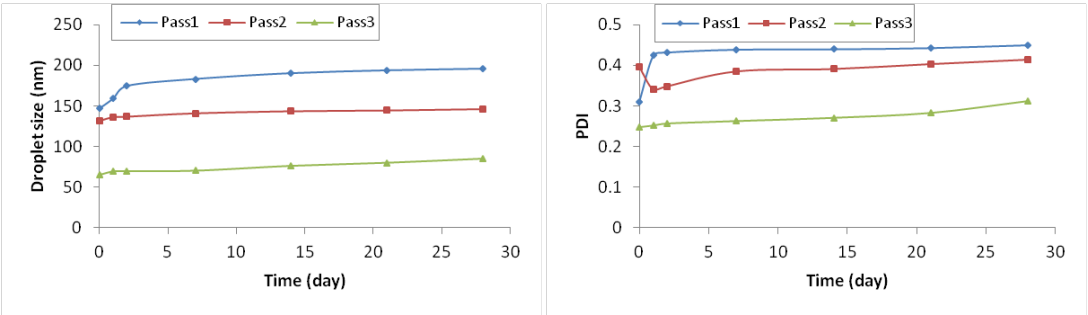

A B

Figure 5.18: Changes of droplet sizes (A) and polydispersity indices (B) over time in emulsions containing 30 % soybean oil and 4 % Tween 20 in oil prepared using the pre-mix membrane emulsification method at 70 °C and 5 bar and passed through a 100 ± 10 nm ceramic membrane three times. (Composition: 30 % Soybean oil-Tween 20 : 70 % water)

As a general trend, emulsions with smaller droplet size and better polydispersity index were obtained by increasing the number of passes. Therefore, emulsions become more transparent as the number of passes increased (see Figure 5.19). Also, results show that emulsions with small droplet size and narrow polydispersity index (i.e. emulsions obtained after three passes) have better stability. This was confirmed by zeta potential measurements which showed an increase in zeta potential values of the samples after each pass.

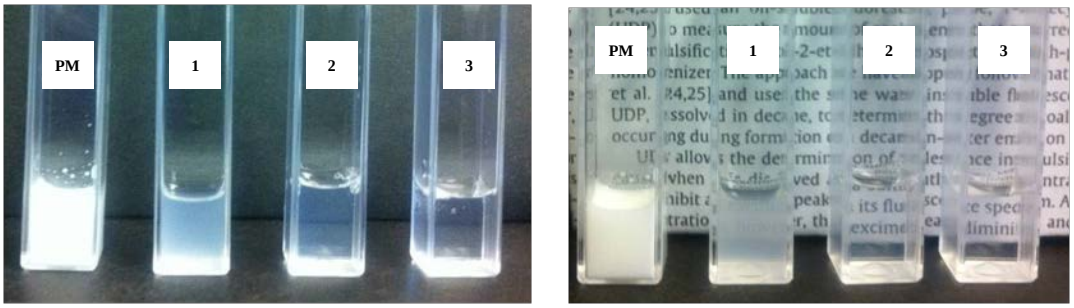

Figure 5.19: The change in appearance of an emulsion after each pass. The emulsion contained 10 % soybean oil, 4 % Tween 20 in oil emulsified at 70 °C and 5 bar and passed through a 100 ± 10 nm ceramic membrane three times.

Cross comparison between Figures 5.16 - 5.18, shows that emulsions with smallest drop size, after first pass, were formed with 10 % oil phase ratio (10 % Soybean oil-Tween 20 : 90 % water), followed by ones with 30 % and 20 % oil phase ratios. However, after three passes, emulsions with 20 % oil phase ratio (20 % Soybean oil-Tween 20 : 80 % water) have smallest drop size, followed by 30 % and 10 % oil phase ratios.

The initial pre-mix coarse emulsions consist of both large and small droplets. The first pass results in droplet break-up; forming droplets with diameters in range of the membrane pore size (see Figures 5.16 - 5.18). At each emulsification cycle, the number of small droplets increases while the number of larger droplets decreases, until a uniform fine emulsion is produced. The droplet size decreases until it reaches a value smaller than the membrane pore diameter for the second and third passes. This is due to the repeated droplet disruption (break-up) inside the pores with each

pass. Different mechanisms have been proposed for droplet break-up inside the membrane pores: 1) Snap-off due to localized shear, 2) break-up due to interfacial tension effects and, 3) break-up due to steric hindrance between droplets [58]. The higher the number of passes through the membrane, the more the droplets are affected by these mechanisms. Effects of different parameters on final droplet size will be discussed in more detail in the following sections.

5.4.2.1 Effect of oil concentration

In order to investigate the effect of oil content on the produced emulsions, the droplet sizes and polydispersity indices of emulsions containing different oil concentrations were determined after three emulsification cycles. The results are compared in Figure 5.20.

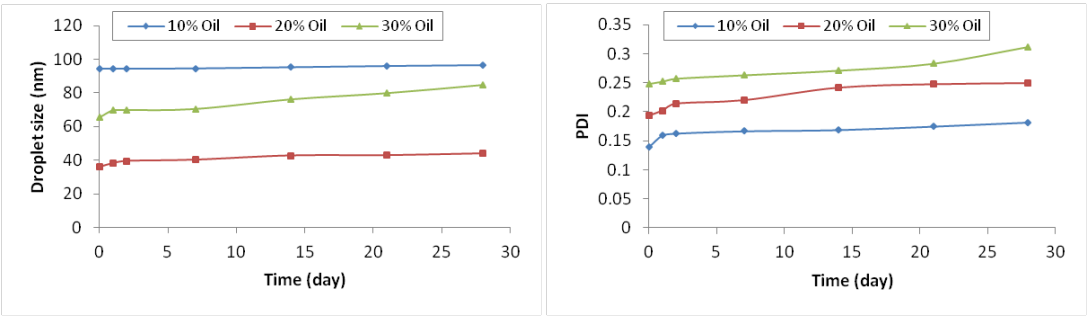

A B

Figure 5.20: Changes of droplet sizes (A) and polydispersity indices (B) over time in relation to different oil concentrations in emulsions prepared using 3-pass pre-mix membrane emulsification. Emulsions contained 4 % Tween 20 in oil and were emulsified at 70 °C under 5 bar.

As can be seen, the emulsions containing 20 % oil had the smallest droplet sizes while the ones with 10 % oil showed the narrowest polydispersity. The droplet sizes in the emulsions containing 30 % oil were larger than those with 20 % oil but smaller than the ones with 10 % oil. These results are similar to those obtained for the 55 ± 6 nm ceramic membrane experiments (see Section 5.4.1.1), therefore, the final droplet sizes were found to be independent of the dispersed phase content. The emulsions

with 10 % oil, however, were more stable since they remained almost unchanged over 1 month. Emulsions having 10 % oil phase ratio have an average droplet size of 100 nm (the largest among the studied emulsions in this section) while it has the lowest polydispersity index. While emulsions with narrow size distribution are achieved with the lowest phase ratio, increasing the phase ratio decreases the droplet size but increases the polydispersity index. Therefore one might argue that the droplet formation for low phase ratios is mostly based on formation of droplets at the pore outlet and the interfacial tension force, producing droplets with narrow size distribution; whereas at higher phase ratios the droplet formation mechanism is mostly due to the wall shear stress inside pore.

Membrane flux rate was used to estimate the wall shear stress inside membrane pore, as explained in Section 5.4.1.6 using Equations 5.7 and 5.5. Viscosities and the wall shear rate for emulsions with 10, 20 and 30 % oil are given in Table 5.5.

Table 5.5: Estimated viscosity and wall shear stress for emulsions with different oil phase ratios at elevated temperatures. Emulsions contained 4 % Tween 20 in oil and were emulsified at 70 °C under 5 bar.

Oil phase ratio (%)	**Pressure (Bar)**	**viscosity (mPa s)**	**wall shear stress (Pa)**
10	5	244.83	260.42
20	5	345.18	260.42
30	5	376.99	260.42

The estimated values show that viscosity increases with oil phase ratio; however, the wall shear rate is independent from oil phase ratio. Therefore, it can be concluded that wall shear rate has the lowest impact on droplet formation at low phase ratio of 10 % as discussed above and droplets are mainly formed at the mouth of the pores. On the other hand, the effect of wall shear rate inside pores, results in formation of smaller droplets at these higher phase ratios. The large droplet size at 30 % phase ratio, compared to 20 %, can also be correlated to the coalescence rate. Emulsions were passed three times through the membrane and therefore the possibility of coalescence rate between droplets increases and it should be higher for emulsions with higher oil phase ratio.

5.4.2.2 Effect of number of emulsification cycles on membrane flux

Typically in pre-mix membrane emulsification, the dispersed phase flux increases with an increase in the number of passes [64]. In order to investigate the effect of emulsification cycle, the permeate flux was determined for each pass of the emulsion process, with emulsions containing 10 % oil, 4 % Tween 20 in oil emulsified at 70 °C under 5 bar (10 % Soybean oil-Tween 20 : 90 % water) and plotted as presented in Figure 5.21.

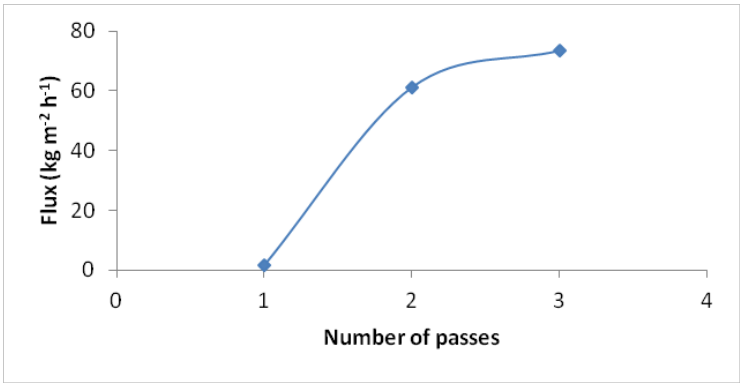

Figure 5.21: Effect of the number of passes through a 100 ± 10 nm membrane on the transmembrane flux. The emulsion contained 10 % oil and 4 % Tween 20 in oil emulsified at 70 °C under 5 bar (10 % Soybean oil-Tween 20 : 90 % water).

It is clear from the graph that in each pass, the dispersed phase flux increases. As droplets are smaller than the pore size the droplets would be expected to pass through the membrane unhindered so that lower energy was required to force the emulsions through the membrane pores at the subsequent pass. The largest change in flux was detected in the second pass, as the largest droplet size reduction happened during the first pass. The reason for the increase in transmembrane flux with each emulsification cycle can be also explained by the following equation [158]:

$$\Delta P_{tm} = \mu_e(R_m + R_{fi})J_i + C\varphi_d\gamma\left(\frac{1}{d_i} - \frac{1}{d_{i-1}}\right) \quad \text{Equation 5.8}$$

Where,

ΔP_{tm} is the trans-membrane pressure (Pa),

μ_e is the viscosity of emulsion within the pores (Pa s),

R_m is the membrane resistance (m^{-1}),

R_{fi} is the fouling resistance in the *i*th pass (m^{-1}),

J_i ($m^3\ m^{-2}\ s^{-1}$) and d_i (m) are the trans-membrane flux and final particle size in the *i*th pass,

C is a constant independent of the number of cycles,

φ_d is the volume fraction of the dispersed phase (vol %),

γ is the interfacial tension ($N\ m^{-1}$).

All parameters in Equation 5.8 are constant in three different passes except for the viscosity of emulsion which varies with the emulsion droplet size. The viscosity of emulsion for each pass was calculated using Equation 5.7 as described earlier. Results are tabulated in Table 5.6. The viscosity of emulsion decreases significantly between pass 1 and 2 which can explain the large increase in the flux between these two stages as expected from Equation 5.8; however the wall shear rate remains constant for all three passes.

Table 5.6: Variation in viscosity and wall shear stress in each pass

Pass	Pressure (Bar)	viscosity (mPa s)	wall shear stress (Pa)
1	5	244.83	260.42
2	5	7.12	260.42
3	5	5.93	260.42

As mentioned earlier, in the membrane emulsification method, the transmembrane pressure is the actual driving force for emulsion flow through the membrane (*i.e.* ΔP_{flow}) and droplet disruption inside the pores (*i.e.* ΔP_{disr}). The first and second terms of Equation 5.8 expresses ΔP_{flow} and ΔP_{disr}, respectively. When a constant pressure is applied to the system, with each emulsification cycle and consequent droplet size reduction, the second term of the equation decreases; resulting in an increase in the first term. In other words, the greater portion of the applied pressure is used for the emulsion flow through the membrane (*i.e.* dispersed phase flux). This increase in flux continues with each pass until the mean droplet size reaches the

smallest possible value at the given experimental conditions. At this point, the transmembrane flux reaches a plateau as d_i almost equal to d_{i-1} [64].

5.4.2.3 Effect of trans-membrane pressure and temperature on membrane flux

The effects of pressure and temperature on the dispersed phase flux through a 100 ± 10 nm ceramic membrane were also investigated by determining the fluxes for the pre-mixed emulsions containing different concentrations of soybean oil and 4 % Tween 20 in oil (10 % Soybean oil-Tween 20 : 90 % water) when emulsified at two different temperatures of 20 and 70 °C under two pressures of 5 and 10 bar. The measured fluxes are compared in the Figure 5.22 for different pressures and temperatures.

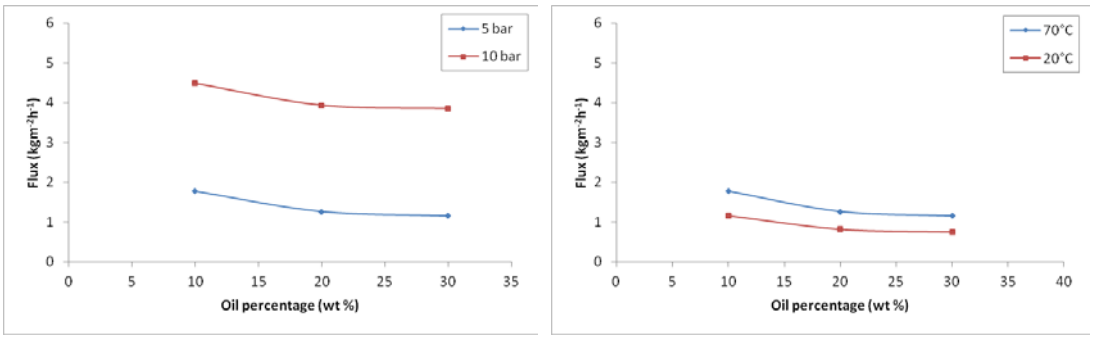

A B

Figure 5.22: Comparison of fluxes through a 100 ± 10 nm ceramic membrane with different oil concentrations: A) emulsified under two different pressures of 5 and 10 bar. Pre-mix emulsions contained 4 % Tween 20 in oil and were emulsified at 70 °C (10 % Soybean oil-Tween 20 : 90 % water), B) emulsified at different temperatures of 20 and 70 °C. Pre-mix emulsions contained 4 % Tween 20 in oil and were emulsified under 5 bar (10 % Soybean oil-Tween 20 : 90 % water)

As can be seen in Figure 5.22, the same as 55 ± 6 nm ceramic membrane, the trans-membrane flux decreased with an increase in the oil concentration and increased with an increase in the transmembrane pressure and/or temperature. Nevertheless, the fluxes were higher than those for the 55 ± 6 nm ceramic membrane as the dispersed phase flux is directly proportional to the membrane pore size (see Figure 5.23).

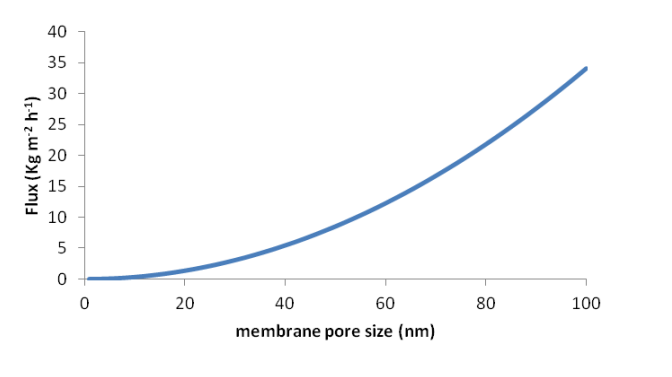

Figure 5.23: Variation in water flux with pore size (for ceramic membranes with tortuosity of 4.04 and porosity of 12 %)

5.4.2.4 Comparison of ceramic membranes with different pore sizes

Finally, in order to compare the emulsions produced by ceramic membranes with two different pore sizes of 55 ± 6 and 100 ± 10 nm, the droplet sizes and polydispersity indices of the emulsions prepared with the same formulation were plotted against time for both membranes, as presented in Figure 5.24. The emulsions were passed through the membrane once in the case of 55 ± 6 nm membrane and three times when the 100 ± 10 nm membrane used.

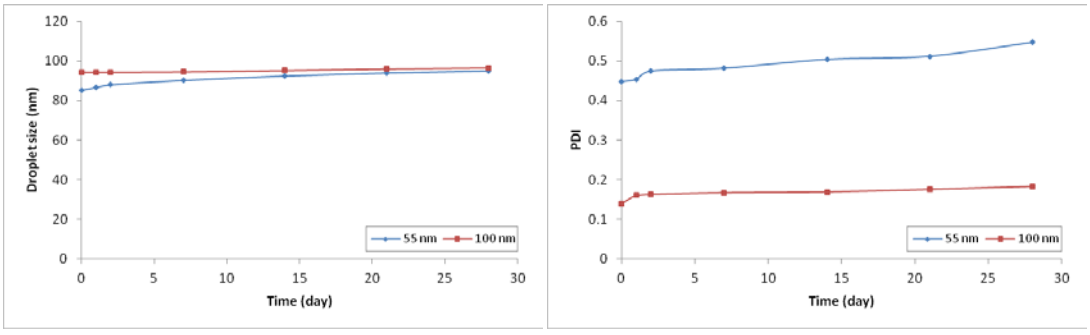

A B

Figure 5.24: Changes of droplet sizes (A) and polydispersity indices (B) over time in emulsions prepared using 55 ± 6 and 100 ± 10 nm ceramic membranes. Emulsions contained 10 % soybean oil, 4 % Tween 20 in oil with RO water and were emulsified at 70 °C under 5 bar. (Number of passes; 55 ± 6 nm: 1 pass, 100 ± 10 nm: 3 passes).

As seen in Figure 5.24, the emulsions with the same formulation and under similar experimental conditions needed to pass three times through a 100 ± 10 nm membrane to reach droplet sizes similar to those passed through 55 ± 6 nm membrane just once. Their polydispersity indices were much lower than the ones emulsified using the 55 ± 6 nm membrane, implying the advantage of multi-cycle emulsification for obtaining monodispersed emulsions. The only drawback was found to be the time and energy consumption of the process when compared to a single pass process.

5.4.3 Emulsification with a 50 nm polycarbonate membranes

As explained in Section 2.3, one of the parameters that can influence the emulsification outcome is the type of membrane being used in the process in terms of material, thickness, pore size and porosity. In this section, in an attempt to compare two different membranes; ceramic and polycarbonate membranes, three sets of emulsions containing 10 % soybean oil and different concentrations of Tween 20 (4, 6 and 10 % in oil) were prepared at 70 °C under 5 bar pressure using 50 nm polycarbonate membrane and the results were compared with those emulsified by means of almost same size ceramic membranes (55 ± 6 nm).

The preliminary experiments (not shown) showed that both using only one membrane and carrying out a one-pass process resulted in opaque and unstable emulsions. This may be explained by the very thin structure of the polycarbonate membranes. Having a thickness of just 10 μm, it produces very high fluxes, indeed, so high that the oil droplets do not stay enough inside the pores to undergo sufficient disruption. For this reason, it was decided to use three membranes inside the extruder and force through the emulsions at least three times in order to obtain finer and more stable emulsions and making comparison studies possible. In order to compare the ceramic and polycarbonate membranes with regard to the permeate flux, the water fluxes through membrane were measured and compared in Table 5.7 along with their theoretical values estimated by Hagen Poiseuille equation (see Section 5.3). As it can be seen in Table 5.7, the polycarbonate membranes can produce fluxes significantly higher than polycarbonate membranes with almost similar pore size even when three membranes are used together. As explained in Section 5.3, the difference between

experimental and theoretical values could be attributed to possible errors in estimating tortuosity values.

Table 5.7: Comparison of ceramic and polycarbonate membranes in term of experimental and theoretical water fluxes at different pressures (Experimental values were estimated at room temperature)

Membrane type	**Number of membrane used**	**Pressure (bar)**	**Theoretical water flux* ($kg\ m^2\ h^{-1}$)**	**Experimental water flux ($kg\ m^2\ h^{-1}$)**
Ceramic (55 nm)	1	5	51.57	45.89
		10	103.15	97.78
Polycarbonate (50 nm)	1	5	1917.61	1576.30
		10	3835.23	3216.61
	3	5	198.62	113.30
		10	397.25	293.35

* Estimated membrane tortuosities: 4.04 (for 55 nm Ceramic), 2.20 (for 50 nm Polycarbonate) and 7.08 (for 3x 50 nm Polycarbonate)

Interestingly, it was noted during early stages of the experiments with polycarbonate membranes that if ethanol was first passed through the membranes prior to any emulsification process, the permeate flux was significantly improved. This may be explained by the potential role of ethanol as co-surfactant acting along with the Tween 20 to reduce the interfacial tension and consequently the droplet sizes. Additionally, ethanol may prevent the accumulation of oil droplets inside the pores and consequent membrane fouling.

A series of experiments were conducted to find the optimum number of cycles for producing emulsions using three layers of polycarbonate membranes. Each experiment was carried out at least three times to check for reproducibility. Results from these experiments, at various surfactant concentrations, are presented in Figures 5.25 to 5.27.

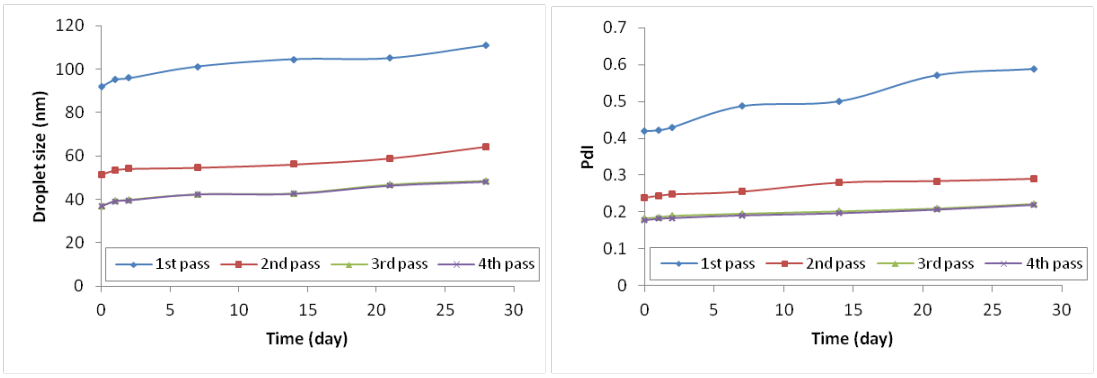

A B

Figure 5.25: Changes of droplet sizes (A) and polydispersity indices (B) over time in emulsions containing 10 % soybean oil and 4 % Tween 20 in oil prepared using the pre-mix membrane emulsification method at 70 °C and 5 bar and passed through 3× 50 nm polycarbonate membranes four times. (Composition: 10 % Soybean oil-Tween 20 : 90 % water)

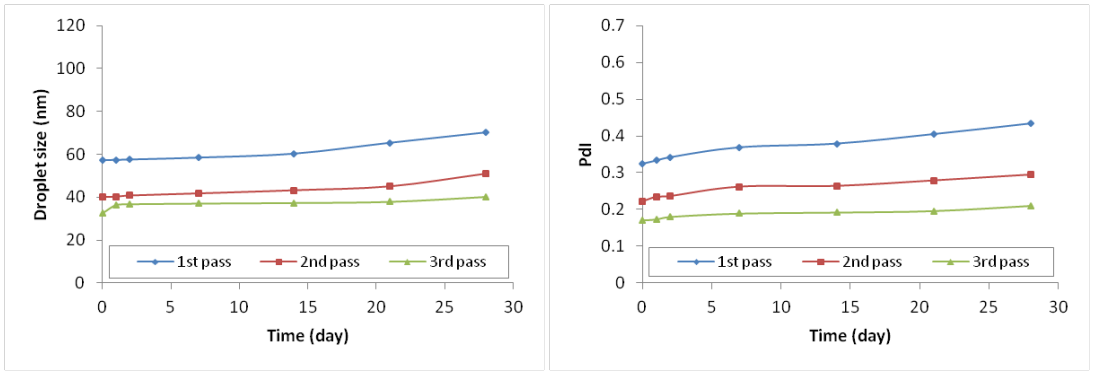

A B

Figure 5.26: Changes of droplet sizes (A) and polydispersity indices (B) over time in emulsions containing 10 % soybean oil and 6 % Tween 20 in oil prepared using the pre-mix membrane emulsification method at 70 °C and 5 bar and passed through 3× 50 nm polycarbonate membranes three times. (Composition: 10 % Soybean oil-Tween 20 : 90 % water)

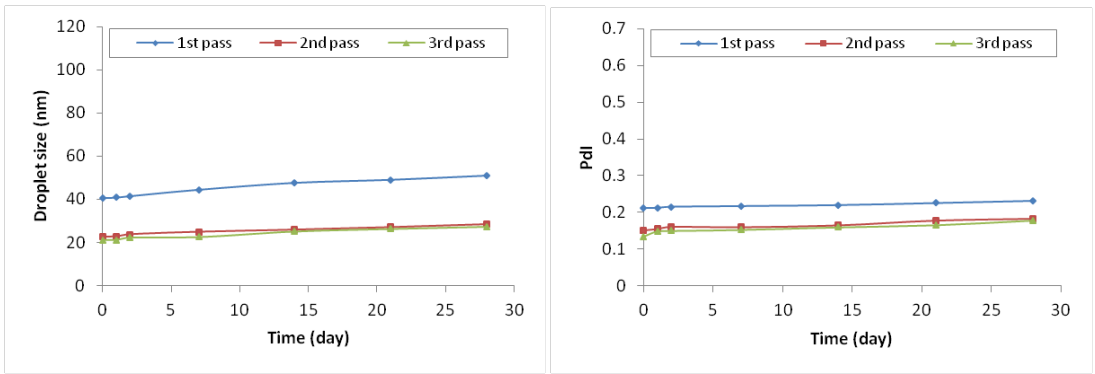

A B

Figure 5.27: Changes of droplet sizes (A) and polydispersity indices (B) over time in emulsions containing 10 % soybean oil and 10 % Tween 20 in oil prepared using the pre-mix membrane emulsification method at 70 °C and 5 bar and passed through 3× 50 nm polycarbonate membranes three times. (Composition: 10 % Soybean oil-Tween 20 : 90 % water)

Results, illustrated in Figures 5.25 to 5.27, show that a smaller droplet size is achieved after each pass of emulsions through membranes. The largest decrease in droplet size is achieved after the second cycle that diminished as the number of cycles increased, with no significant difference between the third and fourth passes. Also, decrease in the droplet size between passes decreases as the surfactant concentration increases. In addition, each pass results in a decrease in polydispersity indices. Therefore, it was concluded that three passes is sufficient to obtain fine stable emulsions with surfactant concentrations as low as 4 % in oil (10 % Soybean oil-Tween 20 : 90 % water) and this number of cycles were used for the rest of experiments in this section. In the case of the emulsions with 10 % Tween 20 in oil (10 % Soybean oil-Tween 20 : 90 % water), the change in droplet size and polydispersity index were almost negligible. It can be concluded that the higher the surfactant concentration, the lower the number of passes required. It was also found that the emulsions that underwent multiple passes showed a better stability over time compared to those forced through the membrane just once. This can be correlated to the narrower size distribution of emulsions (*i.e.* smaller polydispersity index) that passes through the membrane for multiple cycles. Effects of various parameters on produced emulsions with polycarbonate membranes will be discussed in following sections.

5.4.3.1 Effect of surfactant concentration

In order to investigate the effect of surfactant content on the produced emulsions, droplet sizes and polydispersity indices of emulsions after three emulsification cycles in presence of various surfactant concentrations were compared and depicted in Figure 5.28. As expected, the results showed that by increasing the concentration of Tween 20, the mean droplet size and polydispersity of the emulsions decreased.

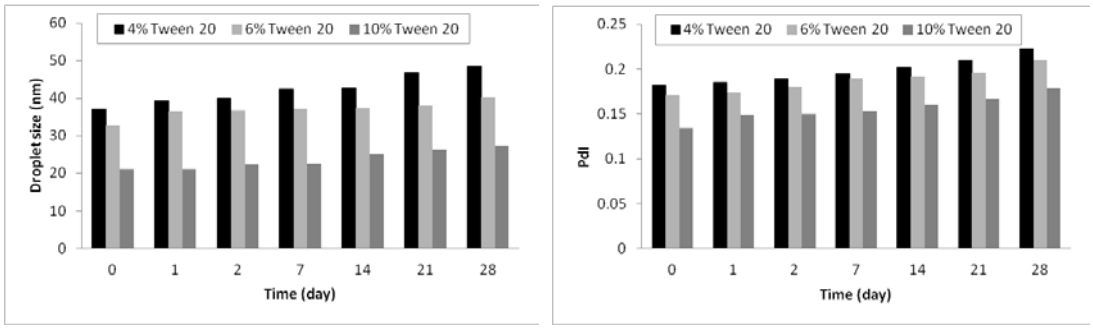

A B

Figure 5.28: Changes of droplet sizes (A) and polydispersity indices (B) over time in emulsions prepared using a 3-pass pre-mix membrane emulsification method with different concentrations of Tween 20 in oil. Emulsions contained 10 % soybean oil and were emulsified at 70 °C under 5 bar, using 3× 50 nm polycarbonate membranes. (Composition: 10 % Soybean oil-Tween 20 : 90 % water)

As discussed earlier, various forces affect droplet formation during membrane emulsification. The decrease in droplet size by increasing the surfactant concentration can be associated with the interfacial force that acts as adhesive force. As this force decreases, detachment of droplet eases. Effect of interfacial force on final droplet size can be calculated with Equation 5.4. Theoretical droplet size, using this equation, was calculated for different surfactant concentrations and tabulated in Table 5.8. Although this equation only considers the interfacial force, it can provide a relatively good estimation and it shows a decrease in droplet size by increasing surfactant concentration. Here it should be noted that these values are estimated using the interfacial tension measured at 20 °C for comparison only and to show effect of surface tension on the final droplet size.

Table 5.10: Calculated droplet size for various surfactant concentrations according to Equation 5.4

Tween 20 %	**Pressure (bar)**	**pore size diameter (nm)**	**Estimated droplet diameter (nm)**
2	5	50	75.32
4	5	50	67.54
6	5	50	58.24
8	5	50	51.20

5.4.3.2 Effect of oil concentration

In an attempt to investigate the effect of oil content on the droplet size and polydispersity of the emulsions produced with polycarbonate membranes, a new series of samples were prepared with the same experimental conditions as the third set of emulsions in Section 5.4.3. The prepared pre-mixtures were then forced through three 50 nm polycarbonate membranes in three subsequent cycles under 5 bar pressure. The experiments for the emulsions containing 30 % oil were not successful since membrane fouling occurred on every attempt. This can probably be explained by the thickness of the polycarbonate membranes in that, having a thickness of just 10 μm, these membranes, in the presence of excess oil are susceptible to fouling as a consequence of oil accumulation on the membrane surface and inside the pores (being defined as external and internal fouling, respectively) [64].

For comparison only, the results for the emulsions containing 20 % oil were plotted together with those obtained from the emulsions prepared earlier with 10 % oil content. As can be seen in Figure 5.29, when the oil concentration was increased to 20 % both the droplet size and the size distribution significantly increased. It was also found that the rate of size alteration over time was higher when the oil concentration was increased. From these results it can be concluded that polycarbonate membranes are not suitable for the emulsification of pre-mixtures with high oil content with a surfactant concentration of up to 10 % in oil.

It should be noted that three layers of polycarbonate membranes were used in these experiments. This means that emulsion passes through the first membrane and then has to find its way through the second and third one. This can result in a delay of passing emulsion between membrane layers, increasing the chance of membrane fouling and droplet coalescence. Therefore, it can be concluded that the higher droplet size resulting from these experiments for 20 % oil phase ratio, compared to the ones from ceramic membranes, could be due to the higher coalescence rate.

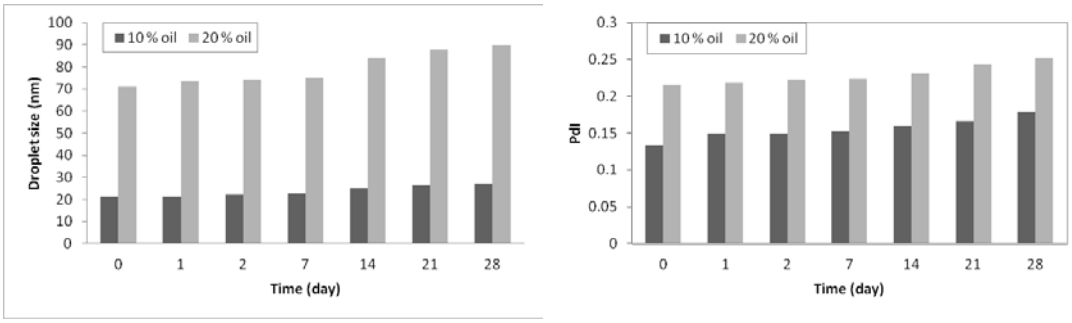

A B

Figure 5.29: Changes of droplet sizes (A) and polydispersity indices (B) over time in emulsions prepared using a 3-pass pre-mix membrane emulsification method with different concentrations of soybean oil. Emulsions contained 10 % Tween 20 in oil and were emulsified at 70 °C and 5 bar using 3× 50 nm polycarbonate membranes.

5.4.3.3 Comparison of polycarbonate and ceramic membranes

Finally, the droplet size and polydispersity indices of the emulsions prepared with the two types of membranes under similar experimental conditions are presented in Figure 5.30 for comparison.

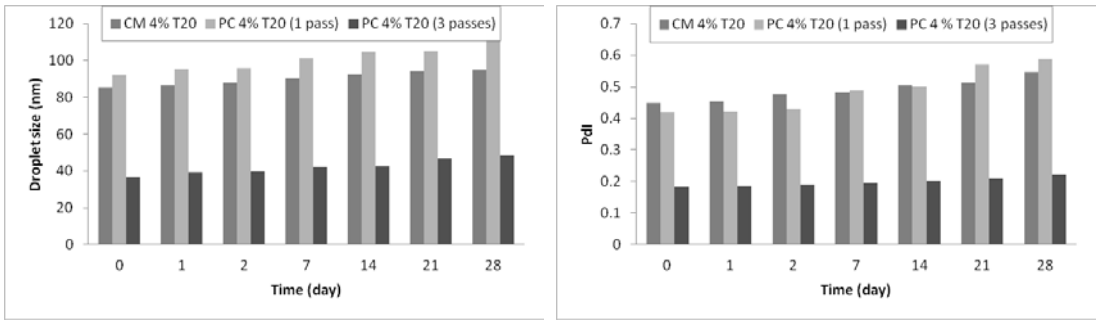

A B

Figure 5.30: Changes of droplet sizes (A) and polydispersity indices (B) over time in emulsions prepared using a pre-mix membrane emulsification method with different membrane materials. Emulsions contained 4 % Tween 20 in oil and were emulsified at 70 °C and 5 bar. (CM: ceramic membrane, PC: polycarbonate membrane (3x), T20: Tween 20)

As can be seen in the Figure 5.30, in the case of one emulsification cycle, the emulsions prepared using 50 nm polycarbonate membranes have larger droplet sizes and wider polydispersity than those produced with the ceramic membranes with an almost similar pore size (55 ± 6 nm), even though three polycarbonate membranes were used. This is probably due to their thicknesses being one tenth of the corresponding ceramic membranes. Formation of large droplets via polycarbonate membrane is due to its hydrophobicity (compared to ceramic membrane). As the polycarbonate membrane is less hydrophilic, it has higher affinity for oil, therefore the oil droplets stay longer at the pore outlets and expand more. This can also result in a higher coalescence rate. In addition, as three layers of membrane are used, the probability of droplets coalescence between these layers increases significantly. Nevertheless, when the number of passes increased, the resulting droplet sizes became noticeably smaller with narrower polydispersity indices and, more importantly, a lower rate of alteration over time, i.e. better stability.

Similar results were obtained with higher surfactant concentrations. As can be seen in Figures 5.31 and 5.32, for any surfactant concentration investigated, the emulsions prepared with three layers of polycarbonate membranes were finer and more stable after 4 weeks compared to those emulsified with a ceramic membrane, although it should be noted that they needed to be passed through the membranes more than once.

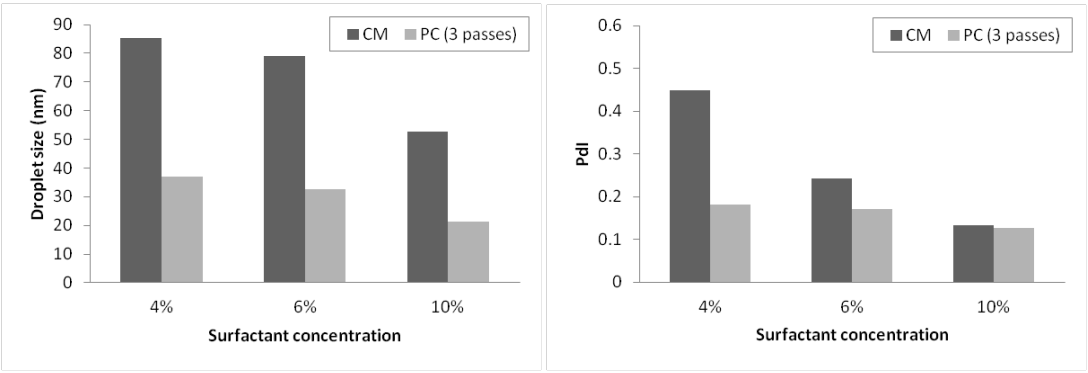

A B

Figure 5.31: Comparison of droplet size (A) and polydispersity indices (B) for emulsions containing different concentrations of Tween 20 in oil (10 % Soybean oil-Tween 20 : 90 % water) prepared using the pre-mix membrane emulsification method with different

membrane materials (emulsified at 70 °C and 5 bar) (CM: ceramic membrane, PC: polycarbonate membrane (3x)).

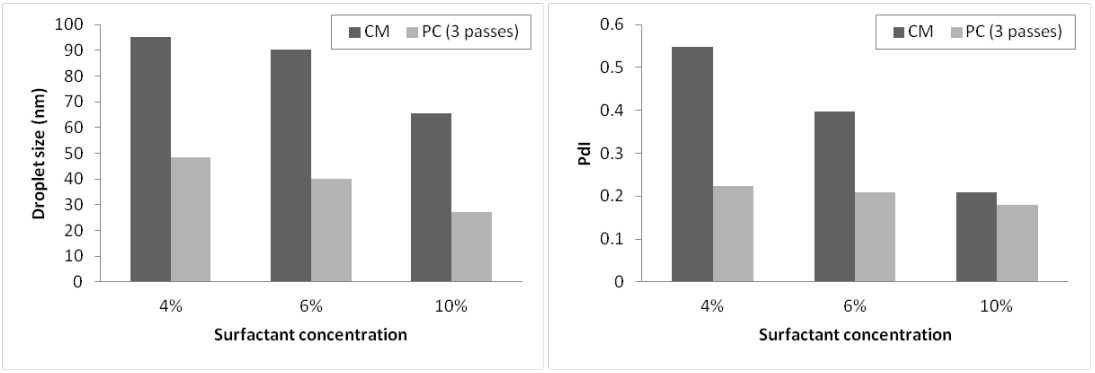

A B

Figure 5.32: Comparison of droplet size (A) and polydispersity indices (B) for emulsions containing different concentrations of Tween 20 in oil (10 % Soybean oil-Tween 20 : 90 % water) prepared using the pre-mix membrane emulsification method with different membrane materials (emulsified at 70 °C and 5 bar) after 4 weeks' storage at room temperature under the same conditions (CM: ceramic membrane, PC: polycarbonate membrane (3x)).

5.4.3.4 Energy consumption

In order to estimate the overall energy consumption during emulsification, the energy consumption for producing the pressure, pre-mixed emulsion and heat (for experiments conducted at elevated temperature) need to be added together. It was considered that the volume inside the extruder is being compressed by the applied pressure from gas cylinder. Therefore, in absence of data for energy consumption for the pressurised cylinder, the power from volume-pressure estimation was used as the energy consumption for membrane emulsification. This compressed volume is considered to be equal to the volume of the emulsion and therefore the work of it can be estimated according to volume-pressure Equation (See Appendix C). The work done by applied pressure was calculated to be 5 and 10 J for experiments conducted at 5 and 10 bar, respectively. Energy consumption for pre-mixed emulsion was also

estimated as discussed in Section 4.3.4. The consumed energy for heating the materials where the experiments carried out at 60° and 70° C were calculated by using the thermal energy equation (see Appendix A). All the estimated energy consumptions for different parts of dead-end membrane emulsification are tabulated in Table 5.9.

Results show that the energy consumption for the dead-end membrane emulsification lies in the range of 9,139 to 9,440 J g^{-1}. These values are within the range of energy consumption estimated for Ultra-Turrax experiments which are significantly higher than the values for phase inversion temperature experiments. This is mainly due to the use of Ultra-Turrax for preparing the coarse premix emulsions and also conducting experiments at elevated temperatures while the membrane emulsification itself does not require high energy consumption.

Table 5.9: Estimated specific energy consumption for different experimental setup studied in this chapter. Energy consumption estimated for pre-mixed emulsion, pressure work for passing emulsion through the membrane and keeping temperature at elevated temperatures.

Surfactant	Temperature (°C)	Applied pressure (bar)	Emulsion composition * in % (w/w)	Specific energy consumption (J g^{-1})			
				Pre-mixed emulsion (J g^{-1})	Temperature increase (J g^{-1})	Membrane emulsification (J g^{-1})	Total (J g^{-1})
Tween 20 (4 % in oil)	20	5	10 : 90	9138.71	0	0.50	9139
			20 : 80	9206.40	0	0.51	9207
			30 : 70	9275.10	0	0.51	9276
		10	10 : 90	9138.71	0	1.01	9140
			20 : 80	9206.40	0	1.01	9207
			30 : 70	9275.10	0	1.02	9276
	70	5	10 : 90	9138.71	228.60	0.50	9368
			20 : 80	9206.40	215.00	0.51	9422
			30 : 70	9275.10	201.20	0.51	9477
		10	10 : 90	9138.71	228.60	1.01	9368
			20 : 80	9206.40	215.00	1.01	9422
			30 : 70	9275.10	201.20	1.02	9477
Tween 80 (4 % in oil)	20	5	10 : 90	9139.63	0	0.50	9140
			20 : 80	9208.27	0	0.51	9209
			30 : 70	9277.95	0	0.51	9278
		10	10 : 90	9139.63	0	1.01	9141
			20 : 80	9208.27	0	1.02	9209
			30 : 70	9277.95	0	1.02	9279
	60	5	10 : 90	9139.63	182.89	0.50	9323
			20 : 80	9208.27	172.02	0.51	9381
			30 : 70	9277.95	160.98	0.51	9439
		10	10 : 90	9139.63	182.89	1.01	9324
			20 : 80	9208.27	172.02	1.02	9381
			30 : 70	9277.95	160.98	1.02	9440

* Soybean oil : surfactant in oil : water

5.5 Summary

Formation of nano-emulsions through pre-mixed membrane emulsification was studied in this chapter. Two sets of experiments, using membranes made with ceramic and polycarbonate, were conducted and effects of various parameters on final droplet size were investigated, with a focus on finding the optimum formulation to produce stable nano-emulsions.

In the first part, emulsions prepared using ceramic membranes with two pore sizes of 55 and 100 nm, under various experimental conditions were investigated. It was found that fine emulsions with a reasonable stability over time can be produced by using both Tween 20 and Tween 80 as surfactant at concentrations as low as 4 % in oil. The size of droplets, size distribution and stability, however, could be improved by increasing the applied pressure, experimental temperature and surfactant concentration. The mean droplet sizes seemed to be independent of the oil content of the dispersed phase. Emulsions produced with Tween 80 have smaller droplets compared to those produced with Tween 20, however the overall stability of the prepared emulsions did not show a noticeable difference when compared to those stabilised by Tween 20. It was found that when using a 100 ± 10 nm ceramic membrane, the premix emulsions need to pass through the membrane at least three times in order to obtain fine and stable emulsions. The obtained droplet sizes after three passes were comparable to the 55 ± 6 nm ceramic membrane but exhibited narrower polydispersity and better stability over time. With each emulsification cycle, the dispersed flux improved significantly until the droplet sizes reached the smallest possible size determined by the experimental conditions.

In the second part, a different type of membrane (polycarbonate) was used to produce emulsions and the results were compared to those prepared with a ceramic membrane with a similar pore size. Because the polycarbonate membrane is thin (just 10 μm), it was found that in order to obtain fine and stable emulsions, three membranes needed to be stacked up in the extruder and the pre-mixtures were required to be forced through the membranes a number of times. It was also realized that by passing ethanol through the membrane before each experiment, the flux could be significantly improved. For emulsions containing 4 % Tween 20, three

emulsification cycles were found to be sufficient to produce stable emulsions. When the surfactant concentration was increased to 10 %, the number of passes could be reduced to two. Furthermore, the effect of oil content on the emulsification outcome was investigated and it was concluded that polycarbonate membranes were not suitable for the emulsification of premix emulsions with high oil concentrations. In comparison, the ceramic membrane could produce smaller droplet sizes with narrower polydispersity than the polycarbonate membrane with just one emulsification cycle, but if emulsions were forced through a polycarbonate membrane more than once the resulting emulsions were finer and more stable.

Energy consumption calculations for membrane emulsification experiments in this study show that the system under study consumed similar amount of energy to the Ultra-Turrax experiments due to the use of this method for preparing the premix emulsions and also conducting experiments at elevated temperatures. As expected, the membrane emulsification itself does not require a high amount of energy.

6. Cross-flow membrane emulsification

6.1 Introduction

As explained in Section 2.2.2.2.2, the cross-flow membrane emulsification method involves passing the dispersed phase through a microporous membrane into flowing continuous phase (Figure 6.1). The aim of the work in this chapter is to investigate the effectiveness of this method in producing stable oil-in-water emulsions. For this purpose and based on the cross-flow membrane emulsification principles, an experimental rig was designed and constructed to produce emulsions (Figure 6.2). In this set-up, the dispersed phase (*i.e.* soybean oil) is pushed through the membrane, by a pressurised vessel, into the continuous phase (*i.e.* RO water & surfactant) while the continuous phase is re-circulated in the system by a pump. Figure 6.3 illustrates the piping and instrumentation diagram/drawing (P & ID) of the rig.

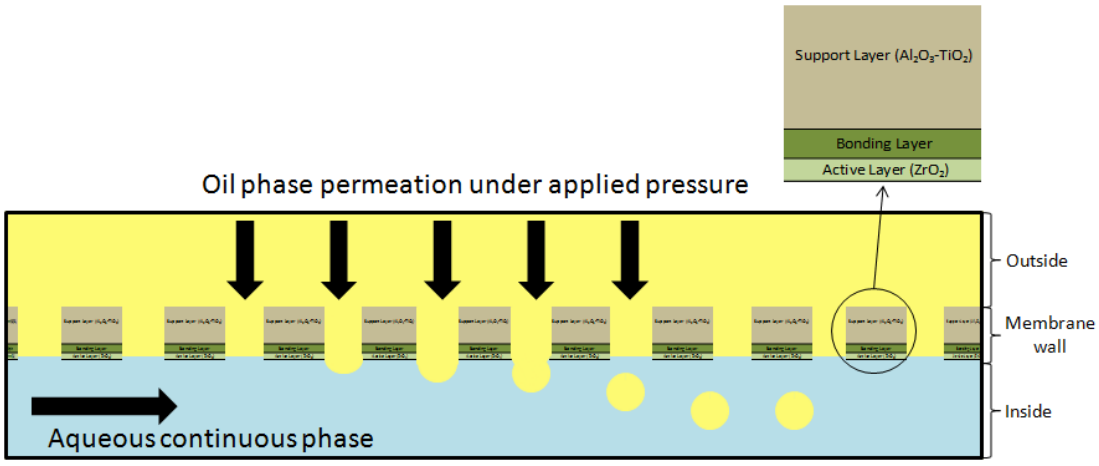

Figure 6.1: Schematic view of cross-flow membrane emulsification method

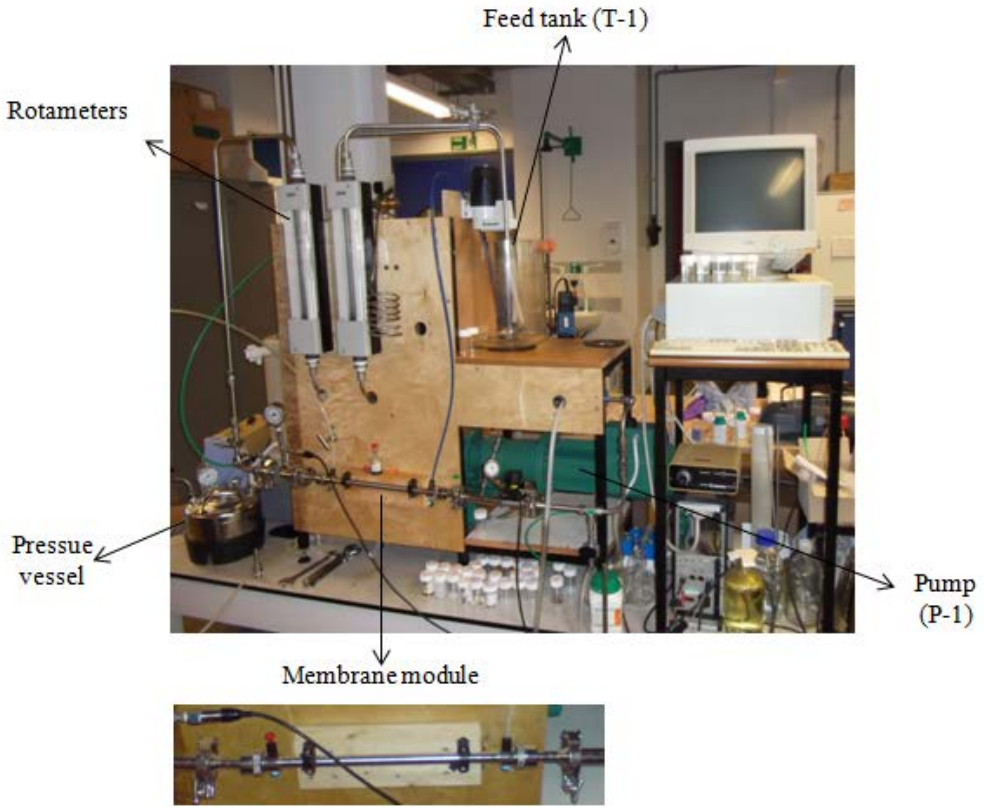

Figure 6.2: Experimental rig for cross-flow membrane emulsification

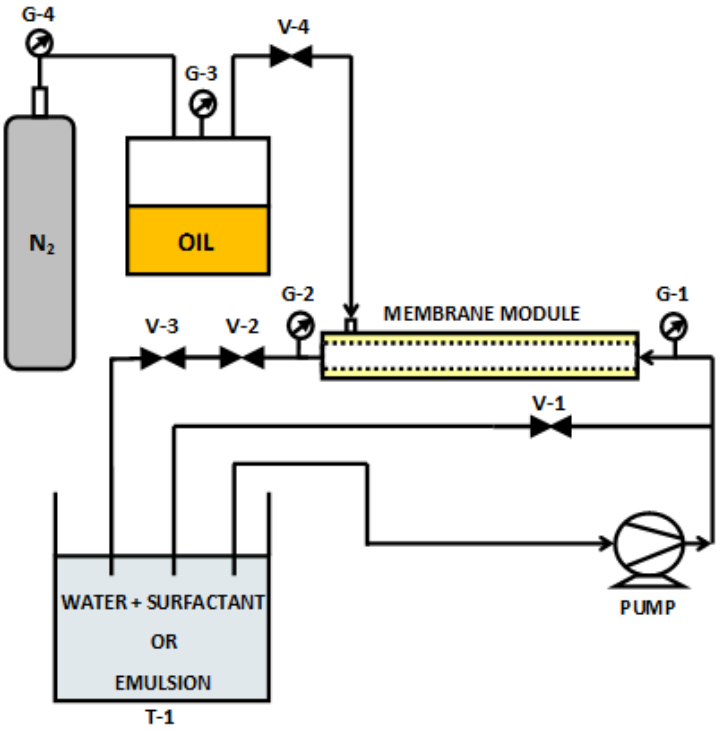

Figure 6.3: P & ID of the final experimental set-up for the production of emulsions using membrane emulsification method (see Appendix D for coding)

Certain steps should be followed when setting the experimental rig for every experimental run. The principles of setting and maintaining the rig can be found in Appendix F. Furthermore, in order to make sure there is accuracy in the process and all the measurements it is important to calibrate the devices in the rig. Calibration can also help to find the limitations of the system which needs to be considered when improving future experiments. The calibration process for both pump and rotameter are explained in detail in Appendix G. After calibrating the experimental rig, a series of emulsions with different surfactant concentrations were prepared and effects of various parameters on resulting droplet size were studied. Each experiment was carried out at least three times to check for reproducibility. The maximum error in the measurements was found to be less than 5 %.

6.2 Experimental results

6.2.1 Membrane characterisation

6.2.1.1 SEM investigation

After scanning prepared samples of 300 kD and 0.1 µm membranes by SEM, the obtained images were analysed by ImageJ software. The images show that the membrane is made up of three separate layers. It can be seen from the membrane cross-section images that the inner (active) layer has the finest grains (Figure 6.4) while the outer (support) layer consists of more coarse grains and also has the greatest thickness (Figure 6.5). The bonding layer which adheres the active layer to the support layer is the thinnest one (Figure 6.4). Figure 6.6 shows the inner and outer surfaces of the membrane, which shows the grains on the outside surface are slightly more close to each other than those inside the membrane. The longitudinal cross-section views were not much different from cross section views regarding the structure and sizes of the grains (Figure 6.7).

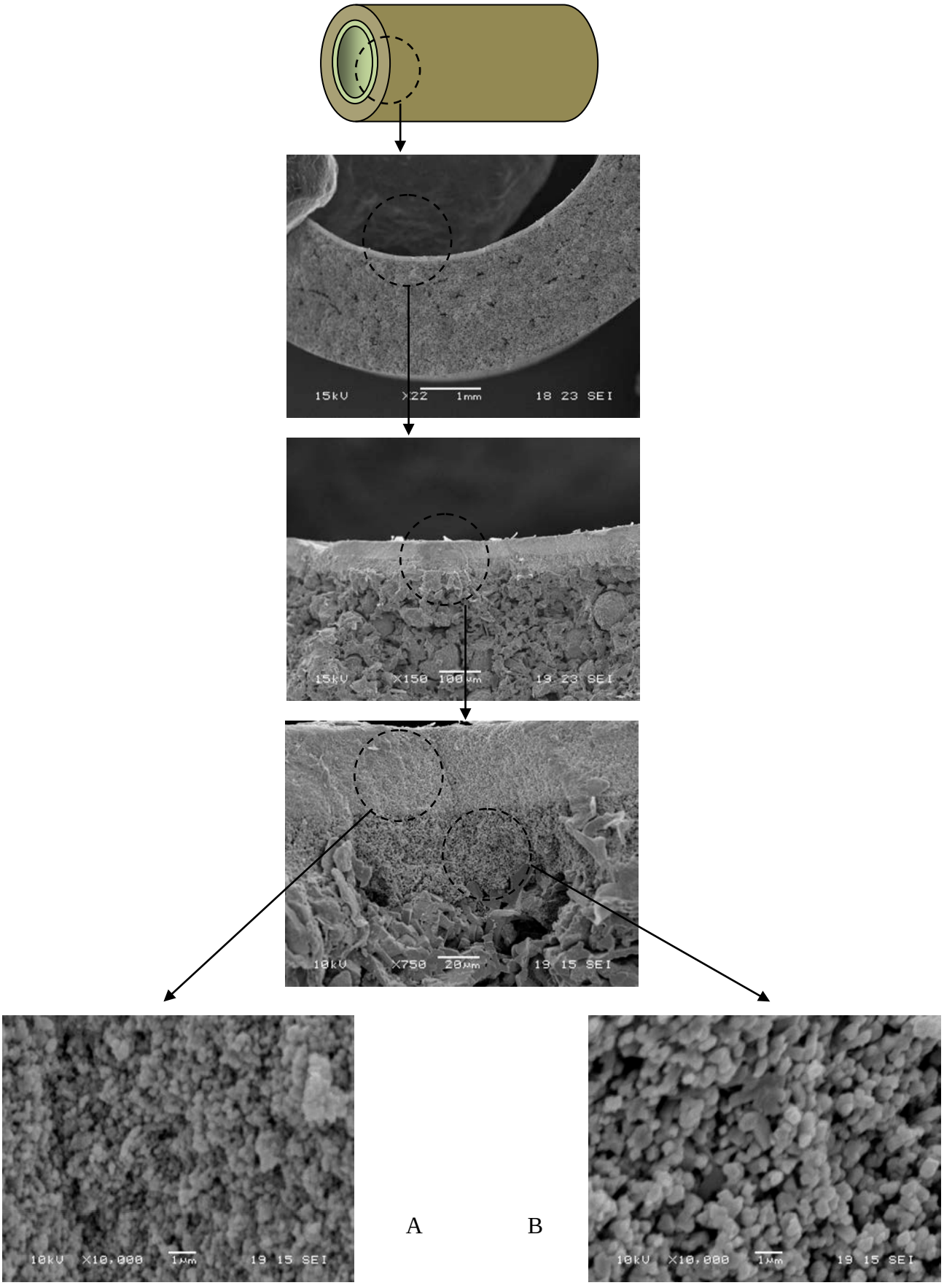

Figure 6.4: SEM images of 300kD membrane cross-section showing the active and bonding layer. The images are in ascending order of magnification. A) Active layer, B) Bonding layer

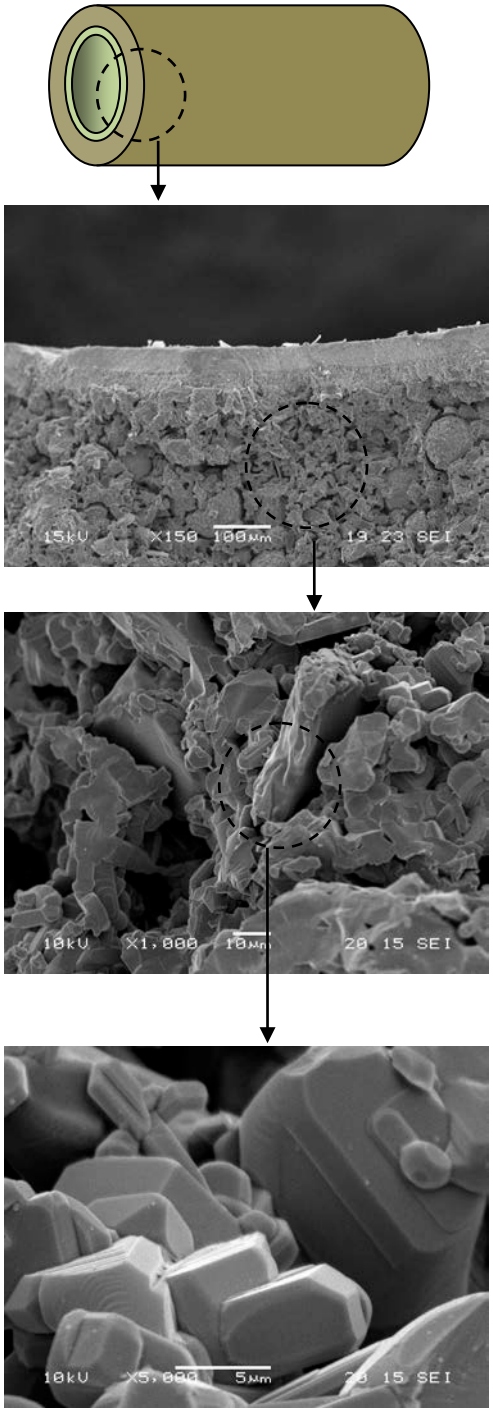

Figure 6.5: SEM images of 300 kD membrane cross-section showing the support layer. The images are in ascending order of magnification.

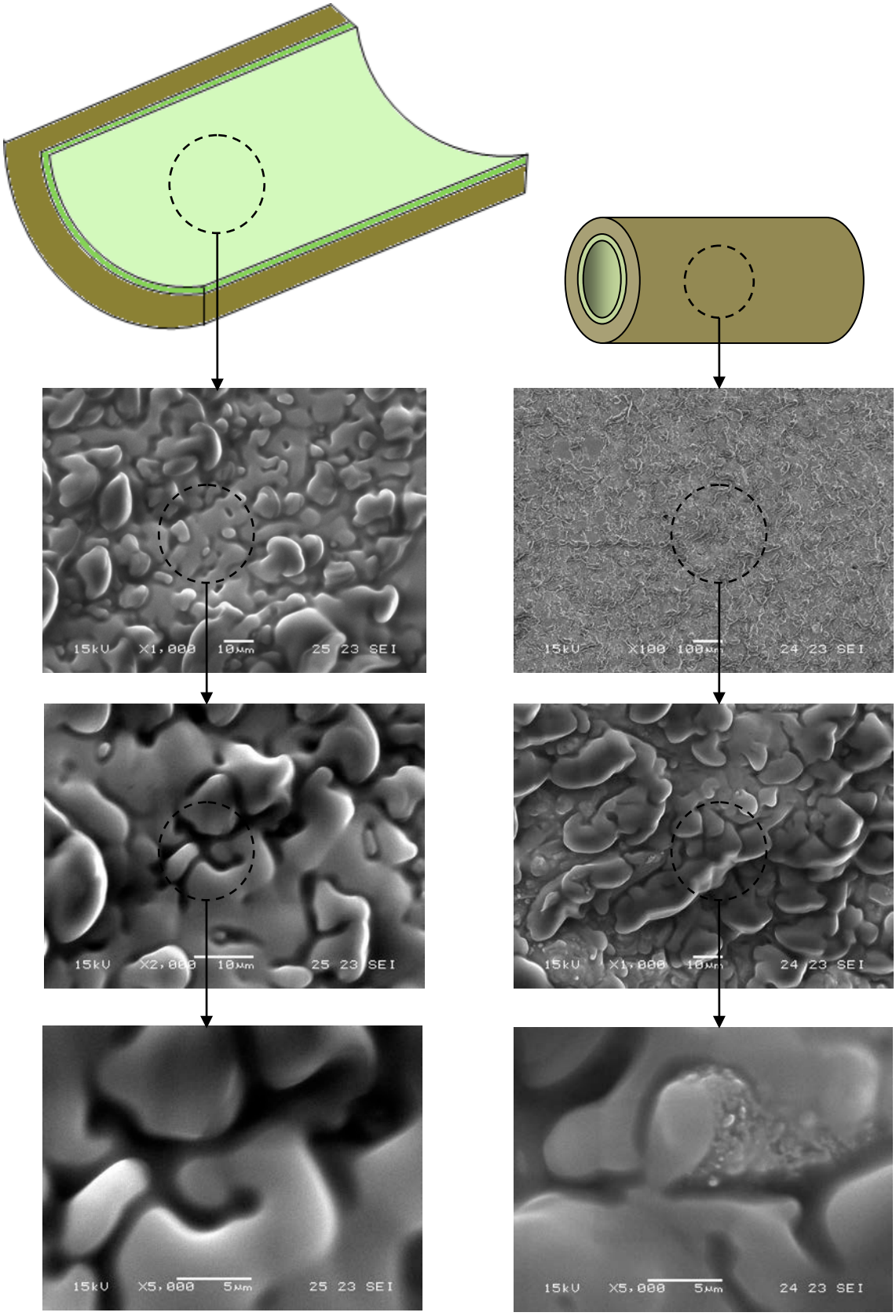

Figure 6.6: A) inner surface and B) Outer surface of the 0.1µm membrane. The images are in ascending order of magnification

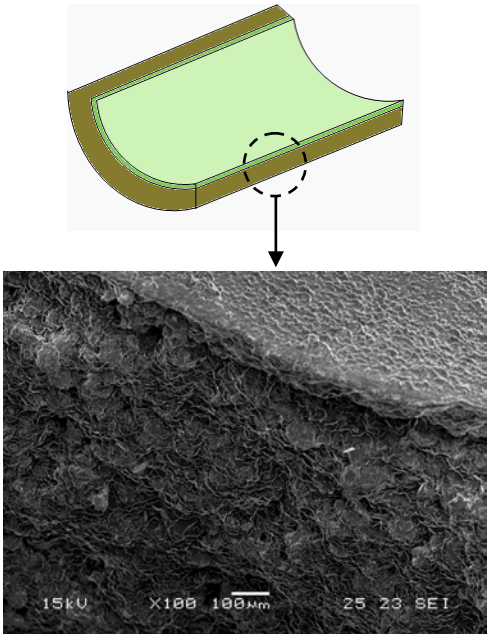

Figure 6.7: Longitudinal cross-section of the membrane showing the three layers

The thickness of different layers was measured using ImageJ and summarised in Table 6.1. The total membrane thickness was 2 mm which gives us an estimate of internal diameter bearing in mind that the external diameter is provided by the manufacturer as 10 mm (Figure 6.8). The calculated internal diameter was later used to determine the cross flow velocity of the system.

Table 6.1: The measured thickness of different membrane layers

Active layer	**Bonding layer**	**Support layer**	**Total membrane thickness**	**External diameter**	**Internal diameter**
42 µm	38 µm	1920 µm	2 mm	10 mm	6 mm

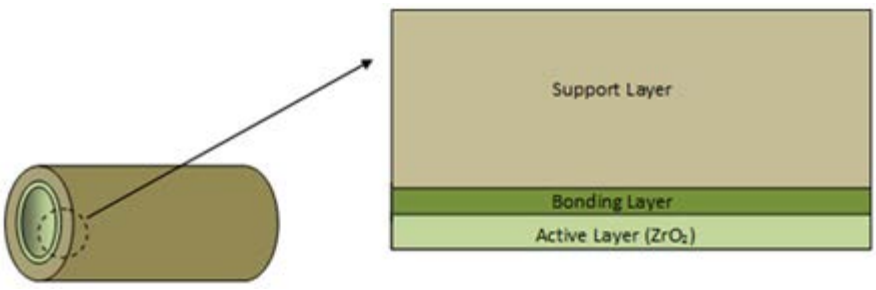

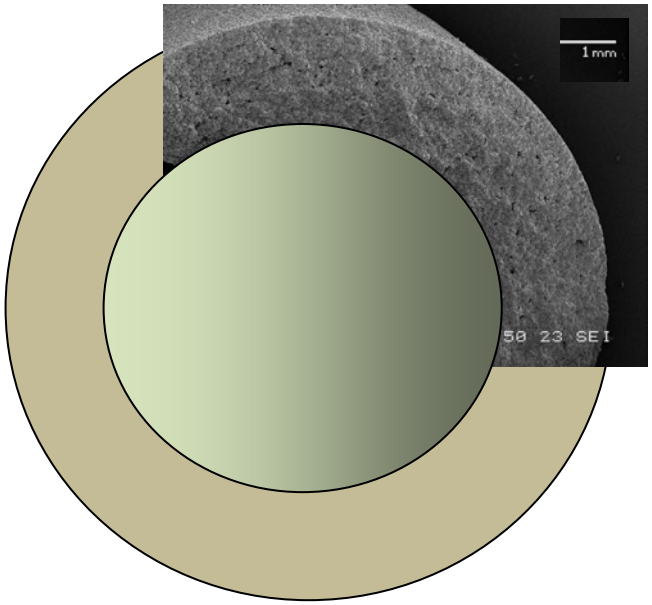

Figure 6.8: Determination of internal diameter

Images of the inner membrane surface were used to estimate the porosity of the active layer for both 300 kD and 0.1 µm membranes. After converting the SEM images to black/white pictures in ImageJ, showing the pores in black on a white background to distinguish the pores from the membrane material (Figure 6.9), the total area of the pores was estimated by the ImageJ software and the porosity was obtained using the following equation.

$$\varphi = \frac{A_t}{A_T} \qquad \text{Equation 6.1}$$

Where,

φ is the porosity of the membrane,

A_t is the total area of the pores in the image (m^2)

and A_T is the total area of the image (m^2).

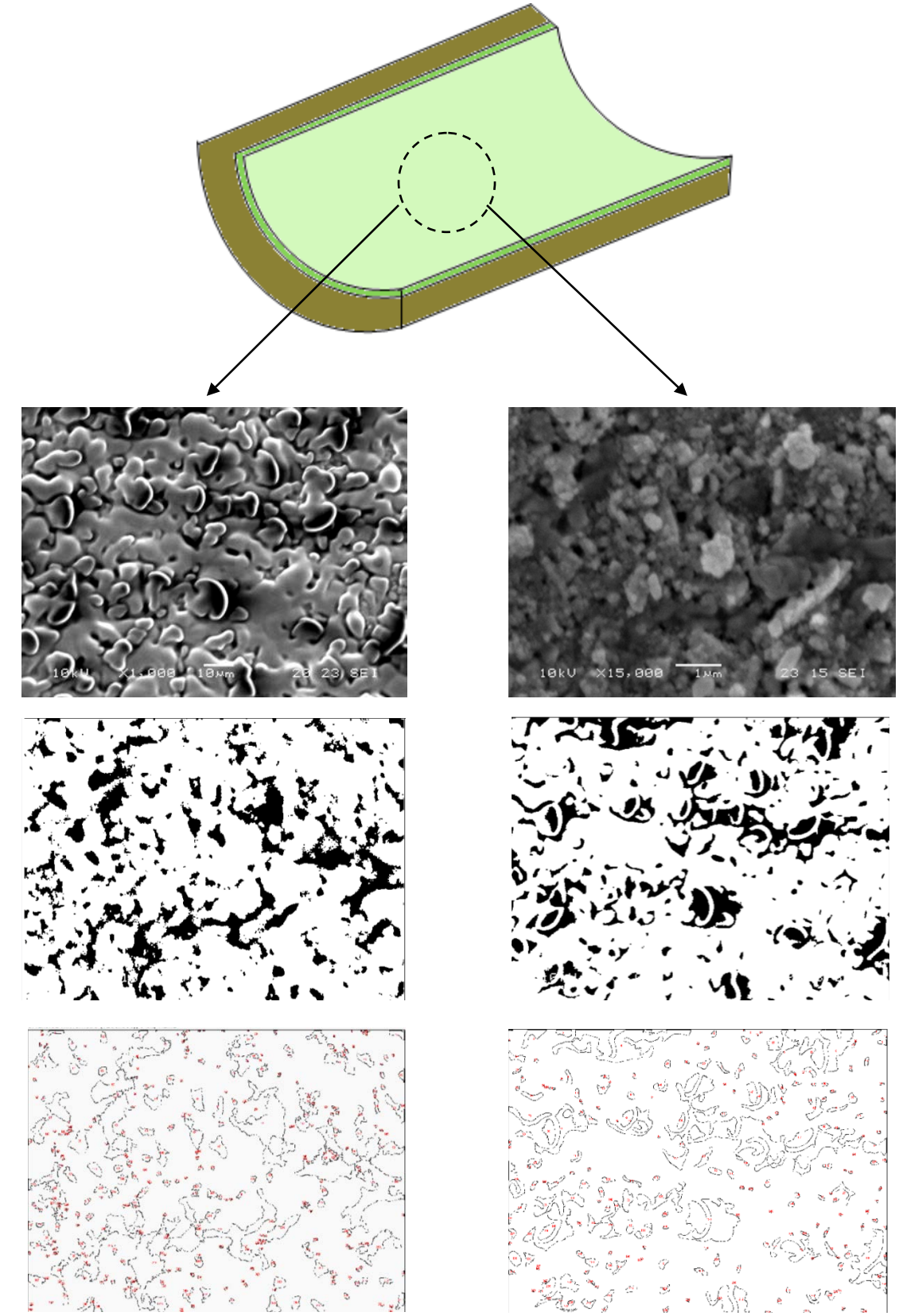

A B

Figure 6.9: SEM images of the inner surface view of the membrane, and images produced by the imageJ software, separating the pores. A) 300 kD, B) 0.1µm.

The characteristics for these two membranes are summarised in Table 6.2. The total area of pores divided by the total area of SEM image determines the membrane porosity. As shown in this table, the porosity of both membranes was calculated as more than 30 %. As the SEM images taken at this stage were not ideal, it is recommended that more clear images with better resolution should be taken to obtain the actual porosity of the membranes. However, the calculated porosity values are within the range of 30-40 %, which is in agreement with previous studies [166].

Table 6.2: Results from ImageJ for calculating the porosity

	Total area of image (m^2)	**Total area of pores (m^2)**	**Porosity (%)**
300 kD	5.32×10^{-5}	1.83×10^{-5}	34.32
0.1 µm	1.18×10^{-2}	3.6×10^{-3}	30.52

6.2.1.2 Determination of membrane water fluxes

In order to get accurate results during emulsification process it is important to make sure the membranes are not fouled. Therefore the membrane pure water fluxes were measured and compared with the manufacturer's data. To determine the membrane water fluxes, tests were carried out for 0.1 µm, 0.2 µm and 0.45 µm membranes using 16 l of water at 20 °C. The pump setting and flow rate were kept constant throughout the tests at 50 % and 2.5 l min^{-1}, respectively. The water flows were measured over time intervals of 1 min by recording the volume of water coming out of the permeate tube while increasing the transmembrane pressure. It should be noted that all the reported pressure values are gauge pressure. In order to get consistent results the readings were repeated as many times as needed. Furthermore, given the membrane area of 0.008 m^2 all the measured flows (l h^{-1}) were converted to water flux (l m^{-2} h^{-1}) and a graph of water fluxes against measured average pressures was plotted for each membrane (Figure 6.10)

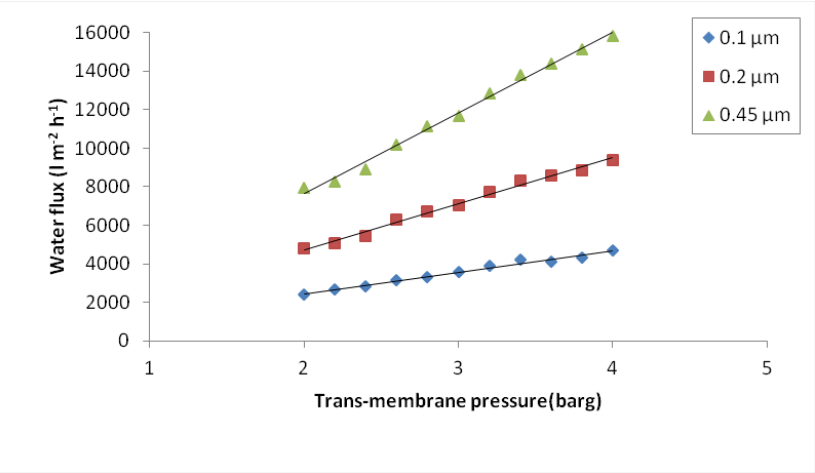

Figure 6.10: Graph of water flux against transmembrane pressure for 0.1, 0.2 and 0.45 µm membranes at 20 °C.

According to the manufacturer's manual the standard water flux values are given at 4 bar transmembrane pressure (TMP) and a temperature of 25 °C. To compare the experimental water fluxes with the standard values, they were normalised to equivalent values at 4 Bar and 25 °C using the Equation 6.2. A summary of this comparison is listed in Table 6.3.

$$J_{4-25} = \frac{4\, J_{Exp,T}\, k_t}{\Delta P_{tm} A} \qquad \text{Equation 6.2}$$

Where:

J_{4-25}: the equivalent of water flux at 4 bar TMP and 25 °C ($m^3\ m^{-2}\ s^{-1}$)

$J_{Exp,T}$: the measured flow at T °C ($m^3\ s^{-1}$)

k_t: Coefficient of temperature

ΔP_{tm}: Average pressure of measurement (Pa)

A: The membrane surface area (m^2)

Table 6.3: Comparison of experimental water fluxes with standard values

Membrane (Kerasep™)	**Experimental water flux at 4 Bar @ 20 °C (l h^{-1} m^{-2})**	**Corrected equivalent water flux at 4 Bar @ 25 °C (l h^{-1} m^{-2})**	**Standard water flux at 4 Bar @ 25 °C (l h^{-1} m^{-2})**
0.1 µm	4697	5294	6500 ± 1500
0.2 µm	9360	10549	12500 ± 4500
0.45 µm	15834	17845	20500 ± 4500

As can be seen from Table 6.3, the experimental water fluxes are all within the standard ranges provided by the manufacturer as expected for these newly-purchased membranes. Thus these membranes are suitable for application in future membrane emulsification experiments.

6.2.2 Membrane emulsification: Determination of process parameters

Membrane emulsification experiments were carried out using three different ceramic membranes with the pore sizes of 0.1, 0.2 and 0.45 µm. The continuous phase consisted of water and different concentrations of Tween 20 as surfactant, and was circulated in the system by the pump set at 50 %, corresponding to a flow rate of 2.50 l min^{-1}. During the membrane emulsification experiments, three important process parameters (cross-flow velocity, transmembrane pressure and dispersed phase flux) were determined.

6.2.2.1 Cross-flow velocity

After reading the flow rates (l min^{-1}) of the continuous phase from the rotameters for two different pump settings, the obtained values were used to calculate the cross-flow velocities (m s^{-1}). To convert the units, the internal cross sectional area of the membrane (m^2) was used. The estimated cross-flow velocities for 50 % and 70 %

pump settings were 1.47 and 2.36 m s^{-1}, respectively. The obtained cross-flow velocities were comparable with literature review as they lie within the typical range of 0.8 to 8 m s^{-1} for cross-flow membrane emulsification [17].

6.2.2.2 Trans-membrane pressure and disperse phase flux

Trans-membrane pressure for a cross-flow emulsification system can be calculated by Equation 2.13 (see Section 2.3.9). However, in this study, it was equal to the pressure of the dispersed phase as the inlet and outlet pressure of the continuous phase remained constantly zero throughout the experiments. Furthermore, dispersed phase fluxes were determined using Equation 2.12 (see Section 2.3.7) for 3 different membranes at an oil phase pressure of 3 bar (3×10^5 Pa). The time taken to see bubbles in the tube connecting the pressurised vessel to the membrane module (*i.e.* process time Δt) was used to obtain the volume flow rate of the dispersed phase. The calculated dispersed fluxes were 0.15, 0.18, 0.23 $m^3\ m^{-2}\ h^{-1}$ for 0.1, 0.2, 0.45 µm, respectively. It can be concluded from these results that the dispersed phase flux increases with increasing membrane pore size. The theoretical dispersed phase flux was calculated using Hagen-Poiseuille relationship (Equation 2.17) to compare with experimental dispersed fluxes. The calculations for 0.45 µm membrane are shown in Appendix H. It is apparent that the calculated flux (0.41 $m^3\ m^{-2}\ h^{-1}$) is close to the estimated experimental flux for 0.45 µm membrane (0.23 $m^3\ m^{-2}\ h^{-1}$). Therefore, it was concluded that the Hagen-Poiseuille equation can be used to predict the disperse phase flux through membrane for given experimental conditions. However, the slight deviation of experimental value from the one calculated by Hagen-Poiseuille equation could be attributed to possible errors in assuming values.

6.2.3 Investigation of prepared emulsions

In this section, the emulsions prepared by 0.1 µm ceramic membrane consisting of two different oil concentrations of 10 & 20 % w/w and surfactant concentration of 1-8 % w/w were compared in terms of appearance, stability and droplet size

distribution. Total mass of 5,000 g was made up for the formulation and the water, oil and surfactant masses were calculated accordingly. Total emulsification process time was found to be between 25 to 40 minutes. All the prepared emulsions had a milky appearance and remained stable for only 2-5 hours after being kept sealed at room temperature. Figures 6.11 to 6.14 show the produced emulsions. It can be seen that creaming occurred in all samples after 5 hours but the one with more surfactant appeared to be more stable.

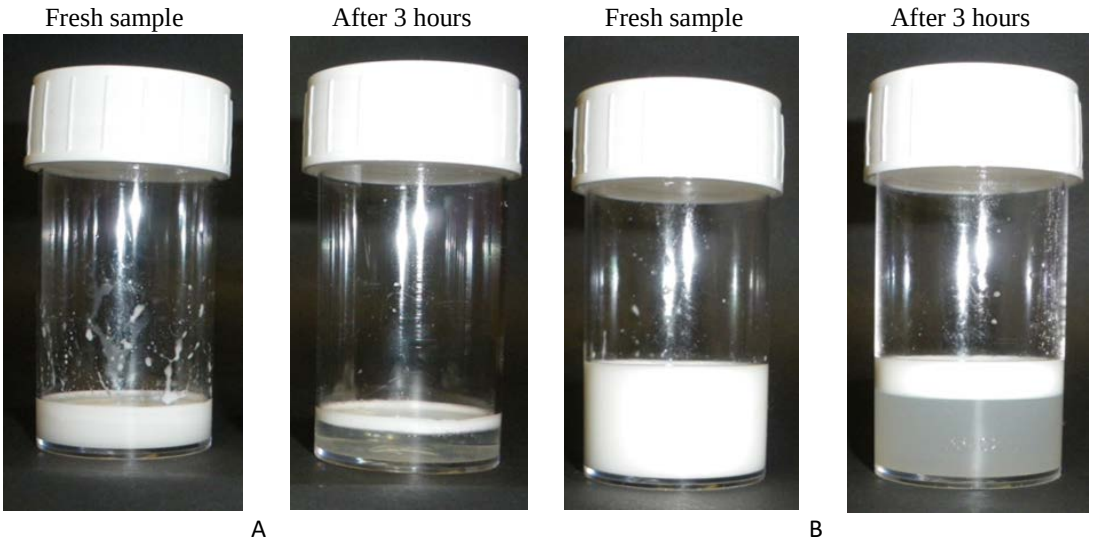

Figure 6.11: A) Prepared emulsion of 10 % soybean oil and 90% water using 1 % Tween 20, and the same sample after being kept at room temperature after 3 hours B) Prepared emulsion of 20 % soybean oil and 80% water using 1 % Tween 20, and the same sample after being kept at room temperature after 3 hours. The samples were emulsified with 0.1 µm ceramic membrane under 3 bar trans-membrane pressure at the ambient temperature of 20 ± 1 °C.

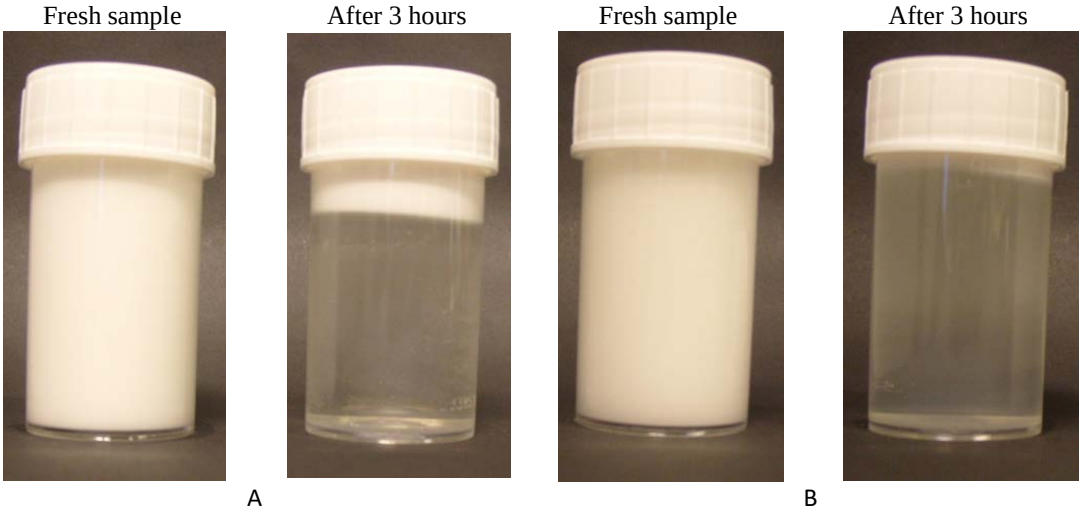

Figure 6.12: A) Prepared emulsion of 10 % soybean oil and 90% water using 2 % Tween 20, and the same sample after being kept at room temperature after 3 hours B) Prepared emulsion of 20 % soybean oil and 80% water using 2 % Tween 20, and the same sample after being kept at room temperature after 3 hours. The samples were emulsified with 0.1 µm ceramic membrane. The samples were emulsified with 0.1 µm ceramic membrane under 3 bar trans-membrane pressure at the ambient temperature of 20 ± 1 °C.

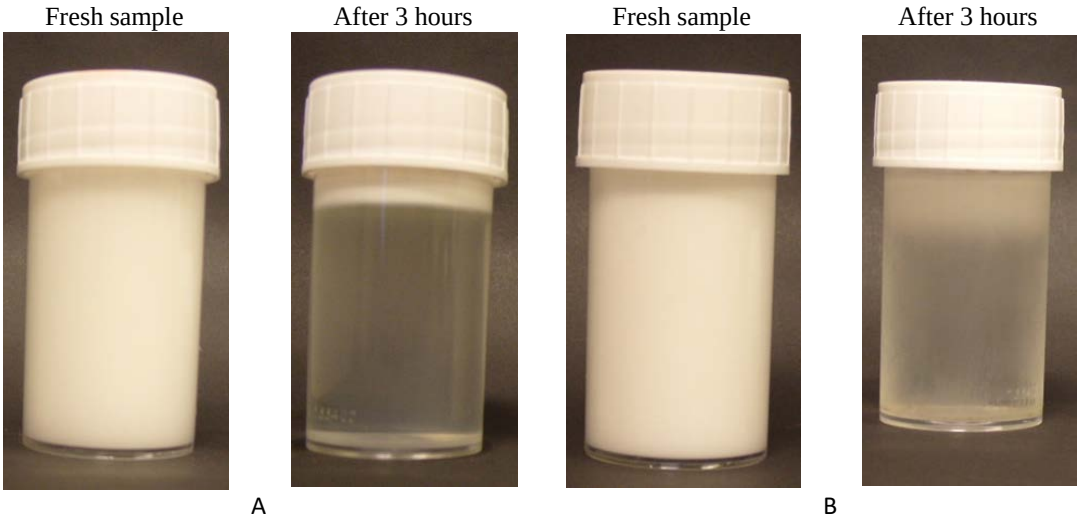

Figure 6.13: A) Prepared emulsion of 10 % soybean oil and 90% water using 4 % Tween 20, and the same sample after being kept at room temperature after 3 hours B) Prepared emulsion of 20 % soybean oil and 80% water using 4 % Tween 20, and the same sample after being kept at room temperature after 3 hours. The samples were emulsified with 0.1 µm ceramic membrane. The samples were emulsified with 0.1 µm ceramic membrane under 3 bar trans-membrane pressure at the ambient temperature of 20 ± 1 °C.

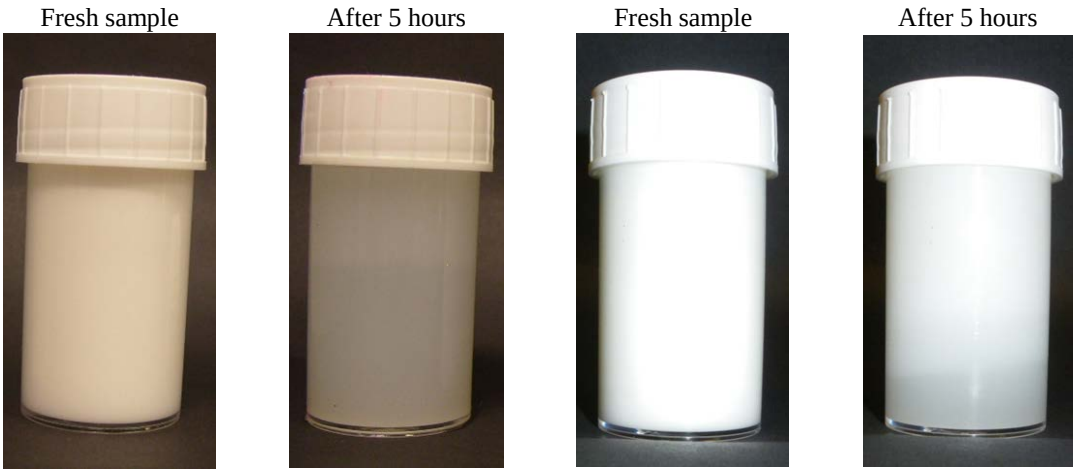

Figure 6.14: A) Prepared emulsion of 10 % soybean oil and 90% water using 8 % Tween 20, and the same sample after being kept at room temperature after 3 hours B) Prepared emulsion of 20 % soybean oil and 80% water using 8 % Tween 20, and the same sample after being kept at room temperature after 3 hours. The samples were emulsified with 0.1 µm ceramic membrane under 3 bar trans-membrane pressure at the ambient temperature of 20 ± 1 °C.

6.2.3.1 Effect of surfactant concentration on droplet size and size distribution

Although the produced emulsions did not show an acceptable level of stability, for comparison purposes, and in order to study the effect of surfactant concentration on the droplet size and size distribution, the emulsions prepared with 10 % soybean oil and different concentrations of Tween 20 were compared in terms of droplet size and polydispersity index and the results are shown in Figure 6.15.

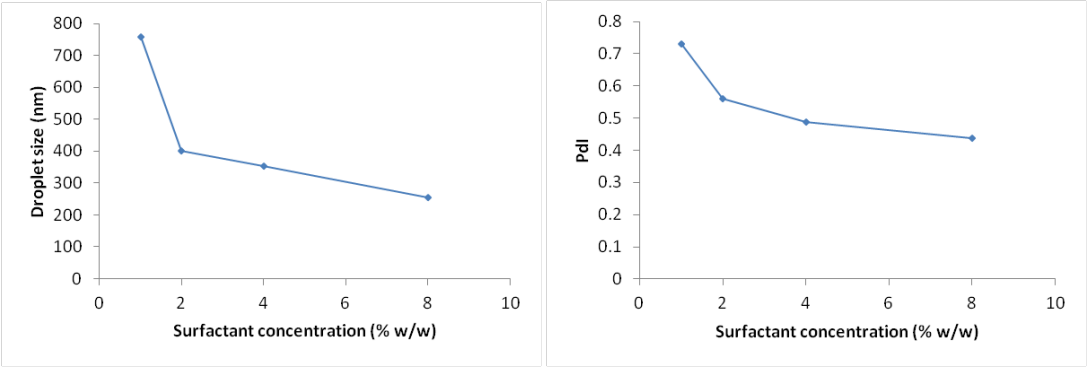

A B

Figure 6.15: Effect of surfactant concentration on droplet size (A) and polydispersity indices (B) of the emulsions containing 10 % soybean oil and 90 % water. The samples were emulsified with 0.1 µm ceramic membrane at 20 ± 1 °C under 3 bar trans-membrane pressure.

As can be seen in Figure 6.15, by increasing the surfactant concentration, the droplet sizes decreases. As discussed in Section 2.4, the final droplet size in cross flow emulsification is a result of applied forces on the droplet. These forces can be categorised as adhesive and detachment forces; former is comprised of interfacial force while latter is comprised of static pressure (due to applied pressure), cross flow and dynamic lift (due to the cross flow) forces [106]. Keeping the cross flow and applied pressure constant, the decrease in droplet size with increasing surfactant concentration can be correlated to decrease in interfacial force. The interfacial tension force, which is directly related to interfacial tension between two phases, decreases by increasing the surfactant concentration and results in formation of smaller droplet. The interfacial tension between soybean oil and water for various concentrations of Tween 20 was estimated using FTA200 (see Section 3.2.6) and plotted as seen in Figure 6.16. It is clear that the surface tension decreases with increasing surfactant concentration. The highest decrease in droplet size was achieved between 1 % and 2 % Tween 20; the emulsions containing 2 % Tween 20 had droplet sizes almost half the ones containing 1 % surfactant. However, at higher surfactant content, the reduction rate in droplet size became less. Depending on the surfactant concentration, the mean droplet sizes were 2.5 to 7.5 times the membrane pore size. The polydispersity indices also decrease when increasing the surfactant

concentration. However, even with 8 % Tween 20, the emulsions were relatively polydispersed which could explain why creaming happened so quickly.

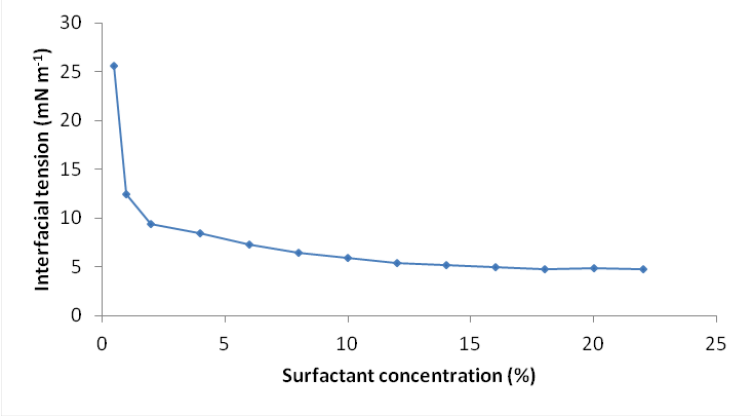

Figure 6.16: Effect of concentration of Tween 20 on interfacial tension between soybean oil and water.

6.2.3.2 Effect of membrane pore size on droplet size

It has been stated by Charcosset *et al.* that for given operating conditions, the ratio of mean droplet size to average pore size is a constant value; between 2 to 10 [22]. Based on the results shown in Section 6.3.4.1, this number was found to be approximately 2.5 for the 0.1 μm membrane when it was used to prepare emulsion with surfactant content of 8 % under 3 bar at 20 ±1 °C. In order to see if this number is applicable for the prediction of droplet size in the case of membrane with larger pore size, a series of emulsions with similar formulation were prepared using 0.2 and 0.45 μm membranes under the same operating condition. The determined average droplet sizes were 519.76 nm and 915 nm for 0.2 and 0.45 μm membranes respectively, showing the same ratio as 0.1 μm membrane. This implies a linear relationship between mean droplet size and average pore diameter as explained by previous studies [17][22].

6.2.3.3 Energy consumption

In order to estimate the energy consumption during membrane emulsification, it was considered that the volume of injected oil through the membrane is compressed and therefore the work of it can be estimated according to volume-pressure equation (see Appendix C). The volume of oil can be estimated using the oil density of 0.92 g ml^{-1} and the applied pressure is 3 bar. However, it should be noted that this is the work done by pressure while the energy consumption for producing the cross flow must be considered as well. The cross flow pump was set to work at 50 % to produce the required cross flow and worked for 25 to 40 minutes according to the formulation and oil concentration. As shown in Figure 6.8, the power of pump at 50 % is around 0.48 kW, therefore, the energy consumption can be estimated accordingly. The estimated energy consumption for pump and oil injection are tabulated in Table 6.4.

Table 6.4: Calculated specific energy consumption for cross flow membrane emulsification according to the energy consumption of the pump and energy required to inject oil through the membrane.

Oil phase ratio (%)	Pressure (Bar)	Emulsification time (s)	Energy consumption (J)			Specific energy consumption (J g^{-1})
			Pump work	Membrane	Total	
10	3	1500	720,000	163.1	720,163	144
20	3	2400	1,152,000	326.2	1,152,326	230

Results show that increasing the oil concentration results in a large increase in the energy consumption as it takes more time to inject the oil. The estimated energy consumption is relatively high; however it should be noted that this energy consumption is for 5000 g of emulsions whereas emulsions produced via the phase inversion temperature and Ultra-Turrax techniques are in range of 50 g. Cross comparison with experimental results from previous chapters show that calculated values of energy consumption for cross flow experiments per mass of emulsion lies within the lowest calculated energy consumption for phase inversion temperature

method which are extremely lower than the energy consumption for Ultra-Turrax experiments. Therefore, it can be concluded that cross flow membrane emulsification method is a very energy efficient method, however in our study it fails to produce stable emulsions.

6.3 Summary

Formation of emulsions via cross flow membrane emulsification was investigated in this chapter. For this purpose, an experimental rig was designed and built, and a series of emulsions with different surfactant concentrations were prepared and effects of various parameters on resulting droplet size were studied. First, pure water fluxes were measured for newly purchased membranes (0.1 µm, 0.2 µm and 0.45 µm). The obtained values were within the standard range provided by the manufacturer which shows they are suitable for using in our emulsification experiments. SEM results for membrane characterization have provided a general view of morphological features such as thicknesses (support and active membrane layer), pore size and shape, the grains' structure, and finally the porosity. The porosity for both 300 kD and 0.1 µm membranes has been calculated as more than 30 %.

Furthermore, the emulsions prepared by 0.1 µm ceramic membrane consisting of two different oil concentrations of 10 & 20 % w/w and surfactant concentration of 1-8 % w/w were compared in terms of appearance, stability and droplet size distribution. Experimental results show that droplet sizes are 2.5 times larger than the pore size. Increasing the surfactant concentration results in formation of emulsions with smaller droplet sizes and narrow size distribution. However, all produced emulsions were not stable and creaming occurred after 5 hours. The ones with higher surfactant concentrations were more stable.

In the next part, the process parameters of trans-membrane pressure, cross-flow velocity and dispersed phase flux have been investigated. Regarding the dispersed phase fluxes, the results show a direct relationship between the oil flux and the membrane pore size when applying a constant pressure. The larger pore size, the greater the flow rate of oil through the membrane for a constant feed pressure.

Furthermore, the dispersed phase flux was calculated using Hagen-Poisieulle equation in order to compare with experimental dispersed fluxes. It was concluded that the Hagen-Poiseuille equation can be used to predict the disperse phase flux through membrane for given experimental conditions. However, the slight deviation of experimental value from the one calculated by Hagen-Poiseuille equation could be attributed to possible errors in assuming values.

Finally, by estimating the energy consumption for this method, it was found that cross flow membrane emulsification technique is very energy efficient; however, in this study, it fails to produce stable nano-emulsions.

7. Conclusions and suggestions for future work

The aim of this project was to find the optimum formulation to produce stable nano-emulsions for food and healthcare applications using different emulsification methods as well as investigating the main parameters affecting the quality of nano-emulsion produced by each method under study. This chapter summarises the conclusions from the experimental findings in this project and suggests potential future works for further investigation in this area of research.

7.1 Conclusions

7.1.1 Rotor-stator homogeniser (Ultra-Turrax)

In this study, it was found that stable nano-emulsions can be produced with mean droplet sizes in the range of 60 - 95 nm when a mixture of 10 % (w/w) soybean oil, RO water and different concentrations of Brij 97 (11 - 25 %) were emulsified by Ultra-Turrax for 15 minutes at 13,500 rpm. This was achievable by pre-heating the emulsion components to 45 °C. However, further increase in temperature failed to produce fine nano-emulsions. It has been stated in the literature that it is relatively easy to produce macroemulsions with the use of high-speed stirrers such as Ultra-Turrax, however, for the production of nano-emulsions a higher concentration of surfactant and/or energy input is required [4]. In most previous studies, the emulsions prepared by Ultra-Turrax were unstable coarse emulsions, therefore, an additional homogenisation process with another high-energy method was required to reduce the droplet size to the nanometre scale [168]. According to Fernandez (2004), the smallest droplet size achieved by Ultra-Turrax so far is known to be approx. 1 µm [54]. Nevertheless, in our study, stable nano-emulsions were prepared by using just the Ultra-Turrax with the surfactant concentration as low as 12 %.

Results also show that increasing the surfactant concentration leads to a better surface coverage of droplets and formation of emulsions with smaller mean droplet size. Also, increasing the oil phase ratio results in formation of emulsions with larger

mean droplet sizes. Considering the Kolmogorov length scale and experimental results, it was found that droplets lie within the viscous regime and therefore viscous equation was employed, as model, to estimate the final mean droplet size of emulsions produced via Ultra-Turrax.

7.1.2 Phase inversion temperature method (PIT)

Emulsions prepared by PIT method containing different concentrations of Brij 97 (10 - 25 %), 10 % (w/w) soybean oil and RO were investigated. The result showed that by PIT method stable nano-emulsions were produced at all surfactant concentrations higher than 11 % (w/w). These nano-emulsions were transparent in appearance, with mean droplet sizes smaller than 20 nm. By increasing the surfactant concentration, the droplet size and polydispersity index decreased which was in agreement with literature [39]. The prepared nano-emulsions showed a good stability over time as no phase separation was noted after 4 weeks and there was only slight change in droplet size with time (4 - 8 %). According to Wang *et al*. (2007), the two most probable breakdown mechanisms in emulsions are coalescence and Ostwald ripening [169], however, it was reported in literature that long chain triglycerides (such as soybean oil), do not undergo Ostwald ripening [170]. Moreover, during the PIT process, the rapid cooling of the prepared emulsion to a temperature approximately 30 °C below its PIT makes droplet coalescence almost negligible as the non-ionic surfactant molecules form an efficient physical barrier preventing the droplets from merging when colliding [39]. It was also found in this study that the phase inversion temperature decreases as surfactant concentration increases. Similar behaviour was observed by Spernath *et al*. [171].

When compared with the emulsions prepared by Ultra-Turrax, it was concluded that PIT method is more favourable than the homogeniser method for producing stable nano-emulsions, especially when shear sensitive materials are used as Ultra-Turrax consumes nearly 50-60 times more energy. By using PIT method, nano-emulsions with smaller droplet sizes, less polydispersed and more stable over time can be produced. According to Tadros (2015), the PIT method is by far the most suitable technique for the production of nano-scale emulsions, however, it only works when

the system contains an ethoxylated surfactant [172]. Nevertheless, for materials with higher heat sensitivity, the homogeniser seems to be the more suitable method.

7.1.3 Dead-end membrane emulsification

Formation of nano-emulsions through pre-mixed membrane emulsification was studied using membranes made with ceramic and polycarbonate, and effects of various parameters on final droplet size were investigated. It was found that fine emulsions with a reasonable stability over time can be produced by using both Tween 20 and Tween 80 as surfactant at concentrations as low as 4 % in oil. The size of droplets, size distribution and stability, however, could be improved by increasing the applied pressure, experimental temperature and surfactant concentration. The mean droplet sizes seemed to be independent of the oil content of the dispersed phase. This was in agreement with previous studies as reported by Vladisavljević *et al*. (2004) [64]. Results showed that surfactant concentration and interfacial tension, regardless of the membrane type, play a great role in droplet formation. However, no direct correlation between the oil phase ratio and final droplet size could be found.

Effect of membrane pore size was investigated by employing two ceramic membranes with average pore sizes of 50 and 100 nm. It was found that emulsions with small droplet size formed using the membrane with 50 nm pore size. It should be noted that the thickness of membrane with 100 nm pore size is half of that of the one with 50 nm pore size. This affects the flux rate and also the shear stress applied inside membrane pores. Increasing the number of passes through the 100 nm membrane results in formation of emulsions with droplets smaller than the pore size. However, results show that this effect is limited to three passes and no further decrease in droplet size was achieved after third pass. This indicates the importance of wall shear rate inside membrane pore size. Flux equation was used to estimate the viscosity and pore wall shear rate in experiments. It was found that the wall shear rate is constant in all passes, however the viscosity of emulsion decreases as the number of passes increases. This shows that droplets break into smaller ones as they pass through the pore and go under shear stress until they reach steady-state droplet size due to the applied shear from pore wall. After this point, no further droplet

breakup occurs, as discussed earlier for high energy emulsification. Also, increasing the pressure results in formation of smaller and finer droplets. The estimated shear wall stress increases as the applied pressure increases; thus emulsions with smaller droplet size are produced. The similar results were reported earlier by Vladisavljević *et al*. (2004) and Kukizaki (2009) [64] [173].

Effect of membrane material was also studied by comparing results from two types of membranes made of ceramic and polycarbonate. Membranes made of polycarbonate are thinner compared to the ones made of ceramic, resulting in a higher flux rate, in fact so high that the oil droplets do not stay enough inside the pores to undergo sufficient disruption. Therefore, three layers of polycarbonate membranes were used to produce emulsions. Results indicate that although the flux rate decreases when employing three layer of polycarbonate membrane, emulsions with small droplet size and good polydispersity index were formed. It was found that oil phase ratio is limited to 20 % when three layers of membranes are used and increasing the oil concentration results in blockage and failure of emulsification. This was correlated to a relatively higher coalescence rate, as the emulsion has to pass through the first layer and then find its way through the next layer. The probability of the droplets stuck between the membrane layers and their collision rate increase significantly, resulting in formation of large droplets, which cannot pass through the membrane pores easily.

Results show that the energy consumption for the dead-end membrane emulsification lies within the range of energy consumption estimated for Ultra-Turrax experiments which are significantly higher than the values for phase inversion temperature experiments. This is mainly due to the use of Ultra-Turrax for preparing the coarse premix emulsions and also conducting experiments at elevated temperatures. As expected, the membrane emulsification itself does not require a high amount of energy. Here it should be noted that phase inversion temperature method requires a higher surfactant concentration compared to the membrane method.

7.1.4 Cross-flow membrane emulsification

Finally, in this study, formation of emulsions via cross-flow membrane emulsification using tubular ceramic membrane was investigated. For this purpose, an experimental rig was designed and built, and a series of emulsions with different surfactant concentrations were prepared and effects of various parameters on resulting droplet size were studied. Experimental results show that droplet sizes are 2.5 times larger than the pore size which was in agreement with literature. According to Charcosset *et al.* (2004), for given operating conditions, the ratio of mean droplet size to average pore size in a cross-flow membrane emulsification system is a constant value; between 2 to 10 [22]. Increasing the surfactant concentration results in formation of emulsions with smaller droplet sizes and narrower size distribution due to the decrease in interfacial tension [86]. However, all produced emulsions were not stable and creaming occurred after 5 hours. The ones with higher surfactant concentrations were more stable. Finally, by estimating the energy consumption for this method, it was found that cross flow membrane emulsification technique is very energy efficient; however, in this study, it fails to produce stable nano-emulsions.

7.1.5 Comparison of energy consumption

The estimated specific energy consumption values (J g^{-1}) for each emulsification method used in this study were converted to energy density (J m^{-3}) for a better comparison with the values reported previously in the literature. Figure 7.1 shows the emulsion droplet size for each method as a function of energy density applied to the system.

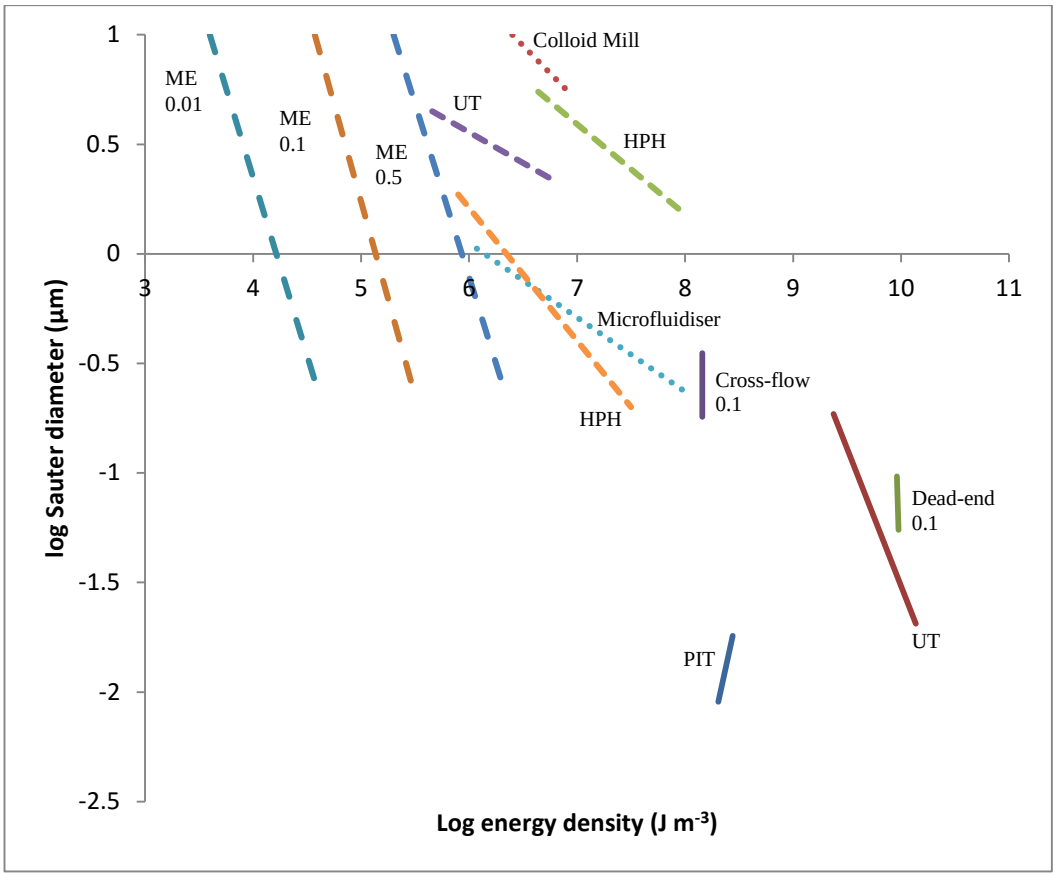

Figure 7.1: Droplet diameter as a function of the energy density for different methods of emulsification. Solid lines represent the estimated energy densities in this study. Dash lines show the reported values in the literature [44]. ME: cross-flow membrane emulsification, numbers denote the disperse phase ratio; HPH: high-pressure homogeniser; UT: Ultra-Turrax.

As it can be seen in Figure 7.1, a cross comparison between the estimated energy densities in this study and the reported values in the literature [44] shows that although energy consumption in our study were higher than those reported in previous studies, smaller droplet sizes were achieved for any emulsification system studied here. As it is expected, the droplet size gets smaller as the energy input goes up. However, it should be noted that the estimation of energy consumption is not easy when running the experiments at such a small scale. More accurate estimation could be expected when the system is operated at a larger scale.

With regard to the estimated energy consumption for the methods used in this study, both cross-flow emulsification and PIT methods showed to be the most energy efficient methods; however, unlike PIT method, the cross-flow emulsification fails to produce stable nano-emulsions in this study.

7.1.6 Final conclusions

The aim of this study was to investigate different emulsification methods with an attempt to find an optimum formulation to produce oil-in-water nano-emulsions for use in food and healthcare applications in which not only the interesting physical properties of nano-emulsions such as their transparency, larger surface area to volume ratio and long-term physical stability are of interest but also the emulsion components should be biocompatible. In this study, the model system soybean oil/water/Brij 97 was used to investigate the emulsification methods. Brij 97 was selected as the main surfactant in this study but it didn't work for the membrane emulsification methods and had to be replaced by food-grade Tween series surfactants which is in fact more biocompatible than Brij 97 especially for food applications. It should be noted that Tween series surfactants were also tried for PIT and Homogeniser but it didn't work either.

In this study, we have succeeded in producing stable nano-size emulsions with Homogeniser, PIT and dead-end emulsification methods. PIT method yielded the smallest drop sizes and lowest energy consumption, however the drawback for this method is that it cannot be used for heat sensitive materials and also more importantly, much higher surfactant concentration is required for PIT method to work. The latter is one of the major concerns for food and healthcare applications as it is more favourable if we can use as little surfactant as possible. For this reason, the dead-end membrane emulsification system appears to be a more suitable option to meet the requirements for food and healthcare applications as our study showed that with this method one can produce stable nano-emulsions with reasonably small droplets while using substantially lower amount of surfactant as opposed to the PIT method, bearing also in mind that Tween 20 is more biocompatible than Brij 97. The only drawback we found in this study for dead-end membrane emulsification is its higher energy consumption than expected as Ultra-Turrax was used to prepare the premix. If a more energy efficient method for mixing the emulsion components is employed, this method could be a more suitable option than PIT method for food and healthcare applications. Nevertheless, PIT method would still be considered as the favourable choice when shear sensitive materials are used.

7.2 Future work

Considering the energy efficiency of the emulsification method when used in a larger scale for food and healthcare applications, the investigation in this work has been proven that two low energy methods of dead-end membrane emulsification and PIT technique can be employed to produce stable nano-emulsions which can be used for potential food and healthcare applications. However, as mentioned, our results showed that both methods have drawbacks. While higher amount of surfactant is required for PIT method which can be an issue when food and healthcare products are involved, dead-end membrane emulsification consumes higher amount of energy compared to phase inversion experiments. Taking all these into consideration, potential future works for further investigation in this area of research are as follows:

PIT method can be used when the emulsion contains shear sensitive components. The next line of research could be to investigate the possibility of adding a food grade co-surfactant or a mixture of surfactants to reduce the Brij concentration in order to make the system more biocompatible. It would be also interesting to try other emulsion systems with different oils as disperse phase. In this study, we have used a batch set-up to prepare emulsions. Another line of research could be to scale-up the production by designing a continuous rig for PIT method in order to investigate the reproducibility of the nano-emulsion formulation at a larger scale. The up-scaling will give us a better understanding of the process and its suitability for the potential applications in industry.

As mentioned, dead-end membrane emulsification was found to be the more favourable choice for food and healthcare applications as it yields stable nano-emulsions by using much lower amount of surfactant. However, as the next line of research, it is required to find a way to lower the energy consumption for this method. It could be achievable by either exploring an alternative way of premixing the emulsion components instead of homogeniser or scaling up the experimental set-up by using a number of parallel dead-end systems. In this case, higher volume of premix emulsions could be prepared at the same time resulting in considerably lower energy consumption for the whole system. In this study, stable nano-emulsions were produced by dead-end membrane emulsification using Tween surfactants with

concentration as low as 4 % in soybean oil. The next step would be to try the same formulations but with other biocompatible oils and surfactants to check the reproducibility of the nano-emulsion formulation with different systems. It would also be interesting to investigate whether the mixture of different surfactants would provide a better oil droplet surface covering, and hence a better stability.

It was noted in literature that most previous studies on the pre-mix membrane emulsification system were focused on the membranes with the pore sizes in the micrometer range. Although the influence of various parameters on the droplet size, polydispersity and emulsion stability such as pore size, number of emulsification cycles, transmembrane pressure and other experimental conditions were investigated before, these effects were mainly explained on the emulsions with droplet sizes more than 1 μm. When it comes to the preparation of nano-emulsions, these affecting parameters are still required to investigate thoroughly in order to understand the droplet formation in nano-porous membranes. Some attempts have been made in this study to explain some of these behaviours but further research is needed in future. Furthermore, the droplet formation and stability of the emulsions are highly dependent on the viscosities of the oil and aqueous phases also the overall viscosity of the prepared emulsion. Nano-emulsions may show different rheological behaviours than the macroemulsions due to very small droplet sizes which could affect the degree of physical stability. Therefore, another interesting line of research would be to investigate the rheological properties of the prepared emulsions and their changes over time using a rotational/ oscillatory rheometer to understand this behaviour more clearly in nano-scale emulsions.

The interest in O/W nano-emulsions as a delivery system for nutraceuticals and pharmaceuticals has been increased in recent years. The majority of these bioactive compounds are greatly lipophilic having very low water solubility. Therefore, using the nanoemulsion-based delivery system not only substantially improves their bioavailability, but also makes the end-product more favourable to consumers. Hence, the other interesting line of research is the encapsulation of drugs or food bioactive components into produced nano-emulsions to investigate the suitability of the obtained formulations in this study for food and healthcare applications.

References

[1] van der Graaf, S., C.G.P.H. Schroen, and R.M. Boom, *Preparation of double emulsions by membrane emulsification - a review.* Journal of Membrane Science, 2005. **251**(1-2): p. 7-15.

[2] Prince, L., *Microemulsions Theory and Practice.* 1977: Academic Press.

[3] Sadurni, N., et al., *Studies on the formation of O/W nano-emulsions, by low-energy emulsification methods, suitable for pharmaceutical applications.* European Journal of Pharmaceutical Sciences, 2005. **26**(5): p. 438-445.

[4] Tadros, T., et al., *Formation and stability of nano-emulsions.* Advances in Colloid and Interface Science, 2004. **108**: p. 303-318.

[5] Mason, T.G., et al., *Nano-emulsions: formation, structure, and physical properties.* Journal of Physics: Condensed Matter, 2006. **18**(41): p. 635-666.

[6] McClements, D.J. and H. Xiao, *Potential biological fate of ingested nanoemulsions: influence of particle characteristics.* Food Funct, 2012. **3**(3): p. 202-20.

[7] McClements, D.J. and J. Rao, *Food-grade nanoemulsions: formulation, fabrication, properties, performance, biological fate, and potential toxicity.* Crit Rev Food Sci Nutr, 2011. **51**(4): p. 285-330.

[8] Acosta, E., *Bioavailability of nanoparticles in nutrient and nutraceutical delivery.* Current Opinion in Colloid & Interface Science, 2009. **14**(1): p. 3-15.

[9] Kumthekar, K.R., *Studies in Mixed Surfactant Systems and Vegetable Oil Emulsions.* 2013.

[10] McClements, D.J., *Crystals and crystallization in oil-in-water emulsions: Implications for emulsion-based delivery systems.* Advances in colloid and interface science, 2012. **174**: p. 1-30.

[11] Baran, R. and H. Maibach, *Textbook of Cosmetic Dermatology, Fourth Edition*. 2010: CRC Press.

[12] Kirk, R.E. and D.F. Othmer, *Encyclopedia of chemical technology: Chocolate and cocoa to Copper*. 1979: Wiley.

[13] Becher, P., *Encyclopedia of Emulsion Technology: Vol.1. Basic Theory*. 1983: Marcel Dekker.

[14] Everett, D.H., *Manual of Symbols and Terminology for Physicochemical Quantities and Units - Appendix 2 - Definitions, Terminology and Symbols in Colloid and Surface-Chemistry.* Pure and Applied Chemistry, 1972. **31**(4): p. 577-638.

[15] Schubert, H., R. Engel, and L. Kempa, *Principles of Structured Food Emulsions: Novel formulations and trends.* 2006: p. 1343.

[16] Moulik, S.P. and B.K. Paul, *Structure, dynamics and transport properties of microemulsions.* Advances in Colloid and Interface Science, 1998. **78**(2): p. 99-195.

[17] Joscelyne, S.M. and G. Tragardh, *Membrane emulsification - a literature review.* Journal of Membrane Science, 2000. **169**(1): p. 107-117.

[18] Schramm, L.L., *Emulsions, Foams, and Suspensions: Fundamentals and Applications*. 2005: Wiley.

[19] Tadros, T.F., *Colloids in Agrochemicals: Volume 5: Colloids and Interface Science*. 2009: Wiley.

[20] Binks, B.P. and R.S.o.C.I. Services, *Modern Aspects of Emulsion Science*. 1998: Royal Society of Chemistry, Information Services.
[21] Joscelyne, S.M. and G. Tragardh, *Food emulsions using membrane emulsification: conditions for producing small droplets.* Journal of Food Engineering, 1999. **39**(1): p. 59-64.
[22] Charcosset, C., I. Limayem, and H. Fessi, *The membrane emulsification process - a review.* Journal of Chemical Technology and Biotechnology, 2004. **79**(3): p. 209-218.
[23] Schröder, V. and H. Schubert, *Production of emulsions using microporous, ceramic membranes.* Colloids and Surfaces a-Physicochemical and Engineering Aspects, 1999. **152**(1-2): p. 103-109.
[24] McClements, D.J., *Food Emulsions: Principles, Practices, and Techniques, Second Edition*. 2004: Taylor & Francis.
[25] Swarbrick, J., *Encyclopedia of Pharmaceutical Technology*. 2007: Informa Healthcare.
[26] Sjoblom, J., *Emulsions and Emulsion Stability: Surfactant Science Series/61*. 2005: CRC Press.
[27] Florence, A.T. and J. Siepmann, *Modern Pharmaceutics, Two Volume Set, Fifth Edition*. 2009: CRC Press.
[28] Butler, H. and W.A. Poucher, *Poucher's Perfumes, Cosmetics and Soaps*. 2000: Kluwer Academic.
[29] *Notes on making cola*. Available: http://sparror.cubecinema.com/cube/cola/chemistry/cola1.htm [accessed 2 March 2010]
[30] Abismaïl, B., et al., *Emulsification by ultrasound: drop size distribution and stability.* Ultrasonics Sonochemistry, 1999. **6**(1–2): p. 75-83.
[31] Williams, P.A., *Handbook of Industrial Water Soluble Polymers*. 2008: Wiley.
[32] Vladisavljević, G.T. and R.A. Williams, *Recent developments in manufacturing emulsions and particulate products using membranes.* Advances in Colloid and Interface Science, 2005. **113**(1): p. 1-20.
[33] Thassu, D. and G.J. Chader, *Ocular Drug Delivery Systems: Barriers and Application of Nanoparticulate Systems*. 2012: Taylor & Francis.
[34] Auernhammer, G., H.J. Butt, and D. Vollmer, *Surface and Interfacial Forces - From Fundamentals to Applications*. 2008: Springer.
[35] Danielsson, I. and B. Lindman, *The definition of microemulsion.* Colloids and Surfaces, 1981. **3**(4): p. 391-392.
[36] Torchilin, V.P., *Nanoparticulates as Drug Carriers*. 2006: Imperial College Press.
[37] Benita, S., *Microencapsulation: Methods and Industrial Applications, Second Edition*. 2005: CRC Press.
[38] Wasan, D.T., M.E. Ginn and D.O. Shah, ed., *Surfactants in Chemical/Process Engineering*. 1988: Taylor & Francis.
[39] Solans, C., et al., *Nano-emulsions.* Current Opinion in Colloid & Interface Science, 2005. **10**(3–4): p. 102-110.
[40] Gutiérrez, J.M., et al., *Nano-emulsions: New applications and optimization of their preparation.* Current Opinion in Colloid & Interface Science, 2008. **13**(4): p. 245-251.

[41] Sonneville-Aubrun, O., J.T. Simonnet, and F. L'Alloret, *Nano-emulsions: a new vehicle for skincare products.* Advances in Colloid and Interface Science, 2004. **108**: p. 145-149.
[42] Schultz, S., et al., *High-pressure homogenization as a process for emulsion formation.* Chemical Engineering & Technology, 2004. **27**(4): p. 361-368.
[43] Tesch, S., C. Gerhards, and H. Schubert, *Stabilization of emulsions by OSA starches.* Journal of Food Engineering, 2002. **54**(2): p. 167-174.
[44] Gijsbertsen-Abrahamse, A.J., A. van der Padt, and R.M. Boom, *Status of cross-flow membrane emulsification and outlook for industrial application.* Journal of Membrane Science, 2004. **230**(1–2): p. 149-159.
[45] Stang, M., H. Schuchmann, and H. Schubert, *Emulsification in High-Pressure Homogenisers.* Engineering in Life Sciences, 2001. **1**(4): p. 151-157.
[46] Weiss, J. *Emulsion Processing: Homogenization*. in *Emulsion Workshop*. 2008.
[47] Urban, K., et al., *Rotor-Stator and Disc Systems for Emulsification Processes.* Chemical Engineering & Technology, 2006. **29**(1): p. 24-31.
[48] Aguilera, J.M. and P.J. Lillford, *Food Materials Science: Principles and Practice*. 2007: Springer.
[49] Kentish, S., et al., *The use of ultrasonics for nano-emulsion preparation.* Innovative Food Science & Emerging Technologies, 2008. **9**(2): p. 170-175.
[50] Wang, L., et al., *Nano-emulsions Prepared by a Two-Step Low-Energy Process.* Langmuir, 2008. **24**(12): p. 6092-6099.
[51] SHlNODA, K. and H. KUNlEDA, *Phase properties of emulsions: PIT and HLB.* Encyclopedia of Emulsion Technology: Basic Theory, 1983. **1**: p. 337.
[52] Hasenhuettl, G.L. and R.W. Hartel, *Food Emulsifiers and Their Applications*. 2008: Springer New York.
[53] Engels, T., T. Förster, and W. von Rybinski, *The influence of coemulsifier type on the stability of oil-in-water emulsions.* Colloids and Surfaces A: Physicochemical and Engineering Aspects, 1995. **99**(2–3): p. 141-149.
[54] Fernandez, P., et al., *Nano-emulsion formation by emulsion phase inversion.* Colloids and Surfaces A: Physicochemical and Engineering Aspects, 2004. **251**(1): p. 53-58.
[55] Nakashima, T., M. Shimizu, and M. Kukizaki, *Particle control of emulsion by membrane emulsification and its applications.* Advanced Drug Delivery Reviews, 2000. **45**(1): p. 47-56.
[56] Suzuki, K., I. Fujiki, and Y. Hagura, *Preparation of Corn Oil/Water and Water/Corn Oil Emulsions Using PTFE Membranes.* Food Science and Technology International, Tokyo, 1998. **4**(2): p. 164-167.
[57] Liu, W., X.L. Yang, and W. Winston Ho, *Preparation of uniform-sized multiple emulsions and micro/nano particulates for drug delivery by membrane emulsification.* Journal of pharmaceutical sciences, 2011. **100**(1): p. 75-93.
[58] van der Zwan, E., et al., *Visualization of droplet break-up in pre-mix membrane emulsification using microfluidic devices.* Colloids and Surfaces A: Physicochemical and Engineering Aspects, 2006. **277**(1–3): p. 223-229.
[59] Drioli, E., A. Criscuoli, and E. Curcio, *Membrane Contactors: Fundamentals, Applications and Potentialities*. 2006: Elsevier.
[60] Suzuki, K., K. Hayakawa, and Y. Hagura, *Preparation of High Concentration O/W and W/O Emulsions by the Membrane Phase Inversion*

Emulsification Using PTFE Membranes. Food Science and Technology Research, 1999. **5**(2): p. 234-238.
[61] Shima, M., et al., *Preparation of fine W/O/W emulsion through membrane filtration of coarse W/O/W emulsion and disappearance of the inclusion of outer phase solution.* Food Hydrocolloids, 2004. **18**(1): p. 61-70.
[62] Park, S.-H., T. Yamaguchi, and S.-i. Nakao, *Transport mechanism of deformable droplets in microfiltration of emulsions.* Chemical Engineering Science, 2001. **56**(11): p. 3539-3548.
[63] Toorisaka, E., et al., *Hypoglycemic effect of surfactant-coated insulin solubilized in a novel solid-in-oil-in-water (S/O/W) emulsion.* International Journal of Pharmaceutics, 2003. **252**(1–2): p. 271-274.
[64] Vladisavljević, G.T., M. Shimizu, and T. Nakashima, *Preparation of monodisperse multiple emulsions at high production rates by multi-stage premix membrane emulsification.* Journal of Membrane Science, 2004. **244**(1–2): p. 97-106.
[65] Spasic, A.M. and J.P. Hsu, *Finely Dispersed Particles: Micro-, Nano-, and Atto-Engineering*. 2005: Taylor & Francis.
[66] Abrahamse, A.J., et al., *Analysis of droplet formation and interactions during cross-flow membrane emulsification.* Journal of Membrane Science, 2002. **204**(1–2): p. 125-137.
[67] Pabby, A.K., S.S.H. Rizvi, and A.M.S. Requena, *Handbook of Membrane Separations: Chemical, Pharmaceutical, Food, and Biotechnological Applications*. 2008: Taylor & Francis.
[68] Charcosset, C., *Preparation of emulsions and particles by membrane emulsification for the food processing industry.* Journal of Food Engineering, 2009. **92**(3): p. 241-249.
[69] van Rijn, C., *Nano and Micro Engineered Membrane Technology*. 2004: Elsevier Science.
[70] Williams, R.A., et al., *Controlled Production of Emulsions Using a Crossflow Membrane: Part II: Industrial Scale Manufacture.* Chemical Engineering Research and Design, 1998. **76**(8): p. 902-910.
[71] Berot, S., et al., *Key Factors in Membrane Emulsification.* Chemical Engineering Research and Design, 2003. **81**(9): p. 1077-1082.
[72] Yanagishita, T., et al., *Preparation of Monodisperse SiO2 Nanoparticles by Membrane Emulsification Using Ideally Ordered Anodic Porous Alumina.* Langmuir, 2004. **20**(3): p. 554-555.
[73] Fuchigami, T., M. Toki, and K. Nakanishi, *Membrane Emulsification Using Sol-Gel Derived Macroporous Silica Glass.* Journal of Sol-Gel Science and Technology, 2000. **19**(1-3): p. 337-341.
[74] Dowding, P.J., J.W. Goodwin, and B. Vincent, *Production of porous suspension polymer beads with a narrow size distribution using a cross-flow membrane and a continuous tubular reactor.* Colloids and Surfaces A: Physicochemical and Engineering Aspects, 2001. **180**(3): p. 301-309.
[75] Liu, X.D., et al., *Preparation of uniform calcium alginate gel beads by membrane emulsification coupled with internal gelation.* Journal of Applied Polymer Science, 2003. **87**(5): p. 848-852.
[76] Giorno, L., N. Li, and E. Drioli, *Preparation of oil-in-water emulsions using polyamide 10 kDa hollow fiber membrane.* Journal of Membrane Science, 2003. **217**(1–2): p. 173-180.

[77] Yamazaki, N., et al., *A Comparison of Membrane Emulsification Obtained Using SPG (Shirasu Porous Glass) and PTFE [Poly(Tetrafluoroethylene)] Membranes.* Journal of Dispersion Science and Technology, 2002. **23**(1-3): p. 279-292.
[78] Gijsbertsen-Abrahamse, A.J., A. van der Padt, and R.M. Boom, *Influence of membrane morphology on pore activation in membrane emulsification.* Journal of Membrane Science, 2003. **217**(1–2): p. 141-150.
[79] Kobayashi, I., et al., *Silicon array of elongated through-holes for monodisperse emulsion droplets.* AIChE Journal, 2002. **48**(8): p. 1639-1644.
[80] Kobayashi, I., M. Nakajima, and S. Mukataka, *Preparation characteristics of oil-in-water emulsions using differently charged surfactants in straight-through microchannel emulsification.* Colloids and Surfaces A: Physicochemical and Engineering Aspects, 2003. **229**(1–3): p. 33-41.
[81] Peng, S.J. and R.A. Williams, *Controlled Production of Emulsions Using a Crossflow Membrane: Part I: Droplet Formation from a Single Pore.* Chemical Engineering Research and Design, 1998. **76**(8): p. 894-901.
[82] Schröder, V., O. Behrend, and H. Schubert, *Effect of Dynamic Interfacial Tension on the Emulsification Process Using Microporous, Ceramic Membranes.* Journal of Colloid and Interface Science, 1998. **202**(2): p. 334-340.
[83] Abrahamse, A.J., et al., *Process fundamentals of membrane emulsification: Simulation with CFD.* AIChE Journal, 2001. **47**(6): p. 1285-1291.
[84] Vladisavljević, G.T. and H. Schubert, *Influence of process parameters on droplet size distribution in SPG membrane emulsification and stability of prepared emulsion droplets.* Journal of Membrane Science, 2003. **225**(1–2): p. 15-23.
[85] Rieger, M. and L.D. Rhein, *Surfactants in Cosmetics, Second Edition*. 1997: Taylor & Francis.
[86] van der Graaf, S., et al., *Influence of dynamic interfacial tension on droplet formation during membrane emulsification.* Journal of Colloid and Interface Science, 2004. **277**(2): p. 456-463.
[87] Morrison, I.D. and S. Ross, *Colloidal Dispersions: Suspensions, Emulsions, and Foams*. 2002: Wiley.
[88] Wilhelm, K.P., et al., *Bioengineering of the Skin: Skin Imaging & Analysis*. 2006: CRC Press.
[89] Kunjappu, J., *Ink chemistry.* Chemistry in Britain, 2003. **39**(3): p. 22-25.
[90] Kobayashi, I., et al., *Microscopic observation of emulsion droplet formation from a polycarbonate membrane.* Colloids and Surfaces A: Physicochemical and Engineering Aspects, 2002. **207**(1–3): p. 185-196.
[91] Güell, C., M. Ferrando, and F. López, *Monitoring and Visualizing Membrane-Based Processes*. 2009: Wiley.
[92] Shui, L., A. van den Berg, and J.C. Eijkel, *Interfacial tension controlled W/O and O/W 2-phase flows in microchannel.* Lab Chip, 2009. **9**(6): p. 795-801.
[93] Griffin, W.C., *Classification of surface-active agents by" HLB"*. J Soc Cosmetic Chemists, 1946. **1**: p. 311-326.
[94] Trotta, M., F. Pattarino, and T. Ignoni, *Stability of drug-carrier emulsions containing phosphatidylcholine mixtures.* Eur J Pharm Biopharm, 2002. **53**(2): p. 203-8.

[95] Israelachvili, J.N., D.J. Mitchell, and B.W. Ninham, *Theory of self-assembly of hydrocarbon amphiphiles into micelles and bilayers.* Journal of the Chemical Society, Faraday Transactions 2: Molecular and Chemical Physics, 1976. **72**(0): p. 1525-1568.
[96] Dunford, N.T., *Food and Industrial Bioproducts and Bioprocessing*. 2012: Wiley.
[97] Kukizaki, M. and M. Goto, *Size control of nanobubbles generated from Shirasu-porous-glass (SPG) membranes.* Journal of Membrane Science, 2006. **281**(1–2): p. 386-396.
[98] Katoh, R., et al., *Preparation of food emulsions using a membrane emulsification system.* Journal of Membrane Science, 1996. **113**(1): p. 131-135.
[99] Innings, F. and C. Trägårdh, *Analysis of the flow field in a high-pressure homogeniser*. Experimental Thermal and Fluid Science, 2007. **32**(2): p. 345-354.
[100] Yuan, Q., et al., *Manufacture of controlled emulsions and particulates using membrane emulsification.* Desalination, 2008. **224**(1): p. 215-220.
[101] Vladisavljević, G.T., et al., *Production of O/W emulsions using SPG membranes, ceramic α-aluminium oxide membranes, microfluidizer and a silicon microchannel plate—a comparative study.* Colloids and Surfaces A: Physicochemical and Engineering Aspects, 2004. **232**(2–3): p. 199-207.
[102] Robinson, J.P., et al., *Solvent flux through dense polymeric nanofiltration membranes.* Journal of Membrane Science, 2004. **230**(1–2): p. 29-37.
[103] Huisman, I., et al., *Determining the zeta potential of microfiltration membranes using the electroviscous effect.* J. Membr. Sci, 1999. **156**: p. 153-158.
[104] Mine, Y., M. Shimizu, and T. Nakashima, *Preparation and stabilization of simple and multiple emulsions using a microporous glass membrane.* Colloids and Surfaces B: Biointerfaces, 1996. **6**(4–5): p. 261-268.
[105] Sheibat-Othman, N., et al., *Preparation of pH-sensitive particles by membrane contactor*. Colloids and Surfaces A: Physicochemical and Engineering Aspects, 2008. **315**: p. 13-22.
[106] Hao, D.-X., et al., *Controlling Factors on Droplets Uniformity in Membrane Emulsification: Experiment and Modeling Analysis.* Industrial & Engineering Chemistry Research, 2008. **47**(17): p. 6418-6425.
[107] Drioli, E. and L. Giorno, *Membrane Operations: Innovative Separations and Transformations*. 2009: Wiley.
[108] Lovelyn, C. and A.A. Attama, *Current state of nanoemulsions in drug delivery.* Journal of Biomaterials and Nanobiotechnology, 2011. **2**(05): p. 626.
[109] Abdulrazik, M., et al., *Ocular delivery of cyclosporin A. II. Effect of submicron emulsion's surface charge on ocular distribution of topical cyclosporin A.* STP pharma sciences, 2001. **11**(6): p. 427-432.
[110] Okonogi, S., et al., *Methods for producing emulsions, low-fat spread and oil-in-water-in-oil type spread*. 1994, Google Patents.
[111] Gershanik, T. and S. Benita, *Positively charged self-emulsifying oil formulation for improving oral bioavailability of progesterone.* Pharmaceutical Development and Technology, 1996. **1**(2): p. 147-157.
[112] Benita, S. and M. Levy, *Submicron emulsions as colloidal drug carriers for intravenous administration: comprehensive physicochemical*

characterization. Journal of pharmaceutical sciences, 1993. **82**(11): p. 1069-1079.
[113] Pal, R., *Effect of droplet size on the rheology of emulsions.* AIChE Journal, 1996. **42**(11): p. 3181-3190.
[114] Malcolmson, C., et al., *Effect of oil on the level of solubilization of testosterone propionate into nonionic oil-in-water microemulsions.* Journal of pharmaceutical sciences, 1998. **87**(1): p. 109-116.
[115] Tamilvanan, S., *Formulation of multifunctional oil-in-water nanosized emulsions for active and passive targeting of drugs to otherwise inaccessible internal organs of the human body.* International Journal of Pharmaceutics, 2009. **381**(1): p. 62-76.
[116] Kruglyakov, P.M., *Hydrophile - Lipophile Balance of Surfactants and Solid Particles: Physicochemical aspects and applications*. 2000: Elsevier Science.
[117] Tenjarla, S., *Microemulsions: an overview and pharmaceutical applications.* Critical Reviews™ in Therapeutic Drug Carrier Systems, 1999. **16**(5).
[118] Wang, Z., et al., *Hexagonal liquid crystalline phases formed in ternary systems of Brij 97-water-ionic liquids.* Langmuir, 2005. **21**(11): p. 4931-4937.
[119] Malcolmson, C. and M.J. Lawrence, *A comparison of the incorporation of model steroids into non-ionic micellar and microemulsion systems.* Journal of pharmacy and pharmacology, 1993. **45**(2): p. 141-143.
[120] Kale, N.J. and L.V. Allen, *Studies on microemulsions using Brij 96 as surfactant and glycerin, ethylene glycol and propylene glycol as cosurfactants.* International journal of pharmaceutics, 1989. **57**(2): p. 87-93.
[121] Warisnoicharoen, W., A. Lansley, and M. Lawrence, *Nonionic oil-in-water microemulsions: the effect of oil type on phase behaviour.* International journal of pharmaceutics, 2000. **198**(1): p. 7-27.
[122] Wang, Z., et al., *Microstructure and rheological properties of liquid crystallines formed in Brij 97/water/IPM system.* Journal of colloid and interface science, 2006. **297**(2): p. 813-818.
[123] Laouini, A., H. Fessi, and C. Charcosset, *Membrane emulsification: A promising alternative for vitamin E encapsulation within nano-emulsion.* Journal of Membrane Science, 2012. **423**: p. 85-96.
[124] Malcolmson, C., D.J. Barlow, and M.J. Lawrence, *Light-scattering studies of testosterone enanthate containing soybean oil/C18: 1E10/water oil-in-water microemulsions.* Journal of pharmaceutical sciences, 2002. **91**(11): p. 2317-2331.
[125] Whitehurst, R.J., *Emulsifiers in Food Technology*. 2008: Wiley.
[126] Masotti, A., et al., *Novel Tween 20 derivatives enable the formation of efficient pH-sensitive drug delivery vehicles for human hepatoblastoma.* Bioorg Med Chem Lett, 2010. **20**(10): p. 3021-5
[127] *Zetasizer Nano Series User Manual MAN 0317*, ed. M.I. Ltd. 2004.
[128] *Size Determination by Dynamic Light Scattering*. Available: http://www.wyatt.eu/index.php?id=dynamic-light-scattering [accessed 22 March 2010].
[129] *Dynamic Light Scattering*. Available: http://www.malvern.com/LabEng/technology/dynamic_light_scattering/dynamic_light_scattering.htm [accessed 22 March 2010].

[130] *NanoSight NTA 2.1 Operating Manual P554B*, NanoSight Ltd. 2010.
[131] Dragovic, R.A., et al., *Sizing and phenotyping of cellular vesicles using Nanoparticle Tracking Analysis.* Nanomedicine: Nanotechnology, Biology and Medicine, 2011. **7**(6): p. 780-788.
[132] NanoSight, *Zeta Potential Analysis using Z-NTA*. Available: http://nanotechweb.org/cws/article/whitepapers/45885 [accessed 16 January 2013].
[133] *ZetaSight Operating Manual P559G*, NanoSight Ltd. 2011.
[134] Seidel, C., et al., *Synthesis and Characterization of Cross-linked Carboxymethyl Potato Starch Ether Gels.* Starch-Stärke, 2004. **56**(5): p. 157-166.
[135] Saravanan, R. and P. Rani, *Metal and Alloy Bonding - An Experimental Analysis: Charge Density in Metals and Alloys*. 2011: Springer.
[136] *ImageJ Manual*. Available: http://rsbweb.nih.gov/ij/docs/pdfs/ImageJ.pdf [accessed 20 November 2010].
[137] Nazarzadeh, E. and S. Sajjadi, *Thermal Effects in Nanoemulsification by Ultrasound.* Industrial & Engineering Chemistry Research, 2013. **52**(28): p. 9683-9689.
[138] Danov, K.D., P.A. Kralchevsky, and I.B. Ivanov, *Dynamic processes in surfactant-stabilized emulsions.* Encyclopedic Handbook of Emulsion Technology, 2001: p. 621-659.
[139] Golemanov, K., et al., *Latex-Particle-Stabilized Emulsions of Anti-Bancroft Type.* Langmuir, 2006. **22**(11): p. 4968-4977.
[140] Brocart, B., et al., *Design of in-line emulsification processes for water-in-oil emulsions.* Journal of dispersion science and technology, 2002. **23**(1-3): p. 45-53.
[141] Fradette, L., B. Brocart, and P. Tanguy, *Comparison of mixing technologies for the production of concentrated emulsions.* Chemical Engineering Research and Design, 2007. **85**(11): p. 1553-1560.
[142] Nazarzadeh, E. and S. Sajjadi, *Viscosity Effects in Miniemulsification via Ultrasound.* Aiche Journal, 2010. **56**(10): p. 2751-2755.
[143] Walstra, P., *Principles of emulsion formation.* Chemical Engineering Science, 1993. **48**(2): p. 333-349.
[144] Pacek, A., C. Man, and A. Nienow, *On the Sauter mean diameter and size distributions in turbulent liquid/liquid dispersions in a stirred vessel.* Chemical Engineering Science, 1998. **53**(11): p. 2005-2011.
[145] McClements, D.J. and J. Weiss, *Lipid Emulsions*, in *Bailey's Industrial Oil and Fat Products*. 2005, John Wiley & Sons, Inc.
[146] Roger, K., B. Cabane, and U. Olsson, *Formation of 10−100 nm Size-Controlled Emulsions through a Sub-PIT Cycle.* Langmuir, 2010. **26**(6): p. 3860-3867.
[147] Aronson, M.P., *The role of free surfactant in destabilizing oil-in-water emulsions.* Langmuir, 1989. **5**(2): p. 494-501.
[148] *LiposoFast LF-50 Operating Instructions*, AVESTIN, Inc. 2011.
[149] *Synkera flat-sheet ceramic membranes*. Available: http://www.synkera.com/index.php?option=com_content&view=article&catid=2:products-and-services&id=9:ceramic-membranes [accessed 10 October 2012].

[150] *Nuclepore™ polycarbonate track-etched (PCTE) membranes*. Available: http://www.whatman.com/NucleporeTrackEtchedMembranes.aspx [Accessed 10 October 2012].
[151] Ghaddar, A., et al., *Thermal evolution of magnetic interactions in Ni nanowires embedded in polycarbonate membranes by ferromagnetic resonance.* Acta Physica Polonica A, 2009. **116**(6): p. 1039-1043.
[152] Rauscher, H., M. Perucca, and G. Buyle, *Plasma Technology for Hyperfunctional Surfaces: Food, Biomedical and Textile Applications*. 2010: Wiley.
[153] Adamson, A.W. and A.P. Gast, *Physical chemistry of surfaces*. 1997: Wiley.
[154] Spasic, A.M. and J.P. Hsu, *Finely Dispersed Particles: Micro-, Nano-, and Atto-Engineering*. 2005: Taylor & Francis.
[155] Hamley, I.W., *Introduction to soft matter: polymers, colloids amphiphiles, and liquid crystals*. 2000: Wiley.
[156] El-Abbassi, A., et al., *Preparation and characterization of highly stable monodisperse argan oil-in-water emulsions using microchannel emulsification.* European Journal of Lipid Science and Technology, 2013. **115**(2): p. 224-231.
[157] Hameed, R.A., et al., *Adsorption studies of non-ionic surfactants at different vegetable oil-water interfaces.* Latin American Journal of Pharmacy, 2012. **31**.
[158] Nazir, A., K. Schroën, and R. Boom, *Premix emulsification: A review.* Journal of Membrane Science, 2010. **362**(1–2): p. 1-11.
[159] Udeagbara, S.G., *Effect of Temperature and Impurities on Surface Tension of Crude Oil*. 2010: Universal Publishers.
[160] Mittal, V., *Advanced Polymer Nanoparticles: Synthesis and Surface Modifications*. 2011: CRC Press.
[161] Sajjadi, S., *Nanoemulsion formation by phase inversion emulsification: On the nature of inversion.* Langmuir, 2006. **22**(13): p. 5597-5603.
[162] Zhou, Q.-Z., G.-H. Ma, and Z.-G. Su, *Effect of membrane parameters on the size and uniformity in preparing agarose beads by premix membrane emulsification.* Journal of Membrane Science, 2009. **326**(2): p. 694-700.
[163] *Kerasep™ membranes catalogue*, Novasep Process, France.
[164] *Micro Carbosep®/ Kerasep™ Operating Instruction*, Novasep Process, France.
[165] Netzsch NEMO® Pump Manual, NETZSCH PUMPS LTD.
[166] Lepercq-Bost, É., et al., Estimating the risk of coalescence in membrane emulsification. Journal of Membrane Science, 2010. 357(1–2): p. 36-46.
[167] Graves, S.M. and L.A. University of California, *The Formation, Optical Properties, and Structure of Nanoemulsions*. 2008: University of California, Los Angeles.
[168] Herrera, M., *Analytical Techniques for Studying the Physical Properties of Lipid Emulsions*. 2012: Springer US.
[169] Wang, L., et al., *Oil-in-water nanoemulsions for pesticide formulations.* Journal of colloid and interface science, 2007. **314**(1): p. 230-235.
[170] Wooster, T.J., M. Golding, and P. Sanguansri, *Impact of oil type on nanoemulsion formation and Ostwald ripening stability.* Langmuir, 2008. **24**(22): p. 12758-12765.

[171] Spernath, L. and S. Magdassi, *A new method for preparation of poly-lauryl acrylate nanoparticles from nanoemulsions obtained by the phase inversion temperature process.* Polymers for Advanced Technologies, 2007. **18**(9): p. 705-711.
[172] Tadros, T.F., *Interfacial Phenomena and Colloid Stability: Industrial Applications*. 2015: Walter de Gruyter GmbH & Co KG.
[173] Kukizaki, M., *Preparation of solid lipid microcapsules via solid-in-oil-in-water dispersions by premix membrane emulsification.* Chemical Engineering Journal, 2009. **151**(1): p. 387-396.

Appendix A

Thermal energy equation

The thermal energy equation was used in this study for the estimation of energy consumption in systems that require the materials to be heated:

$$Q = mC_p\Delta T$$

Where,

Q is the energy required to increase the temperature of a material (J),

m is the mass of the material (kg),

C_p is the specific heat capacity of the material (J kg^{-1} $°C^{-1}$),

and ΔT is the variation in temperature during heating (°C).

In systems comprised of a mixture of materials, the energy required to increase the temperature of the mixture can be estimated as the sum of heat required for each component. Therefore, the energy consumption was estimated by rewriting the equation as:

$$Q = Q_{water} + Q_{surfactant} + Q_{oil}$$

$$= \left(m_{water} \times C_{p_{Water}} \times (\mathrm{T} - 21)\right) + \left(m_{surfactant} \times C_{p_{surfactant}} \times (\mathrm{T} - 21)\right)$$

$$+ \left(m_{oil} \times C_{p_{oil}} \times (\mathrm{T} - 21)\right)$$

It should be noted that the specific heat capacity varies with temperature; however in order to simplify calculations, specific heat of phases at room temperature were used for calculations. Also, specific heat capacity of surfactant could not be obtained and, therefore, it was assumed that specific heat capacity of surfactant is equal to that of oil phase. The specific heat capacities of water and soybean oil are 4.84 and 1.97 J g^{-1} $°C^{-1}$ at 25 °C, respectively. Masses of phases were estimated according to their concentration.

Appendix B

SEM images of flat sheet ceramic membranes

1) SEM images of a new 55 ± 6 nm ceramic membrane showing the porous structure of the anodic alumina.

Top view ($\times$ **50,000**)	**Top view** ($\times$ **100,000**)
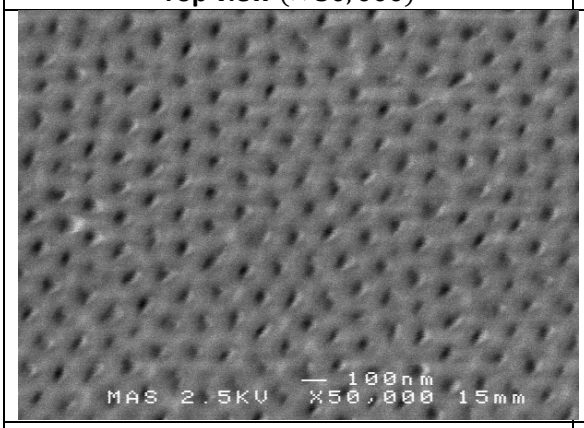	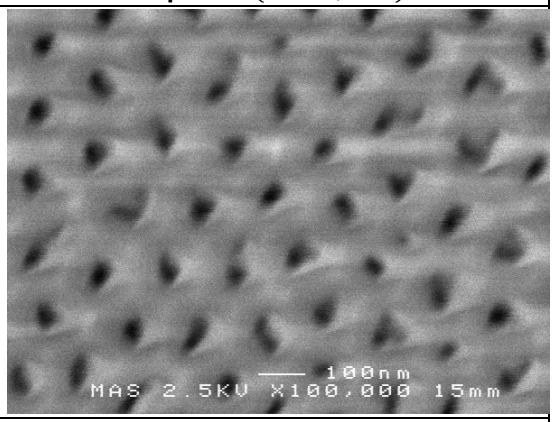
Cross section	**Side view**
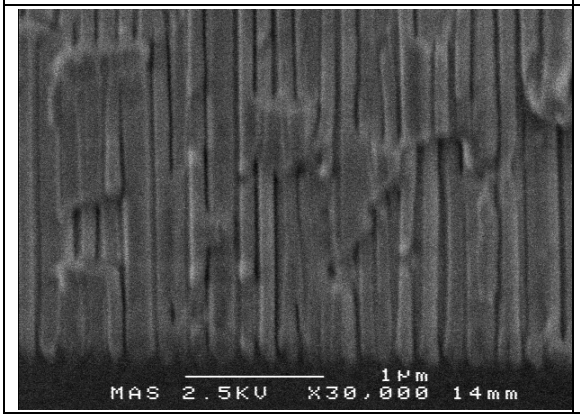	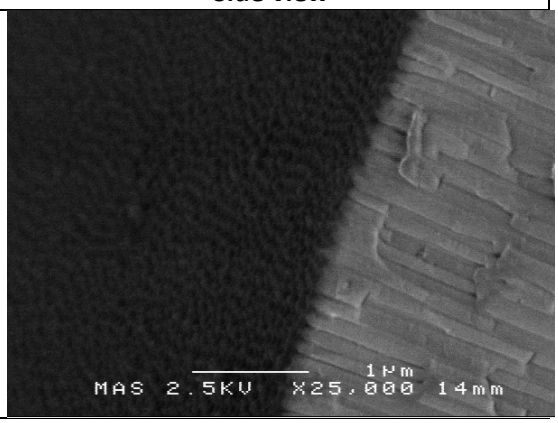

2) SEM images of a new 100 ± 10 nm ceramic membrane showing the porous structure of the anodic alumina.

Top view $(\times \mathbf{50,000})$	**Top view** $(\times \mathbf{100,000})$
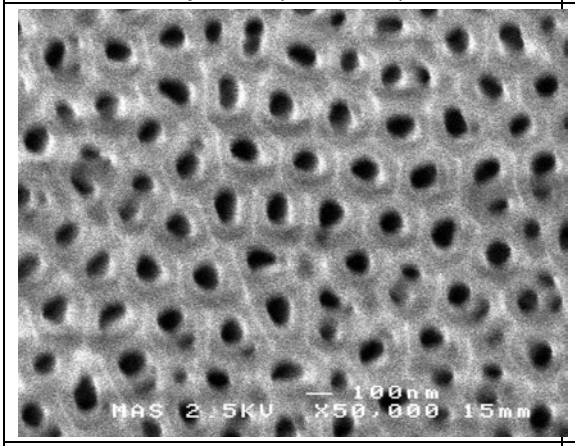	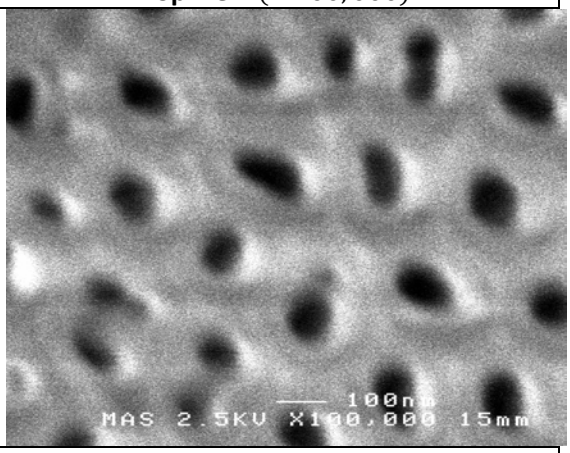
Cross section	**Side view**
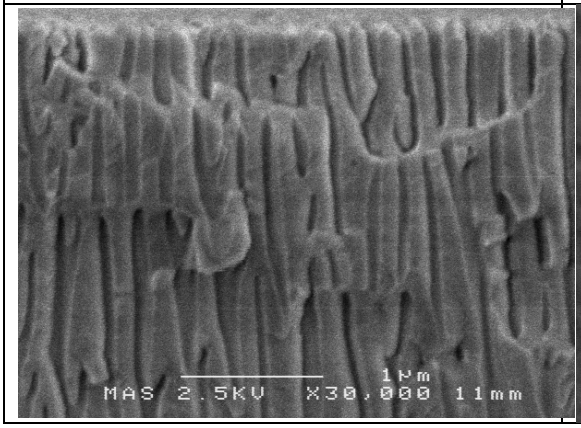	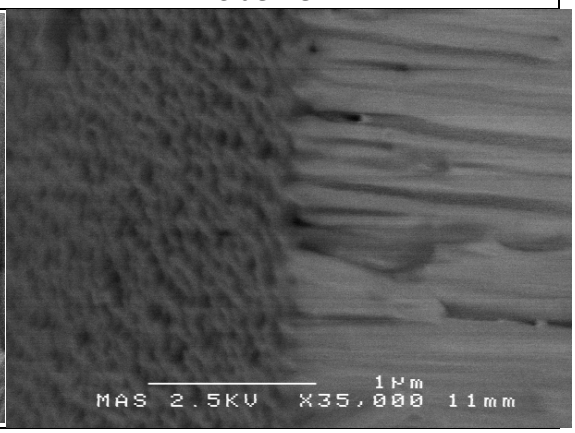

Appendix C

Volume-pressure Equation used for estimating the energy consumption during emulsification

$$W = \Delta P_{tm} \times V_e$$

Where,

W is the work done by applied pressure (J),

ΔP_{tm} is the applied (trans-membrane) pressure (N m^{-2}),

and V_e is the volume of emulsion (m^3).

Appendix D

P & ID coding for the experimental rig designed for the cross-flow membrane emulsification method

V-1	Valve 1 – Recycle Valve (Change and control the flow from recycle to module)
V-2	Valve 2 – Back Pressure Valve (Increase retentate back pressure over the membrane)
V-3	Valve 3 – Sample/Drainage Valve (Collect samples and drain the system)
V-4	Valve 4 – Permeate Valve (Open and close permeate tube)
P-1	Pump
G-1	Pressure Gauge 1 (Pre-module)
G-2	Pressure Gauge 2 (Post-module)
G-3	Pressure Gauge 3 (Pressure vessel)
G-4	Pressure Gauge 4 (N_2 Cylinder)
T-1	Feed Tank

Appendix E

Key features and characteristics of Kerasep™ membranes

1) Key features of Kerasep™ membranes [163]

Key Features	Descriptions
Wide range of cut-offs	15 kD to 0.45 µm (enabling precise separations)
Extreme temperature resistance	wide temperature limits up to 85 °C
Extreme pH resistance	Wide pH limits (pH: 0-14*)
Insensitivity to solvents (chemical resistance)	Wide range of solvents can be used Compatibility with all organic solvents, (ethanol, Methanol, Phenol resistance)
Long lifetime	Requires enough care; cleaning before & after each experiments to avoid fouling
Cleaning	CIP → NaOH, HNO_3, O_3, NaClO SIP → High pressure hot water (121 °C)

*This feature is not essential in this work as there is not a widely different range of pH in the materials used (Water, Oil, Surfactant). Also the pump can only handle pH range of 4-10.

2) Characteristics of Kerasep™ membranes [163]

Membranes	Kerasep™	
Outside Diameter	10 mm	
Inside Diameter	6 mm	
Length	400 mm	
Surface Area	0.008 m²	
Active Layer	ZrO_2- TiO_2	
Cut-off Thresholds (Kerasep™)	15,000 Daltons	Ultrafiltration
	50,000 Daltons	Ultrafiltration
	150,000 Daltons	Ultrafiltration
	300,000 Daltons	Ultrafiltration
	0.1 µm	Microfiltration
	0.2 µm	Microfiltration
	0.45 µm	Microfiltration
Support	TiO_2 - Al_2O_3	

Appendix F

Principles of setting and maintaining the rig

I) Inserting a membrane into the module:

First, the membrane is inserted into the membrane module. Although membranes are resistant to mechanical, chemical and thermal stress, they are susceptible to physical damage and enough care must be taken to avoid any damage when the membranes are inserted or removed from the module. It is very important to check the membrane surface for any possible dust or visible particulates and also to ensure the module is dry and free from any contamination prior to use. The step-by-step guideline for inserting the membrane into the module is as follows:

1. The membrane surface must be checked to remove any dust or visible particulates.
2. Ethylene Propylene Diene Monomer (EPDM) membrane gasket should be attached to one end of the membrane.
3. To ensure the module is dry and free from any contamination it must be removed from the system and inspect carefully. In the presence of any impurities further cleaning with pure water and drying is required.
4. The end of the membrane without the gasket must be inserted carefully into the module while holding it vertically upward. There must be a minimum contact between the membrane and the inner area of the module.
5. When the membrane is placed into the module it must be sealed with the other gasket and ensure there are not any gaps at either ends.
6. By using the brackets the module should be fixed into position.
7. The threads at either ends of the module should be tightened so that the metal piping is sealed against the membrane gaskets. The membrane is now prepared to be rinsed and cleaned.

After inserting the membrane into the module, the membrane module is fixed into position and the threads at either side of the module is tightened in order to make sure the metal piping is completely sealed against the membrane gaskets. Now the system is ready to start up.

II) Start-up the system:

Because of the self-priming capabilities of the pump, starting up the system is an easy and quick procedure. In order to gain enough pressure to prime the pump there should be an extra 2 litres of solution for the system void volume. Therefore the feed tank is required to be filled with at least 5 litres of solution (*i.e* continuous phase). After priming the pump, the system is ready to be rinsed and cleaned. The step-by-step guideline for starting up the system is as follows:

1. Fill the feed tank with the required level of solution, which here is the continuous phase. (In order to gain enough pressure to prime the pump there should be an extra 2 litres of solution for the system void. Therefore at least 5 litres of solution in total is required)

2. Reopen the priming bolt located on the pump to decrease the air-lock within the helical pump mechanism, which allows water to flow through the pump. When water begins to seep out of the priming bolt hole, the bolt should be tightened to prevent liquid loss. The pump is now primed.

3. Fill the water quench pot of the pump with 125ml of water and make sure there is no contaminated water left from before.

4. Open the recycle valve (V-1), turn the pump onto 20 and leave it at this speed until drops of solution begin to return to the feed tank through the recycle tube. Then raise the pump speed gradually to 50 and start to close V-1 partially whilst controlling the rotameters to make sure the module does not undergo too much flow over its surface.

5. When the solution begins to return into the tank through the membrane outlet tube the system is ready for the experiment.

III) Cleaning the system:

It is necessary to clean the system before and after each experiment to avoid membrane fouling and to prepare emulsions free from any contamination. Based on the manufacturer's (Novasep, France), the guideline for cleaning the system is as follows:

1. Rinse and drain

Rinse and drain the system with pure water at temperature between 15 to 50 ºC. 6 litres of water is required in this stage which does not include the system void. After pumping all the water completely through the recycle and membrane module, it will be drained via V-3.

2. Basic Wash

a) Prepare 3 litres of 5-10 gl^{-1} of NaOH (Sodium Hydroxide) solution with boiling water. The pH must be checked to make sure is not more than 10. Including the 2 litres pump void, 5 litres of solution in total is needed.
b) Add the solution to the tank and ensure the temperature is between 80 and 85 ºC.
c) Pump the solution through the recycle for 5 minutes.
d) Close the recycle valve V-1 and pump for further 20 minutes.
e) Open V-1 and increase the pressure over the module to 3 bar by using back pressure valve (V-2) for 5 minutes.
f) Re-open V-2 and make sure the recycle valve (V-1) is completely open and drain the system as much as possible using V-3 without un-priming the pump.

3. Rinse to neutrality

a) Fill the tank with 10 litres of pure water (temperature between 15 to 50 ºC).
b) Pump throughout the system while flushing through V-3.
c) After the tank becomes empty, refill the tank with a further 10 litres of water and flush again.
d) Check the pH. If it is below 7.5 go to Step D. Otherwise, re-flush the system with pure water until the pH becomes neutral.

4. Acid wash

a) Prepare 3 litres of 3-5 $ml.l^{-1}$ of HNO_3 60% (v/v) solution with boiling water. The pH must be checked to make sure is not more than 5.

b) Add the solution to the tank and leave it to cool until it reaches 50 to 60 ºC.

c) Pump the solution trough the recycle for 5 minutes.

d) Close V-1 and pump for a further 20 minutes.

e) Open V-1 and increase the pressure over the module to 2 bar by using back pressure valve (V-2) for 5 minutes.

f) Re-open V-2 and make sure the recycle valve (V-1) is completely open and drain the system as much as possible using V-3 without un-priming the pump.

5. Rinse to neutrality

Carry out Step C again until the pH becomes neutral.

6. Water flow

Fill the tank again with pure water and pump continuously to remove any acid residual.

IV) Operating the Pressure Vessel:

After cleaning the system and before starting any experiment, the pressure vessel needs to be checked as well. First, all of the fittings and connections on the vessel must be examined to ensure there is no leak. Then, in order to check whether the pressure vessel works properly, the opposite end of the line is submerged in a water beaker while opening the valve on the disperse flux line. Seeing bubbles shows that nitrogen is coming out of the line and the system is ready to use. The complete step-by-step protocol for checking the pressure vessel is as follows:

1. For the safety reason, make sure the regulator on the cylinder is completely off before and after each experiment.
2. Ensure the lid on the pressure vessel is fully closed and secured. Check the lid is fixed and does not move.
3. Apply a small amount of pressure to the system by using the N_2 cylinder while the valve on the dispersed phase line is fully closed.

4. All of the fittings and connections on the vessel must be checked to ensure there is not any leak and in case of any leak tighten them accordingly.
5. Open the valve on the dispersed flux line and start to apply pressure. To check whether the pressure vessel is working properly, submerge the opposite end of the line in a water beaker. Seeing bubbles shows the air is coming out of the line. Now the pressure vessel can be filled with relevant dispersed phase.
6. When the experiment is done remove the remaining air from the vessel and release the pressure by gradually lifting up safety valve.
7. Ensure the cylinder is off and check the safety valve again to see there is no air remaining in the vessel. It is now safe to open the vessel.

V) Draining the system:

After the experiment is carried out and the system is thoroughly rinsed, a complete draining as per manufacturer's guideline is required if the system remains un-used for a long time. It is necessary to make sure the pump does not run dry throughout the draining procedure as this will result in excessive pump damage. The guideline for draining system is as follows:

1. Flush the majority of water in the system following the same procedure described in cleaning section.
2. After making sure all valves are open, undo the flexible hose from the pump feed and leave the open end in a container to drain. Undo the fitting attaching the pump outlet and let any remaining solution pouring out into the sink.
3. After undoing the threads at both ends remove the membrane from the module and leave it in a clean place to dry out before placing it in the storage box.
4. Re-attach the membrane module to the system and tighten up all of the gaskets and threads. Then re-attach the flexible hose to the pump and the outlet pipe to the outlet. In order to avoid entry of any kind of contaminants into the system, all the valves should be fully tightened.
5. After removing the feed tank from the system it should be dried and left upside down to keep it away from any dust or air-borne particles.

Appendix G

System calibration for cross-flow experimental rig

I) Calibration of the pump:

A potentiometer ranging from 0-100 % was used to control the pump. Flow rates of water over given time intervals was measured and plotted against the pump settings using manufacturer's data. Each measurement cycle was carried out as follows:

a) After starting up the system, the pump was set to 20 % or increments of that.
b) A pressure of 4 bar was applied over the membrane module using the back pressure valve (V-2).
c) The volume of water that returns to the tank (Figure 6.2, T-1) was measured over 1 minute.

According to the manufacturer's performance curves the maximum power used at the operating pressure of 4 bar is 0.9 kW. Using this information and bearing in mind that the potentiometer worked on a percentage power basis, the power at each pump dial setting can be calculated. Each test was taken without a membrane being inserted into the module. Figure below represents the graphs plotted, using the results obtained and shows a linear relationship between the pump setting and the other variable parameters.

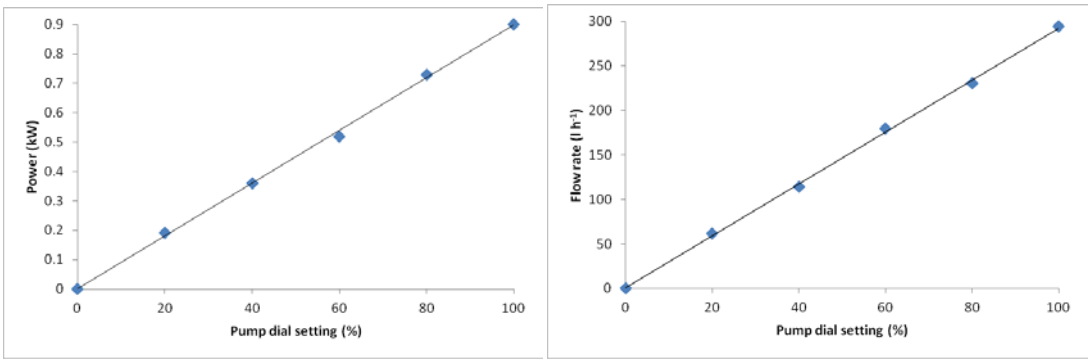

A B

Graph A) Power used by pump as a function of pump setting at the pressure of 4 bar
Graph B) Water flow rate against pump setting at the same pressure (4 bar)

II) Calibration of the Rotameter:

Performances of two rotameters which display the flow rates of the continuous phase in the inlet and outlet of membrane module were checked for accuracy. There is a litre per minute (l min^{-1}) scale on the rotameters, and a calibration test was carried out to find out if the scales were accurate enough for further interpretations. The procedure was simple and was as follows:

a) The pump was set at a fixed flow setting.
b) Readings from both rotameters were recorded.
c) The water which came back into the feed tank (Figure 6.2, T-1) was collected in a measuring cylinder over a given interval time.
d) The recorded values from Step c were compared to the values given on the scale and plotted as presented in figure below.

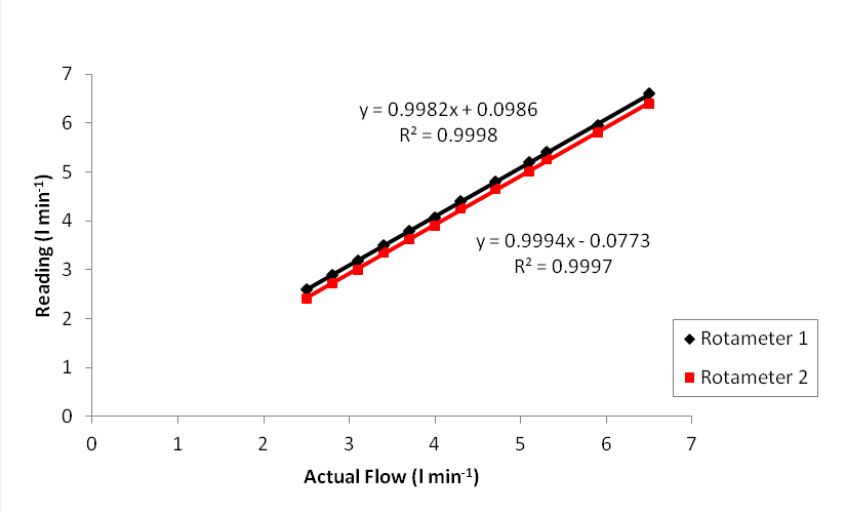

Calibration graphs for inlet / outlet rotameters

It can be concluded from the calibration graphs that the rotameters at the inlet and outlet of the module are accurate within ± 0.1 l min^{-1}. However, for having more accuracy it is better to replace them with more accurate rotameters such as a digital flow meter. On the other hand current rotameters show the flows up to 20 litres per minute while the pump can only deliver up to approximately 7 litres per minute. Therefore downsizing the rotameters would give more accurate and precise measurements.

Appendix H

Calculation of the dispersed phase flux for 0.45 µm membrane using Hagen-Poiseuille equation

Trans-membrane pressure, ΔP_{tm}	=	3×10^5 Pa (kg m^{-1} s^{-2})
Viscosity of soybean oil, μ	=	0.06 Pa s (kg m^{-1} s^{-1})
Pore radius, r_p	=	2.25×10^{-7} m
Membrane porosity, φ	=	0.30 (assumed value)
Membrane tortuosity, τ	=	2 (assumed value)
Membrane active layer thickness, *L*	=	42×10^{-6} m
Membrane internal surface area, *A*	=	0.008 m^2

$$J_d = \frac{\varphi {r_p}^2 \Delta P_{tm}}{8 \mu_d \tau L}$$

Where J_d is the dispersed phase flux (m^3 m^{-2} s^{-1}),

r_p is the pore radius (m),

ΔP_{tm} is the trans-membrane pressure (Pa),

μ_d is the dispersed phase viscosity (Pa s),

τ is the membrane tortuosity and *L* is the membrane thickness (m).

$$J_d = \frac{\varphi {r_p}^2 \Delta P_{tm}}{8 \mu_d \tau L} = \frac{\left(0.30 \times (2.25 \times 10^{-7})^2 \times (3 \times 10^5)\right)}{8 \times 0.06 \times 2 \times (42 \times 10^{-6})}$$

$$= 1.13 \times 10^{-4} \text{ m}^3 \text{ m}^{-2} \text{ s}^{-1}$$

$$= 0.41 \text{ m}^3 \text{ m}^{-2} \text{ h}^{-1}$$